Downloaded from orbit.dtu.dk on: Dec 17, 2017

Technical University of Denmark

DTU

Development of lead-free solders for high-temperature applications

Nachiappan, Vivek Chidambaram; Hattel, Jesper Henri

Publication date:
2010

Document Version
Early version, also known as pre-print

Link back to DTU Orbit

Citation (APA):
Chidambaram, V., & Hattel, J. H. (2010). Development of lead-free solders for high-temperature applications. Kgs. Lyngby, Denmark: Technical University of Denmark (DTU).

DTU Library
Technical Information Center of Denmark

General rights
Copyright and moral rights for the publications made accessible in the public portal are retained by the authors and/or other copyright owners and it is a condition of accessing publications that users recognise and abide by the legal requirements associated with these rights.

- Users may download and print one copy of any publication from the public portal for the purpose of private study or research.
- You may not further distribute the material or use it for any profit-making activity or commercial gain
- You may freely distribute the URL identifying the publication in the public portal

If you believe that this document breaches copyright please contact us providing details, and we will remove access to the work immediately and investigate your claim.

To my parents

Preface

This thesis is submitted in candidacy for a Ph.D degree from the Technical University of Denmark (DTU). The work presented in this thesis was carried out under supervision of Professor Jesper Hattel and affiliated Professor John Hald during the period September 2007 to August 2010 at the Department of Mechanical Engineering.

Part of the present work was carried out under the MATPACK (MATerials and PACKaging) research consortium (project no. 07-003145). The author wishes to acknowledge the financial support from the Danish Ministry of Science, Technology and Development (file no. 07-002236-F).

The following six papers are included in this thesis.

Paper I

Vivek Chidambaram, John Hald and Jesper Hattel. *A feasibility study of lead free solders for level 1 packaging applications*. Journal of Microelectronics and Electronic Packaging. 6: 75-82, 2009.

Author's contribution: Carried out the literature survey on the replacement of high-lead containing solders. Made all the theoretical calculations in the work using ThermoCalc. Wrote the initial draft and incorporated the corrections suggested by the co-authors and also performed the role of the corresponding author during the review process.

Paper II

Vivek Chidambaram, John Hald and Jesper Hattel. *Development of gold based solder candidates for flip chip assembly*. Journal of Microelectronics Reliability. 49: 323-330, 2009.

Author's contribution: Made all the theoretical calculations with respect to solidification, prediction of phases in the bulk solders and also the prediction of intermetallic compounds formation during the wetting reaction/solid state aging. Wrote the initial draft and incorporated the corrections suggested by the co-authors and also performed the role of the corresponding author during the review process.

Paper III

Vivek Chidambaram, John Hald and Jesper Hattel. *Development of Au-Ge based candidate alloys as an alternative to high-lead content solders*. Journal of Alloys and Compounds, 490: 170-179, 2010.

Author's contribution: Produced the prospective candidate solder alloys using the hot-plate microscope and characterized these alloys using microscopy and microhardness measurements. Wrote the initial draft and incorporated the corrections suggested by the co-authors and also performed the role of the corresponding author during the review process.

Paper IV

Vivek Chidambaram, Jesper Hattel and John Hald. *Design of lead-free candidate alloys for high-temperature soldering based on the Au-Sn system*. Journal of Materials and Design, 31: 4638-4645, 2010.

Author's contribution: Performed all the experimental works. Wrote the initial draft and incorporated the corrections suggested by the co-authors and also performed the role of the corresponding author during the review process.

Paper V

Vivek Chidambaram, John Hald, Rajan Ambat and Jesper Hattel. *A corrosion investigation of solder candidates for high-temperature applications*. Journal of Minerals, Metals and Materials Society. 61: 59-65, 2009.

Author's contribution: Made the theoretical calculations with respect to the thermodynamic stability of chlorides and performed all the electrochemical experiments. Wrote the initial draft and incorporated the corrections suggested by the co-authors and also performed the role of the corresponding author during the review process.

Paper VI

Vivek Chidambaram, Jesper Hattel and John Hald. *Status of lead-free solders for high-temperature soldering*. Submitted to Journal of Electronic Materials, 2010.

Author's contribution: Carried out a detailed literature survey on high-temperature soldering and also executed a phase diagram survey with respect to the required solidification criterion for the first level packaging applications. Performed all the experimental works. Wrote the initial draft and incorporated the corrections suggested by the co-authors and also performed the role of the corresponding author during the review process.

Contributions to the following work were also produced during the same period but have not been included because of partial overlap with the work presented in the above mentioned manuscripts.

Vivek Chidambaram, John Hald and Jesper Hattel. *Development of high melting point, environmentally friendly solders, using the calphad approach*. Archives of Metallurgy and Materials. 53: 1111-1117, 2008.

Vivek Chidambaram, John Hald and Jesper Hattel. *Au-Ge based candidate alloys for high-temperature lead-free solder alternatives*. In Conference Proceedings of IMAPS 2009, San Jose, United States.

Acknowledgements

There are several people who have helped me during this work, to whom I owe my sincere gratitude:

First and foremost, I would like to thank my supervisors Prof. Jesper Hattel and affiliated Prof. John Hald for believing in me & providing me the opportunity to perform this Ph.D study and also for the interesting technical discussions during the course of the study. Additionally Jesper is acknowledged for his assistance in compiling the final thesis. Associate Prof. Rajan Ambat deserves thanks for allowing me to use the facilities of CELCORR (Center for Electronic Corrosion) to carry out my corrosion related investigations and also for the intriguing discussions on reliability issues from a corrosion perspective.

Former Ph.D student Rene Bergmann is acknowledged for teaching me the procedure for producing solder alloys precisely using the hot-plate microscope. Many thanks to Steffen Munch for his advice on sample preparation and also for epoxy molding them. I owe my thanks to Laila Leth for familiarizing me with SEM. I would also like to express my gratitude to Peter Clever for carbon sputtering my samples that were subjected to SEM analysis. I am also obliged to John Troelsen and Lars Pedersen in solving technical problems regarding the hot-plate microscope.

Also thanks to

Dr. Torben Tang for always being ready for any kind of support.

Jens Ole Frandsen for providing me a good working place and also for other personal assistances.

Dr. Jesper Thorborg for all the system related assistances.

All my colleagues in the process modelling group and the section of materials science engineering for providing a nice working environment.

My family for all their perpetual support and motivation.

Vivek Chidambaram,
Kgs. Lyngby, August 2010.

Abstract

A survey of phase diagrams for lead-free solders in the high-temperature regime carried out in this work reveals that only a limited number of systems are available. These are Bi based alloys, Au involving alloys and Zn-Al based alloys. This work outlines the criteria for the evaluation of a new high-temperature lead-free solder material with the focus on surface tension, natural radius of curvature, oxidation resistance and environmental oriented issues. Based on the Au involving systems, possible candidate alloys were designed to have a melting range between 270°C and 350°C and were further optimized for a commercially preferred narrow solidification range. These optimized ternary combinations were further scrutinized based on the prediction of phases in the bulk solder and also the possibility of forming intermetallic compounds with the solder wettable layers of the under-bump metallization.

The effort of inducing some softness to the otherwise hard Au-0.28Ge (mole-fraction) and Au-0.30Sn (mole-fraction) hard solders by micro-alloying has been made. The changes in microstructure and microhardness associated with the addition of low melting point metals namely In, Sb and Sn to the Au-Ge eutectic were explored. Similarly the changes in microstructure and microhardness associated with the alloying of Ag and Cu to the Au rich side as well to the Sn rich side of the Au-Sn binary system were also investigated. Furthermore, the effects of thermal aging on the microstructure and the microhardness of these promising Au-Ge and Au-Sn based ternary alloys are extensively reported. A comprehensive comparison of the high-temperature stability of microstructures and mechanical properties of these potential candidate alloys with respect to the currently used high-lead content solders is made.

A corrosion investigation on these potential candidate alloys too was carried out. It was determined that the risk of corrosion of these candidate alloys is much higher when compared to the existing high-lead content solders due to the larger difference in the electromotive force between the respective phases in these candidate alloys. The present work also envisages the possible corrosion scenario between these promising candidate alloys and the under-bump metallization due to combination of materials with different electrochemical properties, high potential bias and high current density. An overview of corrosion related problems that have to be thoroughly investigated before substituting the currently used high-lead content solders has been reported.

This work also reviews the alternative technologies for replacing the high-temperature soldering since it was determined that even the expensive candidate alloys involving Au too could not cover the spectrum of properties required for being accepted as a standard soft solder for high-temperature applications. Unfortunately, even the substitute technologies that are currently being developed cannot address several critical issues of high-temperature soldering. Therefore, further research and development of high-temperature lead-free soldering is obviously needed. It is hoped that this thesis can serve as a valuable source of information to those interested in environmentally conscious electronic packaging.

Contents

List of Figures X

List of Tables XIV

1 Introduction to High-Temperature Soldering 1

1.1. High-Temperature Soldering………………………………………………. 1

1.2. High-Lead Content Solders…………………………………………….... 4

1.3. The Motivation Behind the Lead-Free Drive……………………………… 6

1.4. Legislative Initiatives and Mandates on Lead-Free Electronics…………… 7

2 Engineering Requirements for Lead-Free Solder Alloys for High-Temperature Applications 10

2.1. Solidification Criterion…………………………………………………...... 10

2.2. Environmental Issues……………………………………………………. 11

2.3. Intermetallic Compounds Formation………………………………………. 12

2.4. Surface Tension and Natural Radius of Curvature……………………….... 13

2.5. Oxidation Resistance……………………………………………………. 14

2.6. Corrosion Resistance…………………………………………………..... 16

2.7. Resistance to Thermo-Mechanical Failure……………………………….... 17

2.8. Manufacturing Requirements…………………………………………… 18

2.9. Other Requirements…………………………………………………….... 18

3 Alternative Technologies for High-Temperature Soldering 19

3.1. Electrically Conductive Adhesives………………………………………… 19

3.2. Transient Liquid Phase Bonding………………………………………… 21

4 Bi Based and Zn-Al Based Candidate Alloys **23**

4.1. Bi Based Candidate Alloys…………………………………………………… 23

4.2. Zn-Al Based Candidate Alloys…………………………………………….. 25

5 Thermodynamic Predictions Using the CALPHAD Approach **26**

5.1. Introduction to CALPHAD………………………………………………… 26

5.2. Computational Thermodynamics…………………………………………... 27

5.3. ThermoCalc……………………………………………………………….... 30

5.4. Thermodynamic Databases Used………………………………………….. 31

5.5. Modelling of Solidification………………………………………………… 32

5.6. Selection of Au Rich Candidate Alloys Based on the Prediction of Phases in the Bulk Solder……………………………………………………………. 36

5.7. Selection of Sn Rich Candidate Alloys…………………………………….. 42

5.8. Prediction of Intermetallic Compounds……………………………………. 43

5.9. Candidate Alloys Chosen for Experimental Investigation……………….…. 45

6 Experimental Approaches, Setups and Equipments **46**

6.1. Hot-Plate Microscope……………………………………………………… 46

6.2. Corrosion Testing…………………………………………………………... 50

6.3. Thermal Aging……………………………………………………………... 51

6.4. Cross-Sectioning…………………………………………………………… 51

6.5. Microscopy………………………………………………………………… 51

6.6. Microhardness Measurement………………………………………………. 52

7 Gold Based Candidate Alloys for High-Temperature Applications **53**

7.1. Gold Based Binary Alloys…………………………………………………. 53

7.2. Au-Ge Based Candidate Alloys………………………………………………. 54

7.3. Au-Sn Based Candidate Alloys………………………………………………. 66

8 A Corrosion Investigation of Prospective Candidate Alloys 79

8.1. Corrosion in Advanced Electronic Packaging Applications……………….. 79

8.2. Causes of Corrosion………………………………………………………... 80

8.3. Thermodynamic Stability of Chlorides……………………………………. 80

8.4. Potentiodynamic Polarization Curves……………………………………… 81

8.5. Electrochemical and Galvanic Coupling…………………………………… 84

8.6. Corrosion Surface Morphology After Polarization………………………... 86

8.7. Findings…………………………………………………………………….. 87

9 Summary of Appended Papers 88

10 Concluding Remarks 90

11 Outlook 91

References 92

Appended Papers I - VI

List of Figures

1.1 A BGA packaging involving high-lead alloys…………………………….. 3

1.2 A stacked chip level packaging employing Au wire bonding………………... 3

1.3 Optical microstructure of Pb-5Sn and Pb-10Sn after thermal aging at 150°C for 1 week respectively…………………………………………………….. 4

1.4 SEM-BSE micrograph of the Pb-10Sn solder alloy……………………….. 5

1.5 Microhardness values of the high-lead content solder alloys using 100g load before and after thermal aging for 1 week…………………………….……… 5

2.1 Advanced electronic packaging employing high-lead content solders for first level packaging………………………………………………………….. 11

4.1 Solidification profiles of Bi-2.6Ag, Bi-2Ag and Bi-10Ag alloys respectively……………………………………………….…………... 24

4.2 Comparison of hardness values of high-lead content solders with Bi-Ag based alloys……………………………………………………………... 24

4.3 Zn-Al phase diagram………………………………………………………. 25

5.1 A schematic diagram of CALPHAD Methodology………………………….. 27

5.2 Phases predicted in the bulk solder of eutectic Au-Sn eutectic composition… 37

5.3 Effect of Ag on the precipitation of the brittle Au5Sn phase………………… 38

5.4 Effect of Cu on the precipitation of the brittle Au5Sn phase………………… 39

5.5 Effect of In on the precipitation of the brittle Au5Sn phase…………………. 39

5.6 Effect of Zn on the precipitation of the brittle Au5Sn phase………………… 40

5.7 Phases predicted in the bulk solder of Au-0.13Sn-0.10Si alloy……………… 40

5.8 Phases predicted in the bulk solder of Au-0.18Ge-0.10In and Au-0.24Ge-0.05Sb candidate alloy respectively………………………………………….. 41

5.9 Phases predicted in the bulk solder of Au-0.15Ge-0.12Sn candidate alloy….. 41

5.10 Phases predicted in the bulk solder of Sn-0.29Au-0.08Cu and Sn-0.30Au-0.08Ag candidate alloys respectively……………………………………… 42

5.11 Isothermal section of Au-Sn-Cu system at 300°C….............................. 43

5.12 Isopleth predicting binary Cu-Sn IMCs that could form between Au-0.33Sn-0.04Cu candidate alloy and the Cu metallization…………………………….. 44

5.13 Isopleth predicting binary Cu-Sn IMCs that could form between high-lead content solders and Sn-0.29Au-0.08Cu alloy with the Cu metallization respectively……………………………………………………………….... 45

6.1 Schematic diagram showing the main parts of the hot-plate microscope….…. 46

6.2 Specimen chamber, heating and imaging system of the hot-plate microscope (HPM)………………………………………………………………………… 47

6.3 Schematic diagram showing the solder alloy sample preparation sequence…. 48

6.4 Micro-electrochemical set up……………………………………………… 50

7.1 Au-Ge phase diagram generated using SSOL2 thermodynamic database…… 54

7.2 Elemental mapping of the as-produced Au-0.18Ge-0.10In candidate alloy…. 55

7.3 Elemental mapping of the as-produced Au-0.24Ge-0.05Sb candidate alloy… 55

7.4 Elemental mapping of the as-produced Au-0.15Ge-0.12Sn candidate alloy… 56

7.5 SEM-BSE micrographs of the Au-0.28Ge eutectic alloy before and after thermal aging at 200°C, (a) as-produced (b) 1 day and (c) 1 week………….... 56

7.6 Microhardness values of the Au-Ge eutectic alloy using 100g load before and after aging………………………………………………………………… 57

7.7 SEM-BSE micrographs of the Au-0.18Ge-0.10In candidate alloy before and after thermal aging at 150°C (a) as-produced (b) 1 day (c) 3 weeks…………. 58

7.8 SEM-BSE micrographs of the Au-0.18Ge-0.10In candidate alloy before and after thermal aging at 200°C (a) as-produced (b) 1 day (c) 3 weeks…………. 58

7.9 Optical microstructures of Au-0.18Ge-0.10In candidate alloy after thermal aging for 3 weeks, (a) 150°C (b) 200°C…………………………………….... 58

7.10 Microhardness values of the Au-0.18Ge-0.10In candidate alloy using 100g load before and after aging…………………………………………………… 59

7.11 SEM-BSE micrographs of the Au-0.24Ge-0.05Sb candidate alloy before and after thermal aging at 150°C (a) as-produced (b) 1 week (c) 3 weeks….. 60

7.12 SEM-BSE micrographs of the Au-0.24Ge-0.05Sb candidate alloy before and after thermal aging at 200°C (a) as-produced (b) 1 week (c) 3 weeks…... 61

7.13 Optical microstructures of Au-0.24Ge-0.05Sb candidate alloy before and after thermal aging for 3 weeks (a) as-produced (b) 150°C (c) 200°C………. 61

7.14 Microhardness values of the Au-0.24Ge-0.05Sb candidate alloy using 100g load before and after aging………………………………………………… 62

7.15 SEM-BSE micrographs of the Au-0.15Ge-0.12Sn candidate alloy before and after thermal aging at 150°C (a) as-produced (b) 1 week (c) 3 weeks….. 63

7.16 SEM-BSE micrographs of the Au-0.15Ge-0.12Sn candidate alloy before and after thermal aging at 200°C (a) as-produced (b) 1 week (c) 3 weeks….. 63

7.17 Optical microstructures of Au-0.15Ge-0.12Sn candidate alloy after thermal aging for 3 weeks, (a) 150°C (b) 200°C……………………………………... 64

7.18 Microhardness values of the Au-0.15Ge-0.12Sn candidate alloy using 100g load before and after aging……………………………………………….... 64

7.19 Au-Sn phase diagram generated using COST 531 thermodynamic database.. 66

7.20 SEM-BSE micrographs of the Au-Sn eutectic alloy before and after thermal aging (a) as-produced (b) 150°C-1 week (c) 200°C-1 week………………… 67

7.21 Microhardness values of the Au-Sn eutectic alloy using 100g load before and after thermal aging……………………………………………………. 68

7.22 SEM-BSE micrographs of the Au-0.35Sn-0.03Ag candidate alloy before and after aging (a) as-produced (b) 150°C-1 week (c) 200°C-1 week………. 69

7.23 Microhardness values of the Au-0.35Sn-0.03Ag candidate alloy using 100g load before and after thermal aging………………………………………. 69

7.24 SEM-BSE micrographs of the Au-0.33Sn-0.04Cu candidate alloy before and after aging (a) as-produced (b) 150°C-1 week (c) 200°C-1 week……… 70

7.25 Microhardness values of the Au-0.35Sn-0.04Cu candidate alloy using 100g load before and after thermal aging………………………………………. 71

7.26 Optical micrographs of the Sn-0.30Au-0.08Ag candidate alloy before and after aging (a) as-produced (b) 150°C-1 week (c) 200°C-1 week…………... 72

7.27 SEM-BSE micrographs of the Sn-0.30Au-0.08Ag candidate alloy before and after thermal aging for 1 week, (a) 150°C (b) 200°C………………….... 73

7.28 Microhardness values of the Sn-0.30Au-0.08Ag candidate alloy using 100g load before and after thermal aging………………………………………. 73

7.29 SEM-BSE micrographs of the Sn-0.29Au-0.08Cu candidate alloy before and after thermal aging for 1 week, (a) 150°C (b) 200°C………………….... 75

7.30 Optical micrographs of the Sn-0.30Au-0.08Cu candidate alloy before and after aging (a) as-produced (b) 150°C-1 week (c) 200°C-1 week…………… 75

7.31 Elemental mapping of Sn-0.29Au-0.08Cu candidate alloy aged at 150°C for 1 week……………………………………………………………………. 76

7.32 Elemental mapping of Sn-0.29Au-0.08Cu candidate alloy aged at 200°C for 1 week……………………………………………………………………. 76

7.33 Microhardness values of the Sn-0.29Au-0.08Cu candidate alloy using 100g load before and after thermal aging………………………………….. 77

8.1 Anodic polarization curves for Au-Sn based candidate alloys………………. 82

8.2 Anodic polarization curves for Au-Ge based candidate alloys………………. 82

8.3 Cathodic polarization curves for Au-Sn based candidate alloys…………….. 83

8.4 Cathodic polarization curves for Au-Ge based candidate alloys…………….. 83

8.5 A comparison of Au-Sn and Au-Ge based candidate alloys with respect to their current density……………………………………………………….. 84

8.6 Anodic polarization curves for solder wettable layers………………………. 85

8.7 Cathodic polarization curves for solder wettable layers…………………….... 85

8.8 SEM-BSE micrographs of the surface morphology (a) Au-0.18Ge-0.10In candidate alloy and (b) Au-0.24Ge-0.05Sb candidate alloy…………………. 86

8.9 Corrosion products observed on the surfaces of both the Au-Ge based candidate alloys after polarization tests……………………………………… 86

List of Tables

1.1 Health impacts associated with blood lead levels……………………………. 7

1.2 Limits of lead which can be included in an electronic product to be considered as lead-free from various organizations………………………….. 9

2.1 Toxicity metrics……………………………………………………………. 12

2.2 Surface tension and R values for lead free soldering materials………………. 14

2.3 Standard free energy of formation of stable oxides…………………………... 15

2.4 Critical oxygen partial pressure of the stable oxides…………………………. 15

2.5 Standard free energy of reduction of stable oxides…………………………... 16

2.6 Thermodynamic stability of chlorides………………………………………... 17

5.1 List of wide spectrum of thermodynamic models implanted in the GES module……………………………………………………………………... 30

5.2 List of basic modules and its function in ThermoCalc……………………….. 31

5.3 Ternary combinations optimized for a narrow solidification range based on equilibrium solidification simulations………………………………………... 33

5.4 Minimum and maximum amounts of the alloying elements that can be added to the Au-Sn eutectic based on equilibrium solidification simulations………. 33

5.5 Ternary combinations adhering to the solidification criterion by Scheil solidification simulations…………………………………………………... 35

5.6 Minimum and maximum amounts of the alloying elements that can be added to the Au-Sn eutectic based on equilibrium solidification simulations………. 35

5.7 Candidate alloys in mole-fraction that were chosen for experimental investigation……………………………………………………………….. 45

7.1 Vickers hardness measurement of individual phases using 5g load………….. 59

7.2 Vickers hardness measurement of individual phases using 5g load………….. 62

7.3 Vickers hardness measurement of individual phases using 5g load………….. 65

7.4 Phases of the binary Au-Sn system and their composition ranges…………… 67

7.5 Vickers hardness measurement of individual phases in the Au-0.35Sn-0.03 Ag candidate alloy using 5g load………………………………………………... 70

7.6 Vickers hardness measurement of individual phases in the Au-0.33Sn-0.04 Cu candidate alloy using 5g load………………………………………………... 72

7.7 Vickers hardness measurement of individual phases in the Sn-0.30Au-0.08 Ag candidate alloy using 5g load………………………………………………... 74

7.8 Vickers hardness measurement of individual phases in the Sn-0.30Au-0.08 Cu candidate alloy using 5g load………………………………………………... 78

8.1 Thermodynamic stability of chlorides for potential solder candidates……….. 81

Chapter 1

Introduction to High-Temperature Soldering

High-temperature soldering is a key technology for electronic components & assemblies and requires a high level of process control. This technology can provide value added characteristics to the product including excellent heat conductivity, high reliability and also facilitate the drive for miniaturization. High-lead containing solders have been commonly used as high-temperature solders. The development of high-temperature lead-free solders has become an important issue now because of the health and environmental concerns associated with lead usage. Furthermore, these high-lead content solders still hinder the recycling of electronic products even though the circuit boards are assembled with lead-free Sn based solders.

1.1. High-Temperature Soldering

The needs for ultra high-temperature solders are rapidly increasing to produce the reliable electronics to which a high packaging technology and high-operating temperature are applied [1]. High-lead content solders are currently being used as high-temperature solders for first level packaging applications. Despite numerous studies on lead-free solders in recent years there are only a limited number of reports on the research and development of high-temperature lead-free alternative solders [2]. This is because the volume of solder used in Level 1 packaging is very little when compared to the volume used in Level 2 packaging. However, with the advent of area array packaging concepts, usage of solders in level 1 packaging is increasing sharply [3].

High-temperature solders are widely used as die-attach solders in power semiconductor packaging [4]. The application of power-electronics has been extended to a variety of automotive, aerospace and energy production industries [5]. With the miniaturization drive and increasing power of power electronics, high-temperature operation has become a serious issue. As a response to the growing demand of high-temperature operation, next generation power semiconductors such as SiC & GaN and packaging materials such as AlN & Si_3N_4 have been developed for high-temperature applications. Thus, high-temperature solders are indispensable for power semiconductor packaging [6].

The main applications for high-temperature solders within the electronics industry are for advanced packaging technologies. Advanced packaging technology is required because electronic devices are operating faster and becoming smaller, lighter and more functional. As a result many advanced packaging technologies employing high-temperature solders such as Ball Grid Array (BGA), flip-chip technology, chip-scale package (CSP) and multi-chip module (MCM) have been developed [7].

1.1.1. Die-Attach Material in Power Semiconductor Packaging

The die-attach material should withstand normal working temperatures, thermal loading during soldering and also be sufficiently thermally conducting to transfer heat away from the device. High-lead alloys in die-attach applications are generally used in power circuits where very high levels of conductivity are required. These are commonly found in automotive under-bonnet applications owing to the high current and low voltages produced by car batteries and the high-temperatures occurring within the engine bay [8]. High-lead content solders are also being employed in hybrid vehicles and fuel cell vehicles for the miniaturization of the inverter that converts DC power to three phases AC power to control the motor system. These hybrid vehicles and fuel cells are set to play a vital role in reducing the carbon dioxide emissions exhausted by automobiles [6].

1.1.2. Flip-Chip Technology

Certain kinds of flip-chip packaging use a two level packaging scheme i.e. first chip to ceramic and then ceramic to polymer. High-lead content solders are employed in level 1 packaging i.e. it is used to join the chip to the ceramic module. To join the chip to a ceramic module, the chip is flipped upside down, i.e., the side having the active very-large scale integration (VLSI) of the device is downward. It is known as flip-chip technology. Then the ceramic module is joined to a printed circuit board using a second set of solder bumps, which are eutectic Sn-Pb solder. Usually the bump size is much bigger in second level when compared to the first level packaging. Eutectic Sn-Pb solder is used in the second set because it has much lower melting point (183°C) than high-lead content solders. Hence, the high-lead solder bumps will not melt during the joining of eutectic bumps [9,10]. This kind of packaging concept is mainly used in mainframe computers. The array of solder bumps is usually placed on the silicon die usually by plating or vapor deposition [11].

1.1.3. BGA Technology

A ball grid array (BGA) is a surface-mount technology used for integrated circuits. The BGA is descended from the pin grid array (PGA) which is a package with one face covered (or partly covered) with pins in a grid pattern. These pins used to conduct electrical signals from the integrated circuit to the PCB on which it is placed. In a BGA, the pins are replaced by balls of solder struck to the bottom of the package. The device is placed on a PCB that carries copper pads in a pattern that matches the solder balls. The assembly is then heated, either in a reflow oven or by an infrared heater, causing the solder balls to melt. Surface tension causes the molten solder to hold the package in alignment with the circuit board, at the correct separation distance while the solder cools and solidifies [12].

The BGA is a solution to the problem of producing a miniature package for an integrated circuit with many hundreds of pins. Pin grid array packages were produced with more and more pins and with decreasing spacing between the pins, but this was

causing difficulties for the soldering process. As package pins got closer together, the danger of accidentally bridging adjacent pins with solder grew. BGAs do not have this problem due to the replacement of pins by solder balls. Certain kinds of BGA packaging employ high-lead content solders. Figure 1.1. depicts a BGA packaging involving high-lead alloys [13].

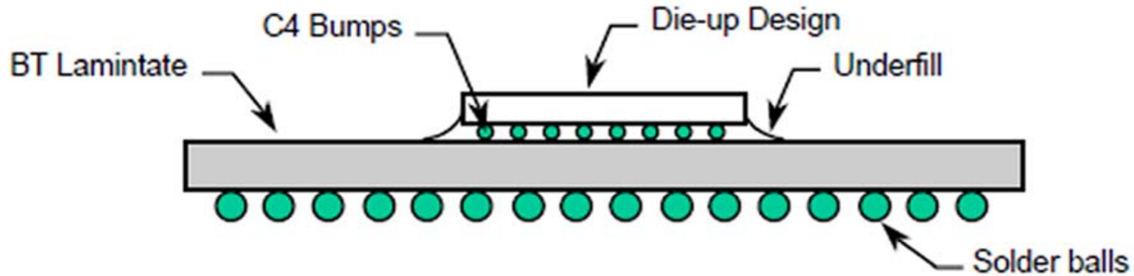

Figure 1.1. A BGA packaging involving high-lead alloys [13].

1.1.4. CSP Technology

A chip scale package (CSP) is a type of integrated circuit chip carrier. In order to qualify as chip scale, the package must have an area no greater than 1.2 times that of the die and it must be a single die, direct surface mountable package. Another criterion that is often applied to qualify these packages as CSPs is that their ball pitch should be no more than 1mm. The advantages offered by chip scale packages include smaller size (reduced footprint and thickness), lesser weight, relatively easier assembly process, lower overall production costs and improvement in electrical performance. CSP's are also tolerant of die size changes since a reduced die size can still be accommodated by the interposer design without changing the CSP's footprint [14].

Chip scale packaging can combine the strengths of various packaging technologies such as the size and performance advantage of bare die assembly and the reliability of encapsulated devices. The significant size and weight reduction offered by the CSP makes it ideal for use in mobile devices like cell phones, laptops, palmtops and digital cameras [15]. High-lead content solders are being employed in certain kinds of CSP technology since it can eliminate wiring, connectors, cooling system needed in a conventional electronic system and thereby, facilitate the miniaturization drive. A CSP packaging using the traditional Au wiring is depicted in Figure 1.2 [1].

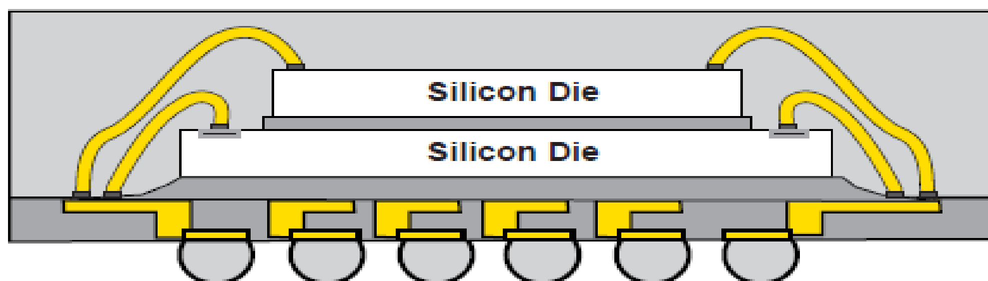

Figure 1.2. A stacked chip level packaging employing Au wire bonding [15].

1.1.5. MCM Technology

The multi-chip module (MCM), one of the most advanced forms of electronic packaging, is a group of highly functional electronic devices interconnected to the substrate by fine-line circuitry, usually in the form of multilayers. The resulting module is capable of handling an entire function. An MCM can in many ways be looked upon as a single component containing several components connected to do some function [16]. The significant benefit of MCM is the increased performance that results from the dramatically shortened interconnection length between integrated circuit devices (chips), lower power supply inductance, lower capacitance loading, less cross talk & lower off-chip driver power [17]. When integrated circuit chips are packaged in MCM, step soldering is used. Step soldering is a method to solder various levels of the package with different solders of different melting points so that the soldering of each successive level or step does not melt the previously soldered joint inadvertently [18]. In general, the 95Pb-5Sn solder with a melting temperature of 308°C-312°C is used for high-temperature applications in step soldering. The MCM technology is currently being used for servers, storage array systems, network management for telecommunications and also for aerospace applications [19].

1.2. High-Lead Content Solders

Pb-Sn and Pb-Ag with a Pb content of more than 85 wt% are the currently used solders for high-temperature soldering. Common versions of high-temperature solders are Pb-5Sn and Pb-10Sn, having a melting range of 308-312°C and 275-302°C respectively [20]. The microstructure composed of Sn particles or (Sn) phase dispersed on the matrix (Pb) phase are depicted in Figures 1.3 and 1.4. The microstructures of the high-lead content solders are very stable and both the aging durations and the aging temperatures do not have a major impact on the microstructures. This facilitates employing high-lead content solders in a wide range of applications since the microstructure does not consist of any intermetallic compounds (IMCs). Moreover, the corrosion of high-lead content solders was never identified as a reliability concern since they form a lead oxide layer, which is fairly stable. Furthermore, the galvanic potential difference between (Pb) and (Sn) is rather small, causing an insignificant corrosion effect even in harsh/humid conditions [21].

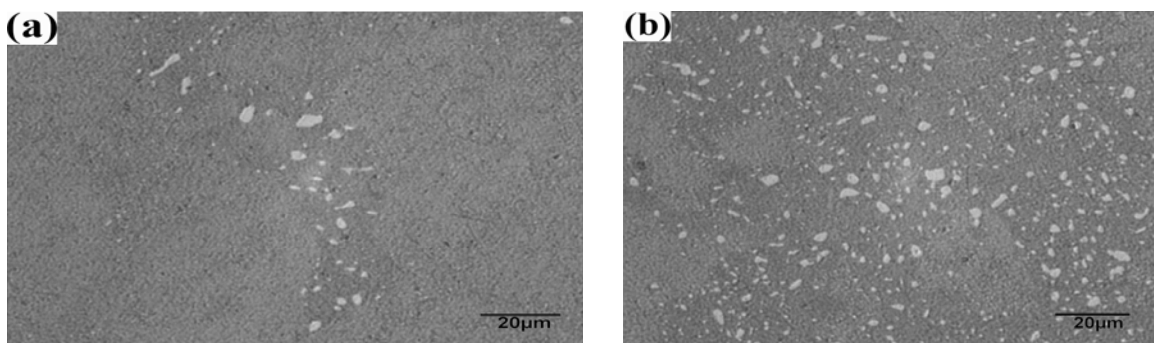

Figure 1.3. Optical microstructure of Pb-5Sn and Pb-10Sn after thermal aging at 150°C for 1 week respectively.

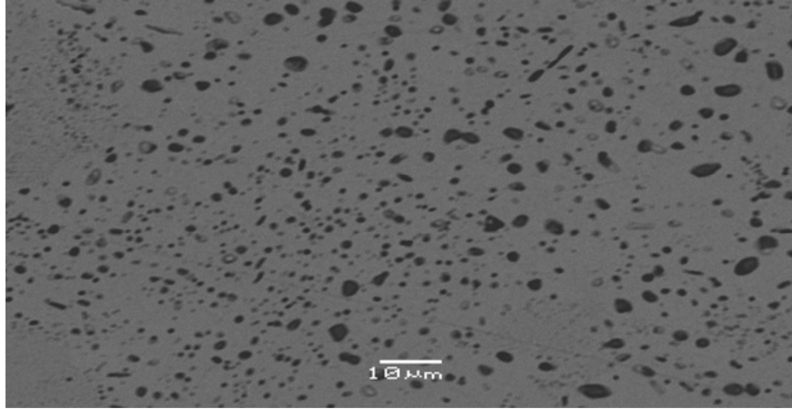

Figure 1.4. SEM-BSE micrograph of the Pb-10Sn solder alloy

High-lead content solders are an extremely soft alloy. It possesses excellent fatigue resistance since the softness of the alloy enables it to maintain a reliable joint structure by relaxation of thermal stresses [22]. On the other hand because of this softness it is prone to thermo-mechanical failure due to creep. In this project (detailed explanation of the experimental procedure has been mentioned in Chapter 6), the overall hardness of the as-produced and the aged samples using 100g load were determined and are illustrated in Figure 1.5. It was not possible to determine the hardness of individual phases even using the 1g load since the alloys are too soft. It was found that the hardness of the alloys during aging were almost similar irrespective of the aging temperatures. Pb-10Sn solder alloy was slightly harder than the Pb-5Sn alloy. This could be attributed to the dispersion hardening of the matrix (Pb) phase by Sn particles or (Sn) phase.

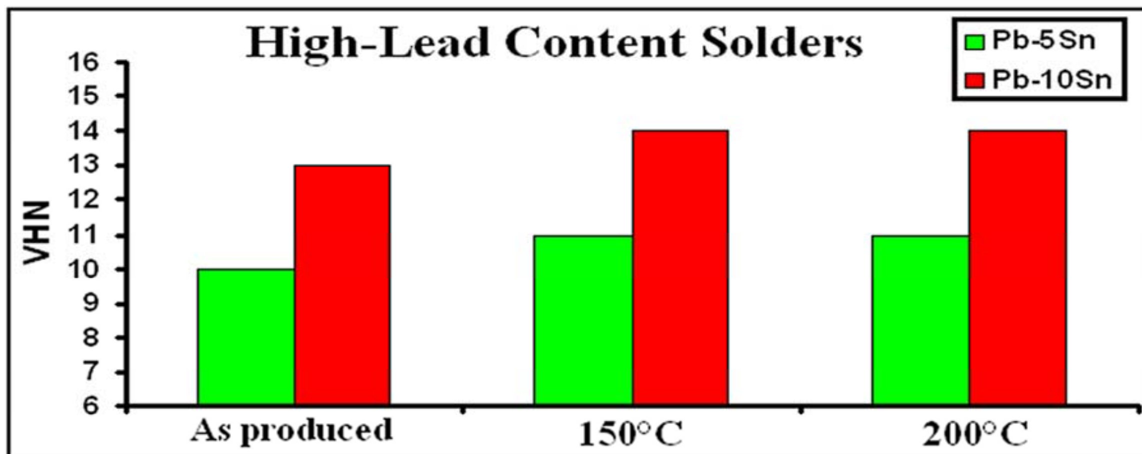

Figure 1.5. Microhardness values of the high-lead content solder alloys using 100g load before and after thermal aging for 1 week.

The surface tension measured experimentally by Somol et al [23] for Pb-5Sn and Pb-10Sn in protective Ar-H_2 atmosphere at 50° C above their respective liquidus temperature are 465 and 470 (mN/m). Surface tension measured for pure tin by Lee et al. [23] at 50°C above the liquidus temperature was 540mN/m in Ar-H_2 atmosphere. Thus, the high-lead in the alloy reduces the surface tension and thereby ensures good wetting since low surface tension generally facilitates good wetting. High-lead content solders also possess

good thermal and electrical conductivity. The thermal conductivity (k) of the Pb-5Sn alloy was determined to be 35W/mK which is fairly good for dissipating heat even for the high power devices that generate high amounts of heat [24]. Thus, mechanically and electrically, high-lead content solders make an excellent choice in the electronics industry since it is corrosion resistant, possess stable microstructure, facilitate good wetting, excellent thermo-mechanical fatigue resistance and good thermal & electrical conductivity. These factors combined with lead being readily available and a low cost metal make it an ideal choice. Despite these beneficial factors, lead is toxic and it is hazardous to the environment [3]. Therefore, the driving factor for lead-free alloys is not related to technical reasons but due to environmental concerns.

1.3. The Motivation Behind the Lead-Free Drive

The Latin word for lead, plumbum may have derived from the original Sanskrit bahu-mala, meaning "very dirty" [25]. Throughout recorded history, lead has been known to be toxic. H.L. Needleman points out that the evidence of lead toxicity existed in $2000_{B.C}$. Having been phased out of Western civilization's staples such gasoline, paint and water distribution pipelines; the elimination of lead in electronic products is imminent [26,27]. The toxic metal's last major refuge is automobile batteries which demand more than 70% of global lead assets but are largely recycled with notable fugitive emissions that contaminate the environment world wide [28]. Unlike automobile batteries; the use of recycled lead for electronics application can be severely limited since recycled lead displays higher α-particle emission. The generation of alpha particles from recycled lead could propagate through the integrated circuit (IC) leaving a track of electron-hole pairs (charge) causing transitory effects such as adding or depleting charge on capacitors and altering circuit timing pulses. These non-repeatable events cause information to be lost (changing bits in the volatile memory) or computers to lock (incorrect timing causes latches to freeze) [29].

Lead and its compounds have been cited by the Environmental Protective Agency (EPA) as one of the 17 chemicals posing the greatest threat to human life and the environment [30]. The main reason for lead posing such a great threat is that unlike many other elements, lead is one which does not have any major or substantial use in the body and thus, cause problems even if present at very low levels. Furthermore, once if lead is mined out from earth, there is no specific way that it could be destroyed or made harmless. Lead bio-accumulates in the body. That is, it is retained over time and can have adverse health impacts when a sufficient accumulation has occurred [31]. The health effects or physiological changes associated with blood lead levels are shown in Table 1.1. Currently, lead poisoning is assumed to have occurred if the level of lead in the blood exceeds 500μg/ml, but recent studies have found that a level of lead well below the official threshold could be hazardous to a child's neurological and physical development [8].

Human toxicity of lead could result in cancer and also could adversely affect the liver and thyroid functions and the resistance to disease. Lead can affect almost every organ in the body including the nervous system, kidneys, and reproductive system. The main

effect of lead toxicity is for the central nervous system of the humans. High exposure of lead could also severely damage the brain and kidneys of humans and could lead to miscarriage in pregnant women. High levels of lead could also affect the brain development of children and organs responsible for sperm production in men.

Table 1.1: Health impacts associated with blood lead levels [19].

Health Impacts	Blood Lead Levels (μg/dL)	
	Children	Adults
IQ Reduction (1-4 points, means of 2.6)[a]	10-20	NA
IQ Reduction (2-5 points, mean of 3.5)[a]	20	NA
Increased Systolic Blood Pressure (1.25mm Hg)	NA	10-15[b]
Increased Systolic Blood Pressure (2.50mm Hg)	NA	15-20[b]
Increases Systolic Blood Pressure (3.75mm Hg)	NA	Above 20[b]
Gastrointestinal Effects	60	NA
Anemia	70	80
Nephropathy	80	120
Encephalopathy	90	140
[a]In children aged 0-1,[b]in men, aged 20-70; NA= not applicable, or data not available		

Lead is very soluble in nature and it can be very dangerous to the environment. The ecological toxicity of lead could occur as a result of direct exposure of algae, invertebrates, and fish to lead. Fish exposed to high levels of lead could exhibit effects such as growth inhibition, mortality, reproductive problems and paralysis. Furthermore, at elevated levels of lead, plants can experience reductions in growth, photosynthesis and water absorption. Birds and mammals could also suffer from lead poisoning resulting in damage to the nervous system, kidneys and lever [32].

The concern about the use of lead in electronics industry stems from occupational exposure, Pb waste derived from the manufacturing process and the disposal of electronic assemblies (landfills and incineration). The Resource Conservation and Recovery Act have classified this electronic waste as hazardous to human health and require special handling and disposal. Electronic products and processes still are significant sources of lead contamination, both through occupational exposure and through waste disposal of electronic assemblies, causing e.g. the contamination of underground water sources. In addition, there is the possibility of lead containing effluents entering sewage disposal systems [3,19]. Although there seems to be no clear understanding of how lead from discarded electronic products enters the ground water stream and from there the animal or human food chain, it is generally agreed that the effect occurs. One theory is that it is connected with the action of water containing oxygen; carbon dioxide and possibly chloride on the lead containing solder materials [8].

1.4. Legislative Initiatives and Mandates on Lead-Free Electronics

Given the legacy of lead as pervasive environmental pollutant and the potency of its health impacts, it is not surprising that jurisdictions across the world have tried to limit its use. The current drive to eliminate lead from solder materials began with concern over

water distribution systems where direct population exposure to lead from potable water was demonstrated [19]. Following this, several countries have enacted legislation to minimize the environmental risks linked to the disposal of electronic waste. In Europe, Denmark was the first country to eliminate lead from most of its industrial activities. The Netherlands and Sweden followed suit with their own respective legislations [33].

In an effort to harmonize these efforts, the European Union adapted two essential directives in January 2003 to reduce the waste of electronic equipment and to ban the use of hazardous materials namely the "Waste Electrical and Electronic Equipment (WEEE)" [34] and the "Restriction of the Use of Certain Hazardous Substances in Electrical and Electronic Equiment (RoHS)" [35]. The WEEE legislation is effective since 13th August 2005. The RoHS directive is expected to work in concert with the WEEE directive to reduce the environmental and human health burden posed by discarded electronic products. A third directive is under consideration [33].

The WEEE mandates the producers of electrical and electronic equipment to finance the collection, recycling or otherwise adapt non-hazardous disposal of their products after consumers are ready to discard them. After July 1, 2006 the European RoHS prohibits the sale of electrical and electronic equipment containing the four metals i.e. Mercury, Lead, Cadmium and Hexavalent chromium. The directive contains an annex with several exemptions and was amended several times since the starting date of 2003 due to the ambiguity in establishing the maximum concentration values of hazardous elements [36].

The following important concentration value is mentioned in the directive:

- "A maximum concentration value of 0.1% by weight in homogeneous materials for lead, mercury, hexavalent chromium and of 0.01% by weight in homogeneous materials for cadmium shall be tolerated".

The explanation for a "homogeneous material" is given by a draft Commissions Guidance Document [37] in August 2004 as follows. Homogenous material means a material that cannot be mechanically disjointed into different materials. Further, the term "homogeneous" is described as "of uniform composition throughout" and "mechanically disjoint" is explained as "separated by mechanical actions such as for example: unscrewing, cutting, crushing, grinding and abrasive process."

The significant exemptions in the directives related to electronic packaging are [38]:

- "Lead in high-melting temperature solders (i.e. lead-based alloys containing 85% by weight or more lead)."

- "Lead in solders for servers, storage and storage array systems, network infrastructure equipment for switching, signaling, transmission as well as network management for telecommunications."

- "Lead in electronic ceramic parts (e.g. piezoelectronic devices)."

- “Lead in solders consisting of more than two elements for the connection between the pins and the package of microprocessors with a lead content of more than 80% and less than 85% by weight.”

- “Lead in solders to complete a viable electrical connection between semiconductor die and carrier within integrated circuit Flip Chip Packages.”

All the exemptions listed in the annex of the RoHS directive “must be subject to a review at least every four years or four years after an item is added to the list” [35].

Beyond these are some technical equipments which are completely exempted from the RoHS directive which is generally valid for all electronic equipment mentioned in the WEEE. Medical devices and monitoring & control devices, including thermostats and smoke detectors are excluded from the RoHS. Further avionic and automotive electronics have not been specifically mentioned in the directions. Additionally in the WEEE, it has been mentioned that equipment which is connected with the protection of the essential parts of the security of EU member states, arms, ammunitions and war material shall be excluded from this directive. This does not, however, apply to products which are not intended for specific military purposes [33,34].

The limits of lead which can be included in an electronic product to be considered as lead-free from different organizations around the world are listed in Table 1.2.

Table 1.2: Limits of lead which can be included in an electronic product to be considered as lead-free from various organizations [39].

Product	Organization	Limit
“Solid state devices”	JEDEC	< 0.2 wt. % of elemental lead
“Lead-free products- no lead intentionally added to the joints”	NEMI	< 0.2 wt. % of lead
“Electrical and electronic equipment”	EU (RoHS)	< 0.1 wt.% of lead

Following the impetus of the EU directives, Japan, China, South Korea and the U.S. state of California have instituted similar regulations to limit the use of lead and other RoHS toxicants in electronic and electrical equipment [19,40]. This convergence of legislative initiatives has increased the geographical scope and pace of activities to redesign electrical and electronic products using lead-free components, despite the fact that materials for high-temperature soldering are amongst those currently not affected by these legislations. It is well acknowledged in the electronics industry that the pressure to remove hazardous substances will continue and spread to other, currently exempt fields. Moreover, market pressures resulting from economies of scale are already having an impact on exempt industries owing to a dwindling availability of Pb-containing high-temperature solders, thereby causing a de facto switch to lead-free [8].

Chapter 2

Engineering Requirements for Lead-Free Solder Alloys for High-Temperature Applications

High-temperature solders are now increasingly being used for the high-performance systems. These systems perform mission-critical operations and are expected to experience virtually no downtime due to system failures. Thus, this chapter outlines the criteria for the evaluation of a new high-temperature lead-free solder material so that the currently used high-lead content solders can be replaced in a responsible and safe manner.

2.1. Solidification Criterion

In designing new lead-free high-temperature solder alloys, the melting behavior is important. The solder design for high-temperature applications needs to consider the proper regime of melting temperature because the soldered parts have to sustain with no melting until it passes the last step of the assembling process. The solidus temperature of the high-temperature solder should be at least 50°C higher than the melting point of the solder used in the second level packaging in order to withstand peak temperatures of the second level soldering. The melting point of the commonly used lead-free solder for second level packaging i.e. SAC (SnAgCu) is 217°C [3]. Therefore, the preferred melting temperature of a potential high-temperature lead-free solder was set to be 270°C by the industries.

The liquidus temperature of the solder alloy should be below 350°C in order to avoid thermal degradation of polymers commonly used in the substrate as dielectric materials since the glass transition temperature of the polymers is around 350°C [7]. This upper limit of 350°C has also been chosen by the industries in order to prevent thermal damage to the die during soldering and also due to the limitation of the thermal stresses of the components to be soldered. Therefore, the melting temperature range (270°C to 350°C) has been chosen by the industries in order to ensure efficient process control. This melting range is generally recommended to be narrower since a narrow solidification range is generally preferred for facilitating rapid production, efficient process control, preventing the movement of components during solidification and also for minimizing segregation and other solidification defects during solidification. In addition, too much liquid at reflow will destroy the package by large-volume expansion. An advanced electronic packaging employing the high-lead content solders for level 1 packaging is depicted in Figure 2.1.

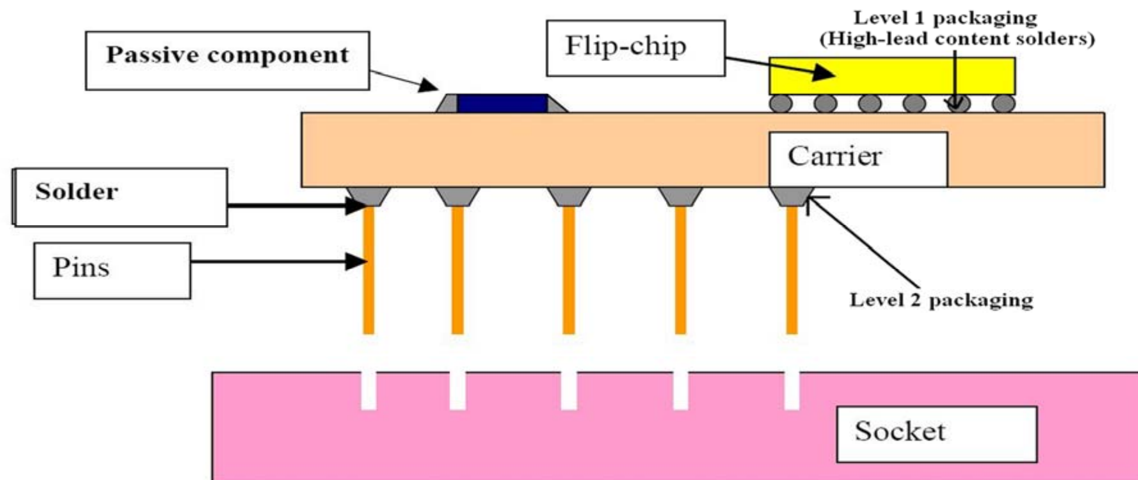

Figure 2.1. Advanced electronic packaging employing high-lead content solders for first level packaging [41].

2.2. Environmental Issues

The extent to which lead-free solders themselves are 'environmentally friendly' is also relevant. There are two basic requirements here: toxicity and recyclability [3]. While a solder might be lead-free, if it contains other toxic metallic elements such as cadmium or thallium or arsenic, the whole motivation behind the lead-free solder development will be violated since they are considered to be more toxic than lead. Of particular importance here are the acceptable concentrations in ground water and potable water and the leachability of solder alloys. In choosing alternatives for lead, it must be ascertained ahead of time that the alternatives will not pose a similar hazard since the main driving force for elimination of lead is its toxic nature [42,43].

Turbini and colleagues in 2001 analyzed the environmental impacts of lead-free alloys that may contain Sb, Bi, Cu, In, Ag or Zn. They have considered resource extraction, product manufacture, transportation and end-of-life management [40]. Indium is reported to be poison, and it affects the lever, heart, kidney and blood. Antimony is also reported to be poisonous to humans. Similarly, Bismuth is also reported to be poisonous to humans, though considered to be one of the less poisonous of the heavy metals. Their conclusion states that the lead-free solders are limited in their ability to decrease the environmental impacts of lead containing solders [44]. Recent research indicates that according to California's hazardous waste classification criteria, most electronic products might still be considered hazardous even if all electronic product manufacturers replace lead-tin solders by solders with high content of copper, nickel, antimony and zinc and thereby, abide by the European RoHS mandate [42].

The elements that are popular candidates for use in lead-free solder alloys are ranked in descending toxicity in Table 2.1, taking into account both EPA (Environmental Protective Agency- U.S) [30] and OSHA (Occupational Safety and Health Administration) [45]. The former threshold values are based on leaching by ground water while the latter are based on occupational exposure in workplace. Thus, the sole objective

of developing not only lead-free but also environmentally friendly high-melting point solders could be accomplished only by Au or Sn based solder alloys.

Table 2.1: Toxicity metrics

Metals	EPA (US) drinking water standard (mg/L)	OSHA PEL (mg/m^3)
Lead	0.015	0.05
Silver	0.05	0.01
Antimony	0.006	0.5
Indium	none	0.1
Bismuth	0.05	none
Copper	1	0.1
Zinc	5	15
Tin	none	2
Gold	none	none

The alloys used must also be recoverable and recyclable, without significant increase in cost. Presently, many recycling points are available for lead-tin alloys. By using gold, the initial costs would be higher but there would potentially be a value to the recycled product and no disposal costs associated with the solders resulting in lower lifetime costs for the product [46]. In addition, the issue of refining costs becomes important when considering initial material selection. For example, refining of gold recovered from electronic waste scrap is easier [47]. It has been reported that 47% of the total consumption of gold was recycled in 2007 [48].

2.3. Intermetallic Compounds Formation

In the first level packaging, the solder joints are made relatively smaller than the ones in the second level packaging and the intermetallic compounds (IMC) occupy a relatively greater portion of the solder joint. Thus, the IMCs too are crucial in determining the thermo-mechanical properties along with the microstructure of the bulk solder. IMCs are generally formed between the solder and the solder wettable layer of the under-bump metallization (UBM) during the wetting reaction and solid-state ageing. It is well known that the formation of IMCs between the solder and the solder wettable layer of the UBM is an indication of a good metallurgical bonding. A thin, continuous and uniform IMC layer is an essential requirement for good bonding. However, the formation of thick IMCs may degrade the reliability of the solder joint due to their inherent brittle nature and their tendency to generate structural defects [49]

In the current high-lead content solders, lead is not a very reactive metal when compared to tin and does not play a major role in the metallurgical reaction with the UBM. This fact has an important influence on the mechanical properties and behavior of the solder joint. Due to the small amount of tin within the high-lead content solders, this alloy forms the essential but only a thin layer of mostly (mostly brittle) IMCs at the solder-UBM interface during the soldering process. This is a big advantage for the high-lead content solders from a reliability perspective [50].

It has been experimentally observed by Tu et.al. [51] that the rate of intermetallic compound formation in wetting reactions between the molten solder and the metals is three to four orders of magnitude higher than those between the solid state solder and the metals. The rate is controlled by the morphology of the IMC formation. In the wetting reaction, the IMC formation has scallop-type morphology, but in solid state aging it has layer type morphology. There are channels between the scallops, which allow rapid diffusion and a rapid rate of compound formation. In the layer-type morphology, the compound layer itself becomes a diffusion barrier to slow down the reaction. These IMCs are generally brittle in nature and are prone to creep and fatigue and thus, such rapid growth of IMCs during the wetting reaction is not favored from a reliability perspective, in which case it would be advantageous that the IMC formation between the proposed promising solder candidates and the metallization is reduced during the wetting reaction.

Among the metals that are popular candidates for use in lead-free alloys, Sn and In have a high tendency of forming IMCs with the metals commonly used as solder wettable layers. The probability of forming Kirkendall porosities and the spalling of IMCs is high with a high content of these metals in the solder alloy. The Kirkendall voids lead to very poor mechanical properties. The spalling phenomenon is extremely undesirable because it leads to chemically and mechanically weak joints since the solder loses contact with the solder wettable layer of the UBM. Thus, from a reliability perspective, it would be desirable to have small amounts of only one element in the lead-free alloy with a tendency of forming IMCs with the UBM just similar to the currently used high-lead content solders. Moreover, it would be an added advantage if the rate of IMC formation during the wetting reaction is kept low [49-51].

2.4. Surface Tension and Natural Radius of Curvature

The surface tension (γ) of a liquid is a thermodynamic quantity and is defined as the amount of work needed to isothermally enlarge the liquid surface area [52]. It quantifies the disruption of intermolecular bonds that occurs when a surface is created. The interfacial forces (surface tension) between the molten solder and the substrate influence the degree of wetting, which in turn determines the formation of proper solder joints. Thus γ is one of the critical properties of a solder that determines its wetting behavior. The dissolution of under-bump metallization (UBM) in the molten solder, the oxidation of the molten solder, the soldering environment, etc., also affect the surface tension of the solder. Studies have shown that the surface tension value of a solder varies with temperature [53] and the extent of solder-UBM (solder wettable layer) interactions [54]. For these reasons the surface tension of solder alloys and most other liquid metals under actual processing conditions is not precisely known [55]. Low γ values generally facilitate better wetting. Other than wetting, γ values also influence the natural radius of curvature, R of the alloys. The relation is shown below.

$$R = \left(\sqrt{\frac{\gamma}{\rho g}} \right) \tag{2.1}$$

γ = surface is tension, ρ = density and g = acceleration due to gravity.

The continuing miniaturization of components in the micro-electronics industry, places ever-increasing demands upon solder alloys to be designed for low *R* values in order to prevent bridging between contacts as the pitch between contacts keeps getting smaller and smaller during the miniaturization drive [3]. The surface tension and natural radii of curvature of elements being considered for this application are listed in Table 2.2 along with the currently used binary alloys. γ and ρ values required for the calculations of R were taken from the SURDAT database [23] measured experimentally at 50°C above the liquidus temperature in Ar+20%H_2 atmosphere. Solder alloys with considerable amounts of Au, Bi, Sb and Sn would facilitate the drive for miniaturization while solder alloys with considerable amounts of Al or Cu would severely hamper the miniaturization drive.

Table 2.2: Surface tension and R values for lead free soldering materials.

Metals	γ (mN/m)	R (mm)
Pb-5Sn (w-p)	465	2.115
Pb-10Sn (w-p)	470	2.147
Ag	890	3.128
Al	863	6.635
Au	1090	2.550
Bi	375	1.960
Cu	1276	4.059
In	547	2.829
Pb	430	2.034
Sb	365	2.402
Sn	540	2.827

2.5. Oxidation Resistance

Oxidation resistance is one of the critical parameters which influence the wetting, formation of intermetallics, etc. The standard free energy of formation of the most stable oxides for the elements being considered for first level packaging applications from room temperature to the temperature during reflow were calculated using the SSUB3 [56] thermodynamic database via Thermo-Calc and is listed in Table 2.3.

Thus, gold and silver having a positive free energy possess a very low tendency to form stable oxides. Gold oxide is not stable above 177°C. Among the elements being widely considered for this application; In, Sb and Si having a very low free energy (negative) possess a very high tendency to form stable oxides. The critical oxygen partial pressures of the stable oxides with negative Gibbs free energy were calculated using the following relation and is listed in Table 2.4 [3].

$$P_{O_2} = \exp\left(\frac{\Delta G_f^0}{RT}\right) \tag{2.2}$$

P_{O_2} = Critical oxygen partial pressure, ΔG_f^0 = Gibbs free energy of formation, R =Gas constant, T =Temperature (K).

Table 2.3: Standard free energy of formation of stable oxides.

Stable Oxides	$\Delta G^0_{f,T}$ (KJ/mole) 25°C	$\Delta G^0_{f,T}$ (KJ/mole) 200°C	$\Delta G^0_{f,T}$ (KJ/mole) 325°C
Ag_2O	-11.25	0.28	8.21
Au_2O_3	77.86	118.57 (177°C)	unstable
Bi_2O_3	-497.10	-450.41	-415.58
Cu_2O	-147.84	-134.51	-125.08
GeO_2	-521.31	-487.02	-462.84
In_2O_3	-827.23	-770.61	-729.17
Sb_2O_5	-829.14	-745.25	-685.32
SiO_2	-856.29	-824.27	-801.54
SnO_2	-515.82	-479.63	-452.78

Table 2.4: Critical oxygen partial pressure of the stable oxides.

Stable Oxides	P_{O_2} 25°C (atm.)	P_{O_2} 200°C (atm.)	P_{O_2} 325°C (atm.)
Bi_2O_3	8.22×10^{-88}	1.89×10^{-50}	5.13×10^{-37}
Cu_2O	1.25×10^{-26}	1.47×10^{-15}	1.20×10^{-11}
GeO_2	4.70×10^{-92}	1.73×10^{-54}	3.84×10^{-41}
In_2O_3	1.19×10^{-145}	8.51×10^{-86}	2.12×10^{-64}
Sb_2O_5	5.51×10^{-146}	5.39×10^{-83}	1.42×10^{-60}
SiO_2	9.68×10^{-151}	1.01×10^{-91}	$1,01 \times 10^{-70}$
SnO_2	4.28×10^{-91}	1.12×10^{-53}	2.89×10^{-40}

atm. = Atmospheric pressure

Thus, it is evident that the critical oxygen partial pressure of the most stable oxide compounds at low temperature for elements like Bi, Ge, In, Sb, Si and Sn are extremely low and even the most sophisticated vacuum equipment available today would not be able to attain such low vacuum levels. While it may not be possible to control the onset of oxidation with the industrial equipment suitable for mass production, the extent to which oxidation proceeds can be controlled by restricting the oxygen content in the environment in which soldering is done so that the oxidation can be kept to a minimum.

An alternative approach frequently taken to prevent oxidation is maintaining a reducing atmosphere such as hydrogen atmosphere during reflow [3]. The effects of a reducing atmosphere on the stable oxide compounds of the elements widely being considered for this application were determined using the SSUB3 thermodynamic database [56]. The formation of stable oxides can be easily controlled if the Gibb's free energy of the reduction reaction is negative. In case of hydrogen atmosphere, the reaction is the reduction of stable oxide to pure element and the formation of water vapor. The effect of the hydrogen atmosphere on the most stable oxides of the popular metals being considered for lead-free alloys is listed in Table 2.5.

Table 2.5: Standard free energy of reduction of stable oxides.

Oxides	ΔG^0_{rxn} (KJ/mole) 25°C	ΔG^0_{rxn} (KJ/mole) 200°C	ΔG^0_{rxn} (KJ/mole) 325°C
Ag_2O	-225.89	-210.23	-202.19
Au_2O_3	-789.28	-754.55 (177°C)	unstable
Bi_2O_3	-214.32	-179.46	-160.65
Cu_2O	-89.30	-75.45	-67.00
GeO_2	47.02	67.10	78.69
In_2O_3	115.80	140.73	152.95
Sb_2O_5	-356.56	-304.54	-275.05
SiO_2	382.01	404.35	417.39
SnO_2	41.54	59.72	68.63

Thus, it is evident that even a hydrogen atmosphere fails to control the onset of oxidation if the solder alloy includes considerable amounts of Ge, In, Si and Sn. Unlike In and Si, the reduction reactions of the stable germanium and tin oxides possess relatively low (positive) free energy. Thus, it would be advantageous from a wetting perspective to avoid Si in the solder alloy. Zinc forms a very stable ZnO_2 phase but this phase has not been assessed in SSUB3 thermodynamic database and therefore, it has not been taken into account.

2.6. Corrosion Resistance

Presently electronic devices are used under service conditions that were never thought of as possible just a few years back [57]. Depending upon the particular design of the electronic component and the manner in which it is mounted, the solder connection can be exposed to the atmosphere [3]. The solder is thus not only exposed to air but also moisture and other corrosives present in the atmosphere such as chlorine compounds. Another source for chlorides is residual chemicals. These are generally introduced during manufacturing and include cleaning compounds, plating solutions and metal processing fluids. Also included here are chemicals from finger prints and saliva [21]. The likelihood of a metal forming a chloride and the stability of the chloride formed is represented by the standard Gibbs free energy of formation (ΔG^0_f) of that chloride. The thermodynamic parameter LNAC (natural logarithm of activity) is useful for investigating metal-gas interaction systems involving formation of various forms of metal-involving oxides, chlorides etc.

$$\mathrm{LNAC} = \frac{\mu}{RT} \tag{2.3}$$

where μ is the chemical potential. The compounds with a large negative LNAC of Cl_2 (g) value are highly stable. The ΔG^0_f values and the LNAC of Cl_2 (g) of the most stable chlorides of the elements commonly being considered for the major constituents in solder alloys were calculated at different room temperatures using the SSUB3 thermodynamic

database and are summarized in Table 2.6. This table shows that all elements currently being considered for replacement solder alloy are prone to attack from chlorine that could be present in the atmosphere but the magnitude is very high for Zinc. Thus, Zinc can be advocated for solder alloys only as a minor constituent and definitely not as a major constituent. The corrosion of the currently used high-lead content solder alloys was never identified as a major concern though it easily reacts with chlorides because they form a lead oxide layer which is fairly stable.

Table 2.6: Thermodynamic stability of chlorides.

Metals	Chlorides	$\Delta G^{0}_{f,T}$ (KJ/ mole)		LNAC of Cl_2 (g) (dimensionless)	
		25°C	45°C	25°C	45°C
Ag	AgCl	-109.8	-108.7	-88.6	-82.2
Au	$AuCl_3$	-53.5	-49.1	-14.4	-12.4
Bi	$BiCl_3$	-315.2	-310.9	-84.8	-78.3
Cu	$CuCl_2$	-173.7	-170.8	-65.2	-59.1
Ge	$GeCl_4$	-462.7	-458.1	-93.3	-86.8
In	$InCl_3$	-455.4	-450.4	-112.9	-104.4
Pb	$PbCl_2$	-314.1	-311.1	-126.7	-117.6
Sb	$SbCl_3$	-324.4	-320.6	-87.3	-80.8
Sn	$SnCl_2$	-291.2	-288.4	-118.7	-109
Zn	$ZnCl_2$	-370.3	-367.3	-149.4	-138.8

2.7. Resistance to Thermo-Mechanical Failure

The two most prominent thermo-mechanical failures encountered by a solder alloy are fatigue and creep. In this context, fatigue is a measure of resistance to failure due to cyclic thermal loading [3]. Likewise, creep is a measure of the time required for a material to fail when it is under a constant load at an elevated temperature [58]. It involves deformation mechanisms, such as grain boundary sliding, vacancy diffusion, etc. which requires thermally driven diffusion processes. Therefore, creep deformations become critical when the operating temperature exceeds about half the absolute melting temperature of the material [58,59]. Thus, for high-temperature solders creep is considered as one of the most important solder deformation mechanisms.

The substitute solder alloy similar to high-lead content solders should be soft since soft solders possess excellent resistance to thermo-mechanical fatigue and thereby facilitate relaxation of thermal stresses [3]. At the same time being too soft would degrade their resistance to creep. Therefore, it is necessary to strike a perfect balance between the ductility and strength. The mechanical properties of a solder alloy are governed primarily by its respective microstructure. Therefore, it is essential that the microstructure of the bulk solder does not possess massive IMCs since massive intermetallic formation degrades the mechanical properties of the joint. Thus, the indispensable requirement for the high-temperature solder selection is considered to be little or no brittle intermetallic formation for the softness and ductility of the alloy.

2.8. Manufacturing Requirements

Electro-deposition is one of the common ways of depositing solder alloys. Thus, it is essential that the elements in the prospective lead-free solder alloys could be easily electrodeposited. Electroplated bumping processes generally are less expensive than other bumping techniques. Electroplating in general has a long history and processes are well characterized. Plating can allow closer bump spacing (35 to 50 microns) than other methods of bump formation. Electroplating has become more popular for high bump count (>3,000) chips because of its small feature size and precision. Among the elements that are popular for lead-free solder alloys; Ag, Au, Cu and Sn are easy ones for electroplating whereas Bi, In and Sb are difficult ones and Ge, Si are currently impossible ones. Thus if a new solder alloy is developed with Ge or Si then a new electroplating technique has to be developed [60,61].

It is very essential that the new lead-free high-temperature solders are compatible with the existing processes and equipments. For instance, the currently used high-lead content solders are used mainly in the forms of wires and ribbons for die-attachments. Therefore, the substitute for high-lead content solders would also have to be manufactured in these forms. Else, introducing these alloys to actual products would be hampered since applying these lead-free alloys then entails an expensive development effort for die-attach machines that handle solder in different forms. It has to be noted that not all proposed lead-free alloys can be manufactured in these forms [62].

2.9. Other Requirements

It is very essential that the solder possesses good thermal and electrical conductivity. A good thermal conductivity is required since the heat generated by the die must be dissipated in order for the device to continue reliable operation. While the main pathway for heat dissipation is through the encapsulation material, the solder joint is also thought of as one pathway for heat dissipation. In high interconnect BGA, the solder balls serve only as a heat dissipation medium and do not serve any electrical function. A good electrical conductivity too is required since the solder also serves as electrical interconnects in most of the advanced electronic packaging, i.e. all the electrical currents going into and out of the silicon device must pass through the solder interconnection [3].

The ability of the molten solders to flow or spread during the soldering process is of prime importance for the formation of a proper metallic bond [63]. The extent of wetting is measured by the contact angle that is formed at the juncture of a solid and liquid in a particular environment. In general, if the wetting contact angle lies between 0 and 90° the system is said to be wet, and if the wetting angle is between 90 and 180°, the system is considered to be non-wetting. Thus, in order to ensure good wetting the lead-free alloys should possess low wetting angle and high wetting force. A high wetting force ensures that the maximum extent of wetting has been attained [3].

Chapter 3

Alternative Technologies for High-Temperature Soldering

There is still no obvious replacement for high-lead content solders covering the spectrum of these properties required for being accepted as a standard soft solder for high-temperature applications. The two emerging alternative technologies that are identified as potential technologies for future electronics and manufacturing are: conductive adhesive technology and the transient liquid phase bonding. These two techniques are briefly evaluated in this chapter. However, further focus has not been given on these alternative technologies since the mission of this Ph.D work is to develop new prospective candidate alloys for replacing the high-lead content solders. Moreover, substituting the existing material is always less complicated than replacing the existing process.

3.1. Electrically Conductive Adhesives

Electrically conductive adhesives (ECA) provide promising alternatives for the high-temperature soldering. The major advantage of ECA over the proposed Pb-free candidate alloys is that the former can be used on a wide range of surfaces including ceramics, glass and other non-solderable surfaces. ECAs are comprised of polymeric binders which provide mechanical strength and conductive fillers which act as channel for charge transport. The characteristics of ECA are essentially the result of its two components. Polymeric binders are either thermosets or thermoplastics. For conductive fillers, metallic materials such as gold, silver, copper, and nickel and nonmetallic materials such as carbon have found applications in ECA. Other advantages of ECA over conventional soldering based interconnection technology are: environmentally friendly; finer pitch capability; higher flexibility; greater fatigue resistance than the high-lead content solders, and the ease of processing [64,65].

ECA can be categorized with respect to conductive filler loading level into anisotropically conductive adhesives (ACA) and isotropically conductive adhesives (ICA). The difference between ACA and ICA is based on the percolation theory. The percolation threshold depends on the shape and size of the fillers but typically in the order of 15-25% volume-fraction. For ICA, the loading level of conductive fillers exceeds the percolation threshold, providing electrical conductivity in all x-, y- and z-directions. For ACA, on the other hand, the loading level of conductive fillers is far below the percolation threshold and the low volume loading is insufficient for inter-particle contact and prevents conductivity in the X-Y plane of the adhesive. Therefore, they provide a uni-directional electrical conductivity in the vertical or Z-axis when pressure is applied with heat treatment. ICA is widely being viewed as a promising

alternative to high-temperature soldering because of its relatively higher conductivity [66].

Although, thermoplastic systems have some advantages like reworkability and assembly speed they are not normally chosen as matrices for ICA. Robust thermosetting systems are the more common choice offering resistance to heat, moisture and mechanical stress [67]. ICA formulations usually include epoxy resin as the polymeric matrix. Epoxy based materials have been used in engineering components because of their outstanding mechanical and thermal properties as well as processability. The use of epoxies has been the state of the art for a long time. Epoxies have many beneficial properties like low shrinkage, good adhesion, resistance to thermal & mechanical shocks and low die-electric constant. They also have a good resistance to moisture, solvents and chemical attacks [68].

The most popular filler material for ICA is Ag which is cheaper than Au and has superior conductivity and chemical stability. Also, it is easy to precipitate into a wide range of controllable sizes and shapes and silver oxides show high conductivity. Filler particles may come in the form of spheres, fibers, flakes or granules but the optimum geometry is that which provides minimum critical filler concentration for low resistance, the best contact between neighboring metallic particles and strong adhesion to the polymer, i.e. flakes due to their high aspect ratio. Small particles are better than large particles, providing more particle to particle contact, greater conductivity and consistency of the product [67].

However, this technology has to address a series of critical reliability issues before being adapted by the electronics industry as an alternative technology to high-temperature soldering. Notable among them are impact strength, electrical and thermal conductivity, adhesion capability of ICA and compatibility with non-noble metal finished components in particular the Sn plated components [69,70]. It also has to be noted that the thermal conductivity of ICA (k=3 W/mK) is even worse than the Bi based candidate alloys [24].

Environmental reliability is also a serious concern for ICA joints. Moisture is the most commonly encountered service environment and must be considered a critical condition in determining the long-term reliability of adhesively bonded joints. For many polymeric systems, warm, moist environments can considerably weaken the performance of the adhesive joints. Moisture may affect the behavior of adhesive joints by attacking the bulk adhesive and the adhesive/substrate interface. Moisture can alter the properties of adhesives in a reversible manner, such as plasticization, which can result in depression of the glass transition temperature and weakening of the mechanical strength of adhesives. Moisture can also change the properties of the adhesives in an irreversible way by causing further cross-linking or chemical degradation and by cracking or crazing in the adhesive. Water can also degrade the adhesive joint by attacking the adhesive/substrate interface. Displacement of the adhesive by water is likely when high surface free energy substrates are utilized and when the adhesion between the adhesive and the substrate is

mainly due to Van Der Waal's forces. In addition water may also hydrate the substrate surface and cause the formation of a weak boundary layer [71].

With the advent of nanotechnology, some of the critical reliability issues with respect to ICA could be addressed. Nano-sized metal particles are being used in ICA to improve electrical conduction and mechanical strength. The desirable properties of the ECA could further be improved with a suitable choice of solvents, colorants, flame retardants, flexibilizers, cure accelerators, coupling agents, corrosion inhibitors etc [68,72].

3.2. Transient Liquid Phase Bonding

The transient liquid phase (TLP) bonding combines the characteristics of liquid–phase joining (soldering and brazing) and diffusion bonding. The process relies on the reaction between a thin low melting interlayer and metal on the components. During the heating cycle, the low melting interlayer diffuses into the high melting point component and by that intermetallic phases are formed by diffusion. After that the remelting temperature of the system is raised and the joint will not remelt thereafter unless it is heated to a higher temperature at which one of the intermetallic phases melts [73]. TLP bonding was originally investigated in the 1960s for multiple soldering operations during assembly. Recently TLP bonding has also attracted great attention in three dimensional (3D) chip stacking technology. Indeed, TLP bonding enables repeated stacking of additional layers without remelting the joints at lower levels of the stack and hence, can facilitate multilevel 3D interconnects [74].

By judicious selection of the component materials or metallizations applied to them, interlayer and process parameters, it is possible to design a joining method that combines the beneficial characteristics of soldering, namely rapid joint filling, tolerance to surface preparation and the formation of fillets, together with the advantages of completeness of joint filling and high remelt temperature of diffusion bonded joints. However, it is usually necessary to apply compressive stress to the assembly in the beginning to minimize the joint gap and a further heat treatment to the assembly after diffusion soldering so that the diffusion of the solder interlayer into the parent materials continues until, ultimately, the joint is homogenous.

The sequence of steps involved in achieving a diffusion soldered joint via TLP bonding are as follows:

- The component surfaces are first metallized in order to provide suitable, solderable surfaces.
- The filler metal (interlayer) is introduced into the joint in the form of thin coating (<10μm). Alternatively, the filler material can also be rolled sheets, rapidly solidified amorphous foils or powders (with or without binders).
- A compressive stress is applied to the assembly to minimize the joint gap, there being insufficient liquid generated during the heating cycle to fill wide joints.
- The assembly is then heated so that the filler metal melts, wets the joint surfaces and fills the joint.

- By maintaining the assembly at the joining temperature for longer than is usual in conventional soldering, the diffusion between the interlayer and the parent materials continues to an extent that results in an isothermal solidification of the filler material through the formation of higher melting point intermetallic phases. Solidification in this manner increases the remelt temperature of diffusion soldered joints above the process temperature.
- The strength and the remelt temperature of diffusion soldered joints can be raised further by heat-treating the assembly so that diffusion of the filler metal into the parent material continues until; ultimately, the joint is homogeneous with them [75].

TLP bonding is conducted in a high vacuum atmosphere to control the formation of oxide layers on the interlayer as well as the faying surfaces. Therefore, it is necessary to select vacuum compatible interlayers. Two possible effects of an oxide layer on the interlayer material can be envisaged. Firstly, the oxide layer could act as a container that restrains the interlayer from spreading and second, the presence of an oxide on the interlayer might modify interfacial energies and/or interface reactions. A further possibility, that arises if the interlayer's oxide layer becomes trapped at the liquid/solid interface, is that the oxide can act as a diffusion barrier that impedes the reaction-driven spreading processes. A wide variety of heating methods can be employed for TLP bonding that include radiant heating in a standard vacuum brazing furnace, induction heating and infrared heating [76].

TLP bonding could easily be achieved around 280°C by using metals like Bi/In/Sn as interlayers [77,78]. Nevertheless, several critical issues are hindering the wide acceptance of TLP bonding as an alternative to high-temperature soldering. These include production delays i.e. the duration of this process could be much longer when compared with seconds for soldering [75]. Most of the possible intermetallic phases that could precipitate between the low melting point metals and the commonly used pad materials and the under-bump metallizations are more brittle than any of the proposed candidate alloys. The possibility of having Kirkendall voids right at the joint is also a matter of great concern.

Chapter 4

Bi Based and Zn-Al Based Candidate Alloys

The binary phase diagrams of Sn and further metallic elements indicate that generally the melting point of pure Sn will be lowered by adding elements that are popular candidates for use in solder alloys. Thus, Bi based alloys and Zn-Al based alloys are the only cost-effective alloys for high-temperature lead-free solder alternatives. The former is not promising enough for this application since Bi rich phases possess very poor thermal conductivity while the latter is not suited for this application due to its highly corrosive nature and also due to its high natural radius of curvature.

4.1. Bi Based Candidate Alloys

Bi is the least toxic of the heavy metals and with a melting point of 270°C it is a natural choice for high-temperature lead-free solder alternatives [6]. It should however be noted that at present Bi is mainly a bi-product of Pb production [79]. The development of Bi based alloys for Pb-free high temperature soldering is severely hindered by the poor thermal and electrical conductivity possessed by the Bi rich phases which is critical for the solder alloy [80]. The thermal conductivity of Bi (k = 8 W/mK) is much lower when compared to the existing high-lead content solders like Pb-5Sn (k = 35 W/mK) [24].

It has been well documented that the addition of Ag to Bi would slightly improve the thermal and electrical conductivity of the alloy. Recent investigation indicates that increasing the Ag content of the Bi-Ag alloy to 10 wt. % promotes an increase in thermal conductivity and ductility [22]. The Bi-Ag system has a eutectic melting point of 262°C corresponding to 2.6 wt% Ag [79]. However, further increasing or decreasing the Ag content from the eutectic point entails an increase of only the liquidus temperature and not the solidus temperature as illustrated in Figure 4.1.

The microstructure of the Bi-Ag consists of Ag rich dendrites dispersed on the matrix (Bi) phase. Coupled growth of the eutectic phases has not been reported since the eutectic point lies on the region with a very high Bi content [79,81]. In addition to being close to the required solidification criterion, Bi-Ag is the only possible candidate alloy that is close in hardness to the high-lead content solders as illustrated in Figure 4.2. The low solubility of silver in bismuth precludes solid-solution strengthening. Thus, the hardness values of Bi-2.6Ag and Bi-10Ag alloys were almost similar.

Bi-2.6Ag is the only possible alloy which is close to the required solidification criterion as well as in hardness to the existing high-lead content solders [22]. Despite this advantage it cannot be used as an alternative since high-temperature solders are currently being employed in applications that generate high amounts of heat and it demands a high heat conductivity of the solder. Moreover, alloying small proportions of Ag cannot

drastically improve the thermal and electrical conductivity of the alloy. Furthermore, Bi-2.6Ag alloy also possesses a higher wetting angle of 39° when compared to the existing high-lead content solders like Pb-5Sn (16°) on Cu substrate [22].

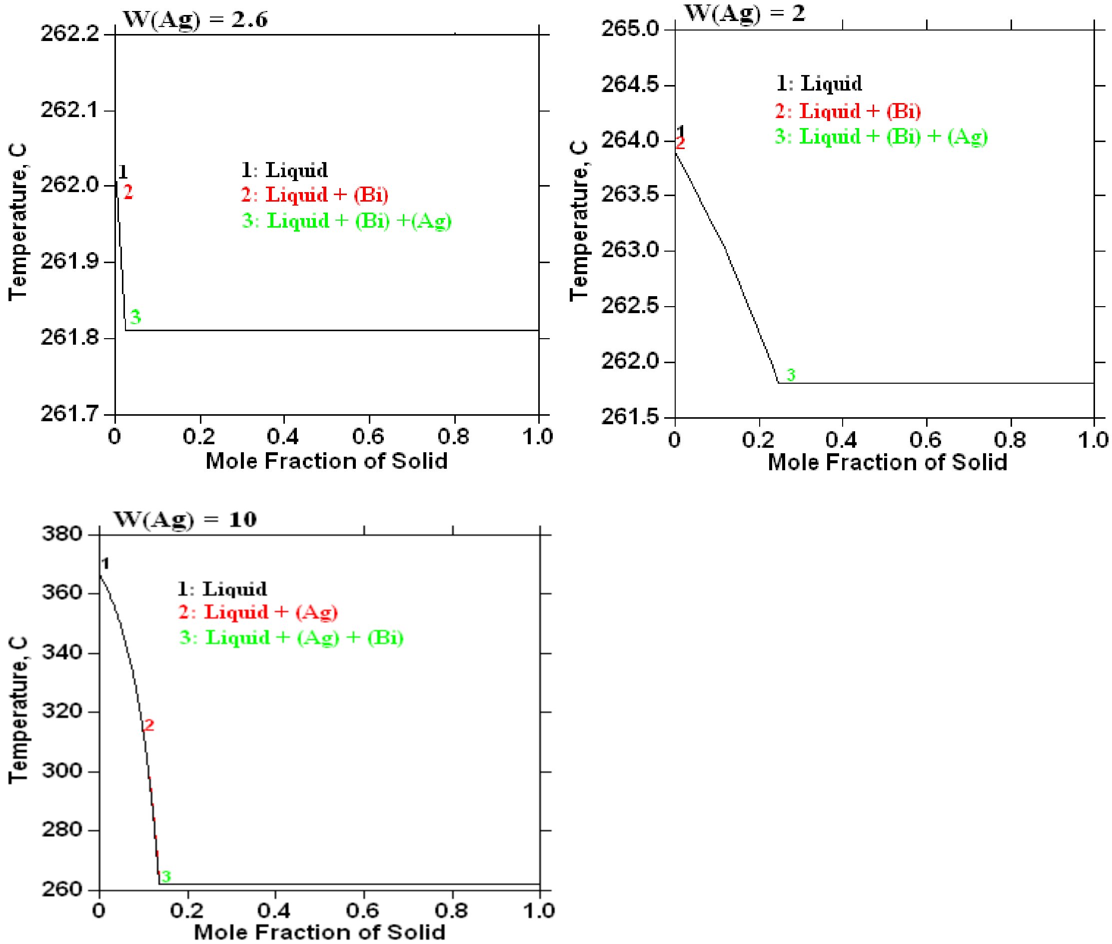

Figure 4.1. Solidification profiles of Bi-2.6Ag, Bi-2Ag and Bi-10Ag alloys respectively.

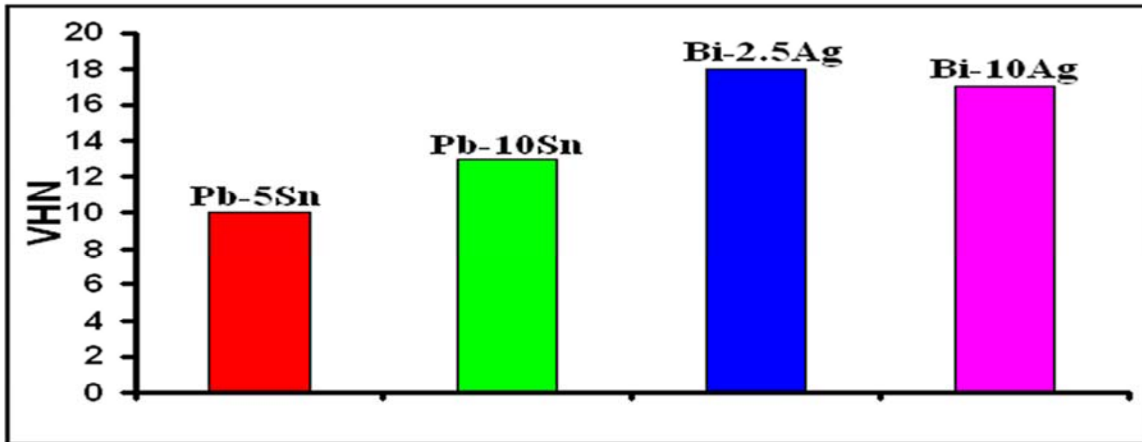

Figure 4.2. Comparison of hardness values of high-lead content solders with Bi-Ag based alloys.

4.2. Zn-Al Based Candidate Alloys

Zn-6Al (wt. %) with a eutectic melting point of 381°C is a very interesting candidate for this application [82]. The corresponding phase diagram as illustrated in Figure 4.3 reveals that this alloy does not form any intermetallic compounds [2]. The microstructure of Zn-Al comprised of the dark α phase (FCC) dispersed on bright η phase (HCP). The solubility of Al in α phase is relatively higher than in the η phase. Zn-Al alloys have long been used as high-temperature solders for structural applications [83,84]. From a commercial perspective, this is a very prospective alloy since Zn is even cheaper than lead [85]. It has also been reported that the thermal conductivity of the Zn-Al based alloys are almost double that of high-lead content solders. Small additions of either Mg or Ge to the Zn-Al eutectic would reduce the melting point of this alloy and make this ternary alloy adhere to the required solidification criterion for high-temperature soldering [86].

However, having Al in the alloy for soldering electronic components would severely hamper the drive for miniaturization in the electronics industry due to the high natural radius of curvature possessed by Al [23]. Above all, the major drawback for developing Zn-Al based alloys as Pb-free solders for high-temperature soldering is the corrosion-oriented reliability issues [3]. Zn is a highly corrosive metal and it can be advocated for solder alloys only as a minor constituent and definitely not as a major constituent since electronic devices are being subjected to service conditions today that were never thought of as possible just a few years back. It has been reported that Zn-Al eutectic is a relatively hard alloy when compared to the existing high-lead content solders [62]. Therefore, it is difficult to fabricate it into wire or ribbon and also some concerns are being expressed about the high hardness of this alloy limiting its use between materials with different co-efficient of thermal expansions. Furthermore, it possesses poor wetting behavior because of the high oxygen affinity of both Zn and Al [3,87,88]. Taking into account its corrosive nature, high natural radius of curvature and wetting constraints, this alloy was also not considered for further investigation in this work.

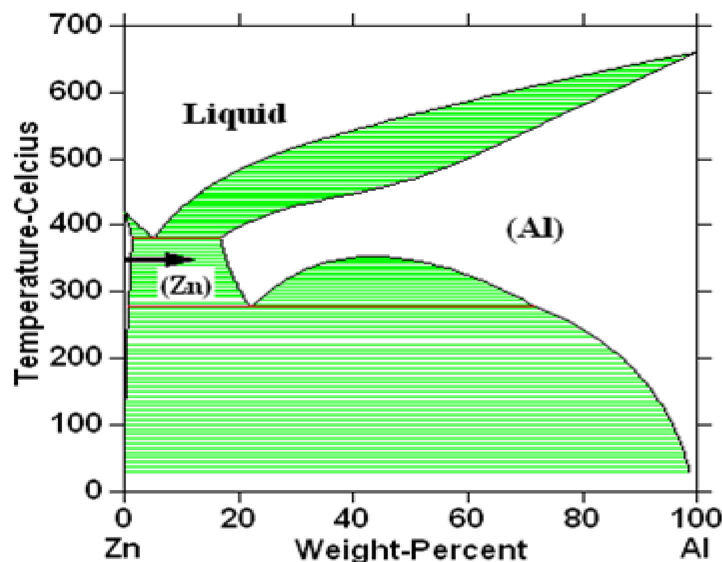

Figure 4.3. Zn-Al phase diagram

Chapter 5

Thermodynamic Predictions Using the CALPHAD Approach

Ternary combinations were extrapolated iteratively from all the well assessed binary systems in the COST 531 and SSOL2 thermodynamic databases involving elements that are popular for solder application using the CALPHAD approach. The ternary combinations which could comply with the required solidification criterion were optimized for a commercially preferred narrow solidification range. These optimized ternary combinations were scrutinized by Scheil solidification simulations, to determine whether they still adhere to the required solidification criterion. The promising candidates were further evaluated by predicting the precipitation of phases in the bulk solder. Focus has also been given to the prediction of IMCs formed between the solder and the commonly used wettable layer of the UBM.

5.1. Introduction to CALPHAD

The history of CALPHAD is a chronology of what can be achieved in the field of phase equilibria by combining basic thermodynamic principles with mathematical formulations to describe the various thermodynamic properties of phases [89]. It started from a vision of combining data from thermodynamics, phase diagrams and atomistic properties such as magnetism into a unified and constant model. Theoretical modelling of the thermodynamic properties of multi-component systems is a modern tool used widely in recent years. It allows the prediction of the thermodynamic behavior of complex systems and reduces the expense of time-consuming experimental studies otherwise necessary for the development of new materials.

CALPHAD methods attempt to provide a true equilibrium calculation by considering the Gibbs energy of all phases and minimizing the total Gibbs free energy of the system (G). One of the most significant advantages of the CALPHAD methodology is that since the total Gibbs energy is calculated, it is possible to derive all of the associated functions and characteristics of phase equilibria, e.g. phase diagrams, chemical potential diagrams etc. The CALPHAD approach is based on the sequential modelling of chemical systems, starting from the simplest being the modelling of the Gibbs energy functions for the pure components followed by modelling of more complex phases such as binary and ternary solutions and intermetallics. The Gibbs energy functions of the phases are stored in the form of polynomial coefficients. It is now a powerful method in a wide field of applications where modelled Gibbs energies and their derivatives are used to calculate properties and simulate transformations of real multi-component materials [90].

The successful use of CALPHAD in these applications relies on the development of multi-component databases which describe many different kinds of thermodynamic functions in a consistent way, all checked to be consistent with experimental data. The construction of these databases is still a demanding task, requiring expertise and experience. There are many subjective factors involved in the decisions to be made when judging and selecting which among redundant experimental data are the most trustworthy. Even more subjective is the assessment of phases of which little or nothing is known, except perhaps in a narrow composition and temperature range. Furthermore, the growing range of applications of these databases increases the feedback and several corrections and modifications are required [91]. The development of new models and the rapid advance of first-principles (ab initio) calculations make the assessment techniques very dynamic and challenging [90].

5.2. Computational Thermodynamics

Thermodynamics describe the equilibrium state of a system. This is necessary for simulations of phase transitions and processes since all systems try to reach this state. In computational thermodynamics (CT), the equilibrium state is described using thermodynamic functions that depend on temperature, pressure and composition. These functions can be extrapolated also outside the equilibrium state and thus, when they are included in a simulation model, provide information.

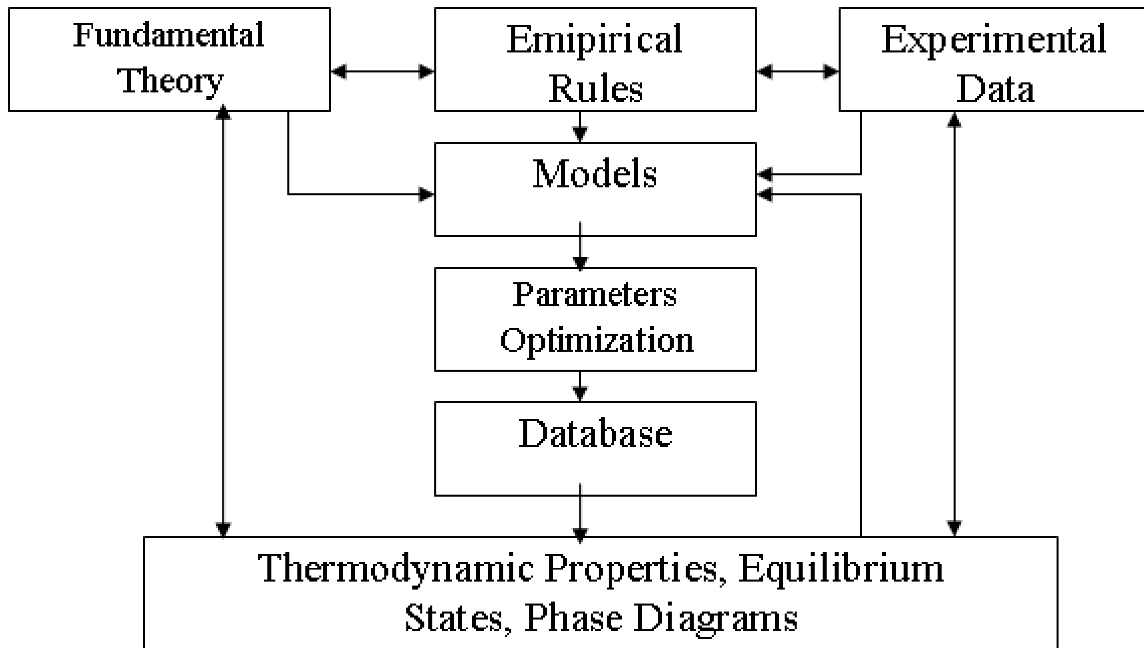

Figure 5.1. A schematic diagram of CALPHAD methodology [89,90].

The thermodynamic models used by CT contain adjustable parameters, which can be optimized in such a way that the models can reproduce many kinds of experimental data as well as theoretical models and first-principle data. Thus, CT is more flexible and has wider possibilities for realistic applications than merely using first-principle data. The

quality of the results of CT is based on the fit to experimental data which is also the criterion for judging the quality of results from the first-principles calculations.

CT can make use of theoretical results as well as traditional experimental data and provides a unique framework of various types of information that can be obtained using rather simple models. Thus, CT is able to provide consistent thermodynamic information with the accuracy required to describe multi-component systems of technological interest. A schematic diagram representing CT using the CALPHAD methodology is illustrated in Figure 5.1.

The primary reason for modelling the Gibbs energy rather than any other thermodynamic function is that most experiments are done at constant temperature and pressure. The other reason for using standardized Gibbs energies rather than lattice stabilities that are frequently used in phase diagram calculations for alloys is that it makes it possible to calculate all other important quantities by using the following relations.

Gibbs energy : $G = (T, p, N_i)$ (5.1)

Entropy : $S = -\left(\frac{\partial G_m}{\partial T}\right)_{p,N_i}$ (5.2)

Enthalpy : $H = G + TS = G - T\left(\frac{\partial G}{\partial T}\right)_{p,N_i}$ (5.3)

Volume : $V = \left(\frac{\partial G}{\partial p}\right)_{T,N_i}$ (5.4)

Chemical Potential : $\mu = \left(\frac{\partial G}{\partial N_i}\right)_{T,N_{j\neq i}}$ (5.5)

Heat Capacity : $C_p = -T\left(\frac{\partial^2 G}{\partial T^2}\right)_{p,N_1}$ (5.6)

Thermal Expansion : $\alpha = \frac{1}{V}\left(\frac{\partial^2 G}{\partial p \partial T}\right)_{N_i}$ (5.7)

Isothermal Compressibility : $k = -\frac{1}{V}\left(\frac{\partial^2 G}{\partial p^2}\right)_{T,N_i}$ (5.8)

Bulk Modulus : $B = 1/k$ (5.9)

The total Gibbs energy of a phase for example θ is generally expressed as

$$G_m^\theta = {}^{srf}G_m^\theta + {}^{Phys}G_m^\theta - T.{}^{cnf}S_m^\theta + {}^{E}G_m^\theta \quad (5.10)$$

in the general form of Gibbs energy model. The pre-superscript “srf” stands for “surface of reference” and represents the Gibbs energy of an unreacted mixture of the constituents of the phase. The pre-superscript “cnf” stands for the configurational entropy of the phase and is based on the number of possible arrangements of the constituents in the particular

phase. The term with pre-superscript "E" stands for the excess Gibbs energy and describes the remaining part of the real Gibbs energy of the phase when the first three terms have been subtracted from the real Gibbs energy, except those included in ${}^{Phys}G_m$. The terms ${}^{srf}G_m$ and ${}^{E}G_m$ will thus include configurational as well as vibrational, electronic and other contributions to the energy.

The selection of the model of the phase must be based on the physical and chemical properties of the phase, for example crystallography, type of bonding, order-disorder transitions and magnetic properties. The models for the phases in the thermodynamic system can be selected independently, except for the case when two phases are members of a structure family. Phases with chemical ordering form structure families and they may be modelled with the same Gibbs energy function. In order to describe the measured phase equilibria and the thermodynamic properties of a system, it is necessary to adjust a number of parameters in the Gibbs-energy model of the phases. The term parameter will be used for a quantity that is part of a model, like excess parameter. Some parameters can be a function of temperature, pressure or even composition and thus, can be split into several other parameters. Each parameter may consist of several coefficients and a coefficient is just like a numerical value.

The integral Gibbs energy for each phase depends on its constitution, temperature and pressure and this is described by a thermodynamic model. The dependence on constitution is usually the most complicated to find a good model for. However, the dependence on temperature and pressure can be very complicated for some phases (such as aqueous solutions). The various thermodynamic models used for describing phases implemented in the GES module (Gibbs Energy System) implanted in ThermoCalc are listed in Table 5.1.

The contributions to the Gibbs energy from other physical phenomena, such as the electronic heat capacity, size mismatch, and short-range order are usually not modelled separately. The reason for this is that, although some of these contributions can be accurately modelled from atomistic theories, the contributions to the Gibbs energy are in most cases much smaller than other contributions that cannot be modelled accurately. In a theoretical approach one can treat some contributions accurately but may ignore others that are equally important. In the CALPHAD technique, the total Gibbs energy is modelled using experimental data on the phase diagram and thermodynamics to fine-tune the models to reality [90,92].

Table 5.1: List of wide spectrum of thermodynamic models implanted in the GES module [93]

Model	Applicable Phases
Ideal Substitutional Model	Ideal gases
Regular Solution Model	Binary alloys
Redlich-Kister Model	Binary alloys
Simple Polynomial Model	Binary phase with no sublattice
Legendre Polynomial Model	Binary phase with no sublattice
Muggianu Extrapolation of R-K Model	Ternary or higher order alloys
Kohler Extrapolation of R-K Model	Ternary or higher order alloys
Toop-Kohler Extrapolation Model	Ternary or higher order alloys
Kohler Extrapolation Model	Ternary or higher order alloys
Muggianu Extrapolation Model	Ternary or higher order alloys
Compound Energy Model (Sub lattice)	Alloys, Liquids, Gases, Oxides
Two-Sublattice Ionic Liquid Model	Liquids
Associate Model	Liquids, Slags
Quasichemical Model of Ionic Liquid	Liquid, Slags
F*A*C*T Quasichemical Model	Liquid, Slags
Isrid Slag Model	Liquid, Slags
Kapoor-Frohberg Cell Model	Liquids
Inden Magnetic Ordering Model	Alloys
Chemical Ordering via CVM Approach	Alloys
Murnaghan Model	High-PT minerals/alloys
Birch-Murnaghan Model	Extra-high PT minerals
Generalized PVT Model	Alloys, Liquids, Minerals, etc.
Super Fluid Model	Real gases & gaseous mixture
Debye-Huckel Model	Dilute aqueous solutions
Specific Ionic Interaction Theory	Dilute aqueous solutions
Generalized Pitzer's Formation	Concentrated aqueous solutions
Revised Helgeson-Kirkham Flowers	Concentrated aqueous solutions
Flory-Huggins Model	Polymers
Generalized Two-State Model	Liquid amorphous phases

5.3. ThermoCalc

Phase-equilibria calculation in this work was carried out using Thermo-Calc (version R) software. ThermoCalc is a general and flexible software system for all kinds of thermodynamic calculations. The primary aim of this software is to make efficient and quick thermodynamic calculations available for applications in science and industry. The ThermoCalc software system is based upon a powerful Gibbs energy minimizer, which has been further enhanced by the so called global minimization technique. The ThermoCalc software is especially designed for complex heterogeneous interaction systems with strongly non-ideal phases and can use many different thermodynamic databases, particularly those developed by SGTE organization (Scientific Group

Thermodata Europe) and CALPHAD community. Furthermore, there are several powerful application programming interfaces of the ThermoCalc software engine, which can be utilized for user-written application programs or within third-party software packages for materials property calculations and materials process simulations. One of the main purposes of the ThermoCalc packages is in its use for planning and reducing the need for several expensive experiments. By thermodynamic calculation it is possible to predict the results of an experiment and this can limit the number of experiments that eventually have to be made. The list of basic modules and its corresponding functions in ThermoCalc is shown in Table 5.2 [93]

Table 5.2: List of basic modules and its function in ThermoCalc [93]

Abbr. Name	Full Name	Primary Functions
SYS	SYSTEM_ UTILITIES	General system utilities for working environmental settings and MACRO creation and opening
TDB	DATABASE_ RETREIVAL	Database selection/combination, system definition, and data retrieval.
GES	GIBBS_ENERGY SYSTEM	Handling of thermodynamic models and thermodynamic quantities.
POLY	POLY	Calculation of complex heterogeneous equilibrium, metastable, local/partial equilibrium
POST	POST_ PROCESSOR	Post processing of all kinds of calculation results and comparison with experimental data.
PARROT	PARROT	Assessment of experimental data and establishment of thermodynamic data.
ED– EXPERIMENTS	EDIT_ EXPERIMENTS	Edit and pre-treatment of experimental data for optimization

5.4. Thermodynamic Databases Used:

The critical assessment of thermodynamic model parameters to describe real systems has already proved to be of industrial interest in understanding material properties, structures and processes. This is because a large effort has been spent on determining the thermodynamic model parameters in all binary and many ternary and some higher order systems with various models [90].

The advantages of critically assessing thermodynamic databases compared to fitting different quantities separately are as follows:

- Unique way to combine and reduce a large amount of experimental data to a few model parameters.
- Consistent assessment of experimental thermo-chemical and phase diagram data.

- Reliable interpolation and extrapolation of thermodynamic data.
- Useful tool for planning new experimental work.
- Basis for modelling and simulation of phase transformations

The following critically assessed thermodynamic databases were used in this work.

SSOL2 [94]:
(Assessed systems interesting for this application)

Ag-Au, Ag-Cu, Ag-Ge, Ag-Si, Ag-Sn, Al-Bi, Al-Ga, Al-Ge, Al-In, Al-Sn, Al-Si, Au-Sn, Au-Bi, Au-Ge, Au-In, Au-Sb, Au-Si, Au-Sn, Bi-Cu, Bi-Ga, Bi-Ge, Bi-In, Bi-Sn, Bi-Zn, Cu-Zn, Ga-Ge, Ga-In, Ga-Sn, Ga-Zn, Ge-In, Ge-Sb, Ge-Sn, Ge-Zn, Sb-Sn, Si-Sn, Si-Zn

COST 531 V. 3.0 [95]:
(Assessed systems interesting for this application)

Ag-Au, Ag-Bi, Ag-Cu, Ag-In, Ag-Sb, Ag-Sn, Ag-Zn, Au-Bi, Au-Cu, Au- In, Au-Sb, Au-Sn, Au-Zn, Bi-Cu, Bi-In, Bi-Sb, Bi-Sn, Bi-Zn, Cu-In, Cu-Sb, Cu-Sn, Cu-Zn, In-Ag, In-Au, In-Bi, In-Cu, In-Sb, In-Sn, In-Zn, Sb-Sn, Sb-Zn.

5.5. Modelling of Solidification

Ternary combinations were extrapolated iteratively from well assessed binary systems involving 10 elements actively being considered for lead-free solders application: Ag, Au, Bi, Cu, In, Ge, Sb, Si, Sn and Zn using the COST 531 v 2.0 [95] and SSOL2 [94] thermodynamic databases. This was done in order to determine the combinations that adhere to the solidification requirement for the first level packaging applications. The ternary combinations which could probably meet the solidification requirement but are not well assessed in the two thermodynamic databases have not been considered. In many cases, the extrapolations have been carried out without taking into account the ternary interaction information since in most cases the excess Gibbs energies of the solution phases in the binary systems relevant to solder alloys are relatively small in magnitude indicating that their ternary interactions are probably less significant [96,97]. The ternary combinations that satisfied the solidification requirement were optimized for a commercially preferred narrow solidification range. The optimized ternary equilibrium combinations were further scrutinized by Scheil solidification simulations to determine whether they still adhere to the solidification criterion.

5.5.1. Equilibrium Solidification

The primary requirement for a solder used in level 1 packaging applications is the solidification requirement i.e. the solidus temperature should be higher than 270°C and the liquidus temperature should be below 350°C. A narrow solidification range is generally preferred for facilitating rapid production, efficient process control, preventing the movement of components during solidification and for minimizing segregation during

solidification. The ternary combinations that satisfied the solidification requirement for first level packaging applications are listed in Table 5.3. The promising replacement solder for first level packaging applications could be either Sn or Au based. Au based systems could be considered for this application since many Au involving binary alloys undergo eutectic reaction very close to the required solidification criterion.

Table 5.3: Ternary combinations optimized for a narrow solidification range based on equilibrium solidification simulations.

S. No.	Ternary Compositions (mole-fraction)	Solidus T (°C)	Liquidus T (°C)	Range (°C)
1.	Au-0.18Ge-0.10In	338.69	339.03	0.34
2.	Au-0.16Sb-0.22In	285.83	287.05	1.22
3.	Au-0.30Sn-0.01Zn	274.96	284.11	9.15
4.	Au-0.31Sn-0.01Cu	279.15	291.44	12.29
5.	Au-0.35Sn-0.21Sb	312.43	329.23	16.80
6.	Au-0.26Sb-0.20Bi	292.44	313.59	21.15
7.	Au-0.13Sn-0.10Si	312.23	333.67	21.44
8.	Au-0.30Sn-0.01In	280.99	302.84	21.85
9.	Au-0.32Sn-0.01Ag	280.86	307.08	26.22
10.	Au-0.15Ge-0.12Sn	285.58	314.16	28.76
11.	Au-0.24Ge-0.05Sb	285.40	347.88	62.48
12.	Bi-0.16Sb-0.04In	269.11	335.84	66.73
13.	Sn-0.25Au-0.20Sb	282.83	305.18	22.35
14.	Sn-0.36Au-0.08Zn	302.95	327.69	24.74
15.	Sn-0.33Au-0.02Ge	314.29	343.43	29.14
16.	Sn-0.30Au-0.08Ag	300.50	334.03	33.53
17.	Sn-0.29Au-0.08Cu	291.75	330.94	39.19

Table 5.4: Minimum and maximum amounts of the alloying elements that can be added to the Au-Sn eutectic based on equilibrium solidification simulations.

S. No.	Minimum (mole-fraction)	Freezing Range (°C)	Maximum (mole-fraction)	Freezing Range (°C)
1.	Au-0.32Sn-0.01Ag	280.84-305.72	Au-0.35Sn-0.03Ag	275.00 -346.81
2.	Au-0.31Sn-0.01Cu	279.51-291.84	Au-0.33Sn-0.04Cu	279.61-347.46
3.	Au-0.30Sn-0.01In	280.99-302.84	Au-0.25Sn-0.07In	303.42-347.06
4.	Au-0.28Sn-0.01Zn	274.96-315.27	Au-0.30Sn-0.09Zn	291.97-347.04

Au-Sn-Ag, Au-Sn-Cu, Au-Sn-In and Au-Sn-Zn ternary systems could be tailored appropriately depending on the microstructure evolution and the type of IMCs developed between the solder and the solder wettable layer of the UBM. They would have very narrow solidification ranges when they are close to the Au-Sn eutectic composition and the content of Ag, Cu, In and Zn could be increased to a maximum of Au-0.35Sn-0.03Ag, Au-0.33Sn-0.04Cu, Au-0.25Sn-0.07In and Au-0.30Sn-0.09Zn respectively and still meet the solidification requirement for this application but with a broader solidification range. The minimum and maximum compositions of Au-Sn based ternary systems are shown in

Table 5.4. The minimum compositions were designed with a view of studying the effect of the addition of the third alloying element to the Au-Sn eutectic composition on the microstructure of the bulk solder. The maximum compositions were designed in order to meet the solidification criterion.

5.5.2. Non-Equilibrium Solidification

Even if the phase diagram shows that a specific alloy has the desired freezing range, it is possible and quite likely for non-eutectic freezing, that a larger freezing range is observed in experiments. This is the case when non-equilibrium solidification occurs. Since the degree to which this non-equilibrium solidification occurs is determined by kinetic factors, it is quite complex to predict unless exact diffusion co-efficients are available. Modelling of solidification very close to reality is currently possible by the CALPHAD approach. Although modelling of real solidification behavior requires the incorporation of kinetic analysis of micro-segregation and back diffusion, the predictions of the Scheil module of Thermo-Calc are close to reality for many alloys for the time scales found in soldering. There are many differences between the traditional Scheil model and the one implemented in the Scheil module of Thermo-Calc i.e. by CALPHAD approach.

The traditional Scheil's equation as shown below is applicable only to dendritic solidification and even not in the case where the solidification is mainly dendritic in nature but contains some final eutectic products. Furthermore, it cannot be used to predict the formation of intermetallic phases during solidification since the partition coefficient is assumed to be constant. However, the partition co-efficient is dependent on both temperature and/or composition and this is not taken into account in the traditional Scheil model.

$$C_s = KC_0(1 - f_s)^{K-1} \quad (5.11)$$

C_s = composition of solid, C_L = composition of liquid K = partition co-efficient and f_s = fraction of solid

Using a CALPHAD approach, all of the above obstacles can be overcome. The process that physically occurs during solidification can be envisaged as follows: A liquid of composition C_0 is cooled to a small amount below its liquidus temperature to T_1. It precipitates out solid with a composition C_1^S and the liquid changes its composition to C_1^L. However, on further cooling to T_2 the initial solid cannot change its composition owing to lack of back-diffusion and it is 'isolated'. A local equilibrium is then set up where the liquid of composition C_1^L transforms to a liquid of composition C_2^L and a solid with a composition C_2^S which is precipitated onto the original solid with composition C_1^S. This process occurs again on cooling to T_3 where the liquid of composition C_2^L transforms to a liquid of composition C_3^L, and a solid with composition C_3^S grows on the existing solid. This process occurs continuously during cooling and when (partition-coefficient) k<1, this leads to the solid phase becoming lean in solute in the centre of the dendrite and the

liquid becoming more and more enriched in solute as the solidification proceeds. Eventually, the composition of the liquid will reach the eutectic composition and the final solidification will occur via this reaction [89].

Table 5.5: Ternary combinations adhering to the solidification criterion by Scheil solidification simulations.

S. No.	Ternary Compositions (mole-fraction)	Solidus T (°C)	Liquidus T (°C)	Range (°C)
1.	Au-0.18Ge-0.10In	338.7	340	1.3
2.	Au-0.16Sb-0.22In	285.7	288	2.3
3.	Au-0.31Sn-0.01Cu	278	292	14
4.	Au-0.30Sn-0.24In	281	303	22
5.	Au-0.32Sn-0.01Ag	278	308	30
6.	Au-0.28Sn-0.01Zn	275	316	41
7.	Au-0.13Sn-0.10Si	271	334	63
8.	Au-0.24Ge-0.05Sb	285	348	63
9.	Sn-0.25Au-0.20Sb	273	290	17
10.	Sn-0.29Au-0.08Cu	305	332	27

Any appearances of secondary phases can be easily taken into account in this approach with the assumption that no back diffusion is involved. Therefore all transformations can be handled including the final eutectic solidification. This approach is based on a series of isothermal steps but as the temperature step size becomes small it provides results which are almost completely equivalent to those which would be obtained from the continuous cooling. The equilibrium thermodynamic calculations were scrutinized using Scheil solidification simulation, to confirm whether the combinations still adhere to the solidification criterion. The ones that satisfied the solidification criterion are listed in Table 5.5.

Table 5.6: Minimum and maximum amounts of the alloying elements that can be added to the Au-Sn eutectic based on equilibrium solidification simulations.

S. No.	Minimum (mole-fraction)	Freezing range (°C)	Maximum (mole-fraction)	Freezing Range (°C)
1	Au-0.32Sn-0.01Ag	281-306	Au-0.35Sn-0.03Ag	278-347
2.	Au-0.31Sn-0.01Cu	279-292	Au-0.33Sn-0.04Cu	278-348
3.	Au-0.30Sn-0.01In	281-303	Au-0.25Sn-0.07In	278-348
4.	Au-0.28Sn-0.01Zn	275-316	Au-0.27Sn-0.015Zn	275-345

Among the elements being actively considered for this application, Sn generally undergoes a peritectic reaction to satisfy the solidification criterion. Equilibrium calculations are less valid for peritectic reactions. Thus, many of the Sn rich candidate alloys did not adhere to the required solidification criterion when subjected to Scheil solidification simulations. Sn-Au-Cu and Sn-Au-Sb ternary combinations still gave positive results. Among the Au-Sn based ternary alloys in the case of Au-Sn-Zn, the composition with which the solidification criterion could be met with the maximum

content of Zn by Scheil solidification simulation is Au-0.27Sn-0.015Zn and is listed in Table 5.6.

5.5.3. Microsegregation

Segregation could be defined as any departure from the uniform distribution of the chemical elements in the alloy. Because of the way in which alloys partition on freezing, alloying elements generally segregate during solidification. It can sometimes be significantly reduced by a homogenizing heat treatment if the distance over which diffusion has to take place to redistribute the alloying elements is sufficiently small [98]. The composition profiles of each phase were studied under both equilibrium and non-equilibrium conditions during solidification. For equilibrium solidification there is no solute segregation and the composition of the solidified material is uniform. The elements were classified as segregated during Scheil solidification simulations if their composition in the solidified material were greater than the one predicted by equilibrium solidification.

The influence of segregation of elements during solidification on the thermo-mechanical properties probably depends on whether the segregated phase appears in the bulk solder as a dispersed phase or as a matrix phase. It could have a small influence on the thermo-mechanical properties if the segregated phase appears as a dispersed phase whereas it could have a high influence on the thermo-mechanical properties if the segregated phase appears as a matrix phase in the bulk solder. The Thermo-Calc software version R is not capable of predicting the resulting microstructure for Scheil solidification simulation.

In many promising Au based ternary systems it was determined that there were no or very little microsegregation during non-equilibrium solidification simulations. The possible explanation for this behavior could be the most of the promising Au based ternary systems were close to the eutectic reactions. As opposed to this, a very high microsegregation was observed in Sn rich candidate alloys. The possible explanation for this behavior could be that Sn generally undergoes a peritectic reaction to satisfy this solidification criterion.

5.6. Selection of Au Rich Candidate Alloys Based on the Prediction of Phases in the Bulk Solder

Au-20Sn (weight-percent), a eutectic composition with a melting point of 280°C adheres to the solidification criterion for the Level 1 packaging applications but this eutectic composition is brittle since it involves ζ' (Au5Sn) hard phase [99]. It has been predicted that the phases in the bulk solder of the eutectic composition in atomic-percent involves around 60% of ζ' (Au5Sn) phase and 40% of δ (AuSn) phase as illustrated in Figure 5.2. The effect of the addition of the third alloying element to the eutectic Au-Sn composition with the objective to suppress the formation of brittle ζ' (Au5Sn) phase and

in turn precipitate relatively ductile phases and still adhere to the solidification criterion was investigated.

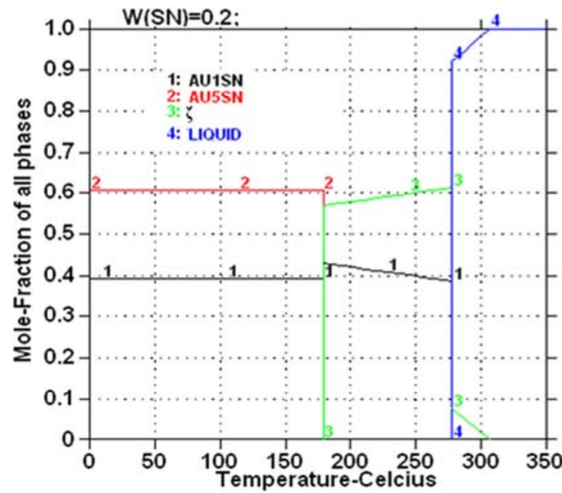

Figure 5.2. Phases predicted in the bulk solder of eutectic Au-Sn eutectic composition.

It was determined that the addition of Ag has a positive effect on the microstructure of the eutectic Au-Sn composition. Phase-equilibria calculations show that the addition of Ag suppresses the precipitation of the brittle ζ’ (Au5Sn) phase and instead proportionally precipitate relatively ductile phases like (Au, Ag) and δ (AuSn) as illustrated in Figure 5.3. Moreover, δ (AuSn) phase is predicted to be the matrix phase. Figure 5.3 demonstrates the fact that the probability of suppression of the hard Au5Sn phase increases proportionally with the content of Ag in the Au-Sn eutectic alloy. However, it has been predicted that the liquidus temperature of this ternary alloy too would increase proportionally with the addition of Ag to the Au-Sn eutectic. Thus, the Au-Sn composition close to eutectic with the maximum content of Ag and still adhering to the solidification criterion is Au-0.35Sn-0.03Ag. It was predicted that the further addition of Ag to the eutectic composition would completely suppress the precipitation of the ζ’ (Au5Sn) phase but with a substantial deviation from the required solidification range. It has been estimated that the liquidus temperature for the composition Au-0.36Sn-0.04Ag is 360.9°C which is much higher than the maximum permissible liquidus temperature.

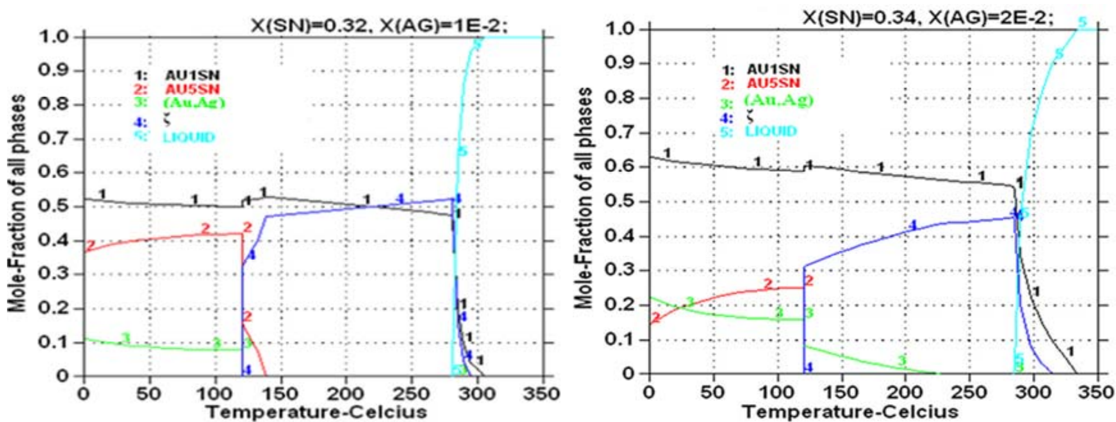

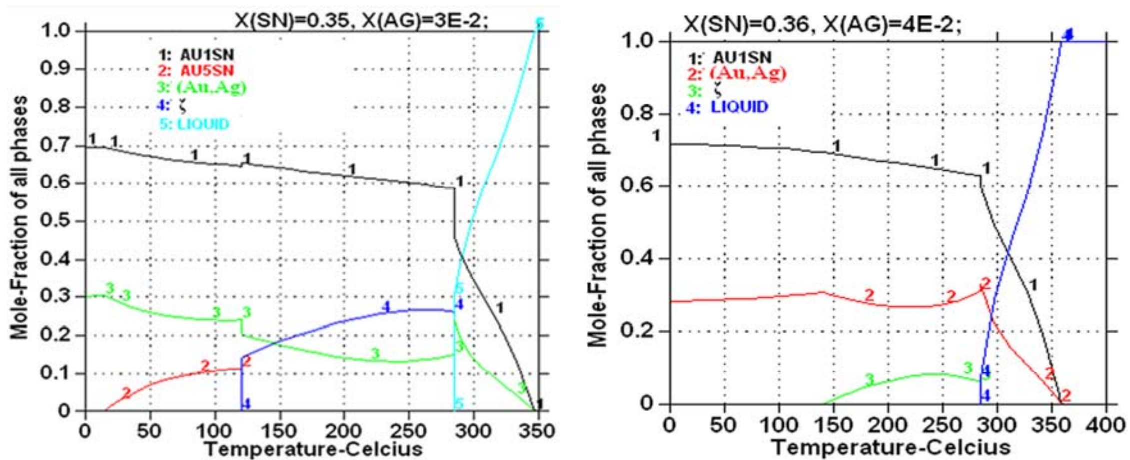

Figure 5.3. Effect of Ag on the precipitation of the brittle Au5Sn phase.

It was determined that the addition of Cu too has a similar effect on the microstructure of the eutectic Au-Sn eutectic. Phase-equilibria calculations show that the addition of Cu suppresses the precipitation of the brittle ζ' (Au5Sn) phase and instead proportionally precipitate relatively ductile phases like (Au, Cu) and δ (AuSn) as illustrated in Figure 5.4. Moreover, δ (AuSn) phase is predicted to be the matrix phase. Figure 5.4 depicts the fact that the probability of suppression of the hard Au5Sn phase increases proportionally with the content of Cu in the Au-Sn eutectic alloy. However, it has been predicted that the liquidus temperature of this ternary alloy too would increase proportionally with the addition of Cu to the Au-Sn eutectic. Thus, the Au-Sn composition close to eutectic with the maximum content of Cu and still adhering to the solidification criterion is Au-0.33Sn-0.04Cu. It was predicted that the further addition of Cu to the eutectic composition would entirely suppress the precipitation of the hard ζ' (Au5Sn) phase (Figure 5.4). Unlike the addition of Ag, in the case of Cu there is only a slight deviation i.e. the liquidus temperature is 351.08°C for the composition Au-0.35Sn-0.05Cu.

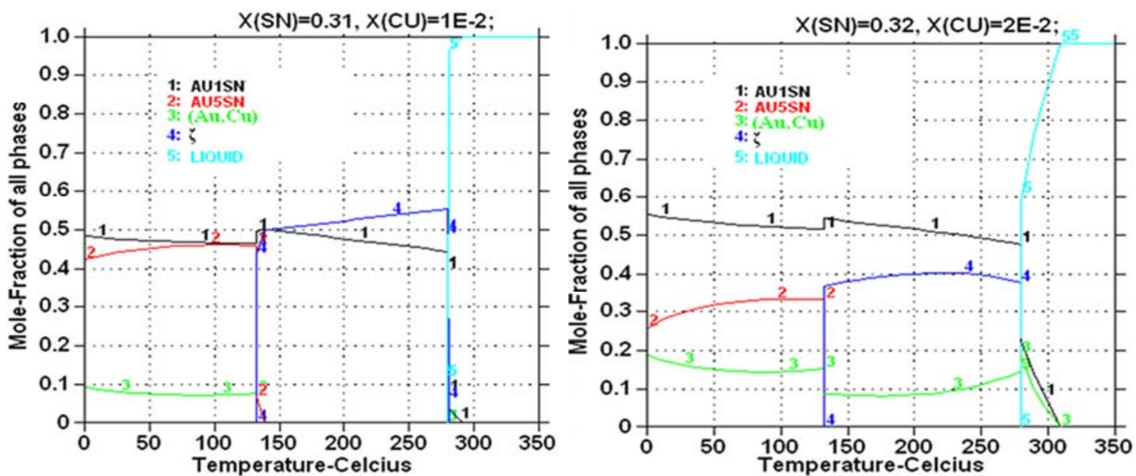

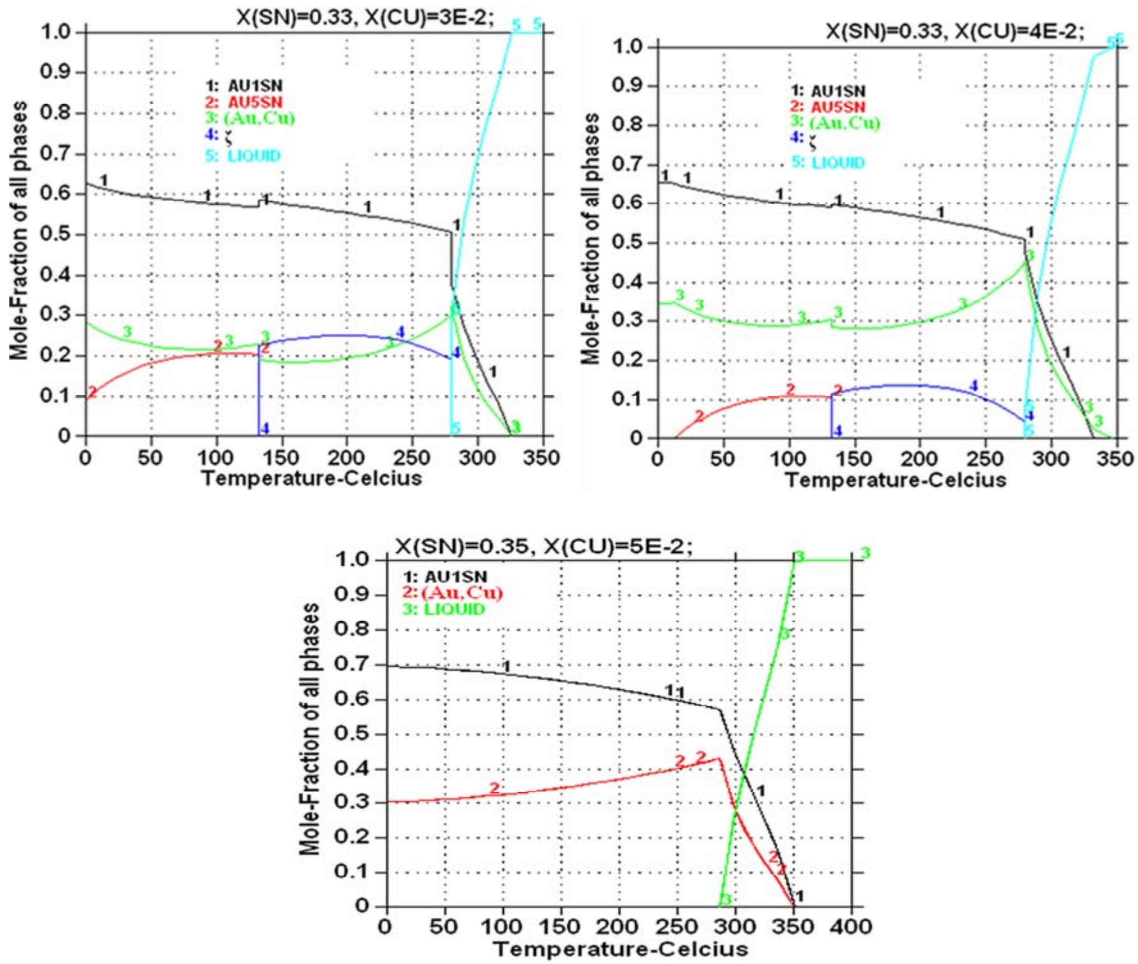

Figure 5.4. Effect of Cu on the precipitation of the brittle Au5Sn phase.

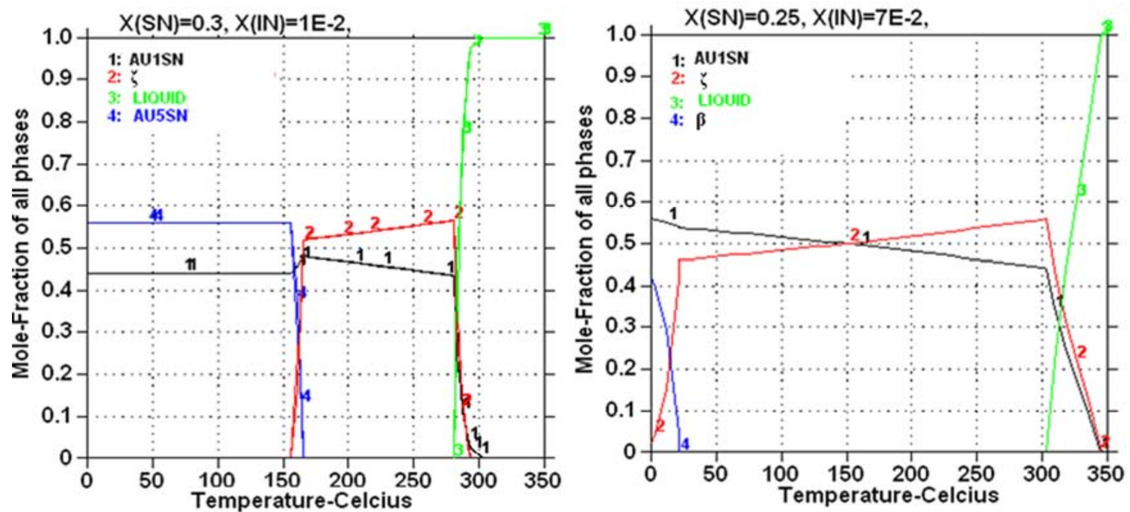

Figure 5.5. Effect of In on the precipitation of the brittle Au5Sn phase.

The effect of indium with the minimum and the maximum additions to the Au-Sn eutectic and still adhering to the solidification criterion are illustrated in Figure 5.5. Indium too like Ag and Cu could suppress the brittle Au5Sn phase but the effect of

indium on Au-Sn eutectic was not considered for further investigation since both indium and tin have a high tendency to form IMCs with the commonly used solder wettable layer of the UBM i.e. Cu/Ni. One of the main advantages of using lead along with tin is that lead does not form IMCs with the commonly used solder wettable layer of the UBM. From the reliability perspective it is not safe to have two elements in the same solder alloy with a high tendency to form IMCs.

Regarding zinc, it was determined that the addition of zinc to the Au-Sn eutectic, would also suppress the ζ' (Au5Sn) phase. The effect of zinc with the minimum and the maximum additions to the Au-Sn eutectic and still adhering to the solidification criterion are illustrated in Figure 5.6. In this figure, it is demonstrated that the effect of suppression of the hard Au5Sn phase is more pronounced with the higher content of Zn in the Au-Sn eutectic alloy. The phases predicted in the bulk solder for the composition Au-0.30Sn-0.09Zn i.e. with the maximum content of zinc in the Au-Sn eutectic alloy while still adhering to the solidification criterion, involves both the matrix and the dispersed phases to be IMCs. Thus, the effect of Zn on the Au-Sn eutectic alloy was not considered for further investigations.

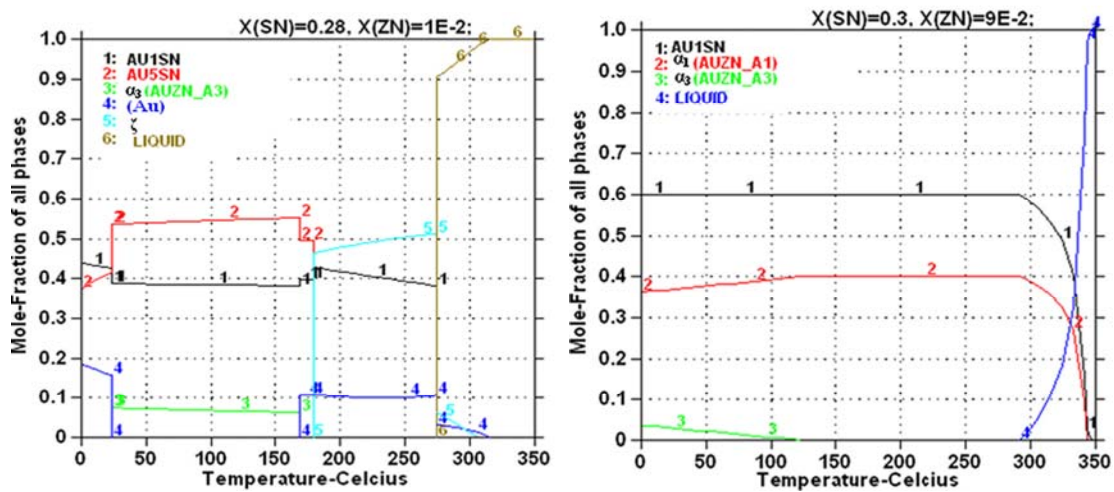

Figure 5.6. Effect of Zn on the precipitation of the brittle Au5Sn phase.

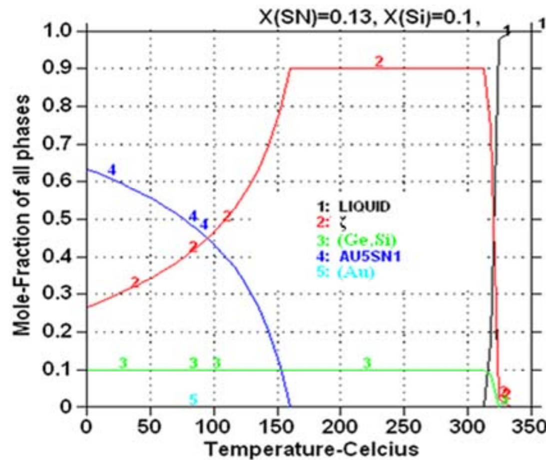

Figure 5.7. Phases predicted in the bulk solder of Au-0.13Sn-0.10Si alloy.

Among the other predicted Au based ternary systems, Au-0.18Sb-0.18In is not interesting as Sb is also in the list of toxic elements. The primary reason behind the drive for the development of alternatives to the high-lead content solders is not due to technical reasons but for environmental concerns only [3]. Thus, developing a solder with high content of Sb is generally not advocated [30,45]. The brittle ζ' (Au5Sn) phase cannot be suppressed for the composition Au-0.13Sn-0.10Si, making this alloy less interesting for this application as shown in Figure 5.7. Furthermore, the presence of Si in the alloy further worsens the wetting properties. Thus, both Au-0.18Sb-0.18In and Au-0.13Sn-0.10Si were not considered for further investigation.

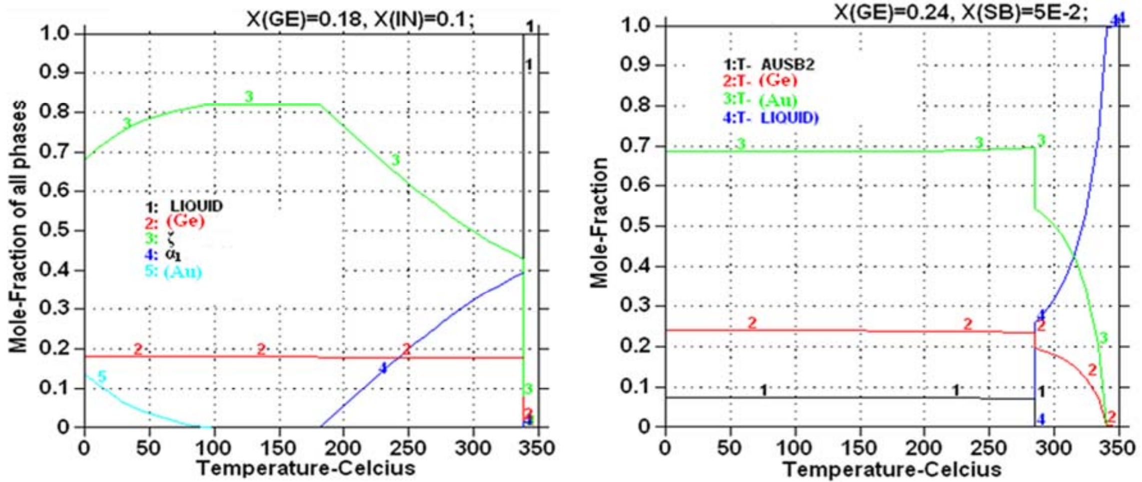

Figure 5.8. Phases predicted in the bulk solder of Au-0.18Ge-0.10In and Au-0.24Ge-0.05Sb candidate alloy respectively.

Among the other promising candidates that adhered to the solidification criterion both by equilibrium calculations and also by the Scheil model; Au-Ge based ternary systems were interesting for this application since the IMC is predicted to exist not as a matrix phase among the following Au-Ge based combinations: Au-0.18Ge-0.10In and Au-0.24Ge-0.05Sb, as depicted in Figure 5.8. No IMC is expected to precipitate in the case of Au-0.18Ge-0.10In alloy while AuSb2 is predicted to exist as a dispersed phase in the case of Au-0.24Ge-0.05Sb alloy.

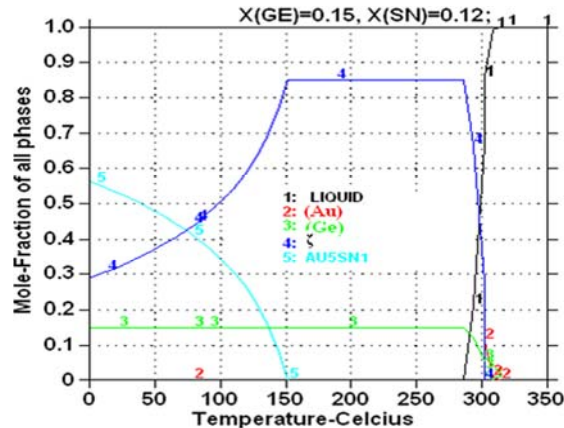

Figure 5.9. Phases predicted in the bulk solder of Au-0.15Ge-0.12Sn candidate alloy.

Despite the presence of the brittle Au5Sn phase as illustrated in Figure 5.9, the Au-0.15Ge-0.12Sn candidate alloy too was considered for further investigation in order to investigate the effect of this low melting point metal i.e. Sn on Au-Ge eutectic along with In and Sb.

Thus, among the predicted Au based compositions that could probably comply with the solidification criterion; Au-0.35Sn-0.03Ag, Au-0.33Sn-0.04Cu, Au-0.18Ge-0.10In, Au-0.24Ge-0.05Sb and Au-0.15Ge-0.12Sn were chosen for further experimental evaluation based on the thermodynamic predictions of their respective solidification profile as well as the phases predicted in the bulk solder.

5.7. Selection of Sn Rich Candidate Alloys

Among the 5 Sn based compositions (Table 5.3) that adhered to the solidification criterion based on equilibrium solidification simulations, only 2 compositions i.e. Sn-029Au-0.08Cu and Sn-0.25Au-0.20Sb complied with the solidification requirement by Scheil solidification simulations. This is because unlike the Au, Sn generally undergoes a peritectic reaction to satisfy this solidification criterion. The phases predicted in the bulk solder of Sn-0.29Au-0.08Cu are illustrated in Figure 5.10. It has been predicted that Cu3Sn and Cu6Sn5 would exist in the bulk solder for this alloy. It has to be mentioned that Cu-Sn IMCs are more brittle than Au5Sn phase itself. Sn-0.25Au-0.20Sb was not considered for further investigation because this composition involves significant amounts of Sb since Sb is also being considered as toxic. Despite not adhering to the solidification criterion by Scheil solidification simulations, the Sn-0.30Au-0.08Ag alloy was also considered for further investigation because the melting temperature measurement using the thermocouple in the hot-plate microscope (comprehensive explanation of the hot-plate microscope has been presented in Chapter 6) shows that even this alloy could probably adhere to the required solidification criterion. Thus, among the Sn rich candidate alloys, Sn-0.29Au-0.08Cu and Sn-0.30Au-0.08Ag were chosen for further investigation.

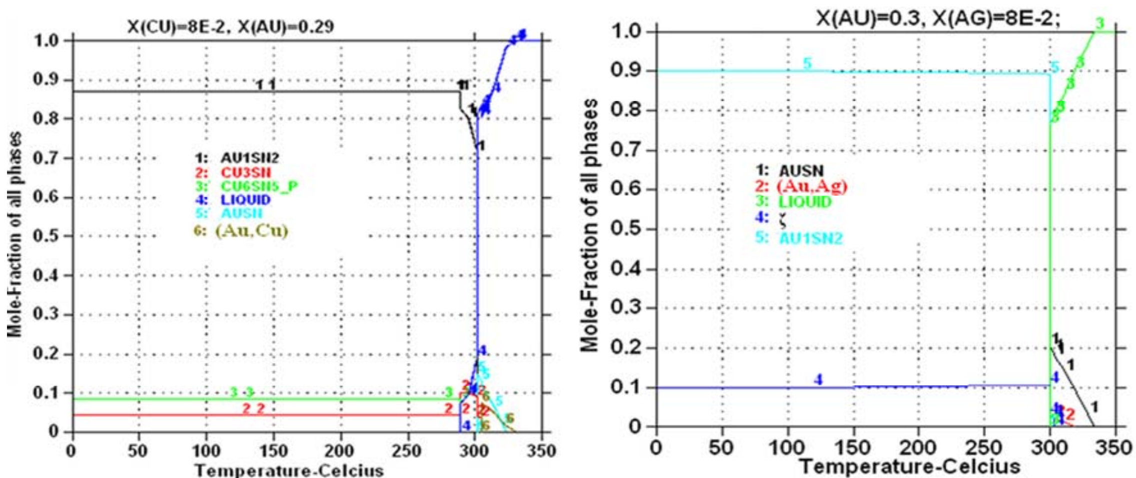

Figure 5.10. Phases predicted in the bulk solder of Sn-0.29Au-0.08Cu and Sn-0.30Au-0.08Ag candidate alloys respectively.

5.8. Prediction of Intermetallic Compounds

The rate of intermetallic compound formation in wetting reactions between the molten solder and the metals (metallization) is faster than those between the solid state solder and the metals. This rate is controlled by the morphology of the IMC formation. In the wetting reaction, the IMC formation has scallop-type morphology, but in solid state aging it has layer type morphology. The stability of scallop-type morphology in wetting reaction and layer type morphology in solid state aging could be attributed to the minimization of surface and interfacial energies. The unusually high rate of scallop-type intermetallic compound formation could be attributed to the gain of rate of free energy change rather than free energy change [51,100]. Thus, from the reliability perspective it would be advantageous that the IMC formation between the proposed promising solder candidates and the metallization is reduced during the wetting reaction [49].

Au-Ge based promising candidate alloys have not been considered for this investigation on IMC formation with the commonly used metallization, as these systems were not critically assessed in the thermodynamic databases used for this work. The focus has been given here only on the IMCs formation of other promising candidates i.e. Au-0.35Sn-0.03Ag, Au-0.33Sn–0.04Cu and Sn-0.29Au-0.08Cu with the commonly used metallization i.e. Au, Cu, Ni, and Pd.

Among the commonly used metallizations, it was predicted that only with Cu these promising solder candidates other than the Sn-0.29Au-0.08Cu alloy i.e. Au-0.35Sn-0.03Ag and Au-0.33Sn-0.04Cu, have a low tendency of forming IMCs during the wetting reaction. The calculated isothermal section during the wetting reaction at 300°C is illustrated in Figure 5.11. This was calculated without taking into account the probability of forming any ternary intermetallic phases.

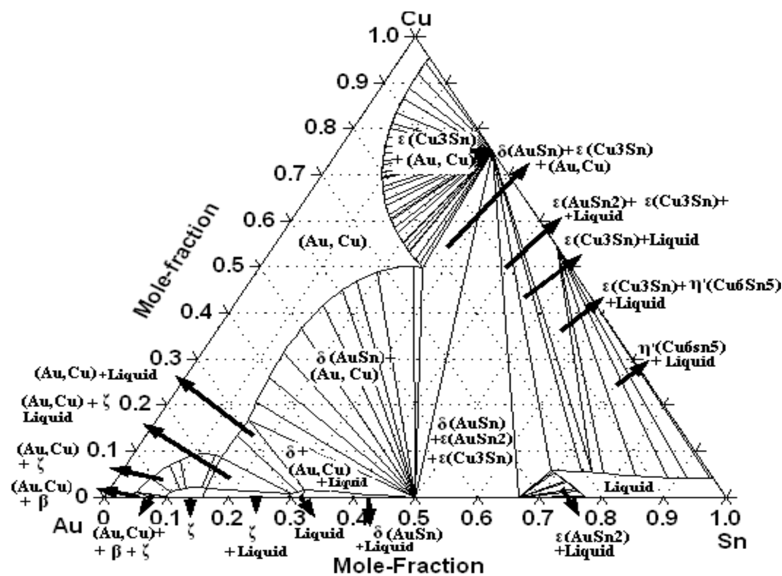

Figure 5.11. Isothermal section of Au-Sn-Cu system at 300°C.

The equilibrium calculations predict that the kinetic path of IMC formation between the Sn containing solder alloy and the Cu metallization has been affected by the high content of gold in the solder alloy. It was found that this effect is highly pronounced when the content of gold (mole-fraction) is more than 0.5 in the proposed solder alloys. IMCs formation have been predicted for the composition close to Au-Sn eutectic with the maximum content of Ag and Cu and still adhering to the required solidification criterion. Figure 5.12 depicts the isopleth, predicting the binary IMCs that could form between the Au-0.33Sn-0.04Cu alloy and the Cu metallization respectively. The isopleth was constructed by allowing the Sn in the Au-0.33Sn-0.04Cu alloy to react and form IMCs with the Cu metallization, i.e. the wettable layer of the UBM. It was constructed without taking into account the formation of any ternary intermetallic phases. However, Chang et. al. [101] have determined $(Cu_{1-x}Au_x)_6Sn_5$ ternary intermetallic phase experimentally but this phase has not been taken into account due to the lack of thermodynamic information.

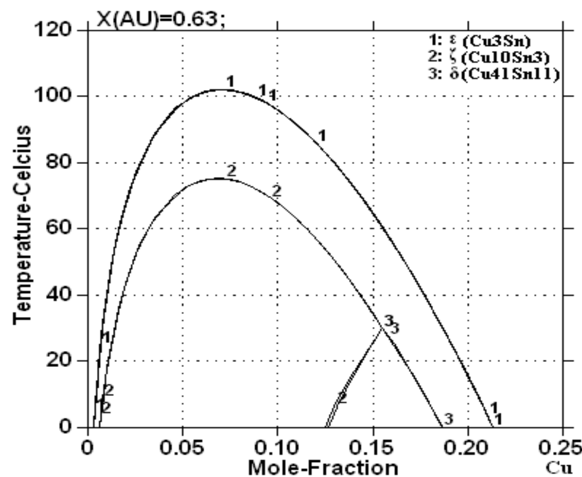

Figure 5.12. Isopleth predicting binary Cu-Sn IMCs that could form between Au-0.33Sn-0.04Cu candidate alloy and the Cu metallization.

Figure 5.12 shows that only one stable binary IMC, i.e. ε (Cu3Sn) phase would form between the promising solder candidate Au-0.33Sn-0.04Cu and Cu, i.e. the wettable layer of the UBM and the prominent η (Cu6Sn5) phase would not form at all. Thus, the high content of gold in the solder alloy greatly influences the precipitation of well known IMCs between the Sn containing solder alloy and the Cu metallization i.e. η (Cu6Sn5) and ε (Cu3Sn). The ε (Cu3Sn) phase too has been predicted to form only at low temperatures and hence, its growth should be slow since the kinetics is likely to be controlled by solid state diffusion. The equilibrium calculation for this proposed solder alloy i.e., Au-033Sn-0.04Cu, shows that the tendency to form IMCs with the Cu metallization decreases proportionally with the increase in the gold content in the solder alloy. Thus, the high content of gold in the solder alloy has a substantial effect on the formation of IMCs between Sn and Cu. The stable ε (Cu3Sn) phase was suspended from the calculation and the isopleth was recalculated and the predicted metastable phases have also been included in Figure 5.12. Thus, there is also a high probability of forming ζ (Cu10Sn3) and δ (Cu41Sn11), meta-stable phases in addition to the ε (Cu3Sn) stable phase. A similar behavior on IMCs formation was predicted between the Au-0.35Sn-

0.03Ag candidate alloy and the Cu metallization too, with little variations in the temperature range.

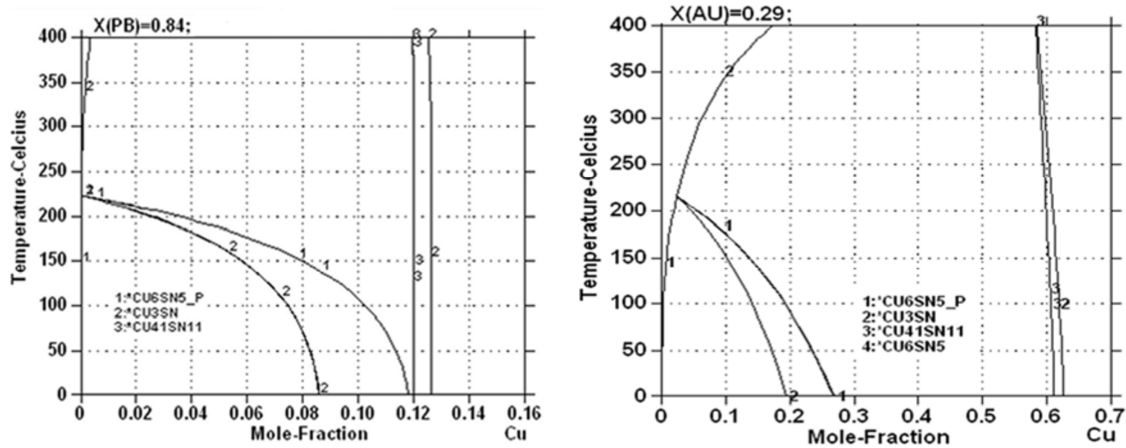

Figure 5.13. Isopleth predicting binary Cu-Sn IMCs that could form between high-lead content solders and Sn-0.29Au-0.08Cu alloy with the Cu metallization respectively

Similar to the Au-0.33Sn-0.04Cu candidate alloy, the isopleths predicting binary Cu-Sn IMCs that could form between high-lead content solder & Sn-0.29Au-0.08Cu with the Cu metallization are illustrated in Figure 5.13 respectively. Unlike the Au rich alloys, the kinetic path of IMC formation between these Sn containing solder alloys and the Cu metallization has not been affected. Thus, the high-content of gold has altered the kinetic path of IMC formation between Sn and Cu and has reduced the probability of IMC formation between the Sn in the solder alloy and the Cu in the solder wettable layer during the wetting reaction. However, this hypothesis is purely based on thermodynamic predictions and it has not been experimentally verified.

5.9. Candidate Alloys Chosen for Experimental Investigation

Thus, among the candidate alloys that could adhere to the required solidification criterion based on the thermodynamic predictions, the following candidate alloys as listed in Table 5.7 were chosen for further experimental investigation for the mentioned reasons.

Table 5.7: Candidate alloys in mole-fraction that were chosen for experimental investigation.

Candidate alloys
Au-0.35Sn-0.03Ag
Au-0.33Sn-0.04Cu
Sn-0.30Au-0.08Ag
Sn-0.29Au-0.08Cu
Au-0.18Ge-0.10In
Au-0.24Ge-0.05Sb
Au-0.15Ge-0.12Sn

Chapter 6

Experimental Approaches, Setups and Equipments

The promising candidate alloys that were determined based on the solidification criterion and the nature of the phases predicted in the bulk solder by the CALPHAD approach were precisely produced using a hot-plate microscope. These candidate alloys were then heat-treated to test their microstructural stability and also corrosion tested in order to evaluate their resistance to corrosive atmospheres.

6.1. Hot-Plate Microscope

The high-lead content solders, Au-Sn eutectic, Au-Ge eutectic and the prospective candidate alloys with a diameter between 3mm to 4mm were precisely produced using the hot-plate microscope. The primary reason for choosing this method for sample preparation was to reduce the consumption of gold for experimental investigation.

6.1.1. Experimental Setup

As schematically shown in Figure 6.1, the hot-plate microscope equipment, consists of three main parts:

1. Vacuum System
2. Specimen chamber with heating system
3. Microscope and imaging system

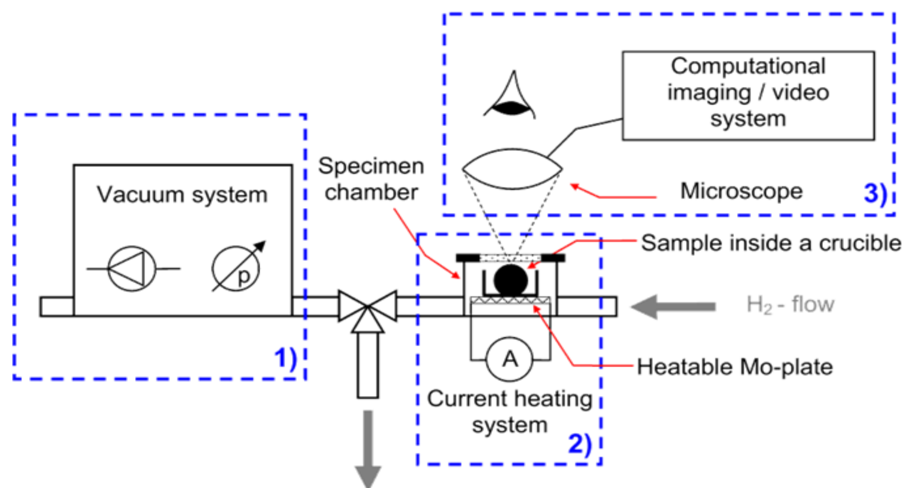

Figure 6.1. Schematic diagram showing the main parts of the hot-plate microscope [102].

The essential part of the equipment is the specimen chamber in which the preparation and investigation of the solder alloy is performed. Therefore, a molybdenum plate (6x8 mm) is mounted between two electrical contacts of a current heating system inside this chamber. During the experimental procedure, as described in the following section, a crucible, up to 6 mm in height can be placed on this Mo plate. Below the Mo-plate, a thermocouple is situated to measure the temperature inside the chamber. The calibration of the thermocouple is done by relating the produced voltage (measured with a digital voltmeter) of the thermocouple to known melting temperatures of pure metal samples out of Sn, Pb, Al, Ag and Au. This results in a linear relation between the measured voltage and the temperature inside the chamber.

The heating system can reach a temperature up to approximately 1400°C and is equipped with water cooling. To prevent oxidation of the hot metal "parts" (Mo plate and contacts) during heating a high-vacuum ($p < 1.\ 10^{-3}$ mbar) as well as an optional flow of reducing hydrogen gas can be applied within the chamber and is controlled by pressure measurement. Moreover, the reducing effect of the hydrogen is used to clean the samples from oxides or at least to prevent the samples from further oxidation during heating. The chamber is sealed by a removable glass lid for optical in-situ observations [102].

Using an Olympus SZ61 stereo-microscope, a digital camera and analysis start imaging software, it is possible to photograph and film the specimen in-situ. Figure 6.2. depicts the described parts of the hot-plate micro1scope as well as a closer view inside the opened specimen chamber.

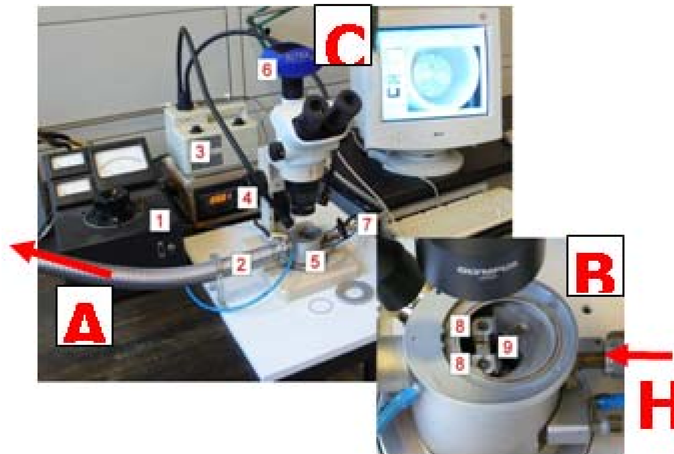

Figure 6.2. Specimen chamber, heating and imaging system of the hot-plate microscope (HPM). (1: current control, 2: tube to vacuum, 3: light source, 4: temperature measurement, 5: specimen chamber, 6: digital camera, 7: hydrogen supply, 8: electrical contacts, 9: molybdenum plate) [103].

6.1.2. Experimental Procedure for Solder Alloy Spheres

Using the HPM, solder alloy samples characterized by a typical spherical shape with a diameter between 3mm to 4mm and a weight of 100-200 mg depending on size and composition, can be prepared.

The experimental procedure to prepare the solder alloy sample spheres is divided into three steps:

1. Weighing and pressing
2. Sphere Forming
3. Heating and Conditioning

As schematically shown in Figure 6.3. the production process of a sample starts with carefully weighing out (accuracy 0.1mg) of high purity metal powders (depending on the composition) followed by slightly mixing and pressing these inside a special pressing tool into a small tablet. Thereto the respective amount of each metal (A, B & C) intend to be comprised in the sample was calculated to form a 3mm diameter sphere in sum.

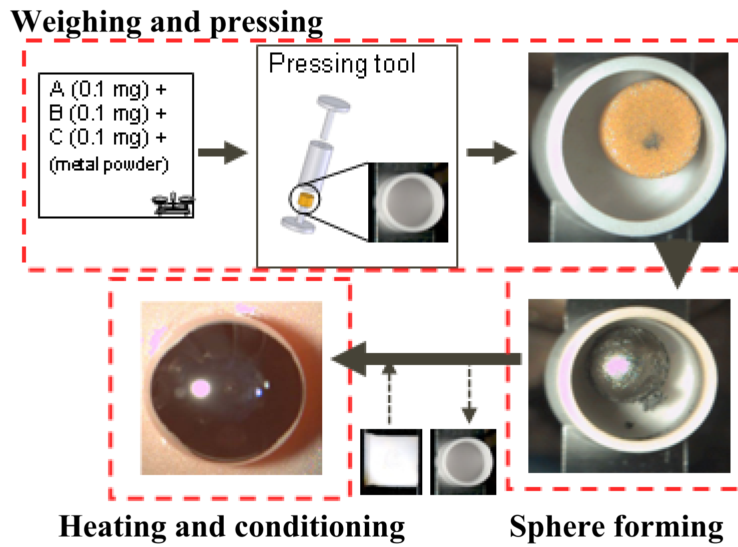

Figure 6.3. Schematic diagram showing the solder alloy sample preparation sequence [103].

According to Equations 6.1, 6.2 and 6.3, the planned compositions of the samples given in at. % has been converted to wt. % for the mass calculation. Thereby is $w_{A,B,C}$ the percentage of weight of the respective element (A,B,C), $a_{A,B,C}$ the atomic mass to be found in periodic tables and $x_{A,B,C}$ the atomic percentage.

$$w_A = \frac{a_A.x_A}{a_A.x_A + a_B.x_B + a_C.x_C} \tag{6.1}$$

$$w_B = \frac{a_B.x_B}{a_A.x_A + a_B.x_B + a_C.x_C} \tag{6.2}$$

$$w_C = \frac{a_C.x_C}{a_A.x_A + a_B.x_B + a_C.x_C} \tag{6.3}$$

The pressing tool was designed in order to reduce the loss of material during the weighing and pressing step and is fitted to the used cylindrical aluminium oxide crucibles (Al_2O_3, V=70µl, d=6mm, h=4mm) to ensure a good transfer of the tablet inside the crucible.

After the weighing and pressing step, the prepared tablet, sitting inside the crucible placed on the Mo-plate of the HPM, is melted to form the solder alloy sphere. It is necessary to use the cylindrical crucible because of the movement of the metal tablet during the forming process from tablet to sphere. It is obvious that the tablet would not stay on the Mo-plate and of course be soldered to this if no non-metal crucible is used.

This forming process is performed under a hydrogen flow to prevent further oxidation of the material and to start the reduction of the oxides on the surface of the developing sphere. Usually, some non-metal impurities pop up during the sphere forming process which makes it necessary to take out the metal sphere of the chamber and clean it carefully.

After washing in ethanol and drying, the solder alloy sphere is placed into the chamber again in order to perform the heating and conditioning step. This means that the sphere is remelted and held at a high temperature (about 1000-1300°C) depending on the composition, to ensure a good homogeneity.

In contrast to the forming, an aluminium oxide plate (6x6mm) is used to carry the specimen instead of a crucible to prevent the sphere from soldering to the Mo-plate. Further the experiments have shown that a flat plate is much better in order to ensure a good flow of hydrogen around the sphere. Doing so, it is possible to in-situ investigate and record the melting and solidification process of a solder sphere using the microscope and the computational imaging and video system.

During heating, some oxides that remained on the surface despite the cleaning usually merge on the liquid surface and form a small area. By further heating and holding on high-temperature it is possible to reduce all oxides and a shiny liquid solder sphere is created which can be cooled down. The melting and solidification can be conducted slowly or fast, depending on the experimental needs of further investigations. Due to the small size of the sphere and the heating on high-temperatures, it is possible to ensure a good homogeneity in the solder sphere [103].

6.1.3. Deviation from the Planned Selected Alloy Composition

Despite performing the sample preparation carefully, a little loss of material occurred during the procedure. Therefore, the previously described general method for sample preparation was slightly modified. The weighing out of the different metal powders was stared and usually ended with the most ductile metal in the alloy so that the pressed tablet showed the most ductile metal at the top and the bottom. Therefore, it is assumed that during transfer of the tablet out of the pressing tool into the crucible, primarily this ductile metal at the top and bottom crumble away. Further, it is assumed that during the

heating and conditioning steps mostly the metals with the low vapor pressure have been removed. Hence an empirical found amount of the ductile metal stacked at the top and the bottom and the metals with the low vapor pressure was added extra (positive tolerance) during every weighing.

6.2. Corrosion Testing

Corrosion testing is essential in order to ensure the reliability of the solder alloy. In engineering materials, corrosion is closely related to materials microstructure. The various microstructural features of the candidate solder alloys possess different electrochemical properties; therefore all of them behave differently to the service environment. In such cases, overall corrosion behavior of the material is determined by the local/electrochemical characteristics and interaction between them.

One major difficulty for corrosion investigation of solder alloys by the electrochemical method is that the measurement needs to be carried out at tiny areas with sizes ranging from few mm to µm. Therefore, a micro-electrochemical technique was employed. A popular idea involves the use of a pipette connected to a system to control the solution flow at the tip. Through addition of reference and counter electrodes, the pipette system becomes a microscopic electrochemical cell which can then be used with high precision to determine the electrochemical characteristics of a small region of interest [104].

6.2.1. Micro-Electrochemical Investigation

The micro-electrochemical set up consists of an electrochemical head containing the 250 ppm NaCl solution, and a counter and reference electrode, which are attached to the carousel of an optical microscope as illustrated in Figure 6.4. A 250ppm NaCl solution was chosen since it is a standard for corrosion testing for electronic products. The cell is connected to a pipette which makes contact with a local region of the working electrode (in this case, the solder alloy). The lateral resolution of the technique is determined by the dimensions of the pipette tip. Potentiodynamic polarization curves were measured to an Ag/AgCl reference electrode starting from an open circuit potential at a scan rate of 1.5 mV/s [105]. The anodic and the cathodic potentiodynamic polarization curves of the commonly used wetting layers of the under-bump metallization (UBM) i.e. Cu and Ni were also measured.

Figure 6.4. Micro-electrochemical set up.

All the candidate alloys and the wetting layers of the UBM were ground on a 4000 SiC paper prior to the experiment. All the surfaces were cleaned with alcohol followed by distilled water and then air dried. All measurements were carried out in naturally aerated 250 ppm NaCl. Separate experiments were used to measure the anodic and the cathodic reactivity. The results were affirmed after measuring the anodic and the cathodic reactivity in several duplicates. The corrosion morphology of the candidate alloys after polarization tests were analyzed using SEM (JEOL 5900).

6.3. Thermal Aging

The aging experiments were conducted at two different temperatures i.e. at 150°C and 200°C in order to investigate the stability of the respective microstructures both at the lower and the upper end of the operating temperature range for high-temperature solders. The samples were carefully placed on an individual alumina crucible and then loaded into an ambient atmosphere resistant furnace and were then heated to these respective temperatures and annealed at the same temperatures for 1 day and 1 week respectively. The candidate alloys were aged up to 3 weeks at these respective operating temperatures in the case of Au-Ge based candidate alloys taking into account the slow reactivity of the system.

6.4. Cross Sectioning

The as-produced and the thermally aged samples were embedded in an epoxy resin, ground for cross sectioning. They were ground with 500, 1000 and 4000 grade abrasive sand papers and then polished with 3 μm and 1 μm diamond suspensions. In the case of high-lead content solders, 0.04 μm alumina and 0.025 μm colloidal silica suspensions were used for final polishing since it is an extremely soft alloy. Appropriate chemical etching was also used to distinguish different phases of the possible candidate alloys. These embedded samples subjected to metallographic preparation methods were used for observations of microstructure and also for the testing of hardness.

6.5. Microscopy

Different types of microscopy techniques have been developed to enable detailed study of the microstructure of materials. Each microscopy technique gives different information about the microstructure. Therefore, in order to obtain the required information about the microstructure, the suitable microscopy technique has to be chosen. Either light or electrons are usually used for microscopy imaging.

In order to investigate the bulk solder material both light optical microscopy (LOM) and scanning electron microscopy (SEM) were used. In the case of LOM, both Leica and Neophot equipped with imaging software and calibrated to a standard for dimension measurement were used. The metallographic microstructure of the various as-produced and aged candidate alloys were also examined using JEOL 5900 SEM. In order to obtain an image in SEM, it is necessary to have a conductive sample. A problem with charging may occur if the sample is not conductive (plastic, ceramic etc.). In the case of metallic

materials which are conductive, the problem with charging can occur when a LOM sample is used, i.e. plastic is used as a mounting. Therefore, it is recommended to use conductive mounting or coating which prevents charging under electron bombardment. To ensure good conductivity of the sample for SEM investigation, carbon film was evaporated on the surface of the specimen. Furthermore, adhesive carbon discs were also applied.

6.5.1. Chemical Composition Analysis

Compositional analysis of the microstructure was carried out using Energy Dispersive X-ray Spectroscopy (Oxford, Link ISIS). It utilizes the fact that the interaction between the accelerated electrons and the specimen excites the involved atoms which then generates X-ray photons. The energy of these X-rays is dependent on the atomic number Z of the atoms they originated from. By measuring the characteristic energy of the emitted X-rays, the composition of the investigated volume can be quantified. Each element has at least one characteristic peak, while higher Z elements have several [106]. Thus, EDX is a fairly good method for chemical composition analysis for solder alloys since all the popular candidates for solder alloys have a reasonable Z.

Backscattered mode of the SEM was used in most cases. Both backscattered as well as secondary electron imaging was used for determining the corrosion products. Elemental mapping was used for Au-Ge based candidate alloys to illustrate the fact that the Ge does not have affinity towards any of the low melting point metals (In, Sb &Sn). It was also carried out on Sn-0.29Au-0.08Cu candidate alloy to show that all the Cu existed in this alloy only in the Sn rich ternary phase and none of the brittle Cu-Sn IMCs precipitated.

6.6. Microhardness Measurement

Vickers hardness measurements were performed using FM-7000 Future Tech, to clarify the relationship of microstructure and microhardness. The microhardness measurement technique is a very sensitive technique to detect structural changes of various candidate alloys at different temperatures. Microhardness testing is one of the easiest ways to determine the mechanical properties of the different phases of the structure [107,108]. The rule of thumb is the higher the hardness, the higher the mechanical strength but with a compromise on ductility [109].

An indentation load of 5g and 100g and a dwell time of 5s were used to measure the hardness of the high-lead content solders and also the possible candidate alloys. The 5g load was used to determine the hardness of individual phases i.e. on the crystal in order to interpret the macro/overall hardness of the alloy. However, in certain cases it was not possible to measure the hardness of individual phases without hitting other phases. The 100g load was also used so that the width of the indentation was large enough to span multiple phases and many eutectic domains. Hence, the test values reflect the overall microhardness of the candidate alloys. The average of the individual measurements was evaluated as the results due to the slight variance of the 10 or more measurements which was especially the case of the 100g load.

Chapter 7

Gold Based Candidate Alloys for High-Temperature Applications

There are several binary eutectic compositions involving gold that could either adhere or be very close to the required solidification criterion for high-temperature solders. Gold also possesses some unique properties required for high-temperature solders like: good corrosion and oxidation resistance, excellent bio-compatibility and workability, good thermal and electrical conductivity, low natural radius of curvature and the tendency of not spontaneously forming intermetallics with the commonly used solder wettable barrier layer. Furthermore, Gold has been ranked as one of the least toxic elements by both EPA-US and OSHA. Thus, this chapter explores the possibility of replacing the high-lead content solders with promising gold based ternary alloys.

7.1. Gold Based Binary Alloys

The microelectronics industry is extremely cost conscious. The history of the industry has been to continuously produce higher performance at lower costs. Cost competitiveness in the electronics industry is maintained by reducing the cost of individual components to a minimum, in order to maximize the overall cost reduction [3]. Considering gold, as a potential substitute for lead would substantially increase the cost of high melting point solders. Though the initial costs would be higher there would potentially be a value to the recycled product and no disposal costs associated with the solders, resulting in lower life time costs for the product [46,110]. In addition, refining costs becomes important when considering initial material selection. The refining of gold recovered from electronic waste scrap is easier and cheaper than refining of other noble elements [47]. It has been reported that 47% of the total consumption of gold was recovered and successfully recycled in 2007 [48].

Au-Ge eutectic as well as Au-Sn eutectic are existing hard solders currently being used for fluxless applications like opto-electronic packaging [2]. However, it cannot be used as a soft solder for high-temperature applications without inducing some softness in it by micro-alloying. Both Au-Ge (k=44 W/mK) and Au-Sn (k=57 W/mK) eutectic alloys possess better thermal conductivities than the existing high-lead content solders like Pb5Sn (k=35 W/mK) [24]. Although Au-0.20Si (mole-fraction) and Au-0.35Sb (mole-fraction) eutectic compositions with a melting point of 363°C and 357°C too, are close to the requirement they are still not prospective candidate alloys [2]. The former is not an appropriate candidate alloy due to the wetting constraints and the latter is not promising

due to the high amounts of Sb involved in it since Sb is also in the list of toxic elements [30,45]. Thus, this chapter focuses only on Au-Ge and Au-Sn based candidate alloys.

7.2. Au-Ge Based Candidate Alloys

Au-Ge is an interesting system for this application since it does not have any intermetallic phases as illustrated in Figure 7.1. Moreover, the tendency of Ge towards forming IMCs with the commonly used wetting layers of the UBM is also very low. Toxicological studies have documented germanium as a therapeutic element [111]. The melting point of the Au-Ge (28 at. % Ge) eutectic composition is 360°C. It slightly deviates from the permissible liquidus temperature. Phase-equilibria calculations show that the addition of a low melting point metal such as In or Sb or Sn decreases the melting point of this alloy below 350°C. The changes in microstructure and microhardness associated with the addition of low melting point metals namely In, Sb and Sn to the Au-Ge eutectic were investigated in this work. Furthermore, the effects of thermal aging on the microstructure and its corresponding microhardness of these promising candidate alloys have been extensively reported.

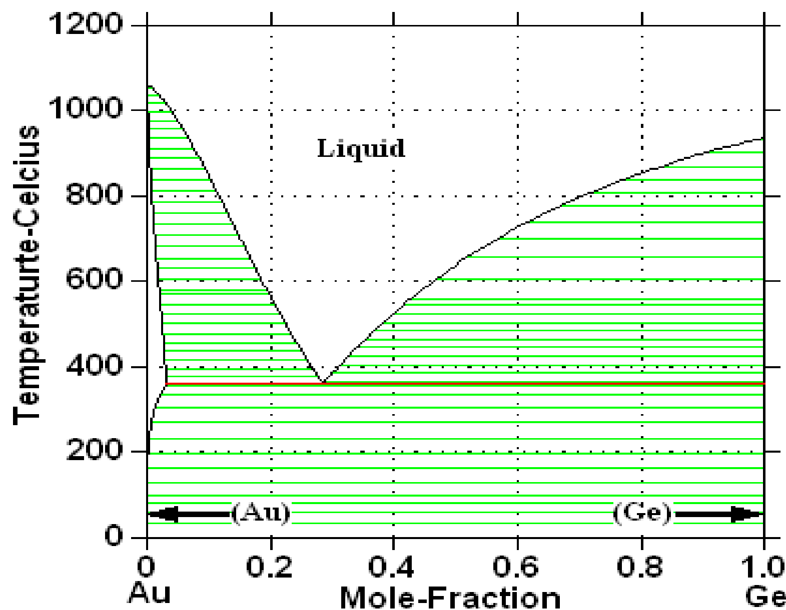

Figure 7.1. Au-Ge phase diagram generated using SSOL2 thermodynamic database.

The other advantage of germanium is that it does not have any affinity towards any of these low melting point metals and also even gold. Elemental mapping as illustrated in Figures 7.2 to 7.4 shows that In and Sb are absolutely insoluble in the (Ge) phase while small amounts of Sn can dissolve in the (Ge) phase. Therefore, Ge does not form any IMC with any of these low melting point metals. Despite these advantages, the major drawback for developing Au-Ge based candidate alloys as an alternative to high-lead content solders is the fact that Ge cannot be easily electrodeposited which is important since electro-deposition is one of the common ways of depositing solder alloys in a commercial scale.

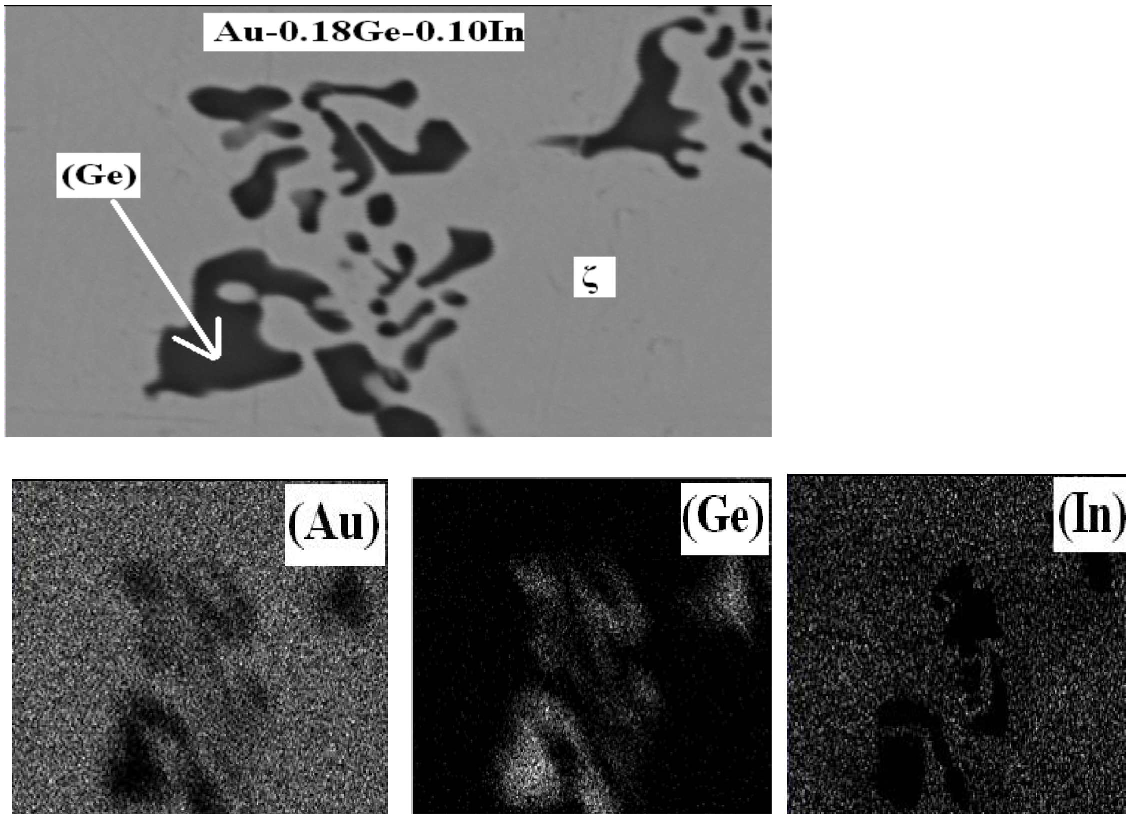

Figure 7.2. Elemental mapping of the as-produced Au-0.18Ge-0.10In candidate alloy.

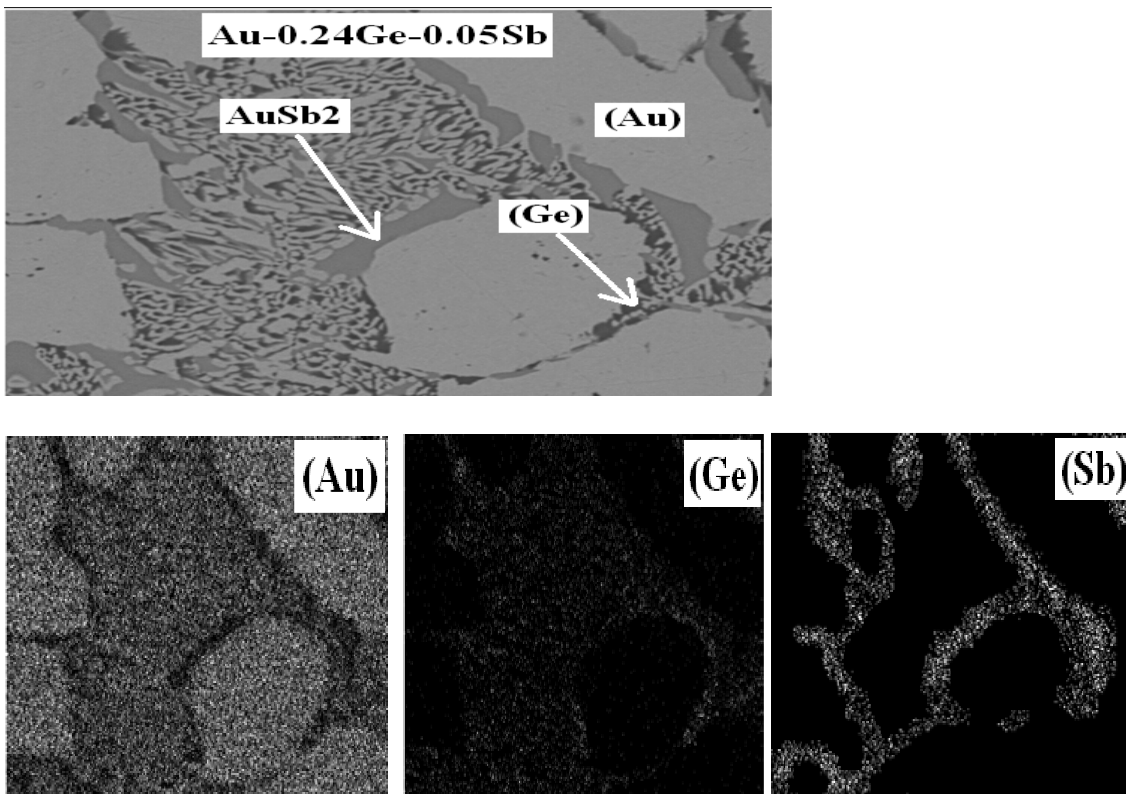

Figure 7.3. Elemental mapping of the as-produced Au-0.24Ge-0.05Sb candidate alloy.

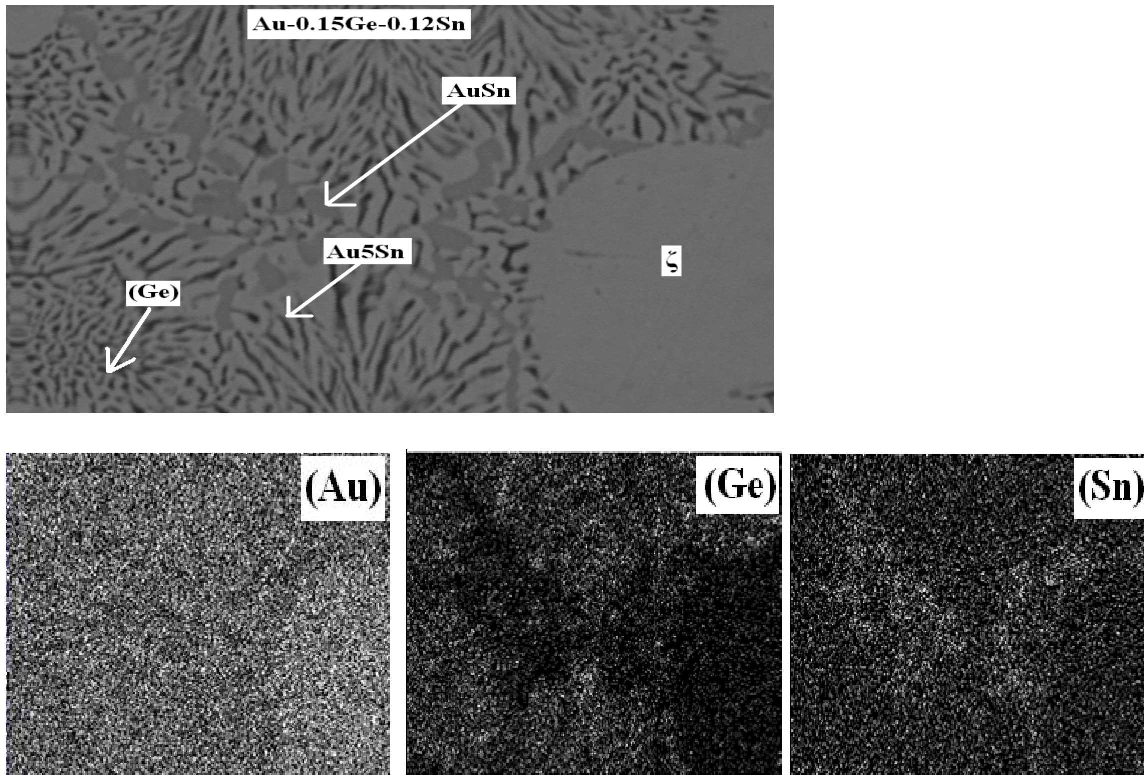

Figure 7.4. Elemental mapping of the as-produced Au-0.15Ge-0.12Sn candidate alloy.

7.2.1. Au-Ge Eutectic Alloy

The microstructure of the Au-Ge eutectic was comprised of the dark (Ge) phase dispersed on the bright (Au) phase. Before being subjected to thermal aging, the as-produced Au-Ge eutectic samples comprised of coarse (Ge) lamellae uniformly distributed on the white (Au) phase. After being subjected to aging at 200°C, instead of coarsening these lamellae were observed to be relatively fine i.e. refined as illustrated in Figure 7.5. This change in morphology was more pronounced with the increase in the thermal aging duration. However, no progressive change in morphology was observed after aging for 1 week at 200°C. No significant variations in the morphology of (Ge) lamellae were observed in the samples aged at 150°C for different durations when compared to the samples aged at 200°C.

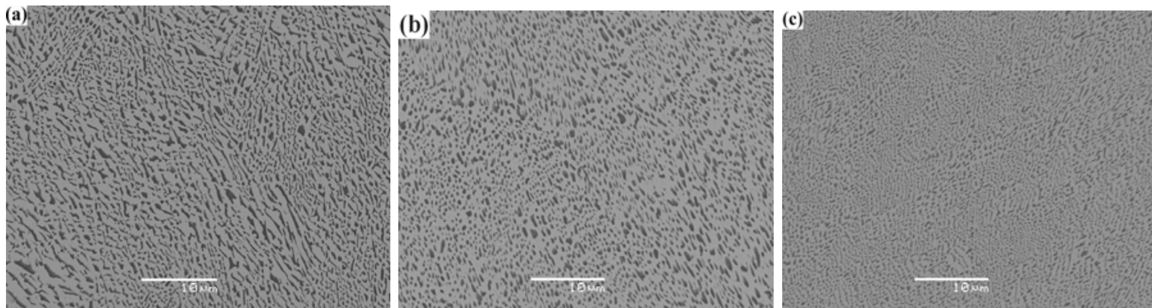

Figure 7.5. SEM-BSE micrographs of the Au-0.28Ge eutectic alloy before and after thermal aging at 200°C, (a) as-produced (b) 1 day and (c) 1 week.

It was not possible to measure the hardness of individual phases without hitting other phases in the case of Au-Ge eutectic even with the 5g load. A eutectic microstructure has a very high surface area per unit volume and it is therefore vey hard for a dislocation line to move within the eutectic structure which causes the structure to be hard. However, Au-0.28Ge eutectic subjected to thermal aging became softer than the as-produced sample as illustrated in Figure 7.6. This age softening effect was more pronounced with the increase in the aging temperature i.e. the samples that were aged at 200°C were found to be much softer than the ones aged at 150°C. This age-softening effect could be attributed to the change in morphology of (Ge) lamellae and its respective distribution on the much softer (Au) phase. Thus, the variation in the morphology and the change in the distribution pattern of (Ge) lamellae during thermal aging have induced some softness to the otherwise hard Au-Ge eutectic.

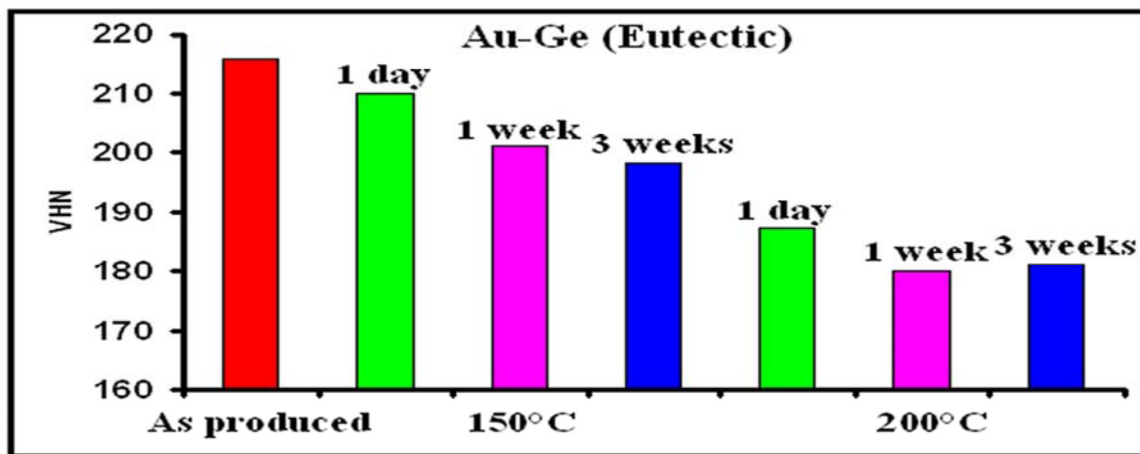

Figure 7.6. Microhardness values of the Au-Ge eutectic alloy using 100g load before and after aging.

7.2.2. Au-0.18Ge-0.10In Candidate Alloy

The microstructure of the as-produced Au-0.18Ge-0.10In candidate alloy was comprised of the (Ge) lamellae that were homogenously distributed over the matrix ζ phase. The microstructure remained relatively stable even after being subjected to aging both at 150°C and 200°C as depicted in Figure 7.7 and Figure 7.8. α_1 phase did not exist in the as-produced samples and also in the samples that were aged at 150°C for different durations. α_1 phase was observed only in the samples that were aged at 200°C for 3 weeks and not even in the samples that were aged at 200°C for 1 day or 1 week. This effect could be attributed to the fast cooling rate employed during the production of these alloys in the hot-plate microscope. Thus, it could be concluded that the microstructure gradually transformed into that of the Au-0.18Ge-0.10In candidate alloy in an equilibrium state at 200°C (as predicted by phase-equilibria calculation) during long-term thermal aging.

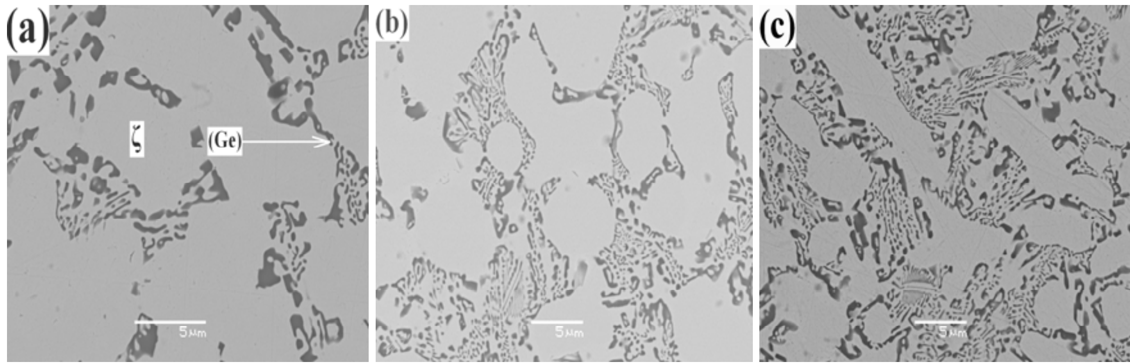

Figure 7.7. SEM-BSE micrographs of the Au-0.18Ge-0.10In candidate alloy before and after thermal aging at 150°C (a) as-produced (b) 1 day (c) 3 weeks.

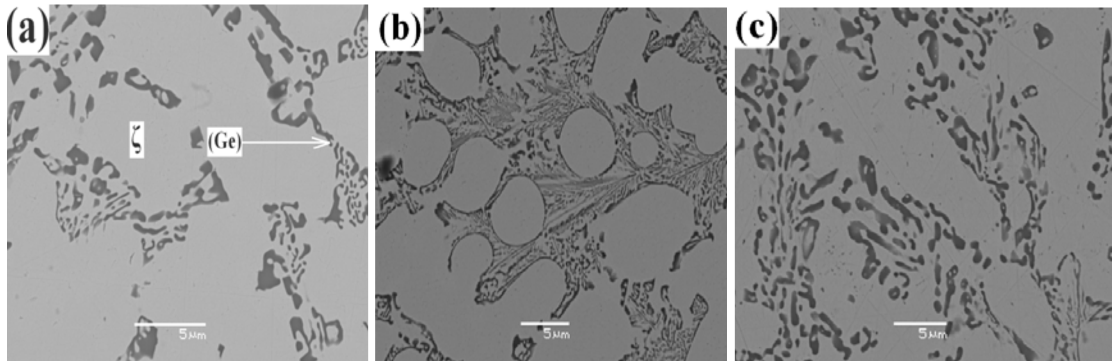

Figure 7.8. SEM-BSE micrographs of the Au-0.18Ge-0.10In candidate alloy before and after thermal aging at 200°C (a) as-produced (b) 1 day (c) 3 weeks.

It was also observed that the volume-fraction of Au rich phases in the matrix was relatively higher in the samples that were aged at 200°C for different durations when compared to those aged at 150°C for similar respective aging durations. Figure 7.9. illustrates the influence of aging temperature on the volume-fraction of Au rich phases in the matrix. The volume-fraction of Au rich phases in the matrix increased proportionally with the aging durations irrespective of the aging temperature. However, this effect was relatively more pronounced at 200°C.

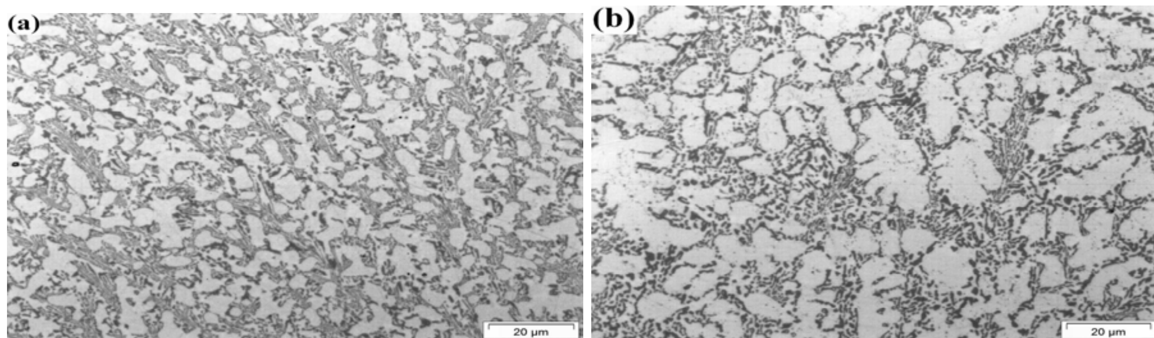

Figure 7.9. Optical microstructures of Au-0.18Ge-0.10In candidate alloy after thermal aging for 3 weeks, (a) 150°C (b) 200°C.

The overall microhardness of the aged Au-0.18Ge-0.10In candidate alloy was higher than the as-produced samples as illustrated in Figure 7.10. This effect could be attributed to the classic solid solution strengthening of the ζ phase (Table 7.1) due to the high solubility limit of In in ζ phase (Figure 7.2). The content of In soluble in the ζ phase calculated thermodynamically at 150°C and 200°C in mole-fraction are 0.122 and 0.124 respectively. The high solubility of In in ζ phase was also confirmed by the SEM/EDX elemental mapping analysis. However, the Au-0.18Ge-0.10In candidate alloy became relatively softer when aged at 200°C for 3 weeks despite the solid solution strengthening of the ζ phase. This effect could be attributed to the precipitation of the softer α_1 phase (Table 7.1). Thus, it could be concluded that the precipitation of α_1 phase during long-term thermal aging at 200°C has induced softness to the Au-0.18Ge-0.10In candidate alloy.

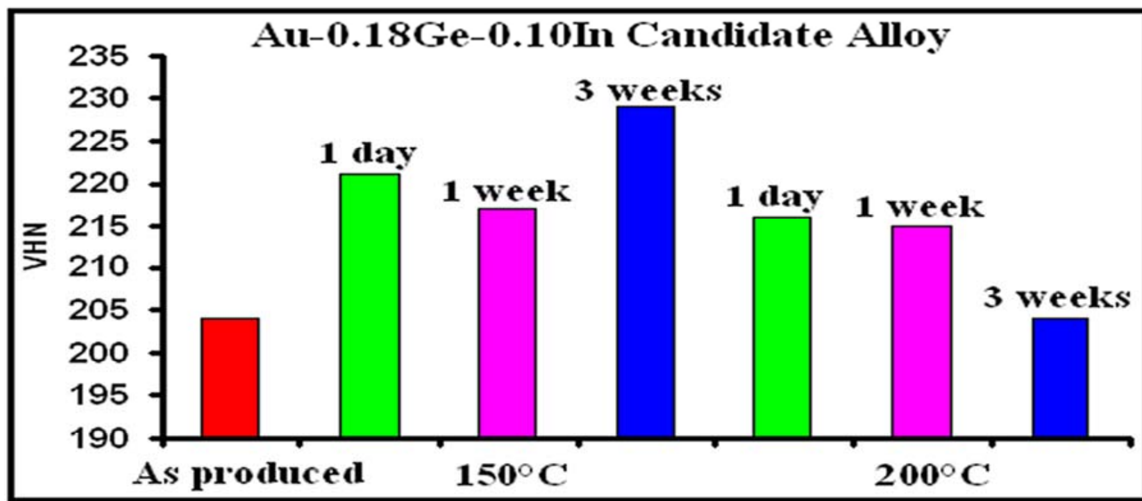

Figure 7.10. Microhardness values of the Au-0.18Ge-0.10In candidate alloy using 100g load before and after aging.

Table 7.1: Vickers hardness measurement of individual phases using 5g load.

Candidate alloy	Phases	Aging time	Hardness (HV)	
			150°C	200°C
Au-0.18Ge-0.10In	ζ	As-produced	183*	183*
		1 day	199	197
		1 week	201	199
		3 weeks	204	202
	(Ge) phase distributed on Au rich phases	As-produced	230*	230*
		1 day	254	241
		1 week	249	240
		3 weeks	247	232
	α_1	3 weeks	—	162

*without heat treatment — unstable

The overall microhardness of the Au-0.18Ge-0.10In candidate alloy aged at 150°C was relatively higher than the ones aged at 200°C. This effect could be attributed to the

presence of low volume-fraction of the softer Au rich phases in the matrix. The initial decrease in microhardness during aging at 150°C could be attributed to the increase in volume-fraction of Au rich phases in the matrix. The microhardness of the samples aged at 150°C was much higher than the ones aged at 200°C. This effect could be attributed to the significant solid solution strengthening of the ζ phase and partly due the presence of low-volume fraction of Au rich phases in the matrix when compared to the ones aged 200°C (Table 7.1). Thus, the microhardness measurement using the 100g load, to a certain extent correlated well with the volume-fraction of Au rich phases in the matrix.

7.2.3. Au-0.24Ge-0.05Sb Candidate Alloy

In the Au-0.24Ge-0.05Sb candidate alloy, the three distinct phases i.e. the white, dark and gray areas were identified as (Au), (Ge) and $AuSb_2$ phases respectively Mixed granules of (Au) and (Ge) phases too existed in the microstructure of as-produced Au-0.24Ge-0.05Sb candidate alloy. Large (Au) phases emerged in the solder matrix instead of many small (Au) phases (as-produced) and few small (Au) phases still existed in the solder matrix when the samples were subjected to aging both at 150°C and 200°C as depicted in Figure 7.11 and Figure 7.12. Thus, during aging irrespective of the aging temperatures, the growth of the (Au) phase was observed in order to reduce the interfacial energy. The growth of the (Au) phase was more pronounced with the aging duration. However, the growth of the (Au) phase at 200°C was relatively higher when compared to the growth of the (Au) phase at 150°C as illustrated in Figure 7.12 and Figure 7.13. Thus, it could be concluded that the growth of the (Au) phase in the Au-0.24Ge-0.05Sb candidate alloy increased proportionally with the aging temperature. Slight dissolution of the bulk (Ge) phase into relatively finer ones during the course of aging at both the aging temperatures was observed. Slight coarsening of the AuSb2 IMC was observed only in the samples that were thermally aged at 200°C for 3 weeks. Mixed granules of (Au) and (Ge) phases still existed in the microstructure of all the thermally aged samples irrespective of the aging durations and aging temperatures.

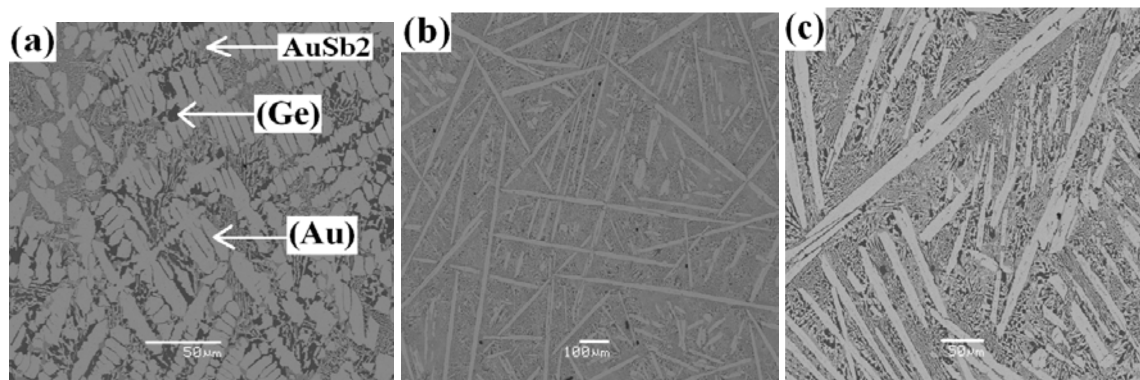

Figure 7.11. SEM-BSE micrographs of the Au-0.24Ge-0.05Sb candidate alloy before and after thermal aging at 150°C (a) as-produced (b) 1 week (c) 3 weeks.

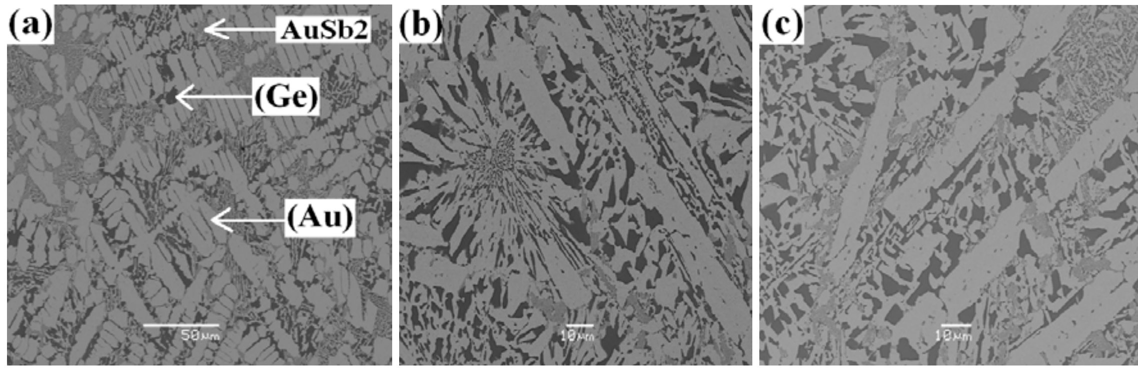

Figure 7.12. SEM-BSE micrographs of the Au-0.24Ge-0.05Sb candidate alloy before and after thermal aging at 200°C (a) as-produced (b) 1 week (c) 3 weeks.

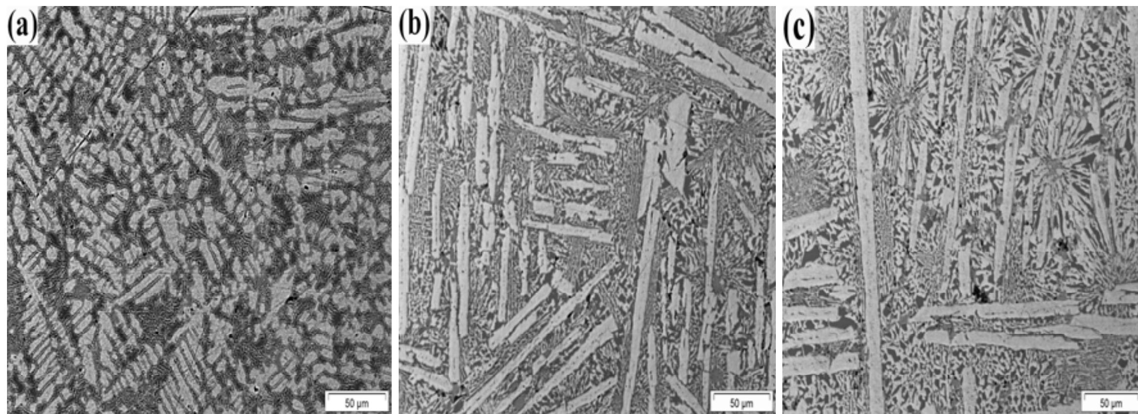

Figure 7.13. Optical microstructures of Au-0.24Ge-0.05Sb candidate alloy before and after thermal aging for 3 weeks (a) as-produced (b) 150°C (c) 200°C.

The overall microhardness of the aged Au-0.24Ge-0.05Sb candidate alloy was higher than the as-produced samples despite the softening induced by the growth of the (Au) phase as illustrated in Figure 7.14. Though the growth of the (Au) phase has induced some softness in the alloy as shown in Table 7.2, the increase in the microhardness (Figure 7.14) can be attributed to the refinement of the (Ge) phase. Because of the relatively large size of the (Ge) phase, composite strengthening (i.e. load transfer from the weaker matrix to the stronger dispersed phase) is more likely than a direct obstruction of dislocation motion such as with solid solution strengthened alloys [112]. Phase-equilibria calculations confirmed by elemental mapping show that Sb does not dissolve in the (Au) phase and all the Sb exists in the microstructure only as AuSb2 IMC. Thus, the refined (Ge) phase can serve as a better reinforcing phase in the Au-0.24Ge-0.05Sb candidate alloy. However, the microhardness fell substantially during long-term thermal aging (3 weeks) at 200°C. This effect could be attributed to the significant growth of the (Au) phase and also due to the slight coarsening of the AuSb2 IMC. The overall microhardness of the Au-0.24Ge-0.05Sb candidate alloy aged at 150°C was relatively higher than the ones aged at 200°C. This is because the softening induced by the growth of the (Au) phase for the samples aged at 150°C was relatively lower than the ones aged at 200°C (Table 7.2).

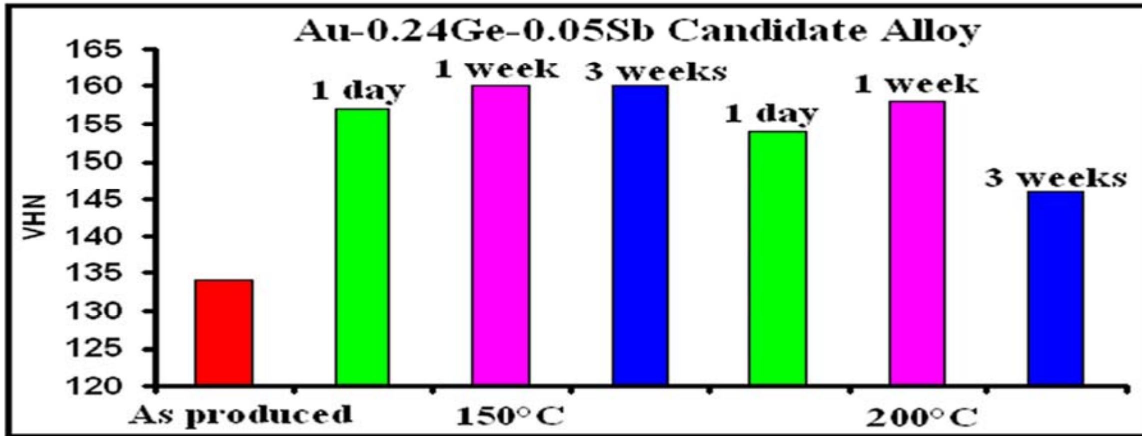

Figure 7.14. Microhardness values of the Au-0.24Ge-0.05Sb candidate alloy using 100g load before and after aging.

Table 7.2: Vickers hardness measurement of individual phases using 5g load.

Candidate alloy	Phases	Aging time	Hardness (HV)	
			150°C	200°C
Au-0.24Ge-0.05Sb	(Au)	As-produced	103*	103*
		1 day	97	94
		1 week	96	95
		3 weeks	96	86
	AuSb2	As-produced	620*	620*
		1 day	619	623
		1 week	628	619
		3 weeks	625	567
	(Ge)	As-produced	320*	320*
		1 day	324	323
		1 week	325	321
		3 weeks	323	325

* without heat treatment

7.2.4. Au-0.15Ge-0.12Sn Candidate Alloy

The matrix of the as-produced Au-0.15Ge-0.12Sn candidate alloy was composed of mixed lamellae [(Ge) & AuSn] phases that were homogenously distributed over ζ and Au5Sn phases. These lamellae were predominantly composed of (Ge) phase [dark] and also a few AuSn phase [gray] were observed. Coarse ζ dendrites and also few Au5Sn granules were found to be dispersed in the matrix. This could be attributed to the fast cooling rate employed during the preparation of solder spheres using the hot-plate microscope. The fast cooling rate to a certain extent has suppressed the precipitation of Au5Sn phase. The presence of AuSn phase in the as-produced samples can be attributed to non-equilibrium solidification since AuSn phase is not expected to precipitate for this specific composition and temperature range, as per phase-equilibria calculation. The microstructure of the Au-0.15Ge-0.12Sn candidate alloy was relatively refined after

thermal aging i.e. the dissolution of bulk ζ dendrites into finer ones was observed during aging both at 150°C and 200°C as illustrated in Figure 7.15 and Figure 7.16 respectively.

Both Au5Sn and AuSn phases did not exist in the microstructure of the Au-0.15Ge-0.12Sn candidate alloy subjected to aging at 200°C for 3 weeks. Thus, both the Au5Sn and AuSn phases that existed in the microstructure of the as-produced Au-0.15Ge-0.12Sn candidate alloy gradually disappeared during thermal aging. Therefore, it could be concluded that the microstructure gradually transformed into that of the Au-0.15Ge-0.12Sn in an equilibrium state during long-term thermal aging at 200°C as depicted in Figure 7.16. However, SEM analysis showed that the volume-fraction of Au5Sn phase increased proportionally with the aging duration in the samples that were aged at 150°C. Similar to the ones aged at 200°C, the AuSn phase gradually disappeared during the course of aging at 150°C and eventually did not exist in the microstructure of the samples that were aged at 150°C. Thus, at both these aging temperatures, the microstructure gradually transformed into that of the Au-0.15Ge-012Sn in an equilibrium state.

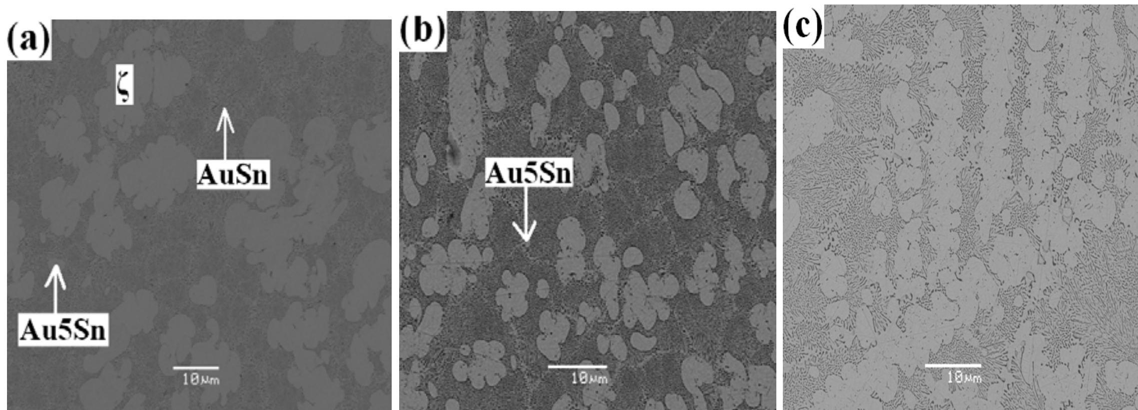

Figure 7.15. SEM-BSE micrographs of the Au-0.15Ge-0.12Sn candidate alloy before and after thermal aging at 150°C (a) as-produced (b) 1 week (c) 3 weeks.

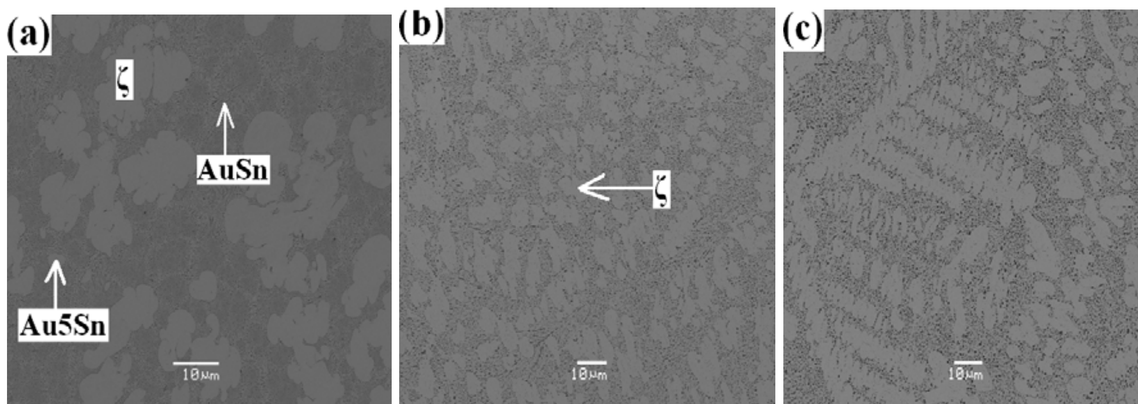

Figure 7.16. SEM-BSE micrographs of the Au-0.15Ge-0.12Sn candidate alloy before and after thermal aging at 200°C (a) as-produced (b) 1 week (c) 3 weeks.

It was observed that the volume-fraction of Au rich phases in the matrix was relatively higher in the samples that were aged at 200°C for different durations when compared to those aged at 150°C for similar aging durations. Figure 7.17 illustrates the influence of

aging temperature on the volume-fraction of Au rich phases in the matrix. The volume-fraction of Au rich phases in the matrix increased proportionally with the aging durations irrespective of the aging temperature. However, this effect was relatively more pronounced at 200°C.

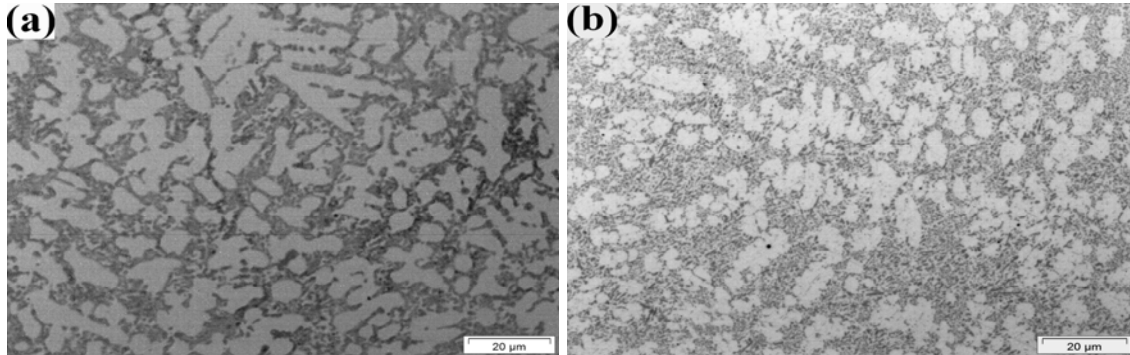

Figure 7.17. Optical microstructures of Au-0.15Ge-0.12Sn candidate alloy after thermal aging for 3 weeks, (a) 150°C (b) 200°C.

The microhardness of the Au-0.15Ge-0.12Sn candidate alloy aged at 200°C was lower than the as-produced samples while the microhardness of the Au-0.15Ge-0.12Sn candidate alloy aged at 150°C was higher than the as-produced samples as depicted in Figure 7.18. The microhardness of the Au-0.15Ge-0.12Sn candidate alloy aged at 200°C decreased proportionally with the aging duration despite the solid solution strengthening of the ζ phase (Table 7.3) and also the refinement of the ζ phase. The content of Sn soluble in the ζ phase calculated thermodynamically at 150°C and 200°C in mole-fraction are 0.140 and 0.141 respectively. The high solubility of Sn in ζ phase was also confirmed by the SEM/EDX elemental mapping analysis (Figure 7.3). The age-softening effect observed at 200°C can be attributed to the gradual disappearance of the brittle Au5Sn phase from the microstructure during thermal aging. The AuSn phase too gradually vanished during aging at 200°C. It was not possible to measure the Vickers hardness of the AuSn phase using the 5g load without hitting other phases.

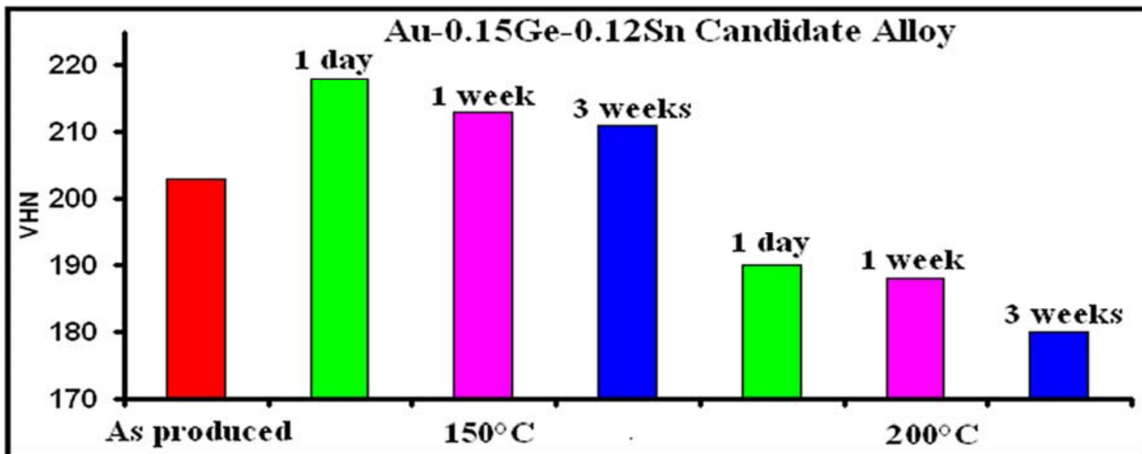

Figure 7.18. Microhardness values of the Au-0.15Ge-0.12Sn candidate alloy using 100g load before and after aging.

The microhardness of the Au-0.15Ge-0.12Sn candidate alloy aged at 150°C was much higher than the ones aged at 200°C as illustrated in Figure 7.18. This effect could be attributed to the solid solution strengthening of the ζ phase, stabilization of the brittle Au5Sn phase and also due to the presence of low volume-fraction of Au rich phases (ζ and Au5Sn phase) in the matrix. Though Au5Sn is a hard phase, it is relatively softer when compared to (Ge) phase as listed in Table 7.3. The microhardness of the Au-0.15Ge-0.12Sn candidate alloy aged at 200°C decreased proportionally with the aging duration. This age-softening effect could be attributed to the increase in the volume-fraction of relatively softer Au rich phases in the matrix during aging.

Table 7.3: Vickers hardness measurement of individual phases using 5g load.

Candidate alloy	Phases	Aging time	Hardness (HV)	
			150°C	200°C
Au-0.15Ge-0.12Sn	ζ	As-produced	150*	150*
		1 day	160	159
		1 week	165	162
		3 weeks	170	169
	Au_5Sn	As-produced	224*	224*
		1 day	226	227
		1 week	221	—
		3 weeks	225	—
	(Ge) phase distributed on (Au) rich phases	As-produced	265*	265*
		1 day	272	206
		1 week	258	192
		3 weeks	240	187

*without heat treatment — unstable

7.2.5. Analysis of Au-Ge Based Candidate Alloys

It was determined that the addition of In to the Au-Ge eutectic would further enhance the hardness of the alloy due to the effective lattice strains induced by the In atoms. In the case of Sn, much softening could not be achieved because of the formation of massive IMCs. Therefore, alloying Au-Ge eutectic with Sn or In would facilitate in adhering to the required solidification criterion for high-temperature soldering but will not induce the required softness to the otherwise hard solder.

Thus, among the three low melting point metals (In, Sb & Sn), it was determined that the addition of Sb to the Au-Ge eutectic would not only decrease its melting point but also would improve its ductility substantially despite the presence of very hard IMC ($AuSb_2$). Therefore, in this context, in addition to the solubility and reactivity of the alloying elements and the characteristics of their IMCs, the distribution of phases played a relatively more crucial role in determining the ductility of the bulk solder alloy. Though the effect of Sb on Au-Ge eutectic has been examined in this work with a holistic approach, it has to be mentioned that Sb is also in the list of toxic elements [30,45]. However, Sb is not as toxic as lead and even small amounts of Sb to the Au-Ge eutectic would make a significant difference in terms of ductility.

7.3. Au-Sn Based Candidate Alloys

The equilibrium phase diagram of the Au-Sn system as shown in Figure 7.19 represents one of the most complicated and intriguing binary systems. Its complexity is caused by the existence of four different stable intermetallic compounds as well as two eutectic and at least three peritectic points. Among the two eutectic compositions, Au-0.30Sn (mole-fraction) and Au-0.94Sn (mole-fraction), the former is widely being considered for soldering because of its favorable melting point [113,114]. Over the past century, a great deal of work has been performed to establish the complete Au-Sn phase diagram and to study the characteristics of the many phases identified. The original diagram was given by Vogel [113] in 1905 and the phase diagram illustrated in Figure 6.19 was generated using ThermoCalc based on the improved version of the Au-Sn phase diagram provided by Ciulik [115]. However, the properties and boundaries of several phases are still not completely determined and the work is still being conducted on the refinement of this phase diagram.

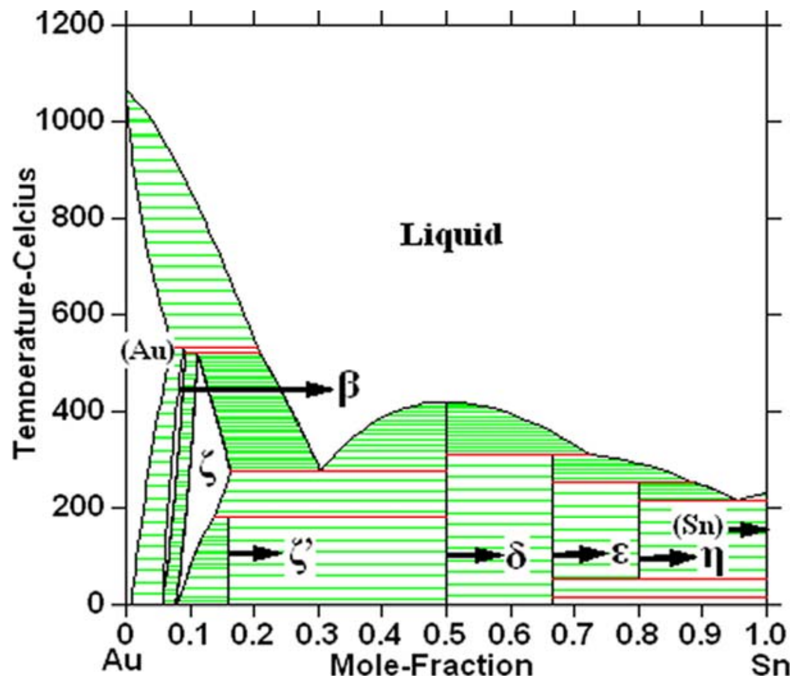

Figure 7.19. Au-Sn phase diagram generated using COST 531 thermodynamic database.

Table 7.4 lists the phases of the binary Au-Sn system and their maximum composition ranges. The values are calculated using the respective thermodynamic description of the phases in COST 531 v 3.0 [95] thermodynamic database. Among the Au-Sn IMCs, ζ' (Au5Sn) was determined to be the hardest in this work. A ranking of the three IMCs that were observed in this work with respect to their hardness on the basis of the obtained results can be given as follows:

$$\delta\ (AuSn) < \varepsilon\ (AuSn2) < \zeta'\ (Au5Sn)$$

Table 7.4: Phases of the binary Au-Sn system and their composition ranges.

Phase	Composition			
	[at.%]		[wt.%]	
	Au	Sn	Au	Sn
(Au)	100-92.8	0-7.2	100-95.5	0-4.5
β	94.4-90.8	5.6-9.2	96.5-94.2	3.5-5.8
ζ	92.2-83.7	7.8-16.3	95.1-89.50	4.9-10.5
ζ' (Au5Sn)	83.3	16.7	89.2	10.8
Eutectic 80Au20Sn (ζ '+ δ)	70	30	80	20
δ (AuSn)	50	50	62.4	37.6
ε (AuSn2)	33.3	66.7	45.3	54.7
η (AuSn4)	20	80	29.3	70.7
Eutectic Au-Sn η + (Sn)	5.5	94.5	5.9	94.1

Au-0.30Sn (mole-fraction) is the only binary eutectic composition with a melting point of 280°C that directly fits into the requirement. Au-Sn eutectic is a hard solder that is currently being used for fluxless applications like opto-electronic packaging [2]. Despite adhering to the solidification criterion, it cannot be used as a soft solder for high-temperature applications without inducing some softness in it by micro-alloying.

7.3.1. Au-Sn Eutectic Alloy

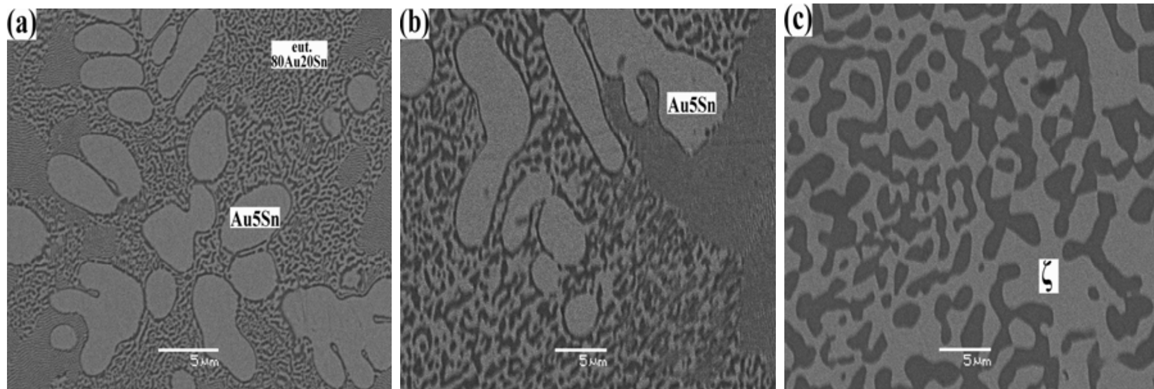

Figure 7.20. SEM-BSE micrographs of the Au-Sn eutectic alloy before and after thermal aging (a) as-produced (b) 150°C-1 week (c) 200°C-1 week.

The microstructure of the as-produced Au-Sn eutectic alloy was comprised of the brittle ζ' (Au5Sn) and ζ phases dispersed on the matrix of Au-Sn eutectic structure (ζ' + δ) as illustrated in Figure 7.20. The presence of ζ phase can be attributed to the fast cooling rate employed during the production of these alloys in the hot-plate microscope. The microstructure of the thermally aged Au-Sn eutectic alloy at 150°C for 1 week was comprised of large Au5Sn IMCs dispersed on the Au-Sn eutectic structure. The ζ phase did not exist in the Au-Sn eutectic alloy subjected to aging at 150°C. The microstructure of the thermally aged Au-Sn eutectic alloy at 200°C was comprised of ζ and δ phases

only. Therefore, it can be concluded that at 200°C, all the brittle ζ' phase of the Au-Sn eutectic alloy has transformed into ζ phase. Microhardness measurements of individual phases supplemented in distinguishing between ζ and ζ' phases since ζ is a soft phase while ζ' is a hard phase.

The overall microhardness of the Au-Sn eutectic alloy aged at 200°C was lower than the as-produced ones while the overall microhardness of the Au-Sn eutectic alloy aged at 150°C was higher than the as-produced ones as depicted in Figure 7.21. The increase in hardness of the Au-Sn eutectic alloy when subjected to aging at 150°C can be attributed to the stabilization of the hard Au5Sn phase while the decrease in the hardness of the Au-Sn eutectic alloy when subjected to aging at 200°C can be attributed to the transformation of the hard Au5Sn phase to a softer ζ phase.

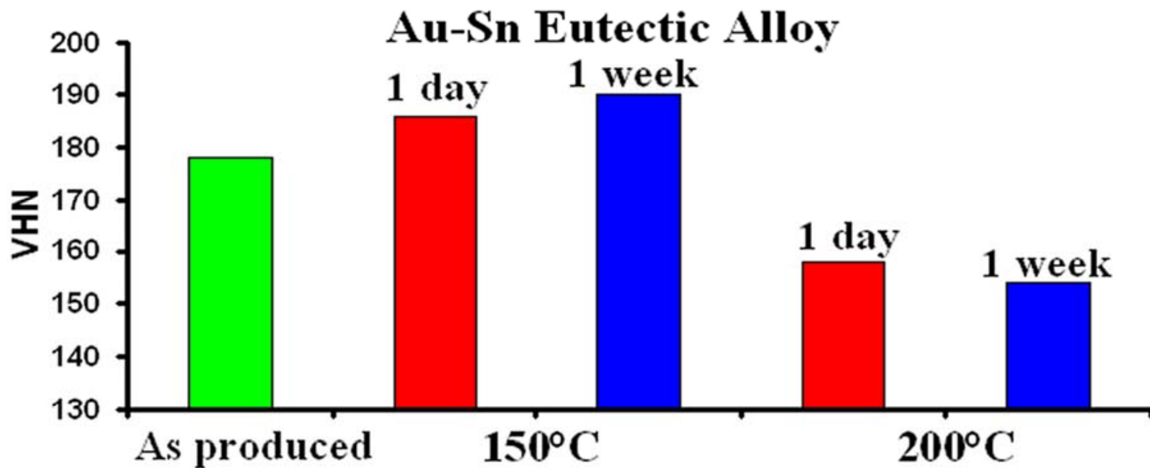

Figure 7.21. Microhardness values of the Au-Sn eutectic alloy using 100g load before and after thermal aging.

7.3.2. Au-0.35Sn-0.03Ag Candidate Alloy

The microstructure of the as-produced Au-0.35Sn-0.03Ag samples as depicted in Figure 7.22, before being subjected to thermal aging was comprised of δ (AuSn) phase dispersed on Au rich phases and also ζ' (Au5Sn) phase. The Au rich phases could be either (Au,Ag) or ζ. It was not possible to distinguish between these two phases by EDX due to the limitations of the technique. This can be attributed to the close solubility limit of these two phases. The Au5Sn phase could be distinguished from the other Au rich phases using EDX since Ag is absolutely insoluble in this phase. SEM analysis showed that the volume-fraction of Au5Sn phase in the matrix of the as-produced samples was too low. This effect could be attributed to the fast cooling rate employed during the production of these alloys in the hot-plate microscope. Thus, it can be concluded that the fast cooling rate employed during the production of these alloys has suppressed the precipitation of the Au5Sn phase to a great extent.

It was observed that the volume-fraction of Au5Sn phase in the matrix of the Au-0.35Sn-0.03Ag alloys subjected to aging at 150°C for different durations was much

higher than that of the as-produced ones. In the samples that were subjected to thermal aging at 200°C for 1 day, the volume-fraction of Au5Sn phase in the matrix was even lower than the as-produced samples. The Au5Sn phase did not exist in the matrix of the samples subjected to aging at 200°C for 1 week.

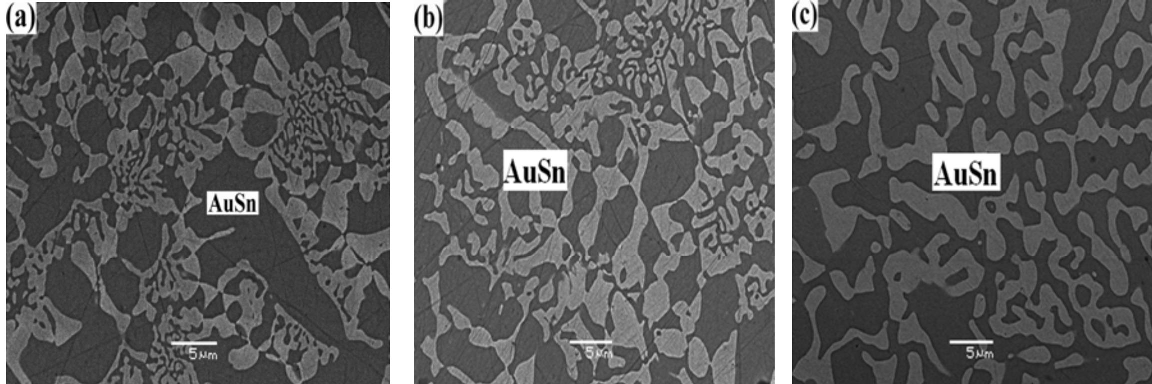

Figure 7.22. SEM-BSE micrographs of the Au-0.35Sn-0.03Ag candidate alloy before and after aging (a) as-produced (b) 150°C-1 week (c) 200°C-1 week.

The overall microhardness of the Au-0.35Sn-0.03Ag candidate alloy aged at 200°C was lower than the as-produced ones while the overall microhardness of the Au-0.35Sn-0.03Ag candidate alloy aged at 150°C was higher than the as-produced samples as depicted in Figure 7.23. The microhardness of the Au-0.35Sn-0.03Ag candidate alloy aged at 200°C decreased proportionally with the aging duration despite the solid strengthening of the Au rich phases [(Au, Ag)/ζ] as listed in Table 7.5. This age-softening can be attributed to the gradual disappearance of the hard Au5Sn phase

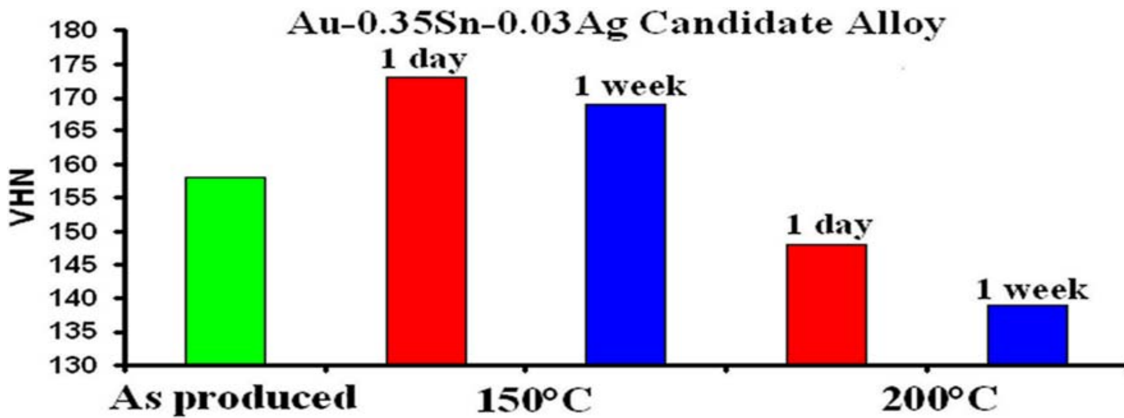

Figure 7.23. Microhardness values of the Au-0.35Sn-0.03Ag candidate alloy using 100g load before and after thermal aging.

The relatively higher hardness of the Au-0.35Sn-0.03Ag candidate alloys aged at 150°C can be attributed to the increase in the volume-fraction of the hard Au5Sn phase. The slight decrease in the hardness of the Au-0.35Sn-0.03Ag candidate alloy aged at 150°C for 1 week when compared to the ones aged at 150°C for 1 day can be attributed to the sensitivity of this technique not resulting in reproducibility within very narrow tolerances.

Table 7.5: Vickers hardness measurement of individual phases in the Au-0.35Sn-0.03Ag candidate alloy using 5g load.

Candidate alloy	Phases	Aging time	Hardness (HV)	
			150°C	200 °C
Au-0.35Sn-0.03Ag	δ (AuSn)	As-produced	140[a]	140[a]
		1 day	139	143
		1 week	142	138
	(Au,Ag)/ζ	As-produced	144[a]	144[a]
		1 day	148	154
		1 week	155	160
	ζ' (Au5Sn)	As-produced	215[a]	215[a]
		1 day	213	217
		1 week	216	—

*without heat treatment — unstable

7.3.3. Au-0.33Sn-0.04Cu Candidate Alloy

The microstructure of the as-produced Au-0.33Sn-0.04Cu candidate alloy as illustrated in Figure 7.24 comprised of δ (AuSn) phase dispersed in the matrix. The matrix comprised of δ (AuSn) and ε (AuSn2) lamellae dispersed on Au rich phases [(Au,Cu) or ζ] and ζ' (Au5Sn). The Au5Sn phase could be distinguished from the other gold rich phases since Cu is absolutely insoluble in this phase. The volume-fraction of Au5Sn phase was too low in the as-produced samples due to the lack of time for precipitation. The major difference that was observed in the as-produced Au-0.33Sn-0.04Cu candidate alloy when compared to that of the as-produced Au-0.35Sn-0.03Ag candidate alloy was related to the presence of a few AuSn2 lamellae in the matrix The presence of AuSn2 phase can be attributed to non-equilibrium solidification since this phase is not expected to precipitate for this specific composition.

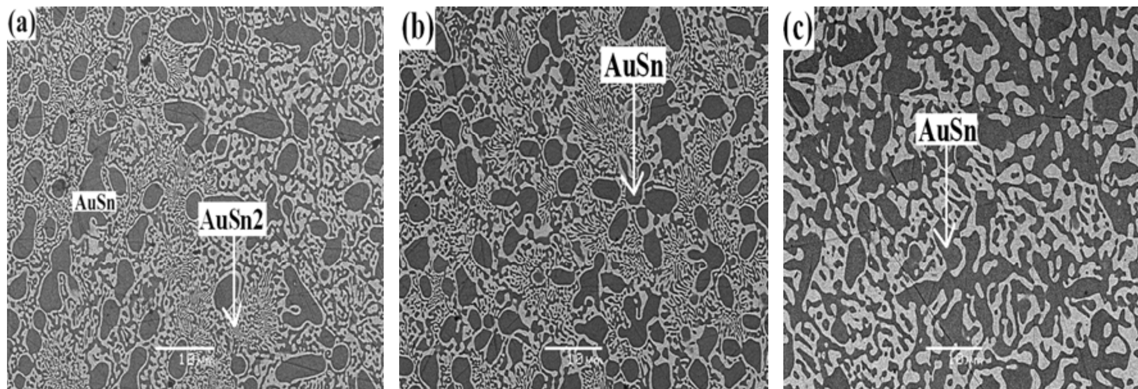

Figure 7.24. SEM-BSE micrographs of the Au-0.33Sn-0.04Cu candidate alloy before and after aging (a) as-produced (b) 150°C-1 week (c) 200°C-1 week.

The volume-fraction of Au5Sn phase increased proportionally with the aging durations when subjected to aging at 150°C while decreased gradually during aging at 200°C. SEM analysis also showed that the volume-fraction of AuSn2 lamellae in the matrix decreased

gradually during aging at 150°C and this phase did not exist in the microstructure of the samples that were subjected to aging for 1week. Both the Au5Sn and the AuSn2 phases did not exist in the microstructure of the samples aged at 200°C for 1 week.

Similar to the Au-0.35Sn-0.03Ag candidate alloy, the overall microhardness of the Au-0.33Sn-0.04Cu candidate alloy aged at 200°C was lower than the as-produced ones while the overall microhardness of the Au-0.33Sn-0.04Cu candidate alloy aged at 150°C was higher than the as-produced samples as depicted in Figure 7.25. The overall hardness of the as-produced Au-0.33Sn-0.04Cu candidate alloy was higher than the as-produced Au-0.35Sn-0.03Ag candidate alloy. This can primarily be attributed to the presence of the hard AuSn2 lamellae in the matrix. Solid-solution strengthening of the Au rich phases [(Au,Cu)/ζ] too was observed irrespective of the aging temperatures as shown in Table 7.6. The solid-solution strengthening of the Au rich phases induced by the Cu atoms was determined to be relatively higher than the ones induced by the Ag atoms. It was not possible to measure the hardness of the AuSn2 phase without hitting the surrounding Au rich phases due to its lamellae structure as shown in Figure 7.24. The slight increase in the hardness of the AuSn2 phase (Table 7.6) irrespective of the aging temperatures can be attributed to the solid-solution strengthening of the surrounding Au rich phases.

The overall hardness of the Au-0.33Sn-0.04Cu candidate alloy aged at 150°C was higher than the as-produced samples despite the gradual disappearance of the hard AuSn2 lamellae from the matrix. This age-hardening effect can be attributed to the increase in volume-fraction of the hard Au5Sn phase. The age-softening effect observed at 200°C can be attributed to the disappearance of both the hard phases i.e. Au5Sn and AuSn2 from the matrix.

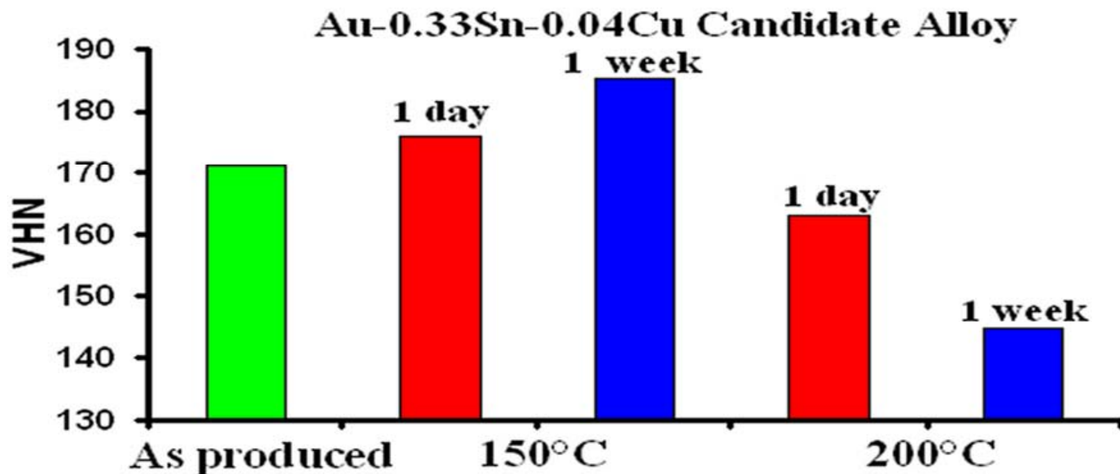

Figure 7.25. Microhardness values of the Au-0.35Sn-0.04Cu candidate alloy using 100g load before and after thermal aging.

Table 7.6: Vickers hardness measurement of individual phases in the Au-0.33Sn-0.04Cu candidate alloy using 5g load.

Candidate alloy	Phases	Aging time	Hardness (HV)	
			150°C	200°C
Au-0.33Sn-0.04Cu	δ (AuSn)	As-produced	141[a]	141[a]
		1 day	143	138
		1 week	143	142
	(Au,Cu)/ζ	As-produced	157[a]	157[a]
		1 day	158	161
		1 week	163	168
	ε (AuSn2) distributed on Au rich phases	As-produced	180[a]	180[a]
		1 day	183	185
		1 week	—	—
	ζ’ (Au5Sn)	As-produced	214[a]	214[a]
		1 day	216	211
		1 week	216	—

*without heat treatment — unstable

7.3.4. Sn-0.30Au-0.08Ag Candidate Alloy

Before thermal aging, the microstructure of the as-produced Sn-0.30Au-0.08Ag candidate alloy comprised of the dark δ (AuSn) phase and the white Au rich phase dispersed in the matrix, as depicted in Figure 7.26. The matrix consisted of ε (AuSn2) phase and an Ag rich ternary phase. It was not possible to identify the Au rich phase with EDX. After thermal aging at different temperatures for different durations, the major difference observed in the aged samples was in relation to the dark AuSn phase dispersed on the matrix (Figure 7.26 & Figure 7.27). The volume-fraction of the Au rich phase was much lower in the aged samples when compared to that of the as-produced ones. It was determined that only the aging temperature had a dramatic impact on the precipitation of the dark AuSn phase and not the aging duration.

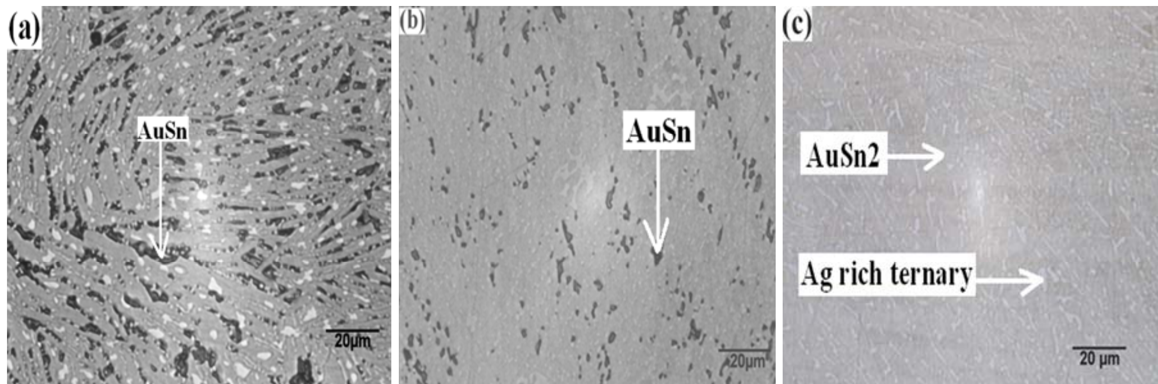

Figure 7.26. Optical micrographs of the Sn-0.30Au-0.08Ag candidate alloy before and after aging (a) as-produced (b) 150°C-1 week (c) 200°C-1 week.

It was observed that the volume-fraction of the dark AuSn phase dispersed in the matrix of the samples aged at 150°C for different durations was much lower when compared to that of the as-produced ones. The AuSn phase did not exist in the samples that were aged at 200°C for different durations. EDX analysis of the as-produced samples and the samples that were aged at different aging temperatures for different durations showed that the Ag content in the Ag rich ternary phase varied between (60-68 at. %) while the Sn content varied between (24-30 at. %) and the Au content varied between (4-14 at. %).

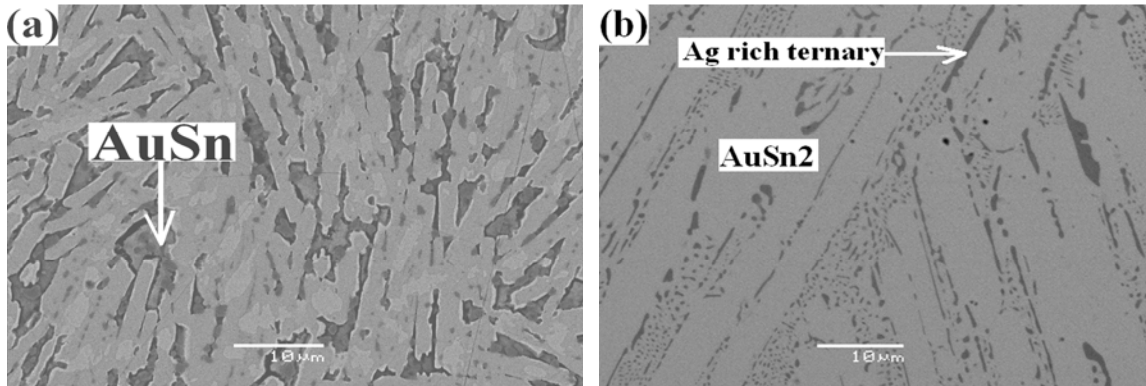

Figure 7.27. SEM-BSE micrographs of the Sn-0.30Au-0.08Ag candidate alloy before and after thermal aging for 1 week, (a) 150°C (b) 200°C.

The trend in the overall hardness of the candidate alloys in the Sn rich region was different from the candidate alloys close to the Au-Sn eutectic. The overall hardness of the samples aged at 150°C for different durations was higher than the as-produced ones. The overall hardness of the samples aged at 200°C was even higher than the ones subjected to aging at 150°C. Unlike the compositions close to the Au-Sn eutectic, only the aging temperature had a notable impact on the microhardness of the Sn-0.30Au-0.08Ag candidate alloy as depicted in Figure 7.28 and not the aging duration. The slight difference in the overall hardness with respect to aging durations irrespective of the aging temperatures can be attributed to the sensitivity of the technique not resulting in reproducibility within very narrow tolerances.

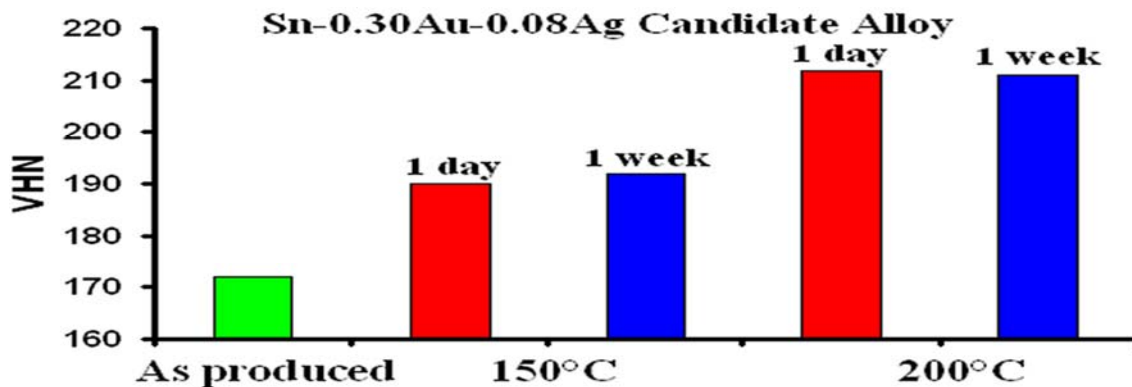

Figure 7.28. Microhardness values of the Sn-0.30Au-0.08Ag candidate alloy using 100g load before and after thermal aging.

The overall hardness values of the Sn-0.30Au-0.08Ag candidate alloy were primarily controlled by the precipitation of the soft AuSn phase. This phase was measured to be relatively softer than the ones measured on the candidate alloys close to the Au-Sn eutectic composition as listed in Table 7.7. This could probably be attributed to the difference in the morphology of the AuSn phase. The as-produced Sn-0.30Au-0.08Ag candidate alloy was much softer than the aged samples due to the high volume-fraction of this soft AuSn phase (Figure 7.26). The Sn-0.30Au-0.08Ag candidate alloy subjected to aging at 150°C was harder than the as-produced ones due to the presence of low volume-fraction of the soft AuSn phase. The Sn-0.30Au-0.08Ag candidate alloy subjected to aging at 200°C was the hardest due to the complete disappearance of this soft AuSn phase. It was not possible to measure the hardness of the Au rich phase in the aged samples without hitting the matrix, i.e. Ag rich ternary phase dispersed on the AuSn2 phase.

Table 7.7: Vickers hardness measurement of individual phases in the Sn-0.30Au-0.08Ag candidate alloy using 5g load.

Candidate alloy	Phases	Aging time	Hardness (HV)	
			150°C	200°C
Sn-0.30Au-0.08Ag	ε (AuSn2)	As-produced	205[a]	205[a]
		1 day	207	204
		1 week	207	206
	δ (AuSn)	As-produced	104[a]	104[a]
		1 day	106	105
		1 week	104	106
	Ag rich ternary phase Ag: [60-68 at. %] Sn : [24-30 at. %] Au: [4-14 at. %]	As-produced	216[a]	216[a]
		1 day	219	220
		1 week	220	219
	Au rich phase	As-produced	161[a]	161[a]

*without heat treatment

7.3.4. Sn-0.29Au-0.08Cu Candidate Alloy

Before thermal aging, the microstructure of the Sn-0.29Au-0.08Cu candidate alloy comprised of the dark δ (AuSn) phase and the gray Sn rich ternary phase dispersed on the ε (AuSn2) matrix as depicted in Figure 7.29. The volume-fraction of the dark δ (AuSn) phase dispersed in the matrix of the as-produced Sn-0.29Au-0.08Cu candidate alloy was higher when compared to that of the as-produced Sn-0.30Au-0.08Ag candidate alloy. After thermal aging at different temperatures for different durations, the major difference observed in the aged samples was in relation to the dark δ (AuSn) phase dispersed on the matrix as illustrated in Figure 7.30. Similar to the Sn-0.30Au-0.08Ag candidate alloy only the aging temperature had a substantial impact on the precipitation of the dark δ (AuSn) phase and not the aging durations.

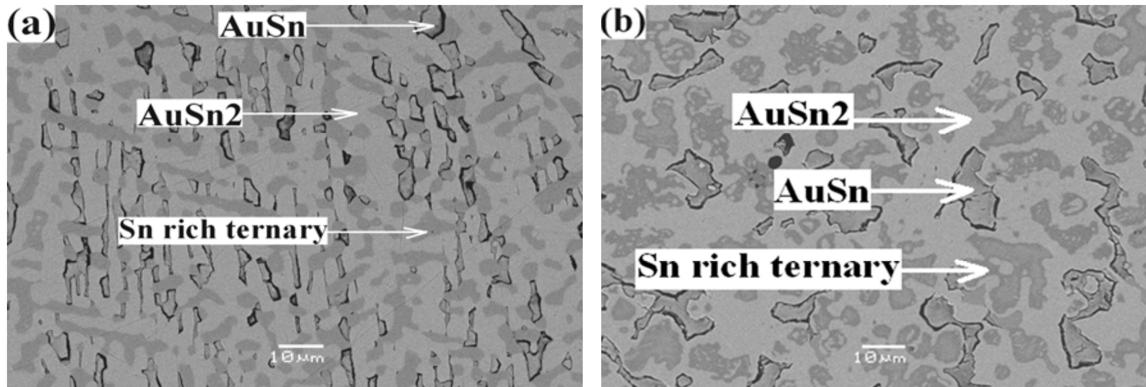

Figure 7.29. SEM-BSE micrographs of the Sn-0.29Au-0.08Cu candidate alloy before and after thermal aging for 1 week, (a) 150°C (b) 200°C.

It was observed that the volume-fraction of the AuSn phase dispersed in the matrix of the samples aged at 150°C for different durations was relatively lower than the as-produced ones. The volume-fraction of the AuSn phase in the samples aged at 200°C for different durations was even lower than the ones aged at 150°C. Slight coarsening of the dark AuSn phase was observed in the samples aged at 200°C for different durations as depicted in Figure 7.29. Thus, unlike for the Sn-0.30Au-0.08Ag candidate alloy, the AuSn phase existed in the samples aged at 200°C for different durations. EDX analysis of the as-produced samples and the samples that were aged at different aging temperatures for different durations showed that the Sn content in the Sn rich ternary phase varied between (51-53 at. %) while the Au content varied between (24-33 at. %) and the Cu content varied between (15-25 at.%). The solubility of Cu in the ternary phase of the as-produced samples was much lower when compared to that of the samples that were subjected to thermal aging for different durations irrespective of the aging temperatures.

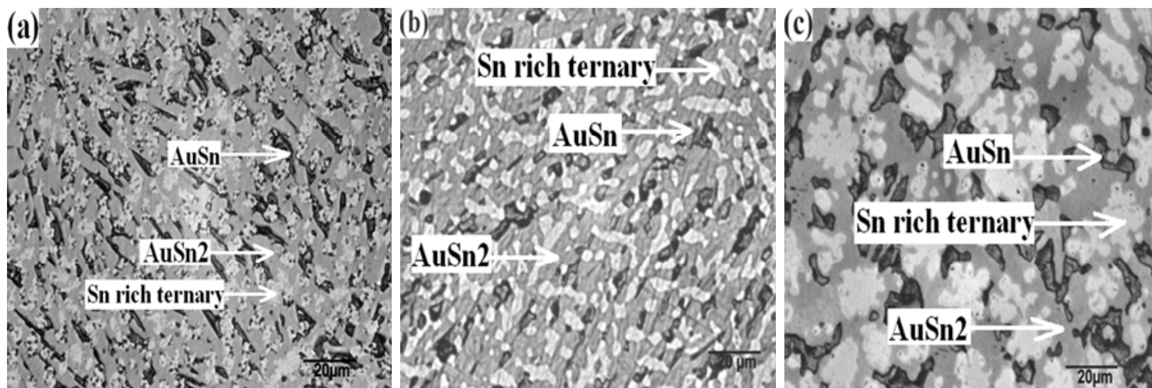

Figure 7.30. Optical micrographs of the Sn-0.29Au-0.08Cu candidate alloy before and after aging (a) as-produced (b) 150°C-1 week (c) 200°C-1 week.

Thus, interestingly none of the brittle Cu-Sn intermetallics [116] precipitated in any of the as-produced and the aged Sn-0.29Au-0.08Cu candidate alloy for this specific composition and aging temperatures. Elemental mapping of the samples subjected to aging for 1 week at 150°C and 200°C respectively as illustrated in Figure 7.31 and Figure 7.32 shows that all the Cu in the aged samples existed only in the Sn rich ternary phase. It

has to be mentioned that Cu-Sn intermetallics are relatively brittle than any of the Au-Sn intermetallics.

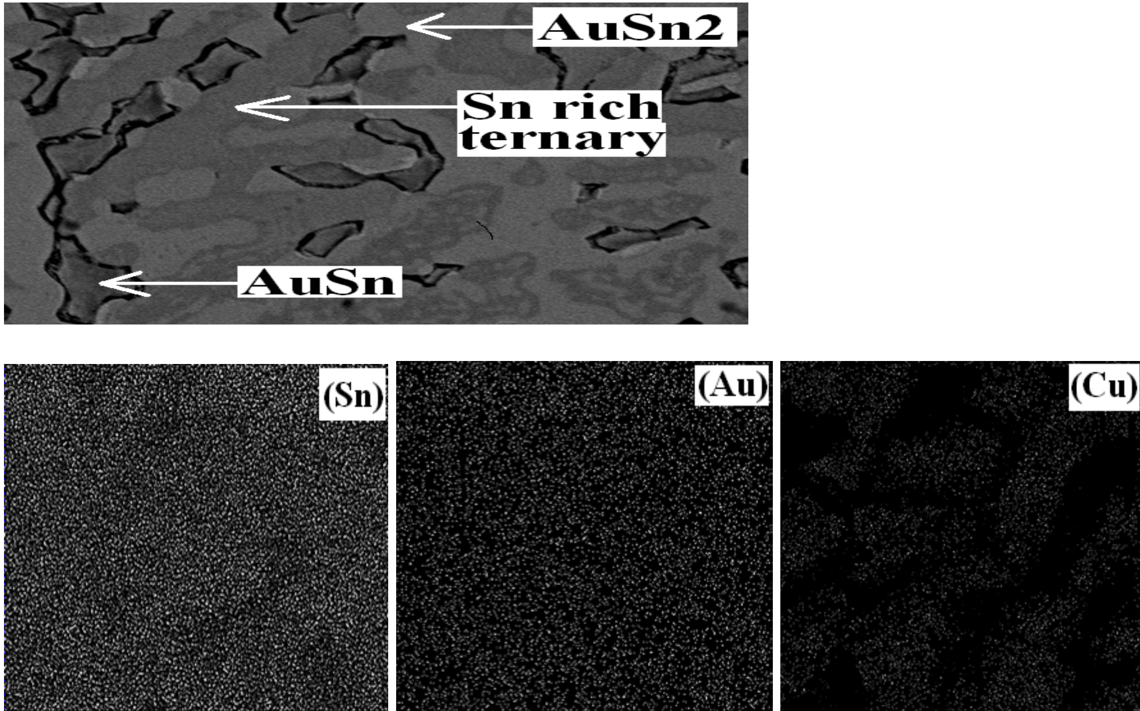

Figure 7.31. Elemental mapping of Sn-0.29Au-0.08Cu candidate alloy aged at 150°C for 1 week.

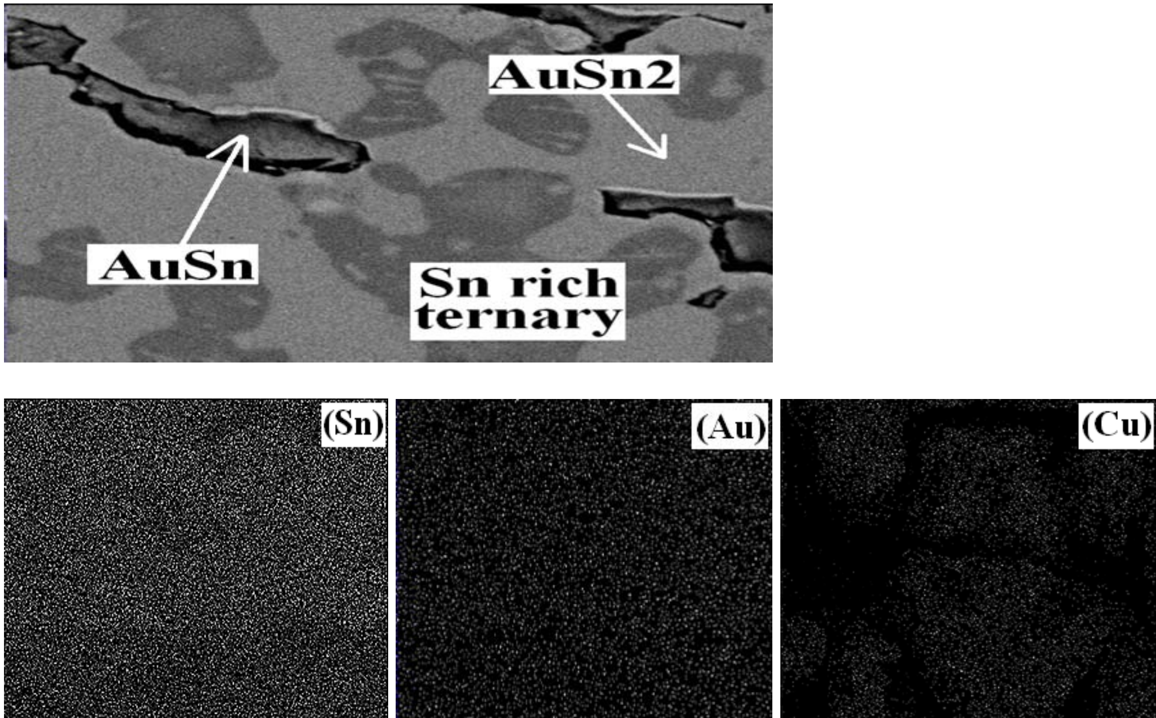

Figure 7.32. Elemental mapping of Sn-0.29Au-0.08Cu candidate alloy aged at 200°C for 1 week.

The trend in the overall hardness of the Sn-0.29Au-0.08Cu candidate alloy was similar to that of the Sn-0.30Au-0.8Ag candidate alloy as depicted in Figure 7.33. The overall hardness of the aged Sn-0.29Au-0.08Cu candidate alloy was higher than the as-produced ones despite the solid-solution strengthening of the ternary phase induced by the Cu atoms as listed in Table 7.8. This age-hardening effect can be attributed to the slight reduction in the volume-fraction of the soft AuSn phase. The as-produced Sn-0.29Au-0.08Cu candidate alloy was even softer when compared to the as-produced Sn-0.30Au-0.08Ag candidate alloy. This could be attributed to the relatively higher volume-fraction of the soft AuSn phase.

Similar to the Sn-0.30Au-0.08Ag candidate alloy, the aging temperature had a notable impact on the microhardness of the Sn-0.29Au-0.08Cu candidate alloy and not the aging duration. The aged Sn-0.29Au-0.08Cu samples were substantially softer than the Sn-0.30Au-0.08Ag candidate alloy subjected to aging at the respective aging temperatures. This effect can be attributed to the fact that the reduction in the volume-fraction of the soft AuSn phase during aging was substantially lower when compared to that of the Sn-0.30Au-0.08Ag candidate alloy. More importantly, the soft AuSn phase existed in the samples subjected to aging at 200°C. No change in the hardness of the AuSn phase in the samples aged at 200°C for different durations was noticed despite the slight coarsening of the AuSn phase.

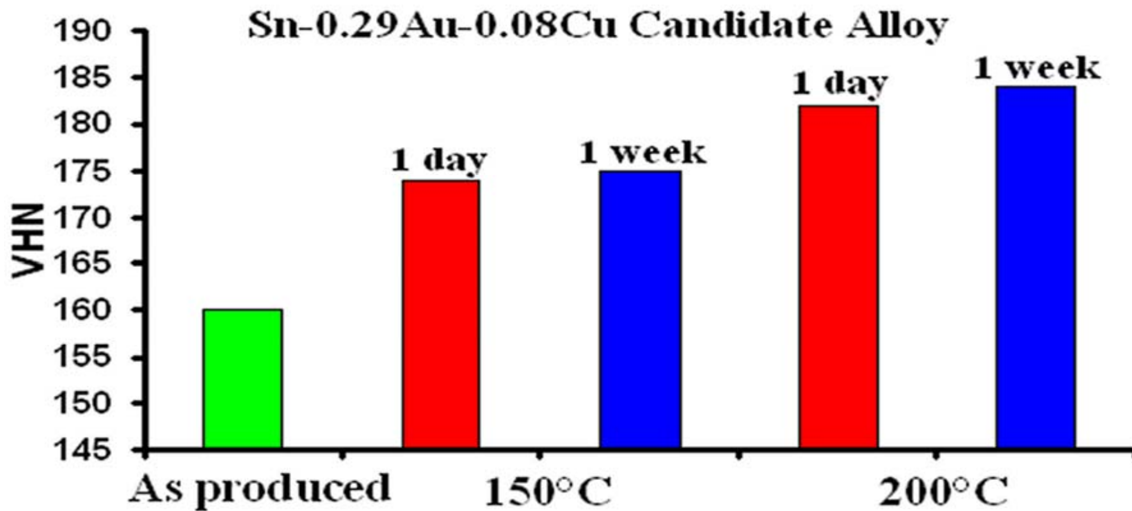

Figure 7.33. Microhardness values of the Sn-0.29Au-0.08Cu candidate alloy using 100g load before and after thermal aging.

Table 7.8: Vickers hardness measurement of individual phases in the Sn-0.30Au-0.08Cu candidate alloy using 5g load.

Candidate alloy	Phases	Aging time	Hardness (HV)	
			150°C	200°C
Sn-0.29Au-0.08Cu	ε (AuSn2)	As-produced	204[a]	204[a]
		1 day	204	203
		1 week	204	204
	δ (AuSn)	As-produced	103[a]	103[a]
		1 day	105	104
		1 week	106	104
	Sn rich ternary phase Sn: [51-53 at. %] Au: [24-33 at. %] Cu: [15-25 at. %]	As-produced	241[a]	241[a]
		1 day	270	277
		1 week	282	285

*without heat treatment

7.3.5. Analysis of Au-Sn Based Candidate Alloys

Both the aging temperature and the aging duration had a notable impact on the microstructure of the candidate alloys close to the Au-Sn eutectic. The candidate alloys on the Sn rich region were considerably more stable, i.e. only the aging temperature had a substantial impact and not the aging durations. Micro-alloying of Ag/Cu has induced some softness to the hard Au-Sn eutectic solder. However, the degree of softness induced to this hard solder by micro-alloying is still not promising enough to be regarded as a soft solder. Despite being hard, Au-Sn eutectic alloys have been reported to exhibit superior thermal fatigue resistance by Suganuma et. al [2]. Thus, among the four Au-Sn based candidate alloys, the ones close to the Au-Sn eutectic were softer than the ones on the Sn rich side. For applications involving an operating temperature of 200°C, candidate alloys close to the Au-Sn eutectic were relatively more ductile than the candidate alloys on the Sn rich side. However, for applications involving an operating temperature of 150°C, the difference in hardness between the alloys on the Au rich side and the Sn rich side was small but still the Au rich candidate alloys had a slight edge over the latter with respect to ductility. This can be attributed to the stabilization of the brittle Au5Sn phase on the Au rich side and to the presence of a high volume-fraction of the soft AuSn phase on the Sn rich side.

Chapter 7

A Corrosion Investigation of Prospective Candidate Alloys

A drive for miniaturization, multiplicity of materials and globalization has resulted in corrosion being a significant issue in the complex electronic packaging systems that are being developed. The solder candidates that could adhere to the solidification criterion required for replacing the high-lead containing solders were investigated from the corrosion perspective. The possible corrosion scenario for these promising candidate alloys in such packaging for high-temperature applications has been envisaged.

7.1. Corrosion in Advanced Electronic Packagings

The demand for miniaturization, multiplicity of materials used, effect of process residues together with unpredictable user environment has opened up serious corrosion problems in the microelectronics industry [67]. Corrosion in electronic components is insidious and can not be readily detected and therefore, the cost of corrosion in the electronic sector can not be estimated. It has been suggested that a significant part of all electronic system failures are actually caused by corrosion but are generally not accounted for [102]. Advanced electronic packagings comprehending high-lead content solders can be exposed to a wide variety of outdoor and indoor environments. The corrosion behavior is determined by the actual environment, which can be as benign as a simple low humidity, purified atmosphere, indoor location, to the aggressive environment existing on the automobile which is subjected to road salt splash and spray [57,103].

Advanced packaging technologies involve the reduction of the distance between components. The close spacing increases the electric field between points and reduces the size of the condensing water droplet needed for connecting the components together for corrosion. The reduction in size and distance between components and the increase in the interconnect density makes the solder alloy susceptible to corrosion problems [104]. A major departure from most corrosion situations in the advanced electronic packaging is the incredible small volume of the material that can be damaged. The tolerance for corrosion loss in such advanced electronic packaging technology is usually on the order of 10-12 picograms [67,102]. Therefore, even a small environmental impact can cause huge damages and when the device is in use, the large voltage gradients will further accelerate the corrosion problems dramatically. Thus, corrosion in the electronics industry has become a significant factor in recent years because of the extremely complex systems that have been developed and the increasing demand on their reliability [105]. Therefore, it is essential to take into account the effects of corrosion during the design of lead-free solder alloys for high temperature applications.

7.2. Causes of Corrosion

As mentioned before, the multiplicity of materials possessing different electrochemical properties and the drive for miniaturization in the advanced electronic packagings being developed, has significantly contributed to the corrosion of high-temperature solders. However, there are several other environmental related factors that could accelerate the corrosion process, which needs to be controlled in order to reduce the corrosion effects in the high-temperature solders.

Among the environmental issues, a significant problem is the residues found on the metallization and the pads. Following classification can be made for residues:

- Process related residues
- Service related residues

Process related residues are the contamination on the surface of the substrate due to the remains of the chemicals used for the manufacturing process. This could be the left over of original chemicals or decomposed fractions of a compound formed during the production cycle. These are the etching medium, plating bath residues, or additives from the polymeric materials. Depending on the temperature cycles and applications, small amount of original compound or decomposed products could remain on the surface of the substrate. In practice, tiny fractions of these chemicals are enough to accelerate the corrosion process.

The service related residues are the residues introduced during exposure to service environments. They can be aggressive ions like chlorides, SO2 (g), NO2 (g), or other types of chemically aggressive ions. Presence of such substances triggers corrosion to a large extent under humid conditions. Formation of water layer is easy on a dusted surface compared to the clean one. Therefore, corrosion is possible even at relatively low humidity such as 50-70%. If the surface of the metallic pads or under-bump metallization which is in contact with the high-melting points solders is not contaminated, then corrosion will not be a major issue. However, in practice significant levels of contamination could be detected on both these metallization and pads. In this work, focus has been given only to the chlorides since it is the most commonly encountered residue [106].

7.3. Thermodynamic Stability of Chlorides

The thermodynamic parameter LNAC of Cl_2 (g) of the most stable chlorides for the promising solder candidates at different room temperatures were determined by coupling both the COST 531 and SSUB3 thermodynamic databases and are listed in Table 7.1. The Au-Ge-Sn candidate alloy has not been considered for corrosion investigation because of the formation of massive intermetallic compounds unlike the other two Au-Ge based candidate alloys (Au-Ge-In & Au-Ge-Sb). Thermodynamic calculations for chlorides when compared to Table 2.6 show that alloying Au with the elements commonly being considered for solder candidates would have an impact on the

chlorides when compared to Table 2.6 show that alloying Au with the elements commonly being considered for solder candidates would have an impact on the thermodynamic stability of chlorides for the respective alloy but unlikely in the case of Ge.

Table 8.1: Thermodynamic stability of chlorides for potential solder candidates.

Potential Candidates (Mole-Fraction)	Predicted Phases		Stable Chlorides	LNAC of Cl_2 (g)	
	Matrix	Dispersed		25°C	45°C
Au-0.18Ge-0.10In	ζ	(Ge) (Au)	$InCl_3$	-109.7	-101.4
Au-0.24Ge-0.05Sb	(Au)	(Ge) AuSb2	$GeCl_4$	-93.3	-86.8
Au-0.35Sn-0.03Ag	δ (AuSn)	(Au, Ag) ζ' (Au5Sn)	$SnCl_2$	-105.4	-97.8
Au-0.33Sn-0.04Cu	δ (AuSn)	(Au, Cu) ζ' (Au5Sn)	$SnCl_2$	-105.8	-98.2
Sn-0.30Au-0.08Ag	ε (AuSn2)	ζ	$SnCl_2$	-115.5	-107.1
Sn-0.29Au-0.08Cu	ε (AuSn2)	ε (Cu3Sn) η^1 (Cu6Sn5)	$SnCl_2$	-116	-107.6

8.4. Potentiodynamic Polarization Curves

The anodic polarization curves of the Au-Sn and Au-Ge based solder alloy candidates in comparison with pure metals are depicted in Figures 8.1 and 8.2 respectively. There was a good agreement in the trend followed by the calculated thermodynamic parameter LNAC of Cl_2 (g) for the most stable chlorides and the experimentally determined E_{corr} values (potential) for the promising solder alloys in chloride environment. The tin was the least noble and it was anodically the most reactive in 250ppm NaCl with highest anodic current density. It was evident that with the increase in the Au content in the Au-Sn based solder alloys there was a gradual improvement in the noble E_{corr} value as well as the gradual reduction in the anodic current density. Ge in comparison with Sn showed ~300mV noble E_{corr} and less anodic current density. Although, the E_{corr} values were different, both pure Ge and Au-Ge based solder alloys showed similar current densities over a range of potentials. Thus, it was determined that even by alloying Ge with substantial fractions of Au in order to adhere to the required solidification criterion no reduction in the anodic current density could be achieved and also the passivation effect exhibited by pure Ge too has been lost.

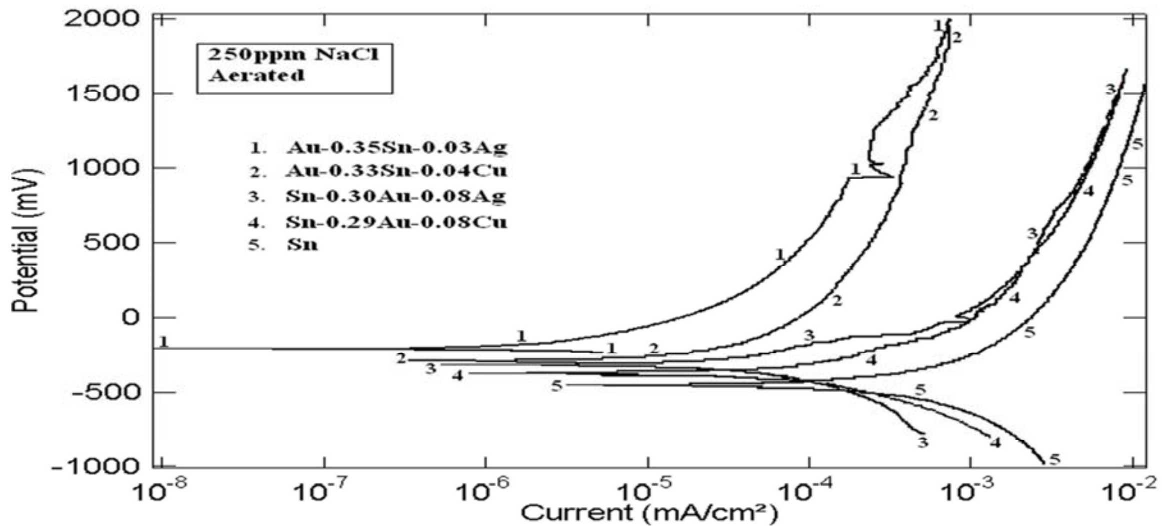

Figure 8.1. Anodic polarization curves for Au-Sn based candidate alloys.

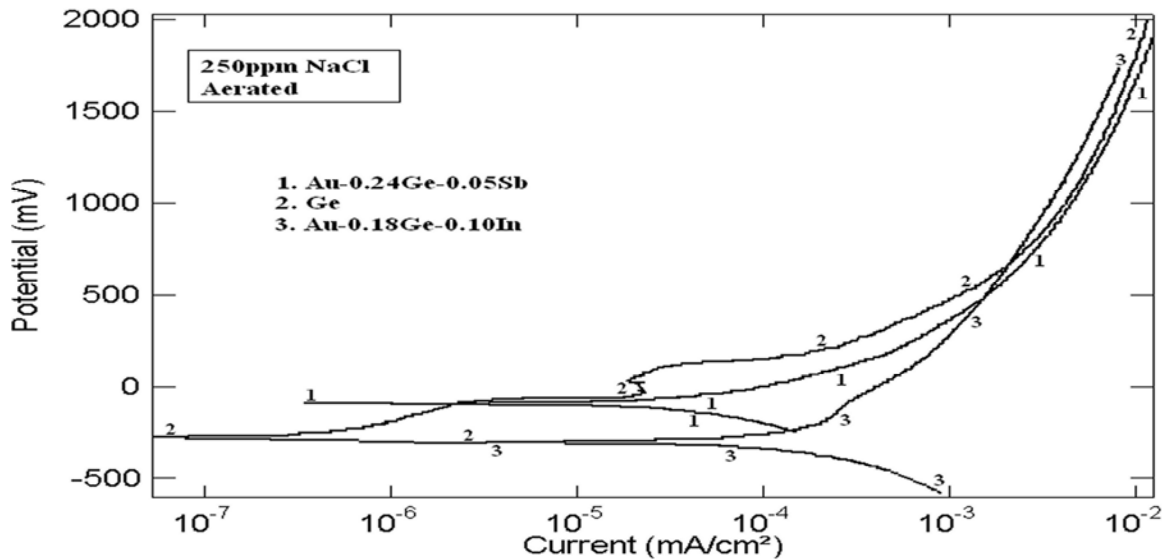

Figure 8.2. Anodic polarization curves for Au-Ge based candidate alloys

The cathodic polarization curves for the Au-Sn and the Au-Ge based solder alloy candidates in comparison with pure metals are depicted in Figures 8.3 and 8.4 respectively. The cathodic activity exhibited by the Au-Ge and Au-Sn based solder candidates showed a trend similar to their respective anodic activity. Again, tin was cathodically the most reactive in 250ppm NaCl with highest cathodic current density and no reduction in the cathodic current density could be achieved even by alloying Ge with substantial proportions of Au. Thus, by alloying Sn with Au, both the anodic and the cathodic reactivities of the alloy could be reduced while no significant reduction in both the anodic and the cathodic reactivities could be achieved by alloying Ge with Au.

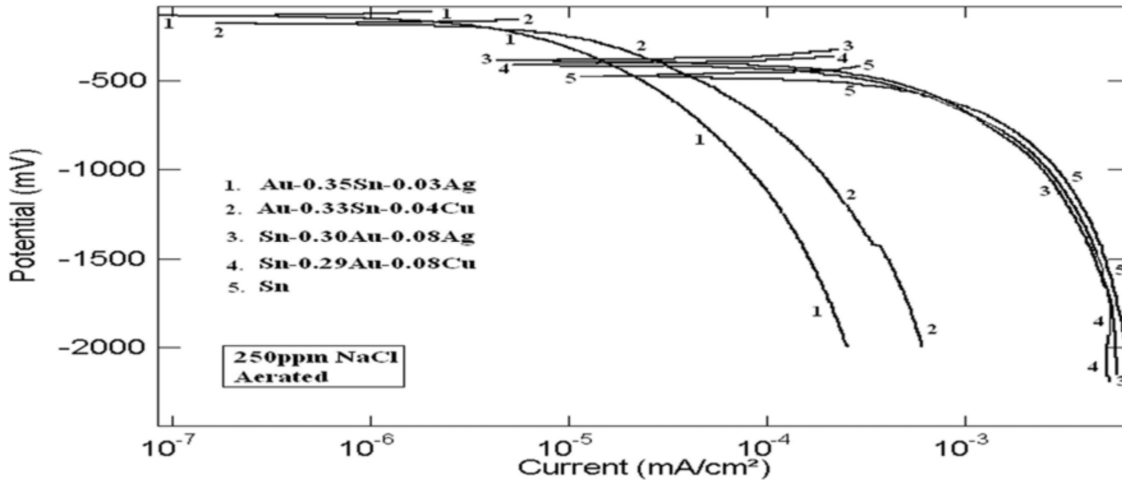

Figure 8.3. Cathodic polarization curves for Au-Sn based candidate alloys.

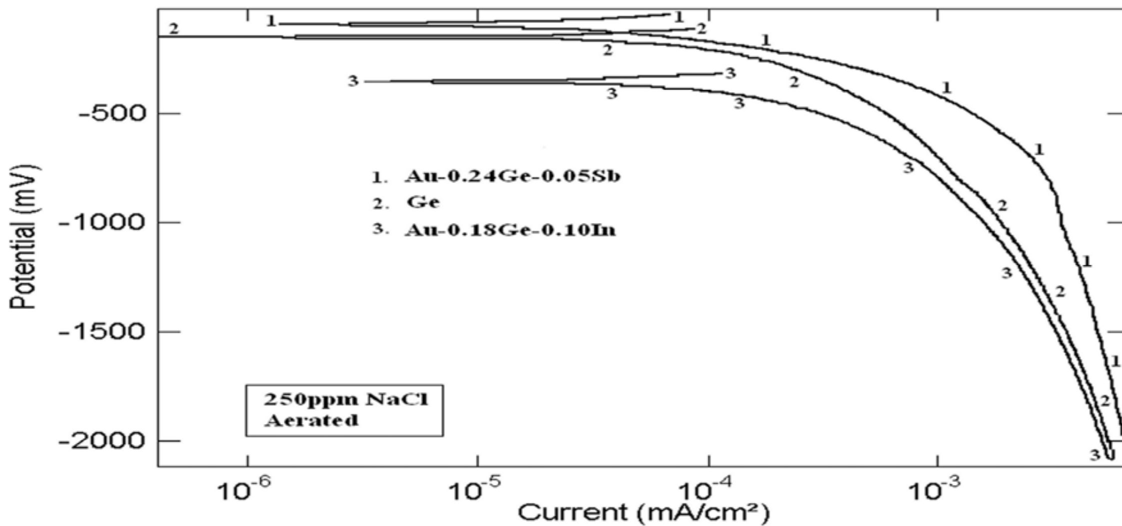

Figure 8.4. Cathodic polarization curves for Au-Ge based candidate alloys.

High-temperature solders are currently being used in applications involving high potential bias. All the solder candidates along with their pure metals were compared at a constant E_{corr} value of 1.5V and are illustrated in Figure 8.5. Ge exhibits both less anodic and cathodic current densities when compared to Sn. However, substantial reduction in both the current densities could be achieved when Sn is alloyed with Au while no significant reduction in any of the current densities could be achieved even by alloying relatively higher proportions of Au to Ge. Thus, Au-Sn based solder alloy candidates close to the eutectic composition are more corrosion resistant compared to the Au-Ge based ones and are much suited to high-temperature applications generally involving high current density. However, the corrosion resistance property of the Au-Ge based solder alloy candidates is almost similar to that of the Au-Sn based solder alloy candidates involving high content of Sn i.e. the Sn rich side of the Au-Sn based systems (Au-Sn-Ag/Au-Sn-Cu).

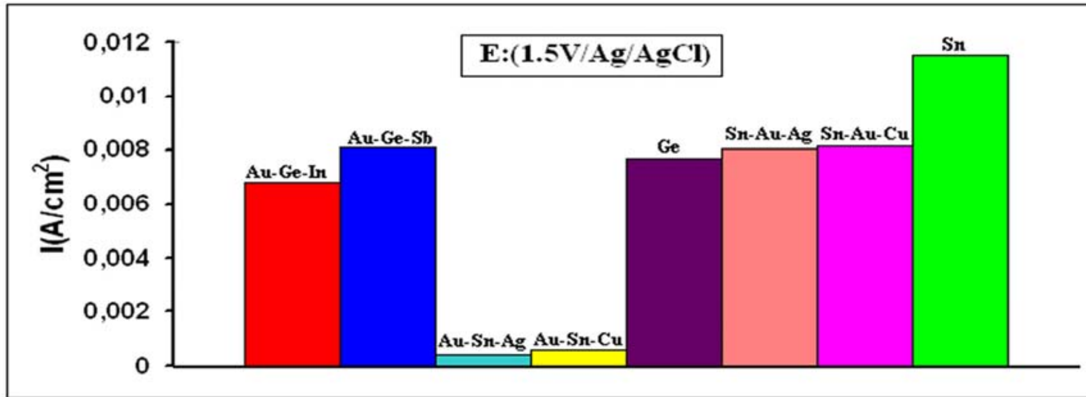

Figure 8.5. A comparison of Au-Sn and Au-Ge based candidate alloys with respect to their current density.

8.5. Electrochemical and Galvanic Coupling

Corrosion of solder alloys, in the presence of a suitable electrolyte can occur either due to the potential difference between the major phases in the alloy or galvanic coupling between one or more phases of the alloy and other parts of the microelectronics device since solder alloys are electrically connected with other metallic components in the electronic devices [3]. Moreover, all these materials including gold are soluble in chloride containing environments at varying pH and potential conditions (Table 2.6).

Temperature fluctuations are common during storage and shipment. These temperature swings can result in a large amount of condensation inside a package. During the warmer period, water vapor penetrates the packaging materials. This gives way to the cooler period. When the temperature reaches the dew point inside, the package condensation occurs. These water droplets (moisture) along with chlorides create conditions conducive to both electrochemical and galvanic corrosion. Electronic devices tend to dissipate heat during operation which leads to reduced relative humidity. During power-down or storage periods, the relative humidity rises and this presents more danger [118]. The risk of corrosion in harsh/humid conditions for these potential ternary solder alloy candidates is higher as compared to the currently used Pb-Sn solder alloy for this application since the galvanic potential difference between lead and tin is rather small while the galvanic potential difference between the constituents in these promising ternary alloys is higher.

Cu and Ni are commonly being used as the solder wettable layers of the UBM [105]. The solder alloys could interact with the wetting layers of the UBM in a hostile environment generating galvanic couples. The anodic and the cathodic polarization curves of these solder wettable layers are illustrated in Figures 8.6 and 8.7. Cu in comparison with Ni has ~300mV noble E_{corr}. Ni exhibited higher anodic current density when compared to Cu over a range of potentials. However, Cu was cathodically more reactive in 250ppm NaCl solution than Ni.

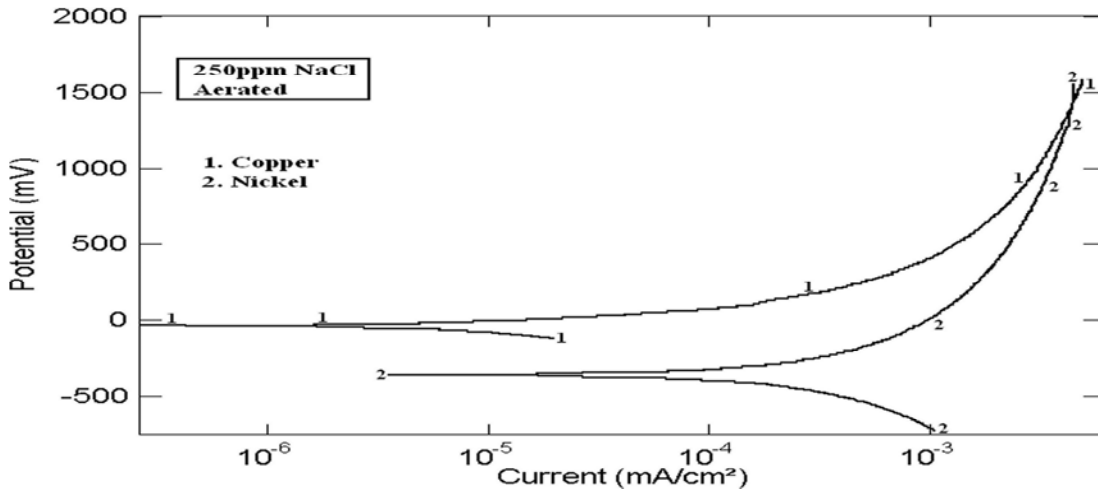

Figure 8.6. Anodic polarization curves for solder wettable layers.

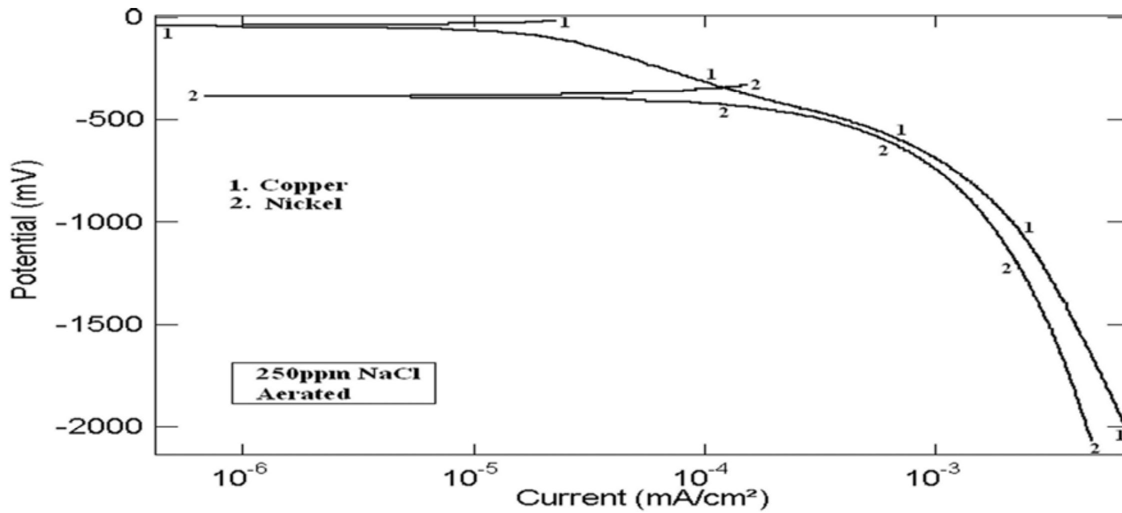

Figure 8.7. Cathodic polarization curves for solder wettable layers.

A comparison between the electrochemistry of potential solder alloys and the solder wettable layers of the UBM shows that a cross galvanic coupling could be feasible between them. Electrochemically as the E_{corr} value suggests, Cu is nobler than all these potential solder alloys. Therefore, ín hostile environments the Cu (UBM) could act as an additional cathode area to drive corrosion on these promising solders alloys. Moreover, the electrochemical results show that the Cu is a good cathode. This could further exacerbate the corrosion mechanism. Similarly as the E_{corr} value suggests, all these potential solder alloys other than Sn-0.30Au-0.08Ag and Sn-0.29Au-0.08Cu are nobler than the Ni (UBM). Therefore, in hostile environments these solder alloy candidates could act as an additional cathode area to drive corrosion on the Ni (UBM). Generally, the potential bias between the solder-UBM would be a key factor in dictating how the corrosion proceeds [105]. If the potential is high enough, it can cause even dissolution of Ni in the chloride solution in the latter scenario. Thus, there is a high risk of corrosion for both these potential candidate alloys and also the solder wettable layers of the UBM.

8.6. Corrosion Surface Morphology after Polarization

The electrochemical results of Au-Sn based candidate alloys were anticipated. SEM analysis was carried out on Au-Ge based solder candidates after polarization tests to determine the corrosion surface morphology and also the corrosion products. The solders were thoroughly washed with water prior to SEM analysis to remove any residual NaCl on the surface. Small pits were found distributed throughout the surface of Au-0.18Ge-0.10In and Au-0.24Ge-0.05Sb solder alloys after polarization tests as shown in Figures 8.8a and 8.8b respectively. In addition, the corrosion products that were predominantly germanium oxides and germanium chlorides were also found on the surfaces of both the Au-Ge based solder alloys along with these pits as shown in Figure 8.9.

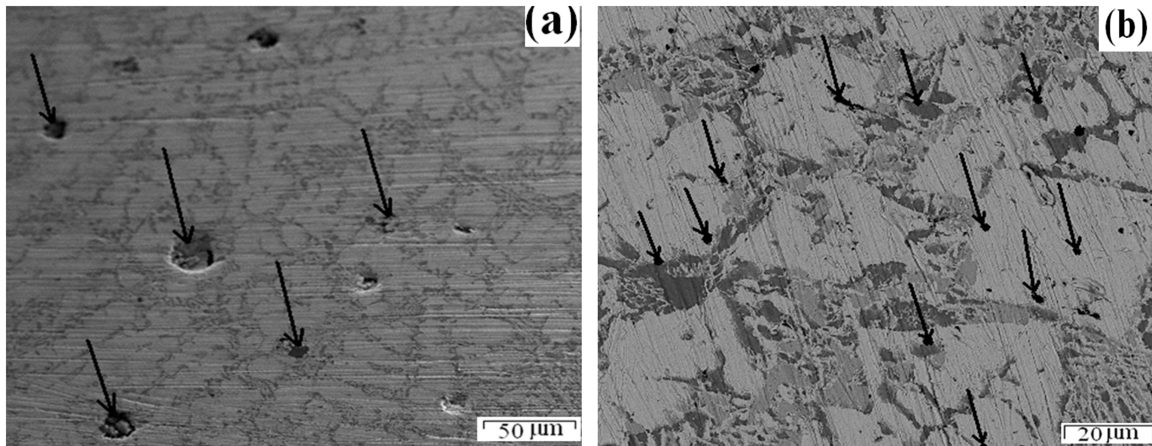

Figure 8.8. SEM-BSE micrographs of the surface morphology (a) Au-0.18Ge-0.10In candidate alloy and (b) Au-0.24Ge-0.05Sb candidate alloy.

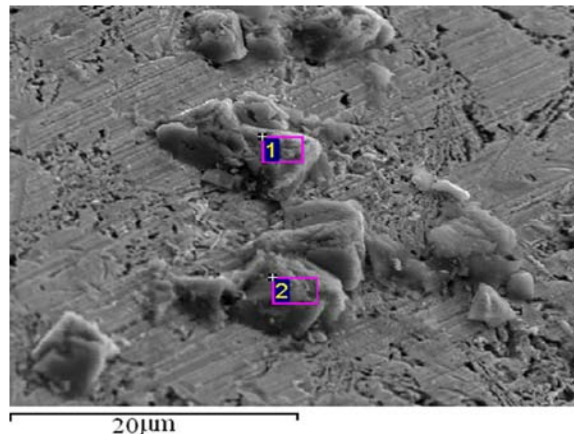

Figure 8.9. Corrosion products observed on the surfaces of both the Au-Ge based candidate alloys after polarization tests.

The EDX spot analysis was used to identify the phases. The gray areas in Figure 7.8a were determined as (Ge) phase. The white areas in the Figure 8.8a could be either (Au) or ζ phase. These two phases could not be distinguished due to the limitations of the technique. The white, pale gray and dark gray areas in Figure 8.8b were identified as (Au), AuSb2 and (Ge) phases respectively.

In the case of Au-Ge based candidate alloys, both Au and Ge exist in the microstructure as (Au) and (Ge) phases respectively. The difference in the electromotive force between these phases is large and hence, corrosion is likely to take place because the electrochemical coupling in the presence of chloride solution is high. Electrochemically, Au is nobler than Ge. Therefore, if there is an electrochemical coupling between the (Au) and (Ge) phases, the (Au) phase could act as a cathode area to drive corrosion on the (Ge) phase. Moreover, Ambat et. al. [105] have determined gold to be an active cathode. Enhanced corrosion could occur because of the low anode [dispersed (Ge) phase]/ cathode [matrix (Au) phase] ratio. Thus, the formation of these pitted areas could be attributed to the severe localized corrosion of (Ge) phase in the Au-Ge based candidate alloys.

8.7. Findings

Au-Sn based candidate alloys close to the eutectic composition are more corrosion resistant than the Au-Ge based ones. The corrosion resistance property of Ge could not be improved even by alloying with very high proportions of Au due to the selective localized corrosion of (Ge) phase in the Au-Ge based candidate alloys. Overall, the results of this investigation present the possible corrosion scenario between these promising candidate alloys and the UBM due to combination of materials with different electrochemical properties. Moreover, applications where high-temperature solders are employed involve high potential bias and high current density and hence, there could be additional issues in the advanced electronic packagings due to combination of potential, environment and material. Therefore, a thorough investigation has to be carried out on these issues related to corrosion before replacing the high-lead containing solder alloys with any of these potential candidate alloys for high temperature applications.

Chapter 9

Summary of Appended Papers

9.1. Paper I

Vivek Chidambaram, John Hald and Jesper Hattel. *A feasibility study of lead free solders for level 1 packaging applications*. Journal of Microelectronics and Electronic Packaging. 6: 75-82, 2009.

This paper presents the possible ternary combinations involving gold that could adhere to the required solidification criterion based on solidification simulations under equilibrium conditions. These combinations were designed for the commercially preferred narrow solidification range. The optimized ternary compositions were further scrutinized based on Scheil solidification simulations and the probability of microsegregation was envisaged. An assessment of all the elements that is popular for this application has been carried out based on surface tension, natural radius of curvature, oxidation resistance and environmental oriented issues.

9.2. Paper II

Vivek Chidambaram, John Hald and Jesper Hattel. *Development of gold based solder candidates for flip chip assembly*. Journal of Microelectronics Reliability. 49: 323-330, 2009.

In this paper, the optimized ternary compositions were further evaluated based on the prediction of phases in the bulk solder and the probability of IMCs formation between the solder and the under-bump metallization (UBM) during the wetting reaction as well as the solid state aging since the reliability of the solder joint is directly influenced by the phases in the bulk solder and the IMCs formed between the solder and the UBM.

9.3. Paper III

Vivek Chidambaram, John Hald and Jesper Hattel. *Development of Au-Ge based candidate alloys as an alternative to high-lead content solders*. Journal of Alloys and Compounds, 490: 170-179, 2010.

In this paper, an attempt has been made to reduce the melting point of the Au-Ge eutectic by micro-alloying it with the low melting point metals namely In, Sb and Sn and thereby adhere to the required solidification criterion. The changes in microstructure and microhardness associated with the alloying of these low melting point metals have been extensively reported. Furthermore, the effects of thermal aging on the microstructure and microhardness of these promising Au-Ge based candidate alloys have been included. The

results were analyzed to determine whether micro-alloying Au-Ge eutectic with these low melting point metals could induce softness to this otherwise hard eutectic solder.

9.4. Paper IV

Vivek Chidambaram, Jesper Hattel and John Hald. *Design of lead-free candidate alloys for high-temperature soldering based on the Au-Sn system*. Journal of Materials and Design. 31: 4638-4645, 2010.

In this paper, an effort has been made to suppress the brittle Au5Sn phase of the Au-20Sn (wt. %) by micro-alloying it with Ag/Cu. The changes in microstructure and microhardness associated with the alloying of Ag and Cu to the Au rich side as well as to the Sn rich side of the Au-Sn binary system were explored since the phase-equilibria calculations show that the required solidification criterion could also be achieved with a high Sn content in these alloys. Furthermore, the effects of thermal aging on the microstructure and microhardness of these promising Au-Sn based ternary systems were investigated.

9.5. Paper V

Vivek Chidambaram, John Hald, Rajan Ambat and Jesper Hattel. *A corrosion investigation of solder candidates for high-temperature applications*. Journal of Minerals, Metals and Materials Society. 61: 59-65, 2009.

In this paper, the prospective lead-free candidate alloys for high-temperature soldering were investigated from a corrosion perspective. The possibility of galvanic coupling between the commonly used wetting layers of the under-bump metallization and these prospective candidate alloys were envisaged. An overview of corrosion related problems; that have to be thoroughly investigated before substituting the currently used one has been reported.

9.6 Paper VI

Vivek Chidambaram, Jesper Hattel and John Hald. *Status of lead-free solders for high-temperature soldering*. Submitted to Journal of Electronic Materials, 2010.

This paper presents the possible alternatives for the high-lead content solders that are currently being employed in advanced electronic packaging applications. It demonstrates the superior characteristics as well as some drawbacks of these promising alternatives. Furthermore, a comprehensive comparison of the high-temperature stability of microstructures and mechanical properties of these potential candidate alloys with respect to the currently used high-lead content solders is made. This paper also reviews other alternative technologies for high-temperature lead-free soldering since none of the prospective candidate alloys could cover the spectrum of properties required for being accepted as a standard soft solder for high-temperature applications.

Chapter 10

Concluding Remarks

The currently used high-lead content solders are being applied for various applications irrespective of the operating temperatures (150-200°C) and this is primarily because their microstructure does not consist of any intermetallic compound. Thus, the operating temperatures do not have a major impact on their microstructure. In the case of lead-free, a single high-temperature solder cannot cover all the applications ranging from 150°C to 200°C.

Among the Au-Sn based candidate alloys, Au-0.35Sn-0.03Ag and Au-0.33Sn-0.04Cu are promising candidate alloys for applications in the higher end of the temperature range i.e. close to 200°C. For applications, involving the lower end of the temperature range i.e. close 150°C, both the candidate alloys close to the Au-Sn eutectic as well as the ones on the Sn rich side can be considered.

Among the Au-Ge based candidate alloys, it was determined that the addition of Sb to the Au-Ge eutectic would not only decrease its melting point but also would improve its ductility substantially despite the presence of a very hard IMC (AuSb2). It was also determined that the addition of In to the Au-Ge eutectic would further enhance the hardness of the alloy due to the effective lattice strains induced by the In atoms and thereby making it ideal for applications like opto-electronic packaging.

The currently used high-lead content solders are used mainly in the form of wires or ribbons for die-attaching. The high hardness of the possible candidate alloys other than Bi-Ag alloys causes some obstacles in introducing these alloys to actual products since it is hard to supply these alloys in the form of wires or ribbons. Thus, applying these alloys entails an expensive development effort for die-attach machines that handle solder in different forms. Furthermore, the risk of corrosion of these prospective candidate alloys is also estimated to be higher than the existing high-lead content solders.

Considering gold as a potential substitute for lead would substantially increase the cost of high-temperature solders. Although the initial costs would be higher there would potentially be a value to the recycled product and no disposal costs associated with the solders, resulting in lower life time costs for the product.

Chapter 11

Outlook

The experimental work done in this Ph.D work characterized the properties of only bulk solders and did not consider factors such as reactions with joining materials which may affect the mechanical properties of actual solder joints. Thus, a comprehensive study on the IMC formation between these prospective candidate alloys and the under-bump metallization has to be carried out since the reliability of the solder joint is directly influenced by both the phases in the bulk solder and also the IMCs formed between the solder and the solder wettable layer of the under-bump metallization during both the wetting reaction or/and the solid state aging.

The contact angle measurements between these prospective candidate alloys and the under-bump metallization have to be carried out since it is very critical for replacing the high-lead content solders due to the high surface tension of gold. The potential candidate alloys are relatively more creep resistant than the high-lead content solders due to their higher strength. However, their thermo-mechanical fatigue resistance has to be investigated in a comprehensive way in order to ensure reliability of the electronic packaging. It is interesting to know from the recent publications that Au-Sn eutectic exhibits superior thermal fatigue resistance despite being hard.

As none of the possible candidate alloys that could adhere to the required solidification criterion for first level packaging applications could emulate the existing high-lead content solders, it is now important to focus on other substitute joining technologies for the traditional soldering. Thus, much work is required to establish a sound scientific basis to promote high-temperature lead-free soldering.

References

[1] N. Kang, H.S. Na, S.J. Kim and C.Y. Kang. Alloy design of Zn-Al-Cu solder for ultra high temperatures. Journal of Alloys and Compounds. 467: 246-250, 2009.

[2] K. Suganuma, S-J. Kim and K-S. Kim. High-temperature lead-free solders: properties and possibilities. JOM. 61: 64-71, 2009.

[3] M. Abtew and G. Selvaduray. Lead-free solders in microelectronics. Journal of Materials Science and Engineering. 27: 95-141, 2000.

[4] S-J. Kim, K-S. Kim, S-S. Kim, K. Suganuma and G. Izuta. Improving the reliability of Si die attachment with Zn-Sn based high-temperature Pb-free solder using a TiN diffusion barrier. Journal of Electronic Materials. 38: 2668-2675, 2009.

[5] S-J. Kim, K-S. Kim, S-S. Kim, C-Y. Kang and K. Suganuma. Characteristics of Zn-Al-Cu alloys for high-temperature solder application. Journal of Materials Transactions. 49: 1531-1536, 2008.

[6] Y. Yamada, Y. Takaku, Y. Yagi, Y. Nishibe, I. Ohnuma, Y. Sutou, R. Kainuma and K. Ishida. Pb-free high temperature solders for power device packaging. Journal of Microelectronics Reliability. 46: 1932-1937, 2006.

[7] J.H. Kim, S.W. Jeong and H.M. Lee. Thermodynamics-aided alloy design and evaluation of Pb-free solders for high-temperature applications. Materials Transactions. 43: 1873-1878, 2002.

[8] COST ACTION MP0602. Memorandum of understanding for the implementation of a European concerted research action. Advanced solder materials for high-temperature applications. Brussels, 2006.

[9] K.N. Tu, A.M. Gusak and M. Li. Physics and material challenges for lead-free solders. Journal of Applied Physics. 93: 1335-1351, 2003.

[10] T. Braun, K-F. Becker, M. Koch, V. Bader, R. Aschenbrenner and H. Reichl. High-temperature reliability of flip chip assemblies. Journal of Microelectronics Reliability. 46: 144-154, 2006.

[11] M. J. Wolf, G. Engelmann, L. Dietrich and H. Reichl. Flip chip bumping technology – status and update. Journal of Nuclear Instruments and Methods in Physics Research. 565: 290-295, 2006.

[12] NexLogic Corporation. Product data sheet. www.nexlogic.com, accessed on April 3, 2010.

[13] Intel Corporation. Product data sheet. www.intel.com, accessed on April 2010.

[14] ChipSupply Corporation. Product data sheet. www.chipscale.com accessed on April 2010.

[15] Intel Corporation. Product data sheet. www.intel.com, accessed on April 2010.

[16] C-Mac Technology. Product data sheet. www.cmac.com, accessed on April 2010.

[17] Palomar Technologies. Product data sheet. www.palomar.com, accessed on April, 2010.

[18] C.J. Yang, M.G. Cho and H.M. Lee. Synthesis of the combination solder of 80Au-20Sn/42Sn-58Bi and thermodynamic interpretation of the microstructural evolution. Materials Transactions. 49: 376-381, 2008.

[19] O.A. Ogunseitan. Public health and environmental benefits of adapting lead-free solders. JOM. 59: 12-17, 2007.

[20] Y. Takaku, I. Ohnuma, R. Kainuma, Y. Yamada, Y. Yagi, Y. Nishibe and K. Ishida. Development of Bi-based high-temperature Pb-free solders with second phase dispersion: thermodynamic calculation, microstructure and interfacial reaction. Journal of Electronic Materials. 35: 1926-1931, 2006.
[21] C. Andersson and J. Liu. Effect of corrosion on the low cycle fatigue behavior of Sn-4.0Ag-0.5Cu lead-free solder joints. International Journal of Fatigue. 30: 917-930, 2008.
[22] Y. Shi, W. Fang, Z. Xia, Y. Lei, F. Guo and X. Li. Journal of Materials Science: Materials in Electronics. DOI 10.1007/s10854-009-0010-5.
[23] Z. Moser, W. Gasior, A. Debski and J. Pstrus. Surface tension and density database. Institute of Metallurgy and Materials Science, Polish Academy of Sciences, Krakow.
[24] J.N. Lalena, N.F. Dean and M.W. Weiser. Experimental investigation of Ge-Doped Bi-11Ag as a new Pb-free solder alloy for power die attachment. Journal of Electronic Materials. 31: 1244-1249, 2002.
[25] P. Van Der Krogt. Elementymology and elements multidict. http://elements.vanderkrogt.net/elem/pb.html, accessed on February 4, 2007.
[26] H.L. Needleman. History of lead poisoning in the world. Implementing a National program in developing countries, The George Foundation, Bangalore, India, 1999.
[27] H.L. Needleman. Low level lead exposure and neurophysical performance. Lead versus wealth, John Wiley and Sons Ltd., New York, 1983.
[28] Blacksmith Institute. The World's worst polluted places. www.blacksmithinstitute.org, accessed on February 2007.
[29] C. Cabral, Jr., K.P. Rodbell and M.S. Gordon. Alpha particle mitigation strategies to reduce chip soft error upsets. Journal of Applied Physics. 101:014902-014906, 2007.
[30] US Environmental Protective Agency (EPA). www.epa.gov, accessed on April 2008.
[31] E.R. Monsalve. Lead ingestion hazard in hand soldering environment. In proceedings of the 8th Annual Soldering and Product Assurance Seminar, Naval Weapons Center, China Lake, CA, February 1984.
[32] S. Heart. Green electronics through legislation and lead free soldering. Journal of Clean-Soil, Air, Water. 36: 145-151, 2008.
[33] A.A. Shapiro, J.K. Bonner, O.A. Ogunseitan, J-D.M. Saphores and J.M. Schoenung. Implications of Pb-free microelectronics assembly in aerospace applications. IEEE Transactions on Components and Packaging Technologies. 29: 60-70, 2006.
[34] European Union. Directive 2002/96/EC of the European Parliament and of the Council of 27 January 2003 on Waste Electrical and Electronic Equipment (WEEE). Official Journal of the European Union, pages L37/24-L37/38, February 13, 2003.
[35] European Union. Directive 2002/95/EC of the European Parliament and of the Council of 27 January 2003 on the Restriction of the Use of Certain Hazardous Substances in Electrical and Electronic Equipment. Official Journal of the European Union, pages L37/19-L37/23, February 13, 2003.
[36] European Union. 2005/618/EC: Commission Decision of 18 August 2005 amending Directive 2002/95/EC of the European Parliament and of the Council for

the purpose of establishing the maximum concentration values for certain hazardous substances in electrical and electronic equipment. Official Journal of the European Union, page L214/65, August 19, 2005.
[37] European Union. Guidance document on RoHS/WEEE. http://europa.eu.int/comm./environment/waste/pdf/faq_weee.pdf, March 16, 2007.
[38] European Union. 2005/747/EC: Commission Decision of 21 October 2005 amending for the purposes of adapting to technical progress the Annex to Directive 2002/95/EC of the European Parliament and of the Council on the restriction of the use of certain hazardous substances in electrical and electronic equipment. Official Journal of the European Union, pages L280/18-L280/19, October 25, 2005.
[39] M. Pecht and S. Ganesan. Lead-free electronics. John Wiley & sons, Inc, Hoboken New Jersey, 1st edition, 2006.
[40] J.M. Schoenung, O.A. Ogunseitan, J-D.M. Saphores and A.A. Shapiro. Adapting lead-free electronics: policy differences and knowledge gaps. Journal of Industrial Ecology. 8: 59-82, 2005.
[41] ERA Technology. Product data sheet. http://www.era.co.uk, accessed on March 2008.
[42] J. D. Lincoln, O.A. Ogunseitan, A.A. Shapiro and J-D.M. Saphores. Leaching assessments of hazardous materials in cellular telephones. Journal of Environmental Science and Technology. 41: 2572-2578, 2007.
[43] A.Z. Miric and A. Grusd. Lead-free alloys. Journal of Soldering and Surface Mount Technology. 10: 19-25, 1998.
[44] N.I. Sax and R.J. Lewis, Sr. Dangerous properties of Industrial Materials, 7th edition, Van Nostrand Reinhold, Newyork, 1989.
[45] US Department of Labor. Occupational Safety and Health Administration. http://www.osha.gov, accessed on February 2008.
[46] J. H. Richard and W. C. Christopher. Trends in the use of gold in current industrial applications. World Gold Council, London, 2002.
[47] H. Baba. An efficient recovery of gold and other noble metals from electronic and other scraps. Journal of Conservation and Recycling. 10: 247-252, 1987.
[48] United States Geological Survey. www.minerals.usgs.gov/minerals/pubs/mcs, accessed on December 2007.
[49] T. Laurila, V. Vuorinen and J.K. Kivilahti. Interfacial reactions between lead-free solders and common base materials. Journal of Materials Science and Engineering. 49: 1-60, 2005.
[50] P. Limaye, B. Vandevelde, R. Labie, D. Vandepitte and B. Verlinden. Influence of intermetallic properties on reliability of lead-free flip-chip solder joints. IEEE Transactions on Advanced Packaging. 31: 51-57, 2008.
[51] K.N. Tu and K. Zeng. Tin-lead (SnPb) solder reaction in flip chip technology. Journal of Materials Science and Engineering. 34:1-58, 2001.
[52] R.J.K. Wassnik. Soldering in electronics. Electrochemical Publications Ltd, G.B-Port Erin, British Isles, 2nd edition, 1989.
[53] F.H. Howie and C. Lea. Blowholing in PTH solder fillets-towards a solution. In proceedings of INTERNEPCON, Brighton, UK, 1984.
[54] R.A. Deighan. Surface tension of solder alloys. International Journal of Hybrid Electronics. 5: 307-313, 1982.

[55] M.A. Caroll and M.E. Warwick. Surface tension of some Sn-Pb alloys: Part I. effect of Bi, Sb, P, Ag and Cu on 60Sn-40Pb solder. Journal of Materials Science and Technology. 3: 1040-1045, 1986.
[56] Scientific Group Thermodata Europe (SGTE), SSUB3 substances database version 3.2, 2001/2002/2004.
[57] P.J. Martin, W.B. Johnson and B.A. Miksic. Corrosion inhibition of electronic materials using vapor phase inhibitors. Presentation at National Association of Corrosion Engineer Meeting, New Orleans, LA, 1984.
[58] J.S. Hwang. Solder paste in electronic packaging. Van Nostrand Reinhold, New York, 1989.
[59] D.R. Frear. The mechanical behavior of interconnect materials for electronic packaging. Journal of Materials. 48: 49-53, 1996.
[60] D.S. Patterson, P. Elenius and J.A. Leal. Wafer bumping technologies: A comparative analysis of solder deposition processes and assembly considerations. In Proceedings of Interpack. 19: 337-351, 1997.
[61] A. Brenner. Electrodeposition of alloys: principles and practice. Vol. 1 and Vol. 2, Academic Press, New York.
[62] T. Shimizu, H. Ishikawa, I. Ohnuma and K. Ishida. Zn-Al-Mg-Ga alloys as Pb-free solder for die attaching use. Journal of Electronic Materials. 28: 1172-1175, 1999.
[63] K.J.R. Wasnik and M.M.F. Verguld. Manufacturing techniques for surface mounted assemblies. Electrochemical Publication Ltd., GB-Port Erin, British Isles, 1995.
[64] Z. Wu, J. Li, D. Timmer, K. Lozano and S. Bose. Study of processing variables on the electrical resistivity of conductive adhesives. International Journal of Adhesion and Adhesives. 29: 488-494, 2009.
[65] D. Wojciechowski, J. Vanfleteren, E. Reese and H-W. Hagedorn. Electro-conductive adhesives for high density package and flip-chip interconnections. Journal of Microelectronics Reliability. 40: 1215-1226, 2000.
[66] Y. Li and C.P. Wong. Recent advances of conductive adhesives as a lead-free alternative in electronic packaging: Materials, processing, reliability and applications. Journal of Materials Science and Engineering. 51: 1-35, 2006.
[67] I. Mir and D. Kumar. Recent advances in isotropic conductive adhesives for electronic packaging applications. International Journal of Adhesion and Adhesives. 28: 362-371, 2008.
[68] F. Tan, X. Qiao, J. Chen and H. Wang. Effects of coupling agents on the properties of epoxy-based electrically conductive adhesives. International Journal of Adhesion and Adhesives. 26: 406-413, 2006.
[69] J.E. Morris. Isotropic conductive adhesives: Future trends, possibilities and risks. Journal of Microelectronics Reliability, 47: 328-330, 2007.
[70] M. Yamashita and K. Suganuma. Improvement in high-temperature degradation by isotropic conductive adhesives including Ag-Sn alloy fillers. Journal of Microelectronics Reliability. 46: 850-858, 2006.
[71] S. Xu, D.A. Dillard and J.G. Dillard. Environmental aging effects on the durability of electrically conductive adhesive joints. International Journal of Adhesion and Adhesives. 23: 235-250, 2003.
[72] H-H. Lee, K-S. Chou and Z-W. Shih. Effect of nano-sized particles on the resistivity of polymeric conductive adhesives. International Journal of Adhesion

and Adhesives. 25: 437-441, 2005.
[73] E. Lugscheider, K. Bobzin and A. Erdle. Solder deposition for transient liquid phase (TLP)-bonding by MSIP-PVD-process. Journal of Surface and Coatings Technology. 174-175: 704-707, 2003.
[74] W. Zhang and W. Ruythooren. Study of the Au/In reaction for transient liquid-phase bonding and 3D Chip Stacking. Journal of Electronic Materials. 37: 1095-1101, 2008.
[75] G. Humpston, D.M. Jacobsen and S.P.S. Sangha. Diffusion soldering for electronics manufacturing. Journal of Endeavour. 18: 55-60, 1994.
[76] W.F. Gale and D.A. Butts. Transient liquid phase bonding. Journal of Science and Technology of Welding and Joining. 9: 283-300, 2004.
[77] A. Kodentsov. On the merits of transient liquid phase bonding as a substitute for soldering with high-Pb alloys. Technical Program Abstract. TMS Annual Meeting, Seattle, WA, February 2010.
[78] N.S. Bosco and F.W. Zok. Critical interlayer thickness for transient liquid phase bonding in the Cu-Sn system. Journal of Acta Materialia. 52: 2965-2972, 2004.
[79] M. Rettenmayr, P. Lambracht, B. Kempf and M. Graff. High meting Pb-free solder alloys for die-attach applications. Journal of Advanced Engineering Materials. 7: 965-969, 2005.
[80] J-M. Song, H-Y.Chuang and Z-M. Wu. Interfacial reactions between Bi-Ag high-temperature solders and metallic substrates. Journal of Electronic Materials. 35: 1041-1049, 2006.
[81] J-M. Song, H-Y.Chuang and T-X. Wen. Thermal and tensile properties of Bi-Ag alloys. Metallurgical and Materials Transactions A. 38A: 1371-1375, 2007.
[82] Y. Takaku, K. Makino, K. Watanabe, I. Ohnuma, R. Kainuma, Y. Yamada, Y. Yagi, I. Nakagawa, T. Atsumi and K. Ishida. Interfacial reaction between Zn-Al based high-temperature solders and Ni substrate. Journal of Electronic Materials. 38: 54- 60, 2008.
[83] E. Gervais. R.J. Barnust and C.A. Loong. An analysis of selected properties of ZA alloys. Journal of Metals. 37: 43-47, 1985.
[84] F. Cay and S.C. Kurnaz. Hot tensile and fatigue behaviour of zinc-aluminum alloys produced by gravity and squeeze casting. Journal of Materials and Design. 26: 479-485, 2005.
[85] London Metals Exchange. http://www.lme.co.uk, accessed on May 2008.
[86] M. Rettenmayr, P. Lambacht, B. Kempf and C. Tschudin. Zn-Al based alloys as Pb-free solders for die-attach. Journal of Electronic Materials. 31: 278-285, 2002.
[87] S-J. Kim, K-S. Kim, S-S. Kim, C-Y. Kang and K. Suganuma. Characteristics of Zn-Al-Cu alloys for high-temperature solder application. Materials Transactions. 49: 1531-1536, 2008.
[88] J. Jiang, J-E. Lee, K-S. Kim and K. Suganuma. Oxidation behavior of Sn-Zn solders under high-temperature and high-humidity conditions. Journal of Alloys and Compounds. 462: 244-251, 2008.
[89] N. Saunders and A.P. Midownik. CALPHAD: Calculation of phase diagrams. Pergamon Materials Series, 1998.
[90] H.L. Lukas, S.Z. Fries and B. Sundman. Computational thermodynamics: The calphad method. Cambridge University Press, United Kingdom, 2007.

[91] A. Kroupa, A.T. Dinsdale, A. Watson, J. Vrestal, J. Vizdal and A. Zemanova. The Development of the COST 531 Lead-Free Solders Thermodynamic Database. JOM. 59: 20-25, 2007.
[92] U.R. Kattner. The thermodynamic modeling of multicomponent phase equilibria. JOM. 49: 14-19, 1997.
[93] B. Sundman. Thermo-Calc user's guide. Division of computational thermodynmics, Department of Materials Science and Engineering, Royal Institute of Technology, Stockholm, Sweden.
[94] Scientific Group Thermodata Europe (SGTE). SSOL2 Solutions Database Version 2.1, 1999/2002/2003.
[95] A.T. Dinsdale, A. Watson, A. Kroupa, A. Zemanova, J. Vrestal and J. Vizdal. COST 531 Database Version 3.0, 2008.
[96] U.R. Kattner and C.A. Handwerker. Calculation of phase equilibria in candidate solder alloys. International Journal of Materials Research. 92: 1-9, 2001.
[97] U. R. Kattner. Phase diagrams for lead-free solder alloys. JOM. 54: 45-51, 2002.
[98] J. Campbell. Castings. Butterworth-Heinemann Ltd, Oxford, 1995.
[99] R.R. Chromik, D-N. Wang, A. Shugar, L. Limata, M.R. Notis and R.P. Vinci. Mechanical properties of intermetallic compounds in the Au-Sn system. Journal of Materials Research. 20: 2161-2171, 2005.
[100] C.E. Ho, S.C. Young and C.R. Kao. Interfacial reaction issues for lead-free electronic solders. Journal of Materials Science: Materials in Electronics. 18: 155-174, 2007.
[101] C.W. Chang, Q.P. Lee, C.E. Ho and C.R. Kao. Cross-interaction between Au and Cu in Au/Sn/Cu ternary diffusion couples. Journal of Electronic Materials. 35: 366-371, 2006.
[102] R. Bergmann, P.T. Tang, H.N. Hansen and P. Møller. Insitu investigation of lead-free solder alloy using a hot-plate microscope. In Proceedings of EPTC Conference, Singapore, 2007.
[103] R. Bergmann. High-temperature lead-free solder for MEMS packaging. Ph.D Dissertation, 2009.
[104] R. Ambat. Localized corrosion information using high resolution measurement devices. In Proceedings of the Eurocorr Conference, Lisbon, Portugal, 2005.
[105] R. Ambat and P. Møller. Corrosion investigation of material combination in a mobile phone dome-pad system. Journal of Corrosion Science. 49: 2866-2879, 2007.
[106] H.K. Danielsen. Z-phase in 9-12%Cr Steels. Ph.D Dissertation, 2007.
[107] C. Wei, Y. Liu, Z. Gao, J. Wan and C. Ma. Effects of thermal aging on microstructure and microhardness of Sn-0.37Ag-0.9Zn-1In solder. Journal of Electronic Materials. 38: 345- 350, 2008.
[108] M. He and V.L. Acoff. Effect of reflow and thermal aging on the microstructure and microhardness of Sn-3.7Ag-xBi solder alloys. Journal of Electronic Materials. 35: 2098-2106, 2006.
[109] R.A. Islam, B.Y. Wu, M.O. Alam, Y.C. Chan and W. Jillek. Investigations on microhardness of Sn-Zn based lead free solder alloys as replacement of Sn-Pb solder. Journal of Electronic Materials. 392: 149-158, 2005.

[110] N.S. Ong. Manufacturing cost estimation for PCB assembly: An activity based approach. International Journal of Production Economics. 38: 159-172, 1995.
[111] P.S. Schein, T. Smythe, D. Hoth, F. Smith, J.S. Mac Donald and P.V. Woolley. Phase I clinical trial of spirogermanium. Cancer Treatment Report. 64: 1051-1056, 1980.
[112] H. Schoeller, S. Bansal, A. Knobloch, D. Shaddock and J. Cho. Microstructure evolution and the constitutive relations of high-temperature solders. Journal of Electronic Materials. 38: 802-809, 2009.
[113] G.S. Matijasevic, C.C. Lee and C.Y. Wang. Au-Sn alloy phase diagram and properties related to its use as a bonding medium. Journal of Thin Solid Films. 223: 276-287, 1993.
[114] V. Grolier and R. Schmid-Fetzer. Thermodynamic evaluation of the Au-Sn system. International Journal of Materials Research. 98: 797-806, 2007.
[115] J. Ciulik and M.R. Notis. The Au-Sn phase diagram. Journal of Alloys and Compounds. 191: 71-78, 1993.
[116] G. Ghosh. Elastic properties, hardness and indentation fracture toughness of intermetallics relevant to electronic packaging. Journal of Materials Research. 19: 1439-1454, 1994.
[117] M.S. Jellesen, D. Minzari, P. Møller and R. Ambat. Corrosion in electronics. In Proceedings of the Eurocorr conference, Edinburgh, Scotland, 2008.
[118] B. L. Rudman. A comparison of several corrosion inhibiting papers in various environments. Presentation at National Association of Corrosion Engineers Meeting, San Diego, March 1998.
[119] R. Baboian. Electronics, Corrosion tests and standards: Applications and Interpretation. West Conshohocken, PA; ASTM, 1996. www.corrosionsource.com/events/intercorr/baboian.htm, accessed on January 2009.
[120] J.W. Nah, F. Ren and K.N. Tu. Electromigration in Pb-free flip chip solder joints on flexible substrates. Journal of Applied Physics. 99: 023520-023526, 2009.
[121] R. Ambat. A review of corrosion and environmental effects on electronics. Center for electronic corrosion, Division of Materials Science and Engineering, Department of Mechanical Engineering, Technical University of Denmark.

Appendix I

A feasibility study of lead free solders for level 1 packaging applications

Vivek Chidambaram, John Hald and Jesper Hattel

Microelectronics and Electronic Packaging, 6: 75-82, 2009.

Journal of Microelectronics and Electronic Packaging (2009) **6**, 75-82
Copyright © International Microelectronics And Packaging Society
ISSN: 1551-4897

A Feasibility Study of Lead Free Solders for Level 1 Packaging Applications

Vivek Chidambaram,* John Hald, and Jesper Hattel

Abstract—**An attempt has been made to determine the lead free ternary combinations that satisfied the solidification requirement for a solder used in level 1 packaging applications, using the CALPHAD approach. The segregation profiles of the promising candidates were analyzed after scrutinizing the equilibrium calculations by Scheil solidification simulations and optimization. A feasibility study has been carried out for the replacement of high-lead-containing solders with the focus on surface tension, natural radius of curvature, oxidation resistance, intermetallic compound formation, and environmental oriented issues.**

Keywords—**Calphad, COST 531 (solder database), level 1 packaging, solder wettable layer, SSOL-2 (solution database), SSUB3 (substance database), SURDAT (surface tension and density database for lead free soldering materials), Thermo-Calc, under-bump metallization**

Introduction

Most of the research earlier devoted to lead free solders had been restricted primarily to the board level assembly process, that is, a level 2 packaging application. In a board level packaging application, the solder used is primarily a eutectic composition Sn-37Pb or a near eutectic composition Sn-40Pb. However, with the advent of array packaging concepts (flip-chip and ball grid arrays), the usage of solders in level 1 packaging is increasing sharply. Common versions of solders primarily used in level 1 packaging for certain applications are Pb-10Sn and Pb-5Sn, having a melting range of 275–302°C and 308–312°C, respectively. These alloys are used for interconnecting a chip to a carrier [1]. The primary requirement for this application is that the solidus temperature should be above 270°C in order to prevent the solder joint within the component from remelting when the component is subsequently soldered to the printed circuit board (PCB), a step that typically involves lower melting point solders and the liquidus temperature should be below 350°C, which is determined by the polymer materials used in the substrate. Lead is used for solders in electronics primarily due to its unique properties such as low melting point, malleability, low surface tension, excellent conductivity, and high resistance to corrosion [2].

Despite all of the beneficial attributes of lead, its potential environmental impact when the products are discarded to landfills has caused the industry to seek out lead free alternatives. Human toxicity of lead can result in cancer and can also adversely affect liver and thyroid function and resistance to disease. Lead can affect almost every organ in the body, including the nervous system, kidneys, and reproductive system. The main effect of lead toxicity is on the central nervous system. High exposure to lead can severely damage the brains and kidneys of humans and can lead to miscarriage in pregnant women. High exposure to lead can also severely damage brain development in children and organs responsible for sperm production in men. The ecological toxicity of lead can occur as a result of direct exposure to algae, invertebrates, and fish to lead. Fish exposed to high levels of lead exhibit effects such as growth inhibition, mortality, reproductive problems, and paralysis. Furthermore, at elevated levels of lead, plants can experience reductions in growth, photosynthesis, and water absorption. Birds and mammals can also suffer from lead poisoning, resulting in damage to the nervous system, kidneys, and liver [3].

Usagewise, electronic solders only account for 1% of the total usage of lead with the majority (80.8%) being used by the battery industry. However, these batteries are largely being recycled. But the use of recycled lead for electronics applications is of limited applicability since recycled lead displays higher α particle emission than virgin lead. When these particles pass through a silicon device, they generate electrons and holes. Before these charge carriers recombine, they may affect the charge stored in the capacitors (memory units) of the device, leading to "soft error" failure. To prevent this problem, Pb-free solders is one of the solutions [4].

At present there are Pb-free solders for level 2 packaging applications but there is none for level 1. One well known binary alloy is Au-20Sn, a eutectic composition with a melting point of 280°C, which could be considered for this application, yet this eutectic alloy is brittle and also known to have poor reflow properties. Thus, only ternary combinations could probably provide an amicable solution [5].

Theoretical modeling of the thermodynamic properties of multicomponent systems is a modern tool widely used in the field of alloy thermodynamics, especially in recent years. It allows the prediction of the thermodynamic behavior of complex systems and reduces the expense of time-consuming experimental studies otherwise necessary for the development of new materials.

The CALPHAD approach, which is the most popular method in use, is based on the sequential modeling of chemical

Manuscript received August 2008 and accepted February 2009
Department of Mechanical Engineering, Technical University of Denmark, Produktionstorvet, Lyngby, DK-2800, Denmark
*Corresponding author; email: vchi@mek.dtu.dk

systems, starting from the simplest—the modeling of the Gibbs energy functions for the pure components—followed by modeling of more complex phases such as binary and ternary solution and intermetallics. The Gibbs energy functions of the phases are stored in the form of polynomial coefficients. The thermodynamic properties of a binary system can be calculated using the Gibbs energy expressions for both elements in each of the phases existing in the system. Interaction parameters can be introduced to describe the mutual interaction between the elements in each phase. It is possible to model such a system with high precision if experimental data are available that describe both the thermodynamic properties of the phases and their equilibria. The deviation of the real behavior of the system from the prediction can be minimized by adding new parameters, but they must not influence the modeled thermodynamic properties and calculated phase diagrams of the lower-order systems [6, 7].

A feasibility study has been carried out to determine a possible replacement solder for high lead containing solders taking into account the solidification requirement, surface tension, natural radius of curvature, oxidation resistance, intermetallic compound formation, and environmental oriented issues.

Methods

Ternary combinations were extrapolated iteratively from well assessed binary systems involving 10 elements actively being considered for lead free solders application: Ag, Au, Bi, Cu, In, Ge, Sb, Si, Sn, and Zn using the COST 531 v 2.0 [8] and SSOL2 [9] thermodynamic databases. This was done in order to determine the ones that adhere to the solidification requirement for the level 1 packaging applications. Ternary combinations which could probably meet the solidification requirement but are not well assessed in the two thermodynamic databases have not been considered. The extrapolations have been carried out without taking into account the ternary interaction information since in most cases the excess Gibbs energies of the solution phases in the binary systems relevant to solder alloys are relatively small in magnitude indicating that their ternary interactions are probably less significant. The ternary combinations that satisfied the solidification requirement were optimized for a commercially preferred narrow solidification range. Extrapolations have been carried out using Thermo-Calc (version R).

The optimized ternary equilibrium combinations were scrutinized by Scheil solidification simulations to determine whether they still adhere to the solidification criterion. Microsegregation during solidification of lead free solder candidates has been predicted by studying the composition profiles of each phase under both equilibrium and nonequilibrium conditions during solidification. The elements were classified as segregated during Scheil solidification simulations if their composition in the solidified material was greater than the one predicted by equilibrium solidification. Focus has also been given to other issues that are critical for a solder such as surface tension, natural radius of curvature, oxidation resistance, intermetallic compound formation, and toxicity related issues. The SSUB3 [10] thermodynamic database has been used to deal with issues related to oxidation resistance.

Results and Discussion

A. Equilibrium Solidification

The primary requirement for a solder used in Level 1 packaging applications is the solidification requirement, that is, the solidus temperature should be higher than 270°C and the liquidus temperature should be below 350°C. A narrow solidification range is generally preferred for facilitating rapid production, efficient process control, preventing the movement of components during solidification and for minimizing segregation during solidification. The ternary combinations that satisfied the solidification requirement for level 1 packaging applications are listed in Table I. The promising replacement solder for level 1 packaging applications could be either Sn or Au based ones. Many Au based systems could be considered for this application since Au undergoes a eutectic reaction with Ge, Sb, Si, and Sn. Bi based systems cannot be considered for this application as its thermal and electrical conductivities are far away from the minimum requirement of a solder. High content of zinc is generally not recommended from a corrosion perspective. Au-Sn-Ag, Au-Sn-Cu, Au-Sn-In, and Au-Sn-Zn could be tailored appropriately depending on the microstructure evolution and ductility of the intermetallics. They would have very narrow solidification ranges when they are close to the Au-Sn eutectic composition and the content of Ag, Cu, In, and Zn could be increased to a maximum of Au-0.35Sn-0.03Ag, Au-0.33Sn-0.04Cu, Au-0.25Sn-0.07In, and Au-0.30Sn-0.09Zn, respectively and still meet the solidification requirement for this application but with a broader solidification range.

B. NonEquilibrium Solidification

Even if the phase diagram shows that a specific alloy has the desired freezing range, it is possible and likely for noneutectic freezing, that a larger freezing range is observed in experiments. This is the case when nonequilibrium solidification occurs. Since the degree to which this nonequilibrium

Table I
Equilibrium Ternary Combinations Optimized for a Narrow Solidification Range

S. No	Ternary Compositions (mole-fraction)	Solidus T (°C)	Liquidus T (°C)	Range (°C)
1.	Au-0.18Ge-0.10In	338.69	339.03	0.34
2.	Au-0.16Sb-0.22In	285.83	287.05	1.22
3.	Au-0.30Sn-0.01Zn	274.96	284.11	9.15
4.	Au-0.31Sn-0.01Cu	279.15	291.44	12.29
5.	Au-0.35Sn-0.21Sb	312.43	329.23	16.80
6.	Au-0.26Sb-0.20Bi	292.44	313.59	21.15
7.	Au-0.13Sn-0.10Si	312.23	333.67	21.44
8.	Au-0.30Sn-0.01In	280.99	302.84	21.85
9.	Au-0.32Sn-0.01Ag	280.86	307.08	26.22
10.	Au-0.15Ge-0.12Sn	285.58	314.16	28.76
11.	Au-0.24Ge-0.05Sb	285.40	347.88	62.48
12.	Bi-0.16Sb-0.04In	269.11	335.84	66.73
13.	Sn-0.25Au-0.20Sb	282.83	305.18	22.35
14.	Sn-0.36Au-0.08Zn	302.95	327.69	24.74
15.	Sn-0.33Au-0.02Ge	314.29	343.43	29.14
16.	Sn-0.30Au-0.08Ag	300.50	334.03	33.53
17.	Sn-0.29Au-0.08Cu	291.75	330.94	39.19

Table II
Ternary Combinations Adhering Solidification Criterion by Scheil Solidification Simulations

S. No	Ternary Compositions (mole fraction)	Solidus T (°C)	Liquidus T (°C)	Range (°C)
1.	Au-0.18Ge-0.10In	338.7	340	1.3
2.	Au-0.16Sb-0.22In	285.7	288	2.3
3.	Au-0.31Sn-0.01Cu	278	292	14
4.	Au-0.30Sn-0.24In	281	303	22
5.	Au-0.32Sn-0.01Ag	278	308	30
6.	Au-0.28Sn-0.01Zn	275	316	41
7.	Au-0.13Sn-0.10Si	271	334	63
8.	Au-0.24Ge-0.05Sb	285	348	63
9.	Sn-0.25Au-0.20Sb	273	290	17
10.	Sn-0.29Au-0.08Cu	305	332	27

solidification occurs is determined by kinetic factors, it is quite complex to predict unless exact diffusion coefficients are available. Modeling of solidification very close to reality is currently possible by the CALPHAD approach. Although modeling of real solidification behavior requires the incorporation of kinetic analysis of microsegregation and back diffusion, the predictions of the Scheil module of Thermo-Calc are close to reality for many alloys for the time scales found in soldering [11]. There are many differences between the traditional Scheil model and the one implemented in the Scheil module of Thermo-Calc, that is, by the CALPHAD approach.

The Scheil equation is applicable only to dendritic solidification and furthermore not even in the case where the solidification is mainly dendritic in nature but contains some final eutectic products. Furthermore it cannot be used to predict the formation of intermetallic phases during solidification since the partition coefficient is assumed to be constant. However, the partition coefficient is dependent on both temperature and/or composition and this is not taken into account in the traditional Scheil model.

Using a CALPHAD approach, all of the above obstacles can be overcome. The process that physically occurs during solidification can be envisaged. Any appearance of secondary phases can easily be taken into account in this approach with the assumption that no back diffusion is involved. Therefore all transformations can be handled including the final eutectic solidification. This approach is based on a series of isothermal steps but as the temperature step size becomes small it provides results that are almost completely equivalent to those that would be obtained from continuous cooling [12]. The equilibrium thermodynamic calculations were scrutinized using Scheil solidification simulation, to confirm whether the combinations still adhere to the solidification criterion. The ones that satisfied the solidification criterion are listed in Table II.

Among the elements being actively considered for this application, Sn generally undergoes a peritectic reaction to satisfy the solidification criterion. Equilibrium calculations are less valid for peritectic reactions. Sn-Au-Cu and Sn-Au-Sb ternary combinations still gave positive results. The Sn-Au-Cu system was optimized with an objective of reducing the solidification range and still meet the solidification criterion. The Sn-Au-Sb system was optimized with an objective of reducing the Sb content in the ternary system and still adhere to the solidification criterion since Sb is considered to be toxic. The results are shown in Fig. 1 and Fig. 2, respectively.

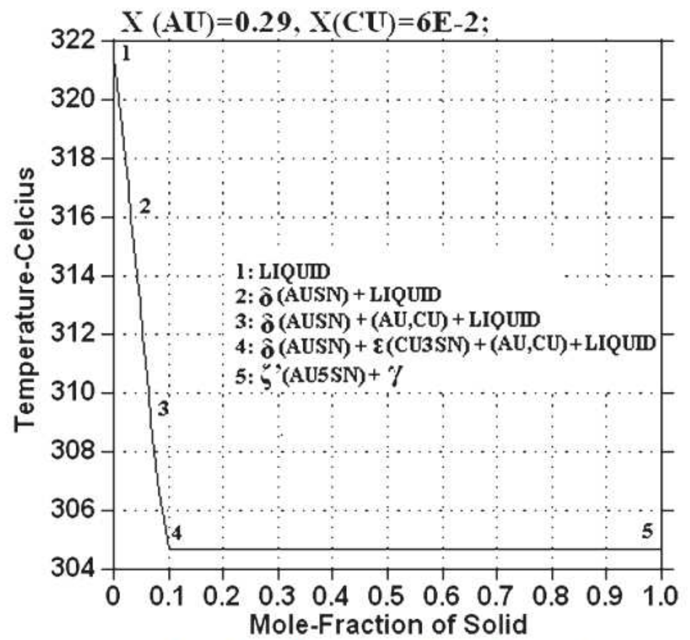

Fig. 1. Scheil solidification simulation of Sn-0.29Au-0.06Cu (mole fraction).

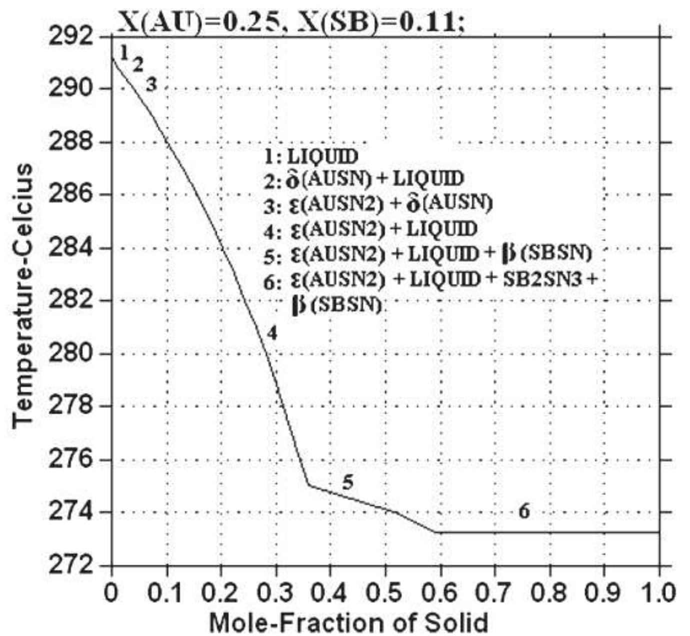

Fig. 2. Scheil solidification simulation of Sn-0.25Au-0.11Sb (mole fraction).

Among these two combinations, the former is more promising since it has a high solidus temperature and it is also environmentally friendly. From a resistance to creep perspective, it would be advantageous to use solder alloys with higher solidus temperature. The latter also has considerable proportion of Sb, even though Sb is considered to be quite toxic but definitely not as toxic as lead.

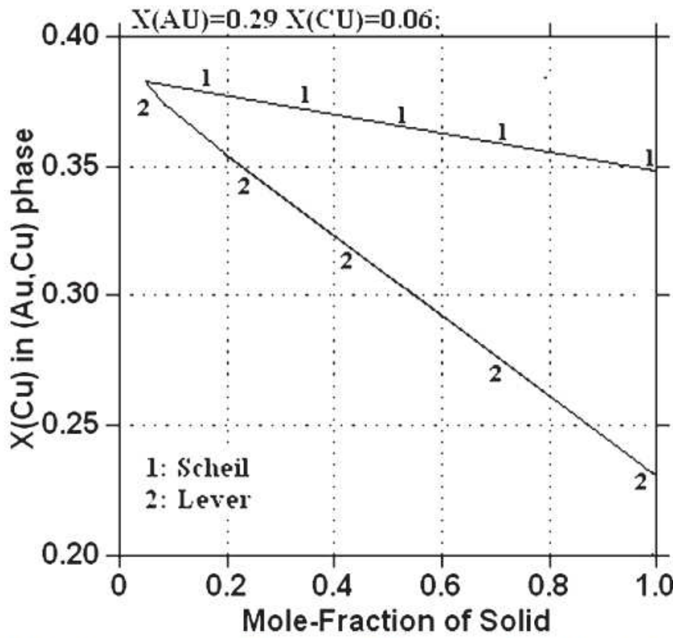

Fig. 3. Microsegregation of Cu in mole fraction (X) predicted in (Au,Cu) phase during solidification of Sn-0.29Au-0.06Cu.

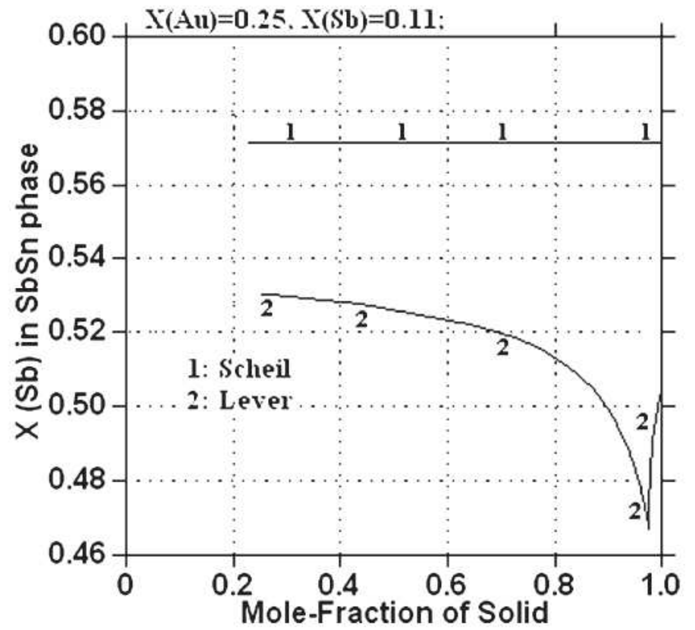

Fig. 4. Microsegregation of Sb in mole fraction (X) predicted in SbSn phase during solidification of Sn-0.25Au-0.11Sb.

C. Microsegregation

Segregation could be defined as any departure from the uniform distribution of the chemical elements in the alloy. Because of the way in which alloys partition on freezing, alloying elements generally segregate during solidification. This segregation can sometimes be significantly reduced by a homogenizing heat treatment if the distance over which diffusion has to take place to redistribute the alloying elements is sufficiently small [13].

The composition profiles of each phase were studied under both equilibrium and nonequilibrium conditions during solidification of Sn-0.29Au-0.06Cu and Sn-0.25Au-0.11Sb. For equilibrium solidification there is no solute segregation and the composition of the solidified material is uniform. The elements were classified as segregated during Scheil solidification simulations if their composition in the solidified material was greater than the one predicted by equilibrium solidification.

Microsegregation of Cu and Sb were observed in the (Au, Cu) phase and the β (SbSn) phase during Scheil solidification simulations of Sn-0.29Au-0.06Cu and Sn-0.25Au-0.11Sb respectively. Fig. 3 and Fig. 4 illustrate the deviations of Cu and Sb composition profiles in the (Au, Cu) phase and the β (SbSn) phase, respectively, from their equilibrium profiles.

The influence of segregation of elements during solidification on the thermomechanical properties probably depends on whether the segregated phase appears in the bulk solder as a dispersed phase or as a matrix phase. It could have a small influence on the thermomechanical properties if the segregated phase appears as a dispersed phase whereas it could have a high influence on the thermomechanical properties if the segregated phase appears as a matrix phase in the bulk solder. The Thermo-Calc software version R is not capable of predicting the resulting microstructure for Scheil solidification simulation. Thus, the phases in the bulk solder of the two promising solder alloys were predicted for optimized compositions that were determined by equilibrium calculations, that is, Sn-0.29Au-0.08Cu and Sn-0.25Au-0.20Sb. The results are depicted in Fig. 5 and Fig. 6, respectively.

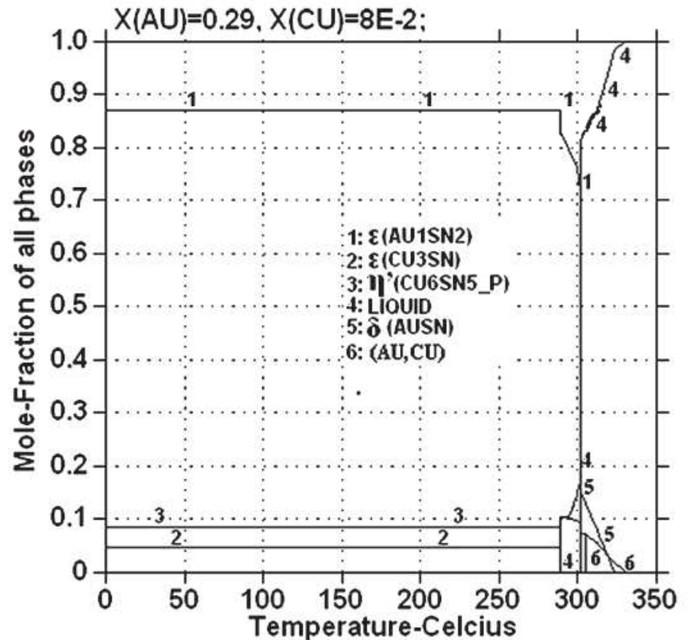

Fig. 5. Prediction of phases in the bulk solder by equilibrium calculation of Sn-0.29Au-0.08Cu alloy.

The phases predicted in the bulk solder by equilibrium calculation of Sn-0.29Au-0.08Cu alloy shows η′ (Cu_6Sn_5) and ε (Cu_3Sn) phases would be dispersed in the ε (Au_1Sn_2) matrix phase. Similarly, the phases predicted in the bulk solder by equilibrium calculation of Sn-0.25Au-0.20Sb shows that

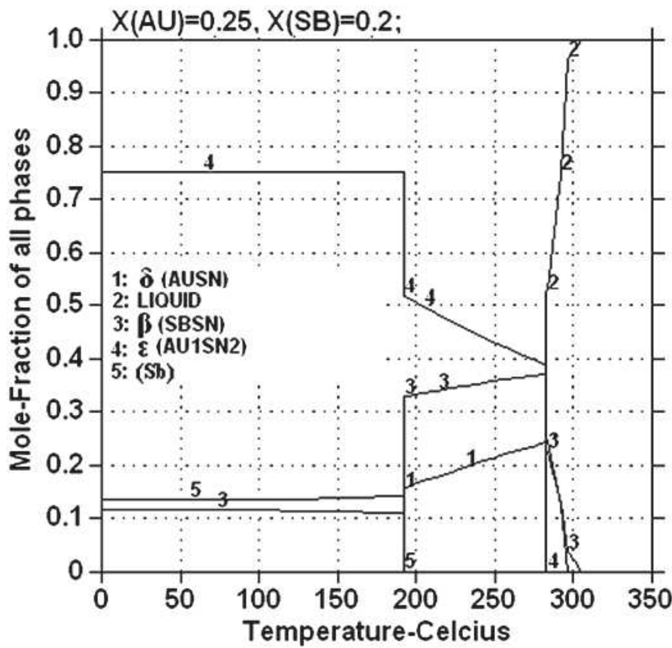

Fig. 6. Prediction of phases in the bulk solder by equilibrium calculation of Sn-0.25Au-0.20Sb alloy.

the (Sb) and β (SbSn) phases are dispersed in the ε (Au1Sn2) matrix phase. Segregation of Cu in the (Au, Cu) phase during solidification will have no influence on the thermomechanical properties since the (Au, Cu) phase is not predicted to exist in the final microstructure of the solidified material. Segregation of Sb in the β (SbSn) phase during solidification may have a small influence on the thermomechanical properties as the β (SbSn) phase is predicted to occur only as a dispersed phase and not as a matrix phase. However, the Thermo-Calc software version R is not capable of predicting the final microstructure for nonequilibrium solidification simulation. Thus, in order to confirm the predictions, it is necessary to perform the microstructure evaluation for the proposed solder candidates for the level 1 packaging applications, that is, Sn-0.29Au-0.06Cu and Sn-0.25Au-0.11Sb.

In many promising Au based ternary systems it was observed that there was no or little microsegregation during nonequilibrium solidification simulations. The possible explanation for this behavior could be that most of the promising Au based ternary systems were close to the eutectic reactions. However, considerable microsegregation of Au was predicted in both the (Au, Ag) phase and the ζ phases during solidification of Au-Sn-Ag, and in both (Au, Cu) and ζ during solidification of Au-Sn-Cu. A high microsegregation of Sn in the ζ phase was observed during solidification of Au-0.13Sn-0.10Si. The equilibrium calculations of these ternary systems have predicted that all these segregated phases appear only as dispersed phases in the bulk solder. Hence, the influence of segregation on the thermomechanical properties should probably be less pronounced.

D. Surface Tension and Natural Radius of Curvature

The surface tension (γ) of a liquid is a thermodynamic quantity and it is defined as the amount of work needed to isothermally enlarge the liquid surface area. The interfacial forces (surface tension) between the molten solder and the substrate influence the degree of wetting, which in turn determines the formation of proper solder joints [14]. Thus, γ is one of the critical properties of a solder that determines its wetting behavior. The dissolution of under-bump metallization (UBM) in the molten solder, the oxidation of the molten solder, the soldering environment, and so on, also affect the surface tension of the solder. Studies have shown that the surface tension value of a solder varies with temperature [15] and the extent of solder-UBM (solder wettable layer) interactions [16]. For these reasons the surface tension of solder alloys and most other liquid metals under actual processing conditions are not precisely known. Low γ values generally facilitate better wetting. Other than wetting, γ values also influence the natural radius of curvature, R of the alloys. The relation is shown below.

$$R = \left(\sqrt{\frac{\gamma}{\rho g}}\right) \quad (1)$$

where γ = surface tension, ρ = density, and g = acceleration due to gravity.

Table III
Surface Tension and R Values for Lead Free Soldering Materials

Metals	γ(mN/m)	R (mm)
Pb-5Sn (w-p)	465	2.115
Pb-10Sn (w-p)	470	2.147
Ag	890	3.128
Al	863	6.635
Au	1090	2.550
Bi	375	1.960
Cu	1276	4.059
In	547	2.829
Pb	430	2.034
Sb	365	2.402
Sn	540	2.827

The continuing miniaturization of components in the microelectronics industry places ever-increasing demands upon solder alloys to be designed for a low R values in order to prevent bridging between contacts as the pitch between contacts keeps getting smaller and smaller during the miniaturization drive [17]. The surface tension and natural radii of curvature of elements being considered for this application are listed in Table III along with the currently used binary alloys. γ and ρ values required for the calculations of R were taken from the SURDAT [18] database measured experimentally at 50°C above the liquidus temperature in Ar+20%H_2 atmosphere. Solder alloys with considerable proportion of Au, Bi, Sb, and Sn would facilitate the miniaturization drive (Table III).

E. Feasibility of Electroplating

One of the primary reasons for preferring flip-clip assembly over the traditional wire bonding in level 1 packaging applications is the miniaturization drive. Reduction of the device size with increased functions means that the pitch between the inputs/outputs (I/O) also needs to be reduced. There are limitations with the different techniques used to deposit these flip-

Table IV
Standard Free Energy of Formation of Stable Oxides

Oxides	25°C (KJ/mol)	200°C (KJ/mol)	325°C (KJ/mol)
Ag_2O	−11.25	0.28	8.21
Au_2O_3	77.86	118.57 (177°C)	unstable
Bi_2O_3	−497.10	−450.41	−415.58
Cu_2O	−147.84	−134.51	−125.08
GeO_2	−521.31	−487.02	−462.84
In_2O_3	−827.23	−770.61	−729.17
Sb_2O_5	−829.14	−745.25	−685.32
SiO_2	−856.29	−824.27	−801.54
SnO_2	−515.82	−479.63	−452.78

Table V
Critical Oxygen Partial Pressure of the Stable Oxides

Stable Oxides	25°C (atm.)	200°C (atm.)	325°C (atm.)
Bi_2O_3	8.22×10^{-88}	1.89×10^{-50}	5.13×10^{-37}
Cu_2O	1.25×10^{-26}	1.47×10^{-15}	1.20×10^{-11}
GeO_2	4.70×10^{-92}	1.73×10^{-54}	3.84×10^{-41}
In_2O_3	1.19×10^{-145}	8.51×10^{-86}	2.12×10^{-64}
Sb_2O_5	5.51×10^{-146}	5.39×10^{-83}	1.42×10^{-60}
SiO_2	9.68×10^{-151}	1.01×10^{-91}	1.01×10^{-70}
SnO_2	4.28×10^{-91}	1.12×10^{-53}	2.89×10^{-40}

atm. = Atmospheric pressure

chip pads, with respect to how low a pitch can be achieved. Ultra fine pitch flip-chip bumping is currently enabled only with electroplating processes [19]. Thus, it is essential that the elements in the potential solder alloy candidates should be easily electroplatable in addition to having a low natural radius of curvature.

Electroplated bumping processes generally are less expensive than other bumping techniques. Electroplating in general has a long history and processes are well characterized. The UBM adheres well to the bond pads and passivation, protecting the aluminum pads. Plating can allow closer bump spacing (35–50 microns) than other methods of bump formation. Electroplating has become more popular for high bump count (>3,000) chips because of its small feature size and precision. Among the elements in the proposed solder alloy candidates Ag, Au, Cu, and Sn are easy ones for electroplating whereas Bi, In, and Sb are difficult ones and Ge, Si are currently impossible ones. Thus, if a new solder alloy is developed with Ge or Si, then a new electroplating technique has to be developed [20, 21]. Thus both Sn and Au, in addition to having low natural radii of curvature, are both easily electroplatable.

F. Oxidation Resistance

Oxidation resistance is one of the critical parameters that influence wetting, formation of intermetallics, and so on. The standard free energy of formation of the most stable oxides for the elements being considered for level 1 packaging applications from room temperature to the temperatures during reflow were calculated using the SSUB3 thermodynamic database in Thermo-Calc and are listed in Table IV.

Thus, gold and silver, having a positive free energy, possess a low tendency to form stable oxides. Gold oxide is not stable above 177°C. Among the elements widely being considered for this application, In, Sb, and Si, having a low free energy (negative), possess a very high tendency to form stable oxides. The critical oxygen partial pressures of the stable oxides with negative Gibbs free energy were calculated using the following relation and are listed in Table V.

$$P_{O_2} = \exp\left(\frac{\Delta G_f^0}{RT}\right) \quad (2)$$

where P_{O_2} = critical oxygen partial pressure, ΔG_f^0 = Gibbs free energy of formation, R = gas constant, T = temperature.

Table VI
Standard Free Energy of Reduction of Stable Oxides

Oxides	25°C (J/mol)	200°C (J/mol)	325°C (J/mol)
Ag_2O	−225.89	−210.23	−202.19
Au_2O_3	−789.28	−754.55 (177°C)	unstable
Bi_2O_3	−214.32	−179.46	−160.65
Cu_2O	−89.30	−75.45	−67.00
GeO_2	47.02	67.10	78.69
In_2O_3	115.80	140.73	152.95
Sb_2O_5	−356.56	−304.54	−275.05
SiO_2	382.01	404.35	417.39
SnO_2	41.54	59.72	68.63

Thus, it is evident that the critical oxygen partial pressure of the most stable oxide compounds at low temperature for elements such as Bi, Ge, In, Sb, Si, and Sn are extremely low and even the most sophisticated vacuum equipment available today would not be able to attain such low vacuum levels. While it may not be possible to control the onset of oxidation with the industrial equipment suitable for mass production, the extent to which oxidation proceeds can be controlled by restricting the oxygen content in the environment in which soldering is done so that the oxidation can be kept to a minimum [22].

An alternative approach frequently taken to prevent oxidation is maintaining a reducing atmosphere, such as hydrogen, during reflow. The effects of reducing atmosphere on the stable oxide compounds of the elements widely being considered for this application were determined using the SSUB3 thermodynamic database. The formation of stable oxides can be easily controlled if the Gibbs free energy of the reduction reaction is negative. In the case of hydrogen atmosphere, the reaction is the reduction of stable oxide to pure element and the formation of water vapor. The effect of the hydrogen atmosphere on the most stable oxides of the elements contained in promising ternary combinations adhering to the solidification criterion by both equilibrium and Scheil solidification simulations from room temperature to the temperatures during reflow, is listed in Table VI.

Thus, it is evident that even hydrogen atmosphere fails to control the onset of oxidation if the solder alloy includes a considerable proportion of Ge, In, Si, and Sn. Unlike In and Si, the reduction reaction of the stable germanium and tin oxides possess relatively low (positive) free energy. Thus it would be advantageous from the wetting perspective to avoid or reduce the content of In and Si in the solder alloy. Zinc also

forms a stable ZnO_2 phase but the phase has not been assessed in the SSUB3 database and so it has not been taken into account.

G. Intermetallic Compounds Formation

In level 1 packaging, the solder joints are made relatively smaller than in level 2 packaging. Thus, the intermetallic compounds (IMC) occupy a relatively greater proportion of the solder joint and are crucial in determining the thermomechanical properties. Intermetallic compounds are generally formed between the solder and the solder wettable layer of the under-bump metallization during wetting reaction and solid-state aging. It is well known that the formation of IMCs between the solder and solder wettable layer of the UBM is an indication of good metallurgical bonding. A thin, continuous, and uniform IMC layer is an essential requirement for good bonding. However, the formation of a thick IMC may degrade the reliability of solder joints due to their inherent brittle nature and their tendency to generate structural defects.

Tin generally has a high tendency of forming IMCs with the elements commonly used as a solder wettable layer. The probability of forming Kirkendall porosities and the spalling of IMCs is high with a high content of tin in the solder alloy. The Kirkendall voids lead to very poor mechanical properties. The spalling phenomenon is extremely undesirable because it leads to chemically and mechanically weak joints, since the solder loses contact with the solder wettable layer of the UBM. Moreover, IMCs are generally brittle and are prone to creep and fatigue [23-25]. Thus, from the IMC perspective, gold based solder alloys would be better than tin based ones.

H. Environmental Impact

The lead-free solder design initiative as a substitute for high-lead-containing solder alloys used in level 1 packaging applications is primarily being driven by the environmental impact of lead [26]. Turbini and colleagues [27] analyzed the environmental impact of Pb-free alloys that may contain Ag, Bi, In, or Sb and concluded that Pb-free solders are limited in their ability to decrease the environmental impacts of high lead content solders.

The Pb-free solder alternatives are ranked in descending toxicity in Table VII, taking into account both EPA (Environmental Protective Agency-US) [28] and OSHA (Occupational Safety and Health Administration) [29]. The former threshold values are based on leaching by groundwater, while the latter are based on occupational exposure, inhalation, and other exposure in workplaces. Thus, the main objective of using Pb-free solders for level 1 packaging applications would be served only with a high proportion of Au and Sn in the solder alloy.

Table VII
Toxicity Metrics

Metals	EPA (US) Drinking Water Standard (mg/L)	OSHA PEL (mg/m^3)
Lead	0.015	0.05
Silver	0.05	0.01
Antimony	0.006	0.5
Indium	none	0.1
Bismuth	0.05	none
Copper	1	0.1
Zinc	5	15
Tin	none	2
Gold	none	none

Concluding Remarks

The main objective of developing an "environmentally friendly" solder would be served only with either Au or Sn based solder alloys. Both Au and Sn have low natural radii of curvature and both are easily electroplatable, hence both would facilitate the miniaturization drive of the microelectronics industry. Thus, the primary objective of the flip-chip assembly concept, that is, the miniaturization drive could be fulfilled only by Au or Sn based systems. Sn based solder alloys have an edge over Au based ones, with respect to its low surface tension and commercial cost. However from the IMC perspective, Au based solder alloys would be better than the Sn based alloys; also, Au based systems generally undergo a eutectic or close to eutectic reaction to adhere to the solidification criterion. By using gold, the initial costs would be higher, but there would potentially be a value to the recycled product and no disposal cost associated with the solders, resulting in lower lifetime costs for the product. Thus, only Au or Sn based alloys could probably be effective substitutes for high-lead-containing solders used currently in level 1 packaging applications.

Acknowledgment

The authors acknowledge the Danish Ministry of Science, Technology and Development for financial support through the innovation consortium "Matpack" (Project no. 07-003145).

References

[1] Y. Takaku, I. Ohnuma, R. Kainuma, Y. Yamada, Y. Yagi, Y. Nishibe, and K. Ishida, "Development of Bi-base high-temperature Pb-free solders with second-phase dispersion thermodynamic calculation, microstructure and interfacial reaction," Journal of Electronic Materials, Vol. 35, pp. 1926-1932, 2006.

[2] S. Herat, "Green electronics through legislation and lead free soldering," Clean: Soil, Air, Water, Vol. 36, pp. 141-151, 2008.

[3] ATSDR, "Lead: Agency for toxic substances and disease registry fact sheet," United States Department of Health and Human Services, 2005, p. 2.

[4] J.F. Ziegler and G.R. Srinivasan, "Terrestrial cosmic rays and soft errors," I.B.M. Journal of Research Development, Vol. 40, pp. 19-39, 1996.

[5] K.N. Tu, A.M. Gusak, and M. Li, "Physics and materials challenges for lead-free solders," Journal of Applied Physics, Vol. 93, pp. 1335-1353, 2003.

[6] H.L. Lukas, S.G. Fries, and B. Sundman, "*Computational Thermodynamics: The CALPHAD Method*," Cambridge University Press, New York, 2007, pp. 1-6.

[7] A. Kroupa, A.T. Dinsdale, A. Watson, J. Vrestal, J. Vizdal, and A. Zemanova, "The development of the COST 531 lead-free solders thermodynamic database," JOM—Journal of the Minerals Metals and Materials Society, pp. 20-25, 2007.

[8] A.T. Dinsdale, A. Watson, A. Kroupa, A. Zemanova, J. Vrestal, and J. Vizdal, "COST 531 database V 2.0," January 2006.

[9] Scientific Group Thermodata Europe (SGTE), "SSOL2-Solutions database version 2.1," 1999/ 2002/ 2003.

[10] Scientific Group Thermodata Europe (SGTE), “SSUB3 Substances database version 3.2,” 2001/ 2002/ 2004.
[11] U.R. Kattner and C.A. Handwerker, “Calculation of phase equilibria in candidate solder alloys,” Zeitschrift fur Metallkunde, vol. 92, pp. 740–746, July 2001.
[12] N. Saunders and A.P. Miodownik, “*CALPHAD*,” Pergamon Materials Series, Vol. 1, 1998, pp. 411-449.
[13] J. Campbell, “*Castings*,” Butterworth-Heinemann, Woburn, MA, pp. 151-162.
[14] R.J.K. Wassink, “Soldering in electronics,” 2nd ed., Electrochemical Publications, Ayr, UK, 1989, pp. 36-37.
[15] F.H. Howie and C. Lea, “Blowholing in PTH solder fillets: Towards a solution,” Proceedings of INTERNEPCON UK, Brighton, 1984, pp. 104-111.
[16] R.A. Deighan, “Surface tension of solder alloys,” International Journal of Hybrid Electronics, Vol. 5, pp. 307-313, 1982.
[17] Y. Yamada, Y. Takaku, Y. Yagi, Y. Nishibe, I. Ohnuma, Y. Sutou, R. Kainuma, and K. Ishida, “Pb-free high temperature solders for power device packaging,” Microelectronics Reliability, Vol. 46, pp. 1932-1937, 1996.
[18] Z. Moser, W. Gasior, A. Debski, and J. Pstrus, “*Surface Tension and Density Database*,” Institute of Metallurgy and Material Science, Polish Academy of Sciences, Krakow, 2007.
[19] P. Limaye, B. Vandevelde, R. Labie, D. Vandepitte, and B. Verlinden, “Influence of intermetallic properties on reliability of lead-free flip-chip solder joints,” IEEE Transactions on Advanced Packaging, Vol. 31, p. 51-57, 2008.
[20] D. S. Patterson, P. Elenius, and J.A. Leal, “Wafer bumping technologies: A comparative analysis of solder deposition processes and assembly considerations,” INTERPACK ’97, EEP, Vol. 19, Advances in Electronic Packaging, pp. 337-351, 1997.
[21] A. Brenner, “*Electrodeposition of Alloys: Principles and Practice*,” Vol. 1 and Vol. 2, Academic Press, New York, p. 963.
[22] M. Abtew and G. Selvaduray, “Lead-free solders in micro electronics,” Journal of Materials Science Engineering, Vol. 27, pp. 95-141, 2007.
[23] N. Jiang, J.A. Clum, R.R. Chromik, and E.J. Cotts, “Thermal expansion of several Sn-based intermetallic compounds,” Scripta Materialia, Vol. 37, pp. 1851-1854, 1997.
[24] K.N. Tu and K. Zeng, “Tin-lead (Sn-Pb) solder reaction in flip chip technology,” Journal of Materials Science Engineering, Vol. 34, pp. 1-58, 2001.
[25] T. Laurila, V. Vuorinen, and J.K. Kivilahti, “Interfacial reactions be tween lead-free solders and common base materials, ” Journal of Materials Science Engineering, Vol. 49, pp. 1-60, 2005.
[26] O.A. Ogunseitan, “Public health and environmental benefits of adapting lead-free solders,” JOM—Journal of the Minerals Metals and Materials Society, Vol. 59, pp. 12-17, 2007.
[27] M.J. Schoenung, O.A. Ogunseitan, J.D.M. Saphores, and A.A. Shapiro, “Adapting lead free solders,” Journal of Industrial Ecology, Vol. 8, pp. 59-85, 2005.
[28] U.S. Environmental Protective Agency (EPA), http://www.epa.gov/.
[29] U.S. Department of Labor, Occupational Safety and Health Administration (OSHA), http://www.osha.gov/.

Appendix II

Development of gold based solder candidates for flip chip assembly

Vivek Chidambaram, John Hald and Jesper Hattel

Microelectronics Reliability, 49: 323-330, 2009.

Microelectronics Reliability 49 (2009) 323–330

Contents lists available at ScienceDirect

Microelectronics Reliability

journal homepage: www.elsevier.com/locate/microrel

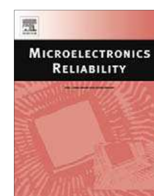

Development of gold based solder candidates for flip chip assembly

Vivek Chidambaram *, John Hald, Jesper Hattel

Department of Mechanical Engineering, Technical University of Denmark, Building 425, Produktionstorvet, Lyngby, DK-2800, Denmark

ARTICLE INFO

Article history:
Received 11 September 2008
Received in revised form 21 December 2008
Available online 5 February 2009

ABSTRACT

Flip chip technology is now rapidly replacing the traditional wire bonding interconnection technology in the first level packaging applications due to the miniaturization drive in the microelectronics industry. Flip chip assembly currently involves the use of high lead containing solders for interconnecting the chip to a carrier in certain applications due to the unique properties of lead. Despite of all the beneficial attributes of lead, its potential environmental impact when the products are discarded to land fills has resulted in various legislatives to eliminate lead from the electronic products based on its notorious legacy as a major health hazard across the spectrum of human generations and cultures. Flip chip assembly is also now increasingly being used for the high-performance (H-P) systems. These H-P systems perform mission-critical operations and are expected to experience virtually no downtime due to system failures. Thus, reliability of the solder joint is a major critical issue. This reliability is directly influenced by both the phases in the bulk solder and also the intermetallic compounds formed between the solder and the solder wettable layer of the under-bump metallization during both the wetting reaction or/and the solid state ageing. In the present work, an attempt has been made to develop new solder alloys for flip chip assembly using the CALPHAD approach based on gold, the safest element among all the elements being considered for this application. Specifically, efforts have been made to predict the phases in the bulk solder of the promising solder candidates and also the intermetallic compounds formation, using the CALPHAD approach.

© 2009 Elsevier Ltd. All rights reserved.

1. Introduction

First level packaging involves interconnecting of the chip to a carrier. The two prominent techniques for doing this are wire bonding and flip chip assembly. Flip chip technology has been widely accepted as a technology for maximum miniaturization and is rapidly replacing wire bonding. Typical applications today are mobile products such as cellular phones or GPS devices [1]. Advanced packaging technologies such as flip chip technology are required because electronic devices are operating faster and becoming smaller, lighter and more functional [2].

Flip chip technology offers several advantages especially for high-density currents because the whole chip surface may be used for a large number of I/O pads in an area array configuration. Short interconnection lengths result in excellent electrical performance of interconnects as well. Flip chip assembly is also being used for automotive diesel control since it is mechanically the most rugged interconnection method. Above all, flip chip technique is probably the lowest cost interconnection for high volume automated production [3,4]. Due to all these advantages, flip chip assembly are now increasingly being used for high-performance (H-P) systems, i.e. servers, storage, network infrastructure/telecommunication systems [5].

Flip chip assembly requires the usage of high melting point solders for certain applications like those of H-P systems. In these cases, the solder should have a solidus temperature above 270 °C in order to prevent the solder joint within the component from remelting when the component is subsequently soldered during second level packaging. The liquidus temperature should also be below 350 °C, which is determined by the polymer materials used in the substrate. Increasing the lead content and reducing the tin content result in solders with substantially high melting points. Common versions of high lead containing solders currently being used for these applications are Pb–10Sn/Pb–5Sn, having a melting range of 275–302 °C and 308–312 °C, respectively, [6]. Lead in particular is being preferred for this application requiring high reliability because of its unique properties like low melting point, malleability, low surface tension, excellent conductivity, high resistance to corrosion and its tendency of not forming intermetallics with the commonly used solder wettable layer of the under-bump metallization (UBM) [7].

Given the legacy of lead as a pervasive environmental pollutant and the potency of its health impacts, it is not surprising that jurisdictions across the world have tried to limit its use. The current drive to eliminate lead from solder materials began with the concern over water distribution systems where direct population

* Corresponding author. Tel.: +45 4525 4711; fax: +45 4593 4570.
E-mail address: vchi@mek.dtu.dk (V. Chidambaram).

0026-2714/$ - see front matter © 2009 Elsevier Ltd. All rights reserved.
doi:10.1016/j.microrel.2008.12.012

exposure to lead from potable water was demonstrated. Subsequently, the European Union (EU) legislation, "Restriction of the Use of Hazardous Substances (ROHS) in Electrical and Electronic Equipment" (Directive 2002/95/EC) effectively bans the use of lead (Pb) and several other substances in electrical products [8]. However, the European commission (EC) specifically granted a special use of lead in solder exemptions, independent of concentration, for certain applications involving the use of flip chip technology [9]. The intent was to preserve the reliability of flip chip solder joints since it is also being used for H-P systems which perform mission-critical operations, so it is imperative that they maintain continuous and flawless operation over their life time. H-P systems are expected to experience virtually no down time due to system failures [5]. It is still unspecified exactly how long the exceptions, covering the Pb-rich solders, will be in force [10].

Au–20Sn (weight-percent), a eutectic composition with a melting point of 280 °C could be considered for flip chip assembly yet this eutectic alloy is brittle. Many Au based ternary alloys adhering to the solidification criterion generally undergo eutectic or close to eutectic reaction since gold undergoes eutectic reaction with Ge, Sb, Sn and Si. Moreover, gold has been classified as the safest element by both EPA – US (Environmental protective agency – United States) and OSHA (Occupational and safety health administration) among all the elements considered for this application [11,12]. Gold also possesses some unique properties required for high melting point solders like: good corrosion and oxidation resistance, excellent bio-compatibility and workability, good thermal and electrical conductivity, low natural radius of curvature and the tendency of not spontaneously forming intermetallics with the commonly used solder wettable barrier layer. Thus, gold based ternary systems could probably be a potential substitute for high lead containing solders used in flip chip assembly for certain applications.

The microelectronics industry is extremely cost conscious. The history of the industry has been to continuously produce higher performance at lower costs. Cost competitiveness in the electronics industry is maintained by reducing the cost of individual components to a minimum, in order to maximize the overall cost reduction [13]. Considering gold, as a potential substitute for lead would substantially increase the cost of high melting point solders. Though the initial costs would be higher, but there would potentially be a value to the recycled product and no disposal costs associated with the solders, resulting in lower life time costs for the product. In addition, refining costs becomes important when considering initial material selection. The refining of gold recovered from electronic waste scrap is easier and cheaper than refining of other noble elements [14]. It has been reported that 47% of the total consumption of gold was recovered and successfully recycled in 2007 [15].

Experimental determination of a ternary system is extremely time consuming. If the thermodynamic description of all the binary systems is available, it is possible to estimate a phase diagram of higher component systems from the extrapolation of the binary systems using the CALPHAD method. This method attempts to provide a true equilibrium calculation by considering the Gibbs energy of all phases and minimizing the total Gibbs free energy of the system. One of the most significant advantages of the CALPHAD methodology is that since the total Gibbs energy is calculated, it is possible to derive all of the associated functions and characteristics of phase equilibria. The quality of the extrapolation to a ternary system from the descriptions of the three binary systems depends not only on the accuracy of the calculation of each binary system but also on the magnitude of possible ternary interactions and the occurrence of ternary intermetallic compounds. The probable magnitude of these ternary interactions can be estimated from the properties of the binary systems. From the calculated phase diagrams, the melting temperature range, i.e. the solidification path, as well as the susceptibility to intermetallic formation with various solder wettable layer of the UBM can be estimated [16,17]. Thus, in the present work, focus has been put on determining all the gold based ternary systems adhering to the solidification criterion of the flip chip assembly, prediction of phases in the bulk solder and the susceptibility of IMCs formation between the solder alloys and the commonly used solder wettable layers like Au, Cu, Ni and Pd.

2. Methods

Ternary combinations were extrapolated iteratively from all the well assessed binary systems involving Au along with nine other elements actively being considered for lead-free solder applications: Ag, Bi, Cu, In, Ge, Sb, Si, Sn and Zn using the COST 531 v 3.0 [18] and SSOL2 [19] thermodynamic databases. This was carried out to identify the ones that adhere to the solidification criterion for the flip chip assembly used in the first level packaging applications. The ternary combinations which could probably meet the solidification requirement but are not well assessed in the two thermodynamic databases have not been considered. In many cases the extrapolations have been carried out without taking into account the ternary interaction information. This is because in most cases the excess Gibbs energies of the solution phases in the binary systems relevant to the solder alloys are relatively small in magnitude indicating that their ternary interactions are probably less significant. The ternary combinations that satisfied the solidification requirement were optimized for a commercially preferred narrow solidification range. Extrapolations have been carried out using the Thermo-Calc (version R) software.

The optimized ternary equilibrium combinations were scrutinized by Scheil solidification simulations, to determine whether they still adhere to the solidification criterion. The promising candidates were further analyzed by investigating their respective microstructures. Focus has also been put on the prediction of intermetallic compounds formed between the solder and the commonly used solder wettable layer of the UBM.

3. Results and discussion

3.1. Equilibrium solidification

The primary requirement for a solder used in flip chip assembly for certain applications is the solidification requirement, i.e. the solidus temperature should be higher than 270 °C and the liquidus temperature should be below 350 °C. A narrow solidification range is generally preferred for facilitating rapid production, efficient process control, preventing the movement of components during solidification and for minimizing segregation during solidification. The Au based ternary combinations that satisfied the solidification requirement of the flip chip assembly are listed in Table 1. Many Au based systems could be considered for this flip chip technology since Au undergoes eutectic reactions with Ge, Sb, Si and Sn.

Au–Sn–Ag, Au–Sn–Cu, Au–Sn–In and Au–Sn–Zn ternary systems could be tailored appropriately depending on the evolution of phases in the bulk solder and the type of IMCs developed between the solder and the solder wettable layer of the UBM. They would have very narrow solidification ranges when they are close to the Au–Sn eutectic composition and the content of Ag, Cu, In and Zn could be increased to a maximum of Au–0.35Sn–0.03Ag, Au–0.33Sn–0.04Cu, Au–0.25Sn–0.07In and Au–0.30Sn–0.09Zn, respectively, and still meet the solidification requirement for this application but with a broader solidification range. The minimum and maximum compositions of Au–Sn based ternary systems are

Table 1
Au based ternary combinations optimized for a narrow solidification range.

S. No.	Ternary compositions (mole-fraction)	Solidus temperature (°C)	Liquidus temperature (°C)	Range (°C)
1.	Au–0.18Ge–0.10In	338.69	339.03	0.34
2.	Au–0.18Sb–0.18In	306.49	314.69	8.20
3.	Au–0.35Sn–0.21Sb	317.05	332.99	16.80
4.	Au–0.13Sn–0.10Si	312.23	333.67	21.44
5.	Au–0.15Ge–0.12Sn	285.58	314.16	28.76
6.	Au–0.27Sb–0.21Bi	296	326.79	30.70
7.	Au–0.24Ge–0.05Sb	285.40	347.88	62.48

shown in Table 2. The minimum compositions were designed with a view of studying the effect of the addition of the third alloying element to the Au–Sn eutectic composition on the microstructure of the bulk solder. The maximum compositions were designed in order to meet the solidification criterion.

3.2. Non-equilibrium solidification

Even if the phase diagram shows that a specific alloy has the desired freezing range, it is possible and quite likely for non-eutectic freezing, that a larger freezing range is observed in experiments. This is the case when non-equilibrium solidification occurs. Since the degree to which this non-equilibrium solidification occurs is determined by kinetic factors, it is quite complex to predict unless exact diffusion co-efficients are available. Modelling of solidification very close to reality is currently possible by the CALPHAD approach.

The process that physically occurs during 'Scheil' solidification can be envisaged as follows: A liquid of composition C_0 is cooled to a small amount below its liquidus temperature to T_1. It precipitates out solid with a composition C_1^S and the liquid changes its composition to C_1^L. However, on further cooling to T_2 the initial solid cannot change its composition owing to lack of back-diffusion and it is 'isolated'. A local equilibrium is then set up where the liquid of composition C_1^L transforms to a liquid of composition C_2^L and a solid with a composition C_2^S, which is precipitated onto the original solid with composition C_1^S. This process occurs again on cooling to T_3 where the liquid of composition C_2^L transforms to a liquid of composition C_3^L, and a solid with composition C_3^S grows on the existing solid. This process occurs continuously during cooling and, when (partition-coefficient) $k < 1$, this leads to the solid phase becoming lean in solute in the centre of the dendrite and the liquid becoming more and more enriched in solute as the solidification proceeds. Eventually, the composition of the liquid will reach the eutectic composition and final solidification will occur via this reaction.

Any appearance of secondary phases can be easily taken into account in this approach with the assumption that no back-diffusion is involved. Therefore all the transformations can be handled, including the final eutectic solidification. This approach is based on a series of isothermal steps but, as the temperature step size becomes small, it provides results, which are almost completely equivalent to those, which would be obtained from continuous cooling. Thus by the CALPHAD approach, all the disadvantages of the traditional Scheil model can be successfully overcome [20]. The equilibrium thermodynamic calculations were scrutinized using the Scheil model by the CALPHAD approach to confirm whether the combinations still adhere to the solidification criterion. The ones that satisfied the criterion are listed in Tables 3 and 4.

Among the Au–Sn based ternary alloys in the case of Au–Sn–Zn, the composition with which the solidification criterion could be met with the maximum content of Zn is Au–0.27Sn–0.015Zn.

Table 2
Au–Sn based ternary combinations optimized for a narrow solidification range.

S. No.	Minimum (mole-fraction)	Freezing range (°C)	Maximum (mole-fraction)	Freezing range (°C)
1.	Au–0.32Sn–0.01Ag	280.84–305.72	Au–0.35Sn–0.03Ag	275.00–346.81
2.	Au–0.31Sn–0.01Cu	279.51–291.84	Au–0.33Sn–0.04Cu	279.61–347.46
3.	Au–0.30Sn–0.01In	280.99–302.84	Au–0.25Sn–0.07In	303.42–347.06
4.	Au–0.28Sn–0.01Zn	274.96–315.27	Au–0.30Sn–0.09Zn	291.97–347.04

Table 3
Au based ternary combinations adhering to the solidification criterion by Scheil solidification simulations.

S. No.	Ternary compositions (mole-fraction)	Solidus temperature (°C)	Liquidus temperature (°C)	Range (°C)
1.	Au–0.18Ge–0.10In	338.7	340	1.3
2.	Au–0.16Sb–0.22In	307	315	8
3.	Au–0.35Sn–0.21Sb	317	333	16
4.	Au–0.13Sn–0.10Si	271	334	63
5.	Au–0.24Ge–0.05Sb	285	348	63

3.3. Reliability of the flip chip solder joint

The reliability of the solder joint depends primarily upon the phases present in the bulk solder and the intermetallic compounds formed between the solder and the metallization during wetting and/or thermal ageing. One of the primary reliability criteria for the phases present in the bulk solder during room and operating temperatures (150 °C) are: the no. of IMCs should be kept low and the IMCs present should be ductile. The criteria for the IMC formation are IMCs should not possess very low (negative) free energy and only one element in the solder alloy should have a positive tendency to react and form IMCs with the solder wettable layer of the UBM. It would be a great advantage from a reliability perspective if the tendency of forming IMCs during the wetting reaction were kept low since generally the growth of IMCs is rapid during the wetting reaction unlike the solid state diffusion [21].

3.3.1. Prediction of phases in the bulk solder

Among the promising candidates, that adhered to the solidification criterion both by equilibrium calculations and also by the Scheil model, Au–Ge based ternary systems were interesting for this application since the IMC is predicted to exist not as a matrix phase among the following Au–Ge based combinations Au–0.18Ge–0.10In and Au–0.24Ge–0.05Sb, as shown in Figs. 1 and 2, respectively. In the case of Au–0.18Ge–0.10In, no IMC is predicted to exist in the bulk solder while it is predicted to exist as a small dispersed phase in the bulk solder of Au–0.24Ge–0.05Sb alloy.

Au–20Sn (weight-percent), a eutectic composition with a melting point of 280 °C adheres to the solidification requirement of the flip chip assembly but this eutectic composition is brittle since it involves ζ' (Au_5Sn) brittle phase. It has been predicted that the

Table 4
Au–Sn based ternary combinations adhering to the solidification criterion by Scheil solidification simulations.

S. No.	Minimum (mole-fraction)	Freezing range (°C)	Maximum (mole-fraction)	Freezing range (°C)
1	Au–0.32Sn–0.01Ag	281–306	Au–0.35Sn–0.03Ag	278–347
2.	Au–0.31Sn–0.01Cu	279–292	Au–0.33Sn–0.04Cu	278–348
3.	Au–0.30Sn–0.01In	281–303	Au–0.25Sn–0.07In	278–348
4.	Au–0.28Sn–0.01Zn	275–316	Au–0.27Sn–0.015Zn	275–345

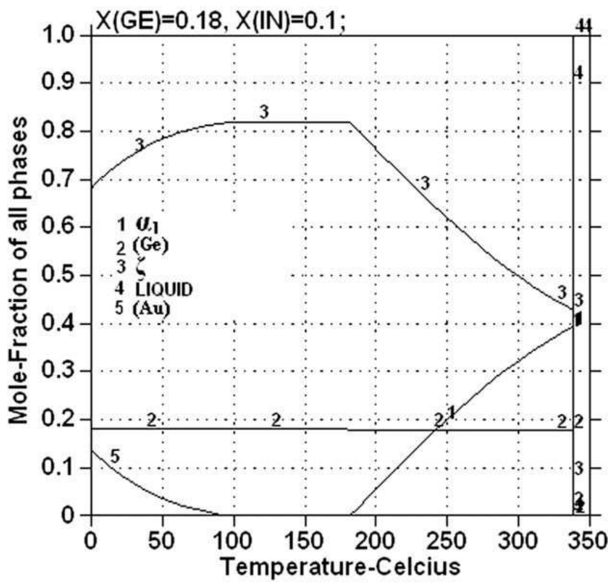

Fig. 1. Phases predicted in the bulk solder of Au–0.18Ge–0.10In alloy.

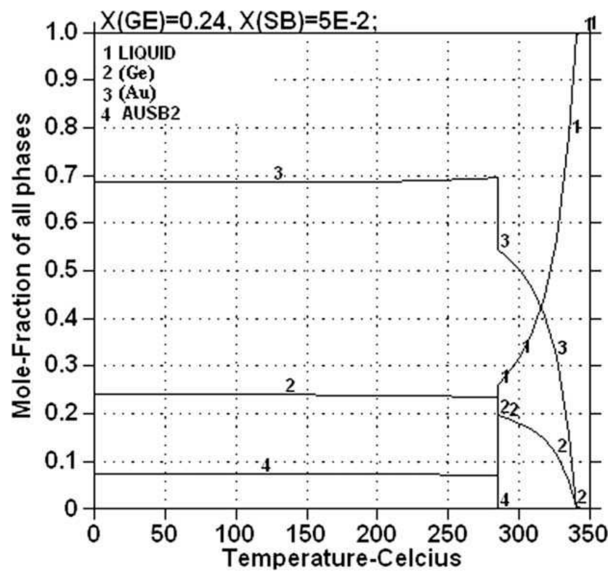

Fig. 2. Phases predicted in the bulk solder of Au–0.24Ge–0.05Sb alloy.

phases in the bulk solder of the eutectic composition in atomic-percent involves around 60% of ζ' (Au_5Sn) phase and 40% of δ (Au–Sn) phase. The effect of the addition of the third alloying element to the eutectic Au–Sn composition with the objective to suppress the formation of brittle ζ' (Au_5Sn) and in turn precipitate relatively ductile phases and still adhere to the solidification criterion was investigated. The hardness values of the Au–Sn binary phases measured by Bergmann et al. [22] and Chromik et al. [23] is shown in Table 5.

The effect of indium on Au–Sn eutectic was not considered for this investigation as both indium and tin have a high tendency to form IMCs with the commonly used solder wettable layer of the UBM. One of the main advantages of using lead along with tin is that lead does not form IMCs with the commonly used solder wettable layer of the UBM. From the reliability perspective it is not safe to have two elements in the same solder alloy with a high tendency to form IMCs. It was determined that both Ag and Cu have a positive effect on the microstructure of the eutectic Au–Sn solder composition from the reliability perspective. It was observed that the addition of both Ag and Cu suppresses the precipitation of the brittle ζ' (Au5Sn) phase and instead proportionally precipitate (Au, Ag) and (Au, Cu) solution phases, respectively. Also relatively ductile δ (Au–Sn) phase is predicted to be the matrix phase. The Au–Sn compositions close to eutectic with the maximum content of Ag and Cu and still adhering to the solidification criterion, are Au–0.35Sn–0.03Ag and Au–0.33Sn–0.04Cu, respectively. The phases predicted in the bulk solder of the eutectic Au–Sn alloy and the effects when having maximum addition of Ag and Cu on the eutectic composition while still adhering to the solidification criterion are illustrated in Figs. 3–5, respectively.

It was predicted that further addition of Ag and Cu to the eutectic composition could also suppress the ζ phase too along with the brittle ζ' (Au5Sn) but with a deviation from the required solidification range. The deviation could be substantial in the case of Ag, i.e. the liquidus temperature for the composition Au–0.36Sn–0.04Ag is 360.89 °C but in the case of Cu, there is only a slight deviation, i.e. the liquidus temperature is 351.08 °C for the composition Au–0.35Sn–0.05Cu. Thus for the composition Au–0.35Sn–0.05Cu even the ζ phase could also be suppressed as shown in Fig. 6. Thus, in the case of Au–Sn–Cu ternary system the final composition for

Table 5
Hardness values of Au–Sn phases.

Phase	Hardness (HV ± σ)	Source
(Au)	66 ± 1.5	[22]
	96 ± 9	[23]
ζ	86 ± 8	[22]
	100 ± 4	[23]
ζ' (Au_5Sn)	143 ± 8	[22]
	236 ± 19	[23]
Eut. $80Au_{20}Sn$	177 ± 7	[22]
($\zeta' + \delta$)	123 ± 19	[23]
δ (AuSn)	107 ± 1	[22]
	104 ± 6	[23]
ε ($AuSn_2$)	207 ± 3	[22]
	274 ± 38	[23]
η ($AuSn_4$)	87 ± 4	[22]
	113 ± 19	[23]
(Sn)	9 ± 0.5	[22]
	24 ± 7	[23]

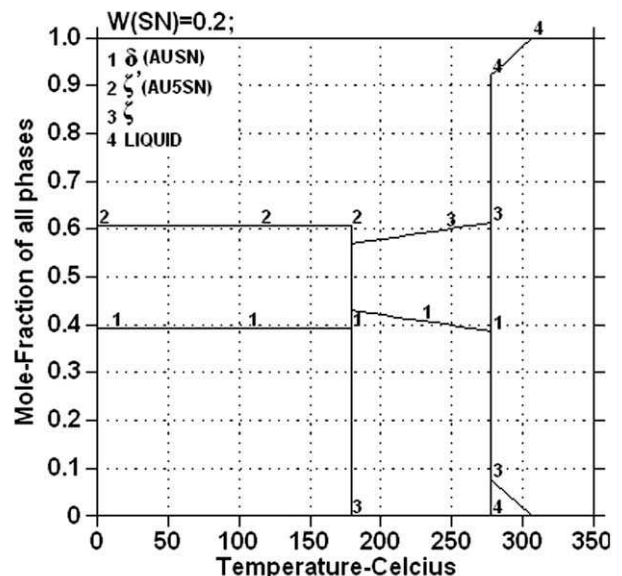

Fig. 3. Phases predicted in the bulk solder of eutectic Au–Sn composition.

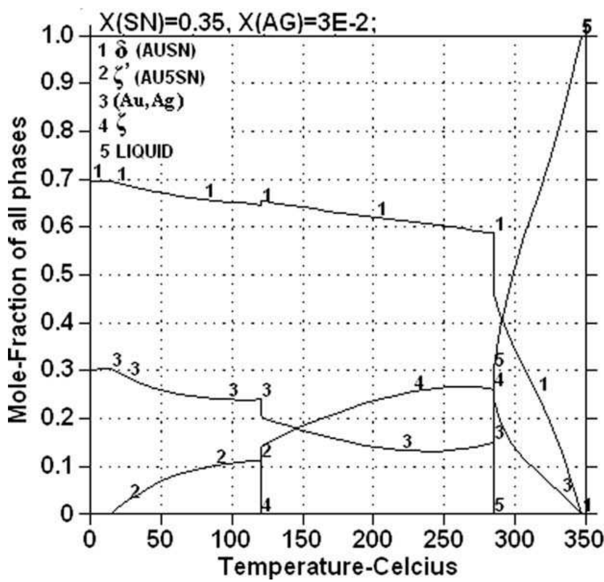

Fig. 4. Phases predicted in the bulk solder of Au–0.35Sn–0.03Ag alloy.

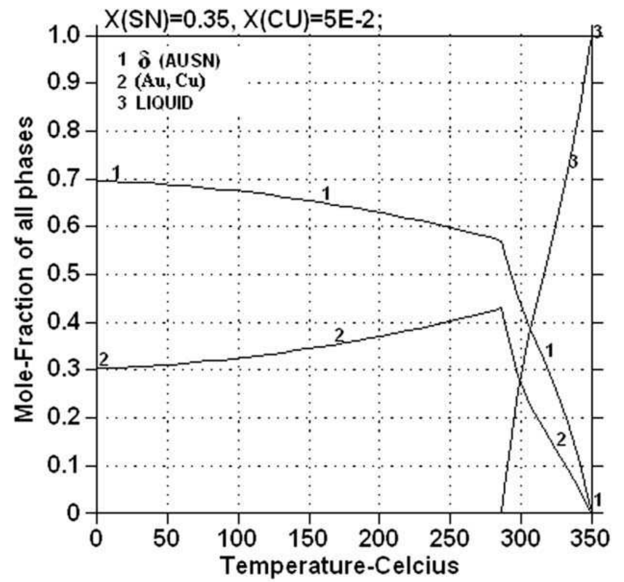

Fig. 6. Phases predicted in the bulk solder of Au–0.35Sn–0.05Cu alloy.

the replacement of high lead containing solders has to be tailored appropriately depending upon the relative ductility between the phases (Au, Cu) and ζ. If the (Au, Cu) phase is more ductile than the ζ phase then Au–0.35Sn–0.05Cu would be the appropriate composition for this application else Au–0.33Sn–0.04Cu would be the better composition since it adheres to the required solidification criterion.

Regarding zinc, it was determined that the addition of zinc to the Au–Sn eutectic, would also suppress the ζ' (Au5Sn) phase but the microstructure predicted for the composition with the maximum content of zinc while still adhering to the solidification criterion, i.e. Au–0.30Sn–0.09Zn, involves both the matrix and the dispersed phases to be IMCs. The effect with the maximum addition of Zn to the eutectic composition while still adhering to the solidification criterion is illustrated in Fig. 7.

Among the other predicted Au based ternary systems, Au–0.18Sb–0.18In is not interesting as Sb is also in the list of toxic elements. The primary reason behind the drive for the development of alternatives to the high lead content solders is not due to technical reasons but for environmental concerns only. Thus, developing a solder with high content of Sb is generally not advocated. The brittle ζ' (Au5Sn) phase cannot be suppressed for the compositions Au–0.15Ge–0.12Sn and Au–0.13Sn–0.10Si, making these alloys less interesting for this application as shown in Figs. 8 and 9, respectively.

Thus, scrutinizing the systems that adhered to the solidification criterion of the flip chip assembly on the basis of the prediction of phases in the bulk solder, the promising solder candidates for the flip chip assembly could be Au–Ge–In, Au–Ge–Sb, Au–Sn–Ag and Au–Sn–Cu. Au–0.18Ge–0.10In and Au–0.24Ge–0.05Sb systems are interesting for this application since the IMC is predicted to exist not as a matrix phase. Au–Ge–Sb has also been included as a potential solder candidate though it includes Sb but still the proportion of Sb in the alloy is small and definitely Sb is not as toxic as Pb. In the case of Au–0.18Ge–0.10In, no IMC is predicted

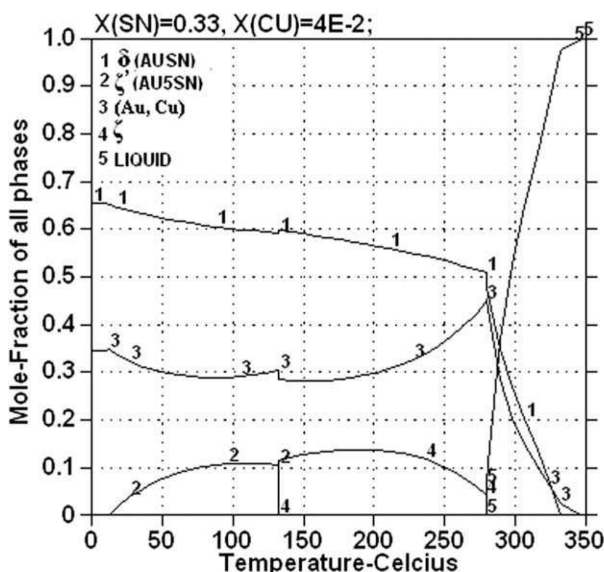

Fig. 5. Phases predicted in the bulk solder of Au–0.33Sn–0.04Cu alloy.

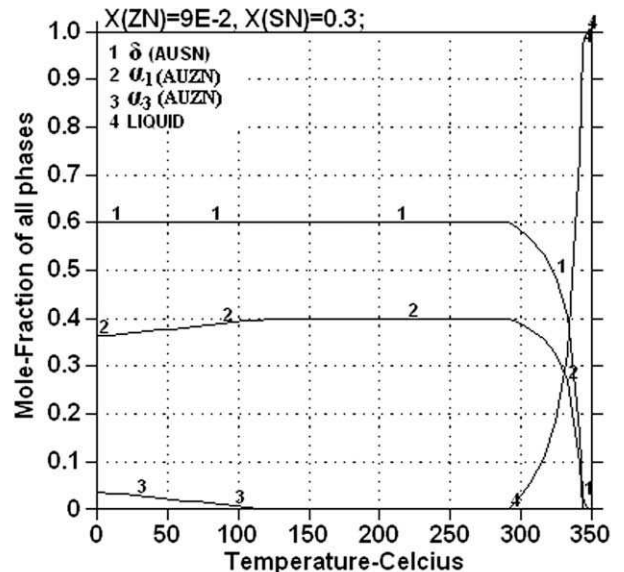

Fig. 7. Phases predicted in the bulk solder of Au–0.30Sn–0.09Zn alloy.

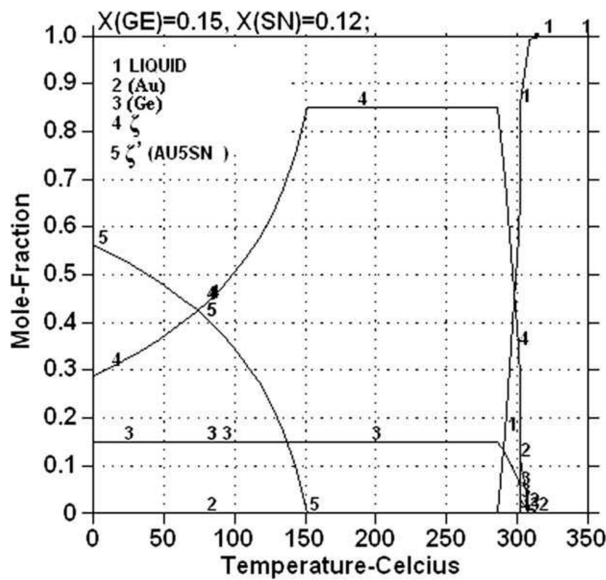

Fig. 8. Phases predicted in the bulk solder of Au–0.15Ge–0.12Sn alloy.

to exist in the microstructure. Au–0.35Sn–0.03Ag and Au–0.33Sn–0.04Cu are also relatively interesting for this application compared to the Au–Sn eutectic itself, even though the matrix phase is predicted to be an IMC, i.e. δ (Au–Sn) phase in the case of Au–0.35Sn–0.03Ag and Au–0.33Sn–0.04Cu but still it is relatively ductile compared to the ζ' (Au5Sn) phase of the Au–Sn eutectic.

3.3.2. Prediction of intermetallic compounds

In the first level packaging, the solder joints are made relatively smaller than the ones in the second level packaging and the intermetallic compounds (IMC) occupies a relatively greater proportion of the solder joint. Thus, the IMCs too are crucial in determining the thermo-mechanical properties along with the microstructure of the bulk solder. IMCs are generally formed between the solder and the solder wettable layer of the under-bump metallization during the wetting reaction and solid state ageing. It is well known that the formation of IMCs between the solder and the solder wettable layer of the UBM is an indication of good metallurgical bonding. A thin, continuous and uniform IMC layer is an essential requirement for good bonding. However, the formation of thick IMCs may degrade the reliability of the solder joint due to their inherent brittle nature and their tendency to generate structural defects [24].

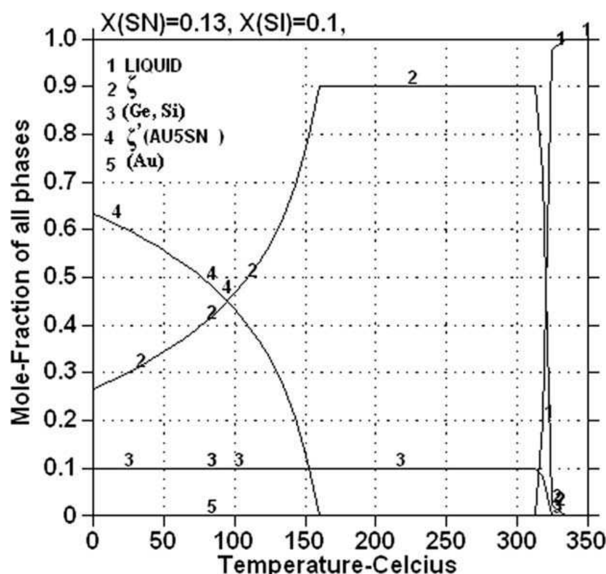

Fig. 9. Phases predicted in the bulk solder of Au–0.13Sn–0.10Si alloy.

It has been experimentally observed by Tu et al. [25] that the rate of intermetallic compound formation in wetting reactions between the molten solder and the metals is three to four orders of magnitude faster than those between the solid state solder and the metals. The rate is controlled by the morphology of the IMC formation. In the wetting reaction, the IMC formation has scallop-type morphology, but in solid state ageing it has layer-type morphology. There are channels between the scallops, which allow rapid diffusion and a rapid rate of compound formation. In the layer-type morphology, the compound layer itself becomes a diffusion barrier to slow down the reaction. These IMCs are generally brittle in nature and are prone to creep and fatigue and thus, such rapid growth of IMCs during the wetting reaction is not favored from a reliability perspective, in which case it would be advantageous that the IMC formation between the proposed promising solder candidates and the metallization is reduced during the wetting reaction.

Au-Ge based promising solder candidates have not been considered for this investigation on IMC formation with the commonly used metallization, as these systems were not critically assessed in the thermodynamic databases used for this work. The focus has been given here only on the IMCs formation of other promising Au based candidates, i.e. Au–0.35Sn–0.03Ag and Au–0.33Sn–0.04Cu with the commonly used metallizations, i.e. Au, Cu, Ni and Pd.

Among the commonly used metallizations, it was predicted that only with Cu these promising solder candidates have a low tendency of forming IMCs during the wetting reaction. The calculated isothermal section during the wetting reaction at 300 °C is illustrated in Fig. 10. This was calculated without taking into account the probability of forming any ternary intermetallic phases.

The equilibrium calculations predict that the kinetic path of IMC formation between Sn containing solder alloy and the Cu metallization has been affected by the high content of gold in the solder alloy. It was determined that this effect is highly pronounced when the content of gold (mole-fraction) is more than 0.5 in the proposed solder alloys. IMCs formation have been predicted for the composition close to Au–Sn eutectic with the maximum content of Ag and Cu and still adhering to the required solidification criterion. Fig. 11 depicts the isopleth, predicting the binary IMCs that could form between the Au–0.33Sn–0.04Cu alloy and the Cu metallization, respectively. The isopleth was constructed by allowing the Au–0.33Sn–0.04Cu alloy to react and form IMCs with the Cu metallization, i.e. the wettable layer of the UBM. It was constructed without taking into account the formation of any ternary intermetallic phases. However, Chang et al. [26] has determined $(Cu_{1-x}Au_x)_6Sn_5$ ternary intermetallic phase experimentally but this phase has not been taken into account due to the lack of thermodynamic information.

Fig. 11 shows that only one stable binary IMC, i.e. ε (Cu3Sn) phase would form between the promising solder candidate Au–0.33Sn–0.04Cu and Cu, i.e. the wettable layer of the UBM and the prominent η (Cu6Sn5) phase would not form at all. Thus, the high content of gold in the solder alloy greatly influences the precipitation of well known IMCs between the Sn containing solder alloy and the Cu metallization, i.e. η (Cu6Sn5) and ε (Cu3Sn). The ε (Cu3Sn) phase too has been predicted to form only at low temperatures and hence, its growth should be slow since the kinetics is likely to be controlled by solid state diffusion. The equilibrium calculation for this proposed solder alloy, i.e. Au–033Sn–0.04Cu,

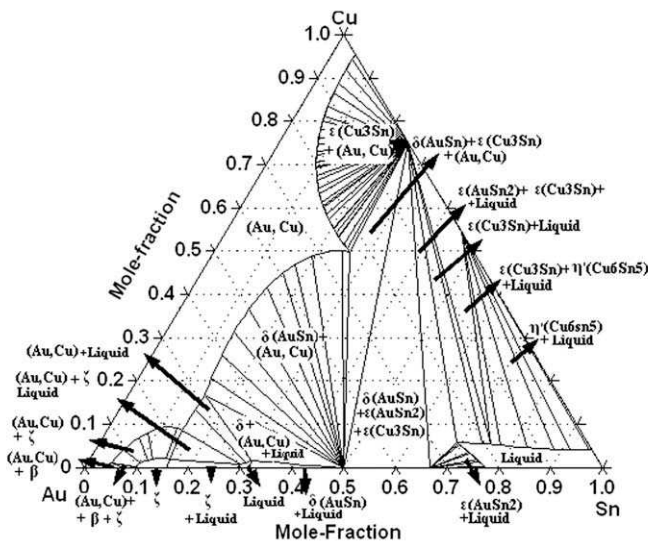

Fig. 10. Isothermal section of Au–Sn–Cu system at 300 °C.

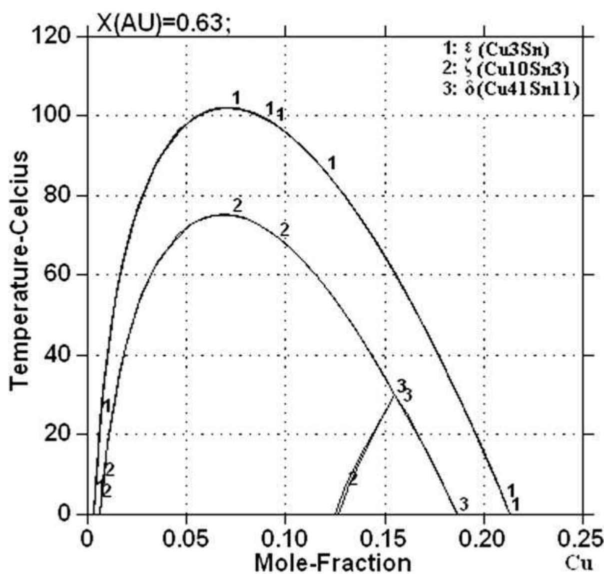

Fig. 11. Isopleth predicting possible binary IMCs that could form between Au–0.33Sn–0.04Cu alloy and the Cu metallization.

shows that the tendency to form IMCs with the Cu metallization decreases proportionally with the increase in the gold content in the solder alloy. Thus, the high content of gold in the solder alloy has a substantial effect on the formation of IMCs between Sn and Cu. The stable ε (Cu3Sn) phase was suspended from the calculation and the isopleth was recalculated and the predicted meta-stable phases have also been included in Fig. 11. Thus, there is also a high probability of forming ζ (Cu10Sn3) and δ (Cu41Sn11), meta-stable phases in addition to the ε (Cu3Sn) stable phase. A similar behavior on IMCs formation was predicted between the Au–0.35Sn–0.03Ag solder candidate and the Cu metallization too, with little variations in the temperature range.

4. Concluding remarks

Based on the present work's findings it can be stated that, the motivation behind the drive of lead-free solders, i.e. developing 'environmentally friendly' solders, will be served only by adapting to gold based solder alloys. Among the various gold based ternary combinations that could probably adhere to the solidification criterion, the most promising ones with respect to the predicted phases in the bulk solder are Au–Ge–In, Au–Ge–Sb, Au–Sn–Ag and Au–Sn–Cu. The final Au–Sn–Cu solder alloy composition has to be tailored for this application depending upon the relative ductility between the phases; (Au, Cu) and ζ.

Among the commonly used solder wettable layers for the flip chip assembly, it was predicted that the most promising one is Cu, based on the IMC formation between the promising candidates, i.e. Au–Sn–Ag and Au–Sn–Cu with the commonly used metallizations. It was predicted that the high content of gold in the solder alloy has a substantial effect on the formation of IMCs between Sn and Cu. However, the present understanding of the behavior of these intermetallic structures during longer term use is very low and hence needs more research from the reliability perspective since it is being employed in mission-critical operations.

Acknowledgement

The authors acknowledge the Danish Ministry of Science, Technology and Development for financial support through the innovation consortium "Matpack" (Project No. 07-003145).

References

[1] Braun T, Becker KF, Koch M, Bader V, Aschenbrenner R, Reichl H. High-temperature reliability of flip chip assemblies. J Microelectron Reliab 2006;46:144–54.
[2] Lau John H. Low cost flip chip technologies. New York: Mc Graw-Hill; 2000.
[3] Juergen Wolf M, Engelmann Gunter, Dietrich Lothar, Reichl Herbert. Flip chip bumping technology – status and update. J Nucl Instrum Meth Phys Res A 2006;565:290–5.
[4] Deborah S. Patterson, Peter Elenius, James A. Leal. A wafer bumping technologies – a comparative analysis of solder deposition processes and assembly considerations. EEP-vol 19-1. Hawaii, USA; June 1997, p. 337–51.
[5] Puttlitz Karl J, Galyon George T. Impact of the ROHS on high-performance electronics systems. J Mater Sci: Mater Electron 2007;18:347–65.
[6] Takaku Yoshikazy, Ohnuma Ikuo, Kainuma Ryosuke, Yamada Yasushi, Yagi Yuji, Nishibe Yuji, et al. Development of Bi-base high-temperature Pb-free solders with second – phase dispersion: thermodynamic calculation, microstructure and interfacial reaction. J Electron Mater 2006;35:1926–32.
[7] Herat S. Green electronics through legislation and lead free soldering. Clean 2008;36:141–51.
[8] Ogunseitan Oladele A. Public health and environmental benefits of adapting lead-free solders. JOM 2007:12–7.
[9] European Union, Directive 2002/95/EC of the European Parliament and of the Council of 27 January 2003 on the restriction of the use of certain hazardous substances in electrical and electronic equipment. OJEU 2002; 37: p. 19–23.
[10] European Union, 2005/747/EC: commission decision of 21 October 2005 amending for the purposes of adapting to technical progress the annex to directive 2002/95/EC of the European Parliament and of the council on the restriction of the use of certain hazardous substances in electrical and electronic equipment. OJEU 2005; 280: p. 18–19.
[11] US Environmental Protective Agency (EPA). <http://www.epa.gov/>.
[12] US Department of Labor. Occupational Safety and Health Administration (OSHA). <http://www.osga.gov/>.
[13] Mulugeta Abtew, Guna Selvaduray. Lead – free solders in microelectronics. J Mater Sci Eng 2007;27:95–141.
[14] Holiday Richard J, Corti Christopher W. Trends in the use of gold in current industrial applications. London: World Gold Council; 2002.
[15] United States Geological Survey. <http://www.minerals.usgs.gov/minerals/pubs/mcs/>; [accessed 31.12.07].
[16] Kattner Ursula R, Handwerker Carol A. Calculation of phase equilibria in candidate solder alloys. Z Metallkd 2001;92:1–9.
[17] Lukas HL, Fries SG, Sundman B. Computational thermodynamics – the Calphad method. Cambridge University press; 2007.
[18] Dinsdale AT, Watson A, Kroupa A, Zemanova A, Vrestal J, Vizdal J. COST 531 database V 3.0; June 2008.
[19] Scientific Group Thermodata Europe (SGTE). SSOL2 Solutions Database Version 2.1, 1999/2003/2003.
[20] Saunders N, Miodownik AP. CALPHAD, Pergamon Materials Series; 1998.
[21] Aloke Paul. The Kirkendall effect in solid state diffusion. PhD. Dissertation 2004, ISBN 90-386-2646-0.
[22] Bergmann Rene, Tang Peter Torben, Hansen Hans Nørgaard, Møller Per. In-situ investigation of lead free solder alloy formation using a hot-plate microscope. IEEE Conf Proc 2007.

[23] Chromik RR, Wang D-N, Shugar A, Limata L, Notis MR, Vinci RP. Mechanical properties of intermetallic compounds in the Au–Sn system. J Mater Res 2005;20:2161–71.
[24] Laurila T, Vuorinen V, Kivilahti JK. Interfacial reactions between lead-free solders and common base materials. J Mater Sci Eng 2005;49:1–60.
[25] Tu KN, Zeng K. Tin–lead (Sn–Pb) solder reaction in flip chip technology. J Mater Sci Eng 2001;34:1–58.
[26] Chang CW, Lee QP, Ho CE, kao CR. Cross-interaction between Au and Cu in Au/Sn/Cu ternary diffusion couples. J Electron Mater 2006;35:366–71.

Appendix III

Development of Au-Ge based candidate alloys as an alternative to high-lead content solders

Vivek Chidambaram, John Hald and Jesper Hattel

Alloys and Compounds, 490: 170-179, 2010.

Journal of Alloys and Compounds 490 (2010) 170–179

Contents lists available at ScienceDirect

Journal of Alloys and Compounds

journal homepage: www.elsevier.com/locate/jallcom

Development of Au–Ge based candidate alloys as an alternative to high-lead content solders

Vivek Chidambaram*, John Hald, Jesper Hattel

Department of Mechanical Engineering, Technical University of Denmark, Building 425, Produktionstorvet, Lyngby DK-2800, Denmark

ARTICLE INFO

Article history:
Received 28 September 2009
Received in revised form 10 October 2009
Accepted 14 October 2009
Available online 23 October 2009

Keywords:
High-temperature solders
Precipitation
Phase transitions
Solid solution strengthening
Composite strengthening
Phase-equilibria

ABSTRACT

Au–Ge based candidate alloys have been proposed as an alternative to high-lead content solders that are currently being used for high-temperature applications. The changes in microstructure and microhardness associated with the addition of low melting point metals namely In, Sb and Sn to the Au–Ge eutectic were investigated in this work. Furthermore, the effects of thermal aging on the microstructure and its corresponding microhardness of these promising candidate alloys have been extensively reported. To investigate the effects of aging temperature, candidate alloys were aged at a lower temperature, 150 °C for up to 3 weeks and compared with aging at 200 °C. After being subjected to high-temperature aging, the microstructure varied a lot in morphology in the case of both Au–Ge–Sb and Au–Ge–Sn candidate alloys while the microstructure remained relatively stable even after long-term thermal aging in the case of the Au–Ge–In candidate alloy. The microhardness measurement is well correlated with the solubility and reactivity of these alloying elements, characteristics of their intermetallic compounds (IMCs) and the distribution of phases. The primary strengthening mechanism in the case of Au–Ge–In and Au–Ge–Sn combinations was determined to be the classic solid solution strengthening. The Au–Ge–Sb combination was primarily strengthened by the refined (Ge) dispersed phase. The aging temperature had a significant influence on the microhardness in the case of the Au–Ge–Sn candidate alloy. The distribution of phases played a relatively more crucial role in determining the ductility of the bulk solder alloy. The findings of this work are: the addition of Sb to the Au–Ge eutectic would not only decrease its melting point but would also improve its ductility substantially and the lattice strains induced by the In atoms were the most effective strengthening mechanism.

© 2009 Elsevier B.V. All rights reserved.

1. Introduction

High-lead content solders are being widely used in advanced electronic packagings to provide stable interconnections that resist a severe thermal environment and also to facilitate the drive for miniaturization [1,2]. However, these high-lead content solders still hinder the recycling of electronic products even though the circuit boards are assembled with lead-free Sn-based solders. Thus, the establishment of high-temperature lead-free solders is an urgent priority in the electronics and automotive industries [3]. The primary indispensable requirement for the high-temperature solder selection is the melting temperature range (270–350 °C) [4].

The selection of high-temperature solders is still a challenge since a survey of phase diagrams reveals that there is no drop-in replacement. Among the cheaper alternatives being proposed, Zn–Al based alloys have several limitations since Zn is highly corrosive while Al possesses a high natural radius of curvature (R) that would hamper the drive for miniaturization. The continuing miniaturization of components in the microelectronics industry places ever increasing demands upon solder alloys to be designed for low R values in order to prevent bridging between contacts as the pitch between contacts keeps getting smaller and smaller during the miniaturization drive [5].

$$R = \left(\sqrt{\frac{\gamma}{\rho g}}\right) \tag{1}$$

where γ = surface tension, ρ = density and g = acceleration due to gravity. Bi based alloys too have several drawbacks such as low electric and thermal conductivity and brittleness [6]. Thus, the present work focuses on the development of Au–Ge based candidate alloys as an alternative to high-lead content solders.

Au–Ge is an interesting system for this application since it does not have any intermetallic phases. Moreover, the tendency of Ge towards forming intermetallic compounds (IMCs) with the commonly used wetting layers of the under-bump metallization (UBM)

* Corresponding author at: Department of Mechanical Engineering, Technical University of Denmark, Room No. 31, Building 425, Produktionstorvet, Lyngby DK-2800, Copenhagen, Denmark. Tel.: +45 4525 4880; fax: +45 4593 4570.
E-mail address: vchi@mek.dtu.dk (V. Chidambaram).

0925-8388/$ – see front matter © 2009 Elsevier B.V. All rights reserved.
doi:10.1016/j.jallcom.2009.10.108

is also very low. Gold has been ranked as one of the least toxic elements by both EPA-US (Environmental protective agency-United States) and OSHA (Occupational and safety health administration) [7,8]. Toxicological studies have documented germanium as a therapeutic element [9]. The eutectic melting temperature of the Au–Ge (28 at.% Ge) composition is 360 °C. It slightly deviates from the permissible liquidus temperature. Phase-equilibria calculation shows that the addition of a low melting point metal such as In or Sb or Sn decreases the melting point of this alloy below 350 °C [5]. Thus, the effect of these low melting point metals on the Au–Ge eutectic with respect to microstructure and its corresponding mechanical properties has been investigated in this work.

High-temperature solders are used for wide applications in the electronics and automotive industries. The operating temperature that the high-temperature solders are being subjected to varies between 150 and 200 °C depending on the applications. At high-temperature, the microstructure of these promising solder candidates could significantly change and consequently their mechanical properties could be affected [10,11]. Therefore, in this work, the high-temperature stability of microstructures and mechanical properties of Au–Ge based solder candidates are extensively reported. This work only characterizes the properties of bulk solders and does not consider factors such as reactions with joining materials, which may affect the mechanical performance of actual solder joints. Instead the work focuses on specific microstructural features that can explain solder performance at elevated temperatures.

Table 1
Phases predicted in the bulk solder for the optimized ternary compositions in mole-fraction.

Optimized ternary compositions	Phases predicted (150 °C)		Phases predicted (200 °C)	
	Matrix	Dispersed	Matrix	Dispersed
Au–0.18Ge–0.10In	ζ	(Ge)	ζ	(Ge), α_1
Au–0.24Ge–0.05Sb	(Au)	(Ge), $AuSb_2$	(Au)	(Ge), $AuSb_2$
Au–0.15Ge–0.12Sn	ζ	Au_5Sn, (Ge)	ζ	(Ge)

2. Materials and methods

Phase-equilibria calculations in this work have been carried out using a thermodynamic description of the phases in SSOL2 [12] and COST 531 v 3.0 [13] thermodynamic databases via the Thermo-Calc (version R) software. The promising Au–Ge based candidate alloys that were determined based on the solidification criterion and optimized for a narrow solidification range by the CALPHAD approach, were precisely produced using a hot-plate microscope [14].

The high purity metal powders were carefully weighed and were mixed inside a specially designed pressing tool to form small tablets. The tablet was placed inside a cylindrical aluminium oxide crucible on a molybdenum plate that is mounted between the electrical contacts of the heating system inside the specimen chamber of the hot-plate microscope. The heating system can reach a temperature up to approximately 1400 °C and is equipped with water cooling. A high-vacuum ($<1 \times 10^{-3}$ mbar) was created in the specimen chamber and it was controlled by pressure measurements. The melting process was carried out under hydrogen flow to prevent further oxidation of the material and to start the reduction of oxides on the surface of the developing sphere. Usually, non-metal impurities pop up during the sphere forming process and it is necessary to clean the metal sphere. Normally it is done by washing it by ethanol followed by drying [15]. The solder sphere is remelted a couple of times for homogenization. A

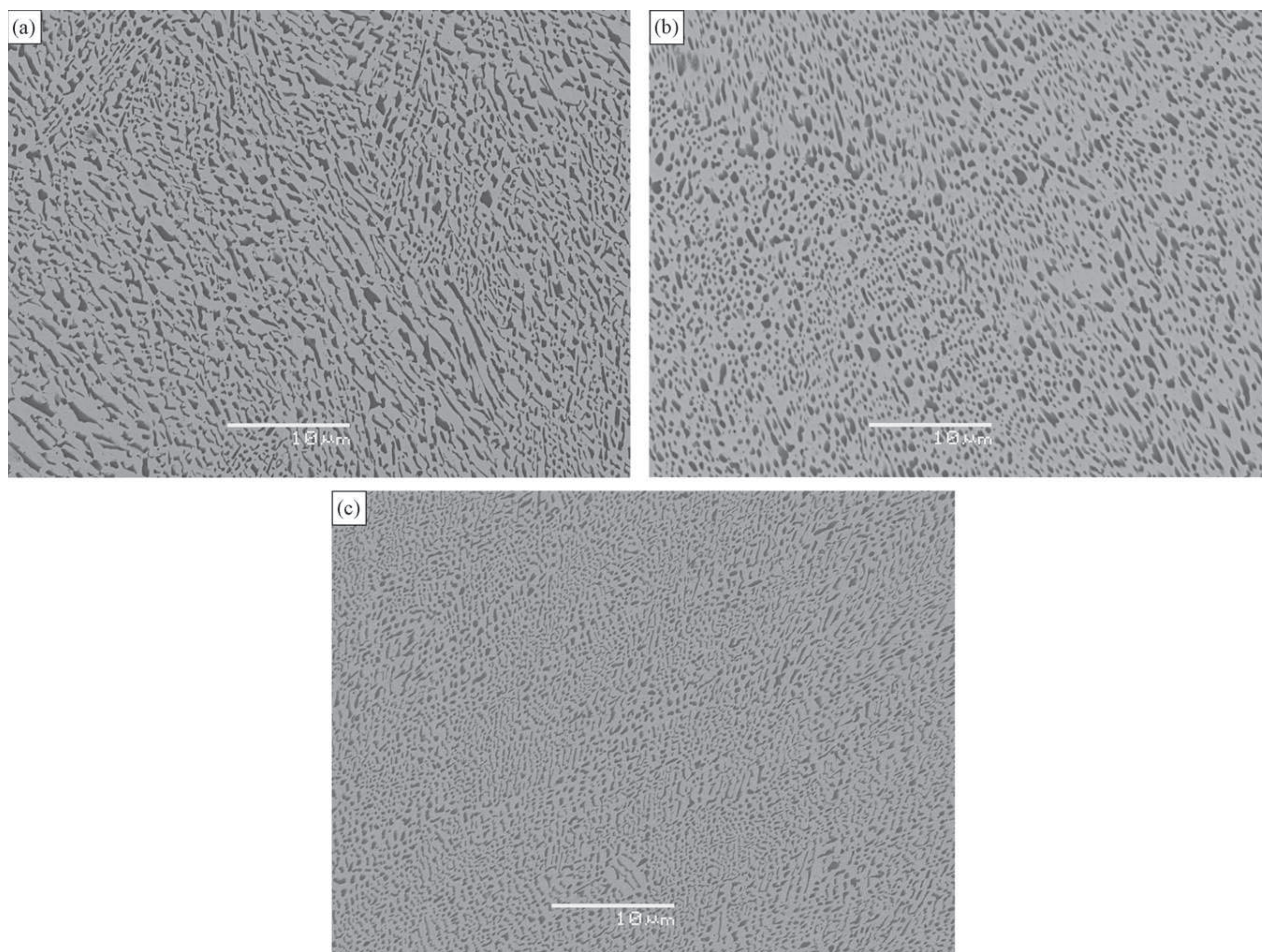

Fig. 1. SEM-BSE micrograph of the Au–0.28Ge eutectic alloy before and after thermal aging at 200 °C, (a) as-produced, (b) 1 day, and (c) 1 week.

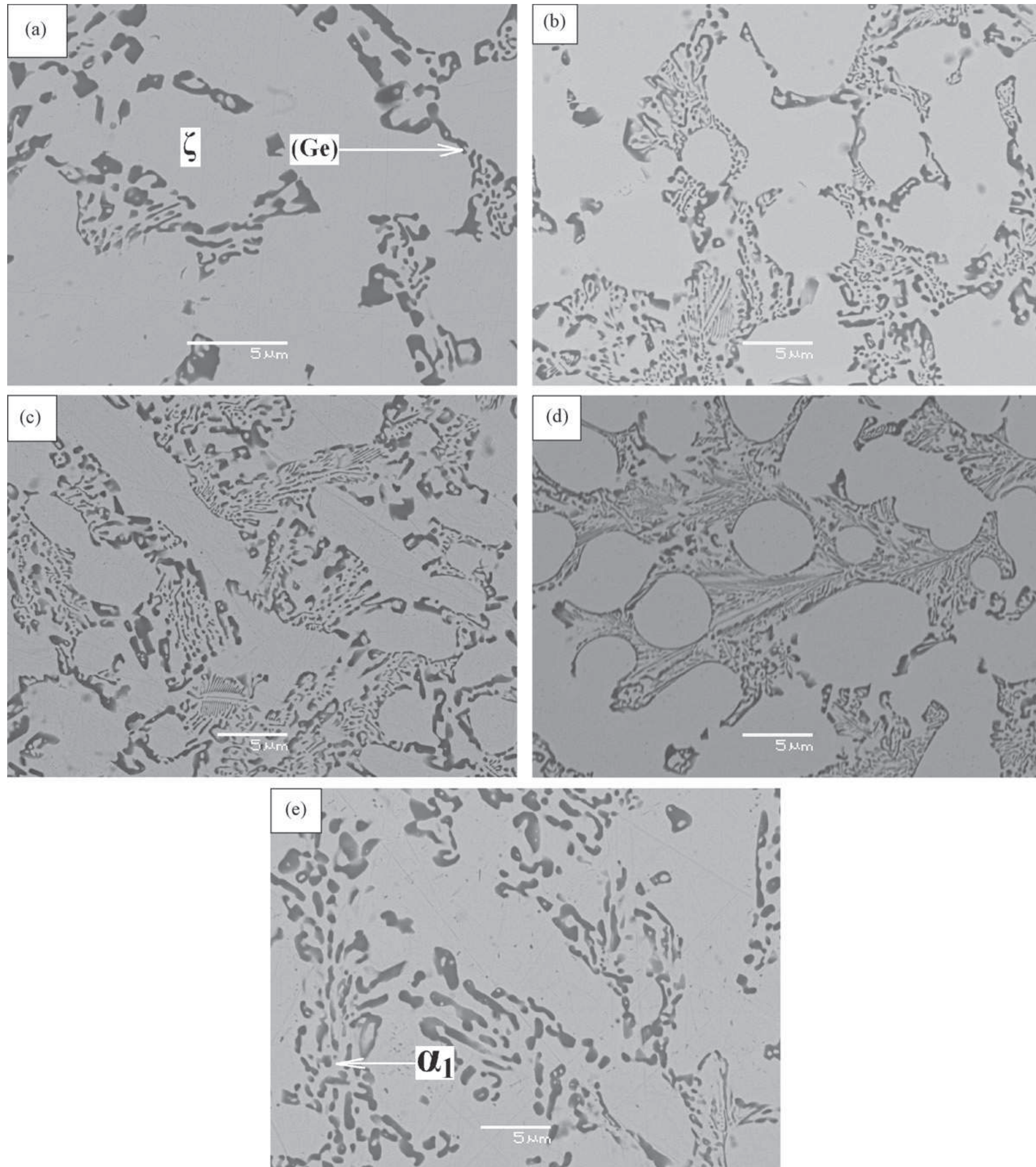

Fig. 2. SEM-BSE micrograph of the Au–0.18Ge–0.10In candidate alloy before and after thermal aging, (a) as-produced, (b) 150 °C-1 day, (c) 150 °C-3 weeks, (d) 200 °C-1 day, and (e) 200 °C-3 weeks.

high cooling rate (300 K/s) was employed during the production of these solder spheres.

The solder spheres were split into six batches and loaded into an ambient atmosphere-resistance furnace for thermal aging at 200 and 150 °C for either 1 day or 1 week or 3 weeks, respectively. The as-produced and thermally aged samples were embedded in an epoxy resin, ground and polished in accordance with the standard metallographic preparation methods for observations of the microstructure and also for the testing of microhardness. Both mechanical polishing and chemical etching were used to expose grain boundaries and examine different phases of the solder alloys. Microstructural analysis of the as-solidified and aged solder alloys was performed by optical microscopy and scanning electron microscopy (JEOL 5900). SEM/EDX analysis was used to identify the developed phases inside the sphere and it was carried out on unetched samples.

The microhardness measurements were carried out using a Vickers microhardness measurement system, FM-700 Future-Tech and JK Lab software. In this work, the loading time used was 5 s and the loading force was 5 and 100 g. 5 g load was used to determine the hardness of individual phases. However, in certain cases it was not possible to measure the hardness of individual phase without hitting other phases. 100 g load was also applied so that the width of the indentation is large enough to span multiple phases and many eutectic domains. Hence the test values reflect the overall microhardness of solder candidates. For each sample at least 10 random points were measured and the arithmetical mean values were evaluated as the results due to the slight variance of the 10 measurements.

3. Results and discussion

3.1. Thermodynamic predictions

Phase-equilibria calculation shows that the addition of a low melting point metal such as In or Sb or Sn to the Au–Ge eutectic decreases the melting point of the ternary alloy and thereby making it adhere to the required solidification criterion. These ternary combinations were then optimized for a narrow solidification range

since a narrow solidification range is commercially preferred for facilitating rapid production, efficient process control, preventing the movement of components during solidification and for minimizing segregation during solidification [4,5]. Phases predicted in the bulk solder for these optimized ternary combinations at 150 and 200 °C are shown in Table 1. The phases in this context were classified as matrix and dispersed only based on the thermodynamic estimation of mole-fraction of the corresponding phases under equilibrium conditions.

3.2. Structural variation during aging

Before being subjected to thermal aging, the as-produced Au–Ge eutectic samples comprised of coarse (Ge) lamellae uniformly distributed on the white (Au) phase. After high-temperature aging at 200 °C, these lamellae were observed to be relatively fine as illustrated in Fig. 1. This change in morphology was more pronounced with the increase in the thermal aging duration. However, no progressive change in morphology was observed after aging for 1 week at 200 °C. No significant variations in the morphology of (Ge) lamellae was observed in the samples aged at 150 °C for different durations when compared to the samples aged at 200 °C.

The microstructure of the as-produced Au–0.18Ge–0.10In candidate alloy was comprised of ζ phase dispersed in the matrix. The matrix was composed of (Ge) lamellae that were homogenously distributed over the ζ phase and the α_1 phase (200 °C-3 weeks). Surprisingly the microstructure remained relatively stable even after high-temperature aging both at 150 and 200 °C as depicted in Fig. 2. α_1 phase did not exist in the as-produced samples and also in the samples that were aged at 150 °C for different durations. α_1 phase was observed only in the samples that were aged at 200 °C for 3 weeks and even not in the samples that were aged at 200 °C for 1 day or 1 week. This effect could be attributed to the fast cooling rate employed during the production of these alloys in the hot-plate microscope. Thus, it could be concluded that the microstructure gradually transformed into that of the Au–Ge–In candidate alloy in an equilibrium state at 200 °C (as predicted by phase-equilibria calculation) during long-term thermal aging.

It was observed that the volume-fraction of Au rich phases in the matrix was relatively higher in the samples that were aged at 200 °C for different durations when compared to those aged at 150 °C for similar respective aging durations. Fig. 3 illustrates the influence of aging temperature on the volume-fraction of Au rich phases in the matrix. The volume-fraction of Au rich phases in the matrix increased proportionally with the aging durations irrespective of the aging temperature. However, this effect was relatively more pronounced at 200 °C.

In the Au–0.24Ge–0.05Sb candidate alloy, the white, dark and gray areas were identified as (Au), (Ge) and $AuSb_2$ phases respectively as illustrated in Fig. 4. Mixed granules of (Au) and (Ge) phases too existed in the microstructure of as-produced Au–0.24Ge–0.05Sb candidate alloy. Large (Au) phases emerged in the solder matrix instead of many small (Au) phases (as-produced) and few small (Au) phases still existed in the solder matrix when the samples were subjected to high-temperature aging both at 150 and 200 °C as depicted in Fig. 4. Thus, during aging irrespective of the aging temperatures, the growth of the (Au) phase was observed in order to reduce the interfacial energy. The growth of the (Au) phase was more pronounced with the aging duration. However, the growth of the (Au) phase at 200 °C was relatively higher when compared to the growth of the (Au) phase at 150 °C as illustrated in Fig. 5. Thus, it could be concluded that the growth of the (Au) phase in the Au–0.24Ge–0.05Sb candidate alloy increased proportionally with the aging temperature. Slight dissolution of the bulk (Ge) phase into relatively finer ones during the course of aging at both the aging temperatures was observed. Slight coarsening of the $AuSb_2$ IMC was observed only in the samples that were thermally aged at 200 °C for 3 weeks. Mixed granules of (Au) and (Ge) phases still existed in the microstructure of all the thermally aged samples irrespective of the aging durations and aging temperatures.

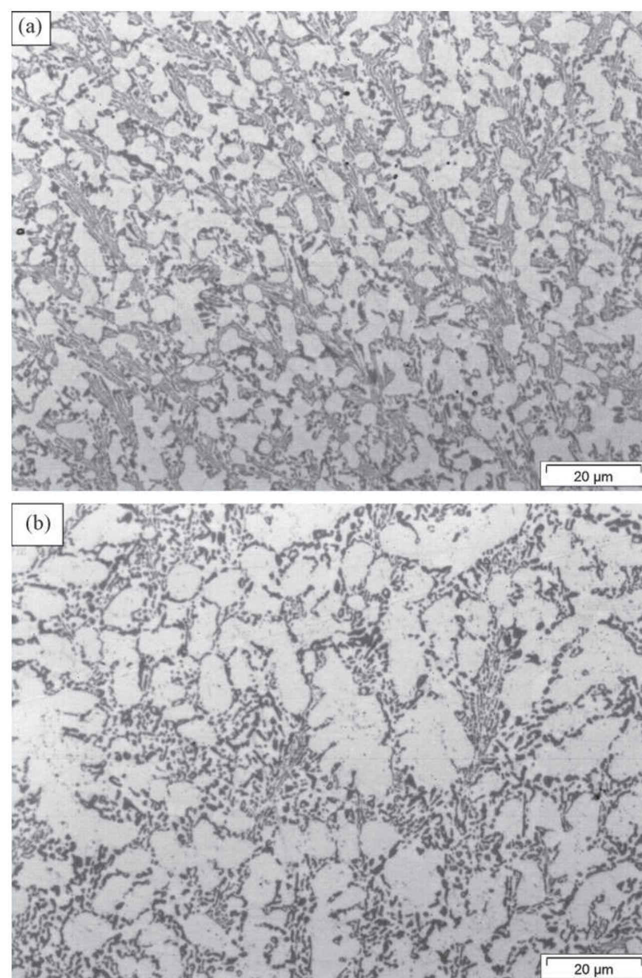

Fig. 3. Optical microstructure of Au–0.18Ge–0.10In candidate alloy after thermal aging for 3 weeks, (a) 150 °C and (b) 200 °C.

Before thermal aging, the matrix of the Au–0.15Ge–0.12Sn candidate alloy was composed of mixed lamellae [(Ge) and AuSn] phases that were homogenously distributed over ζ and Au_5Sn phases. These lamellae were predominantly composed of (Ge) phase [dark] and also a few AuSn phase [gray] were observed. Coarse ζ dendrites and also few Au_5Sn granules were found to be dispersed in the matrix. This could be attributed to the fast cooling rate employed during the preparation of solder spheres using the hot-plate microscope. The fast cooling rate to a certain extent has suppressed the precipitation of Au_5Sn phase. The presence of AuSn phase in the as-produced samples can be attributed to non-equilibrium solidification since AuSn phase is not expected to precipitate for this specific composition and temperature range, as per phase-equilibria calculation. The microstructure of the Au–0.15Ge–0.12Sn candidate alloy was relatively refined after thermal aging, i.e. the dissolution of bulk ζ dendrites into finer ones was observed during high-temperature aging both at 150 and 200 °C as illustrated in Fig. 6.

Both Au_5Sn and AuSn phases did not exist in the microstructure of the Au–0.15Ge–0.12Sn candidate alloy subjected to high-temperature aging at 200 °C for 3 weeks. Thus, both the Au_5Sn and AuSn phases that existed in the microstructure of the as-produced Au–0.15Ge–0.12Sn candidate alloy gradually disappeared during

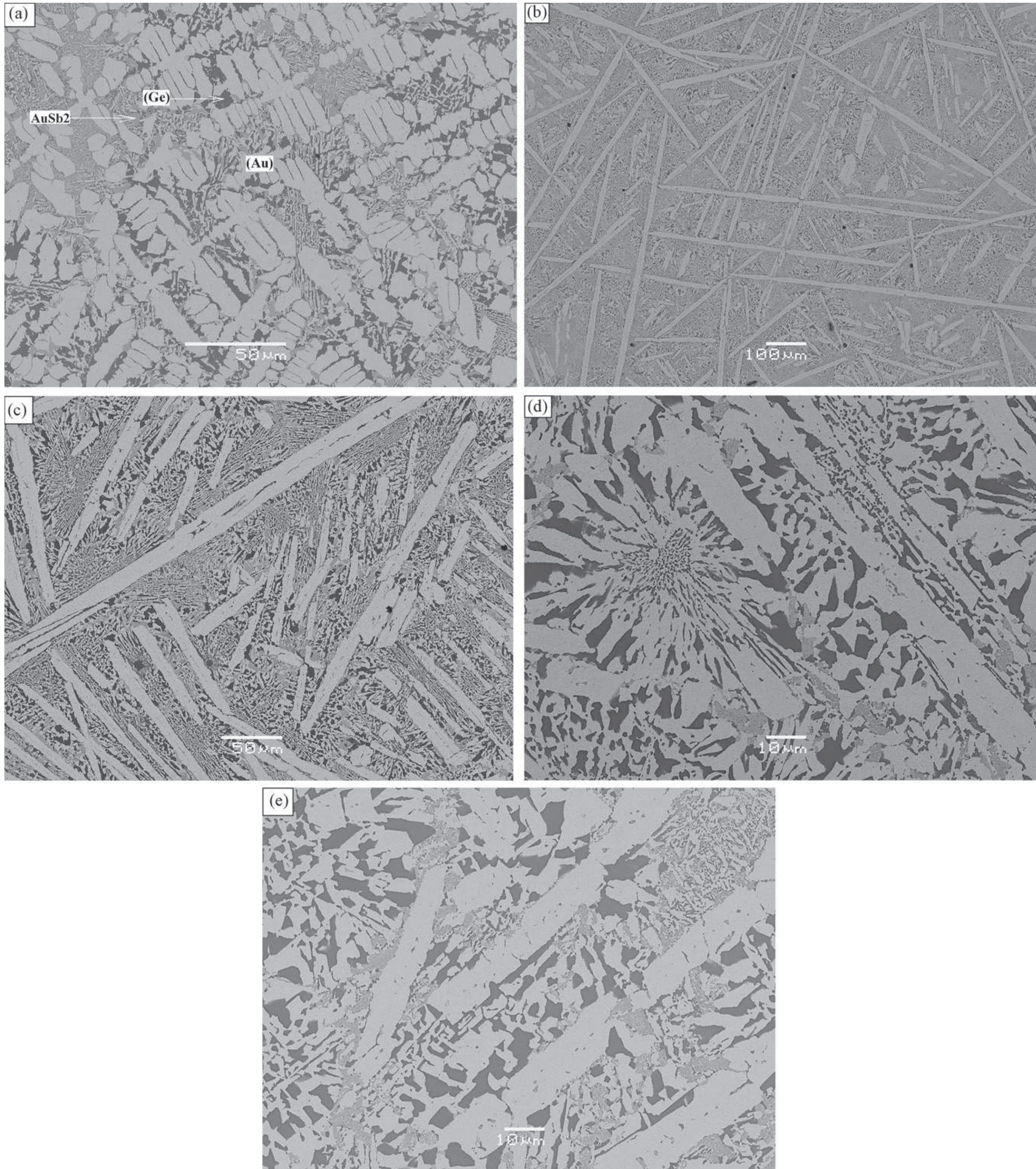

Fig. 4. SEM-BSE micrograph of the Au–0.24Ge–0.05Sb candidate alloy before and after thermal aging, (a) as-produced, (b) 150 °C-1 week, (c) 150 °C-3 weeks, (d) 200 °C-1 week, and (e) 200 °C-3 weeks.

thermal aging. Therefore, it could be concluded that the microstructure gradually transformed into that of the Au–0.15Ge–0.12Sn in an equilibrium state during long-term thermal aging at 200 °C. However, SEM analysis showed that the volume-fraction of Au_5Sn increased proportionally with the aging duration in the samples that were aged at 150 °C. Similar to the ones aged at 200 °C, the AuSn phase gradually disappeared during the course of aging at 150 °C and eventually did not exist in the microstructure of the samples that were aged at 150 °C. Thus, at both the aging temperatures, the microstructure gradually transformed into that of the Au–0.15Ge–012Sn in an equilibrium state.

It was observed that the volume-fraction of Au rich phases in the matrix was relatively higher in the samples that were aged at 200 °C for different durations when compared to those aged at 150 °C for similar respective aging durations. Fig. 7 illustrates the influence of aging temperature on the volume-fraction of Au rich phases in the matrix. The volume-fraction of Au rich phases in the matrix increased proportionally with the aging durations irrespective of

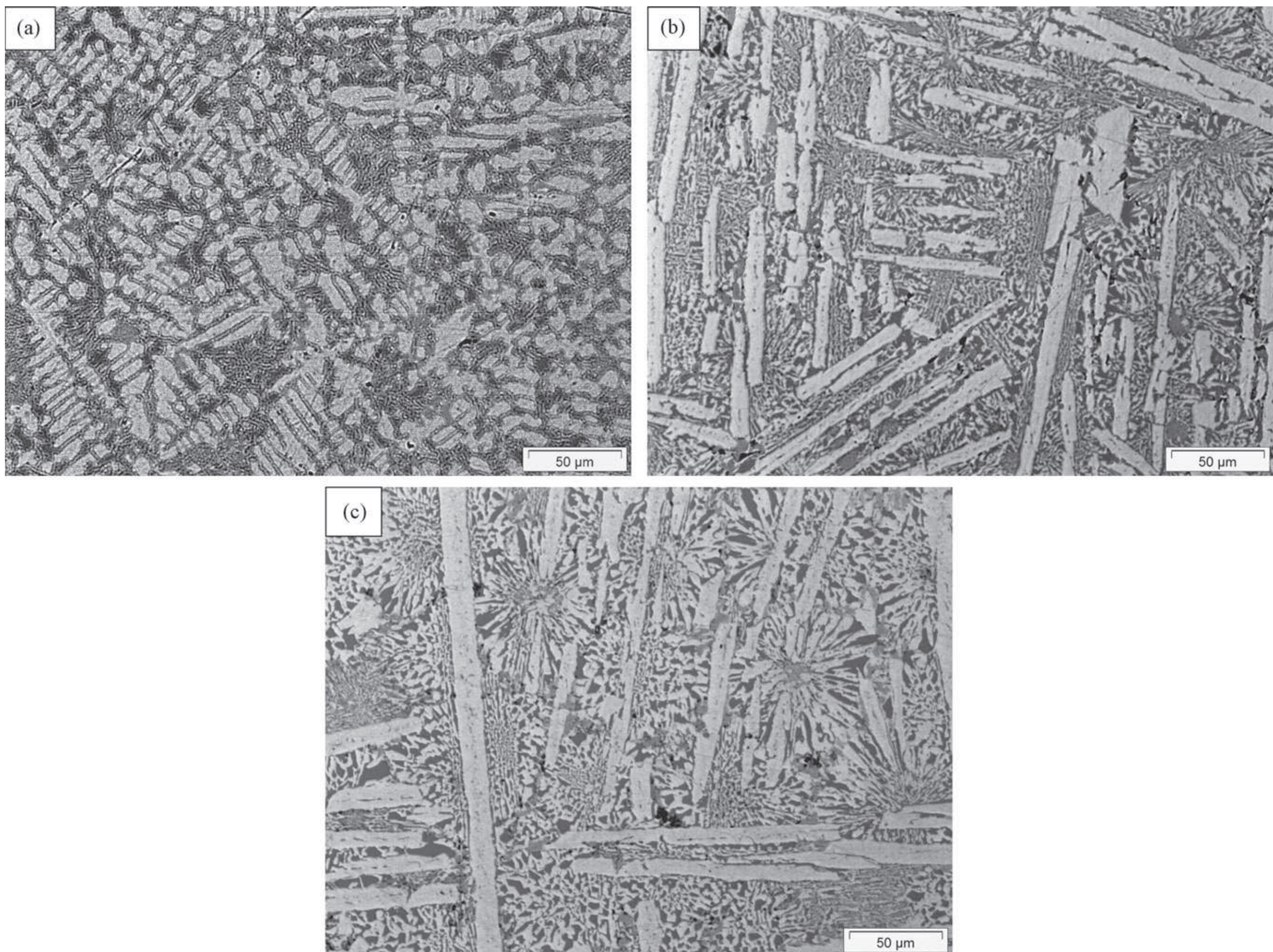

Fig. 5. Optical microstructure of Au–0.24Ge–0.05Sb candidate alloy before and after thermal aging for 3 weeks, (a) as-produced, (b) 150 °C, and (c) 200 °C.

the aging temperature. However, this effect was relatively more pronounced at 200 °C.

3.3. Microhardness of candidate alloys before and after aging

The microhardness of the solders is tested because it is considered the most convenient way to determine the mechanical properties of materials, especially for solder alloys, which are normally composed of soft and hard phases [16]. The test can be performed in a very small zone and can determine the hardness of individual grains, phases and structural components of the alloys. The rule of the thumb is the higher the hardness, the higher is the mechanical strength but with a compromise on ductility. Although eutectic alloys have high mechanical strength and a considerable amount of hardness, the introduction of a third element even in small proportions to a binary eutectic alloy could result in a significant variation in terms of its mechanical properties [17].

It was not possible to measure the hardness of individual phases without hitting other phases in the case of Au–Ge eutectic even with the 5 g load. A eutectic microstructure has a very high surface area per unit volume and it is therefore very hard for a dislocation line to move within the eutectic structure, which causes the structure to be hard. However, Au–0.285Ge eutectic subjected to thermal aging became softer than the as-produced sample as illustrated in Fig. 8. This age-softening effect was more pronounced with the increase in the aging temperature, i.e. the samples that were aged at 200 °C were found to be much softer than the ones aged at 150 °C. This age-softening effect could be attributed to the change in morphology of (Ge) lamellae and its respective distribution on the much softer (Au) phase. Thus, the variation in the morphology and the change in the distribution pattern of (Ge) lamellae during thermal aging have induced some softness to the otherwise hard Au–Ge eutectic.

The overall microhardness of the aged Au–0.18Ge–0.10In candidate alloy was higher than the as-produced samples (Fig. 9). This effect could be attributed to the classic solid solution strengthening of the ζ phase (Table 2) due to the high solubility limit of In in ζ phase. The content of In soluble in the ζ phase calculated thermodynamically at 150 and 200 °C in mole-fraction are 0.122 and 0.124, respectively. The high solubility of In in ζ phase was also confirmed by the SEM/EDX elemental mapping analysis. However, the Au–0.18Ge–0.10In candidate alloy became relatively softer when aged at 200 °C for 3 weeks despite the solid solution strengthening of the ζ phase. This effect could be attributed to the precipitation of the softer α_1 phase (Table 2). Thus, it could be concluded that the precipitation of α_1 phase during long-term thermal aging at 200 °C has induced softness to the Au–0.18Ge–0.10In candidate alloy.

The overall microhardness of the Au–0.18Ge–0.10In candidate alloy aged at 150 °C was relatively higher than the ones aged at 200 °C. This effect could be attributed to the presence of low-volume-fraction of the softer Au rich phases in the matrix. The initial decrease in microhardness during aging at 150 °C could be attributed to the increase in volume-fraction of Au rich phases in the matrix. The microhardness of the samples aged 150 °C was much higher than the ones aged at 200 °C. This effect could be attributed to the significant solid solution strengthening of the ζ phase and partly due the presence of low-volume-fraction of Au

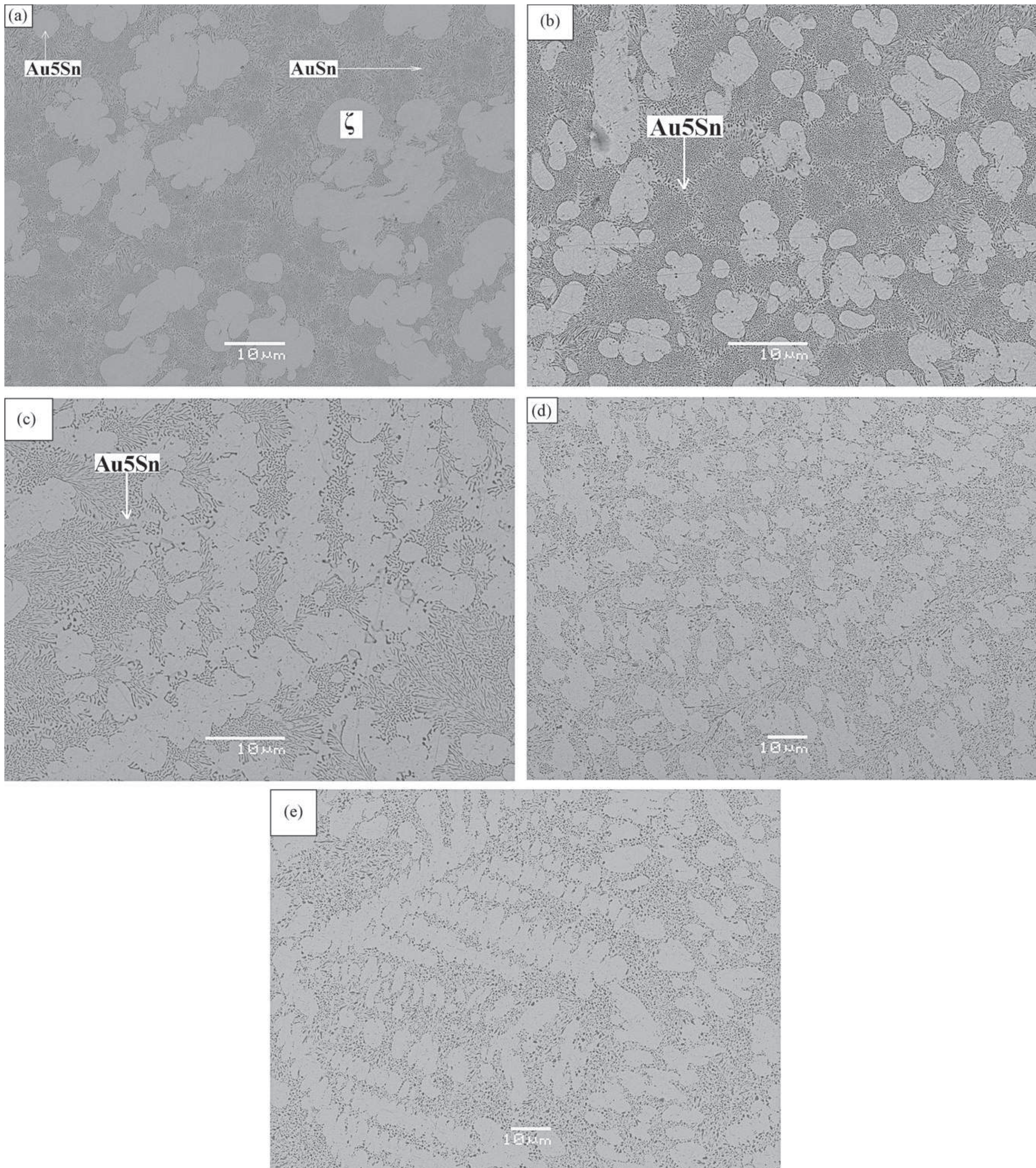

Fig. 6. SEM-BSE micrograph of the Au–0.15Ge–0.12Sn candidate alloy before and after thermal aging, (a) as-produced, (b) 150 °C-1 week, (c) 150 °C-3 weeks, (d) 200 °C-1 week, and (e) 200 °C-3 weeks.

rich phases in the matrix when compared to the ones aged 200 °C (Table 2). Thus, the microhardness measurement using the 100 g load, to a certain extent correlated well with the volume-fraction of Au rich phases in the matrix.

The overall microhardness of the aged Au–0.24Ge–0.05Sb candidate alloy was higher than the as-produced samples despite the softening induced by the growth of the (Au) phase. Though the growth of the (Au) phase has induced some softness in the alloy as shown in Table 3, the increase in the microhardness (Fig. 10) can be attributed to the refinement of the (Ge) phase. Because of the relatively large size of the (Ge) phase, composite strengthening (i.e. load transfer from the weaker matrix to the stronger dispersed phase) is more likely than a direct obstruction of dislocation motion such as with solid solution strengthened alloys. Phase-equilibria calculations show that Sb does not dissolve in the (Au) phase and all the Sb exists in the microstructure only as $AuSb_2$ IMC. Thus, the refined (Ge) phase can serve as a better reinforcing phase in the Au–0.24Ge–0.05Sb candidate alloy. However, the

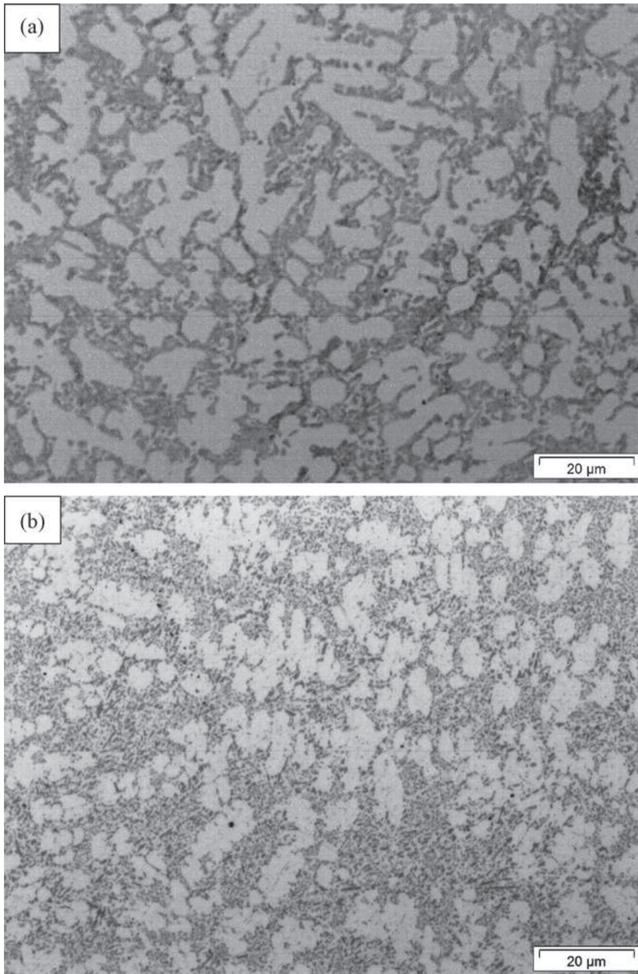

Fig. 7. Optical microstructure of Au–0.15Ge–0.12Sn candidate alloy after thermal aging for 3 weeks, (a) 150 °C and (b) 200 °C.

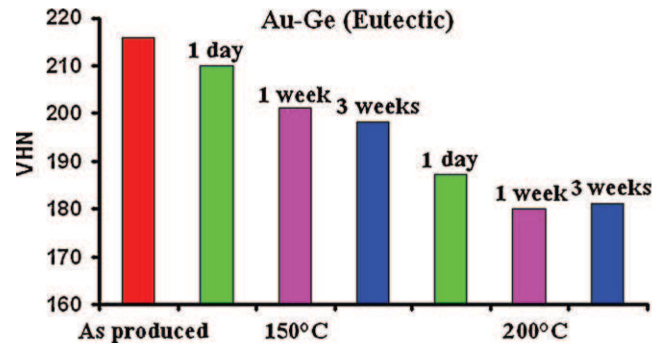

Fig. 8. Microhardness values of the Au–Ge eutectic alloy using 100 g load before and after thermal aging.

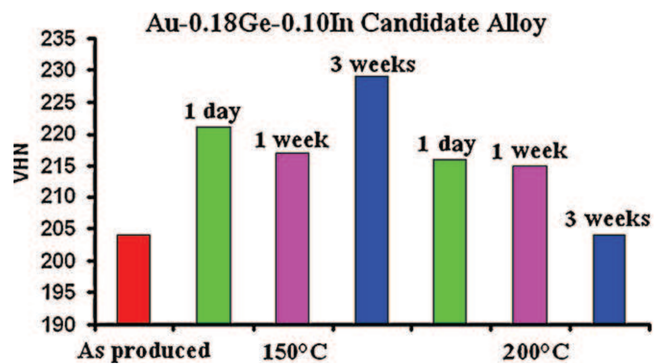

Fig. 9. Microhardness values of the Au–0.18Ge–0.10In candidate alloy using 100 g load before and after thermal aging.

microhardness fell substantially during long-term thermal aging (3 weeks) at 200 °C. This effect could be attributed to the significant growth of the (Au) phase and also due to the slight coarsening of the $AuSb_2$ IMC. The overall microhardness of the Au–0.24Ge–0.05Sb candidate alloy aged at 150 °C was relatively higher than the ones aged at 200 °C. This is because the softening induced by the growth of the (Au) phase for the samples aged at 150 °C was relatively lower than the ones aged at 200 °C (Table 3).

The microhardness of the Au–0.15Ge–0.12Sn candidate alloy aged at 200 °C was lower than the as-produced samples while the microhardness of the Au–0.15Ge–0.12Sn candidate alloy aged at 150 °C was higher than the as-produced samples as depicted in

Table 3
Vickers hardness measurement of individual phases using 5 g load.

Candidate alloy	Phases	Aging time	Hardness (HV)	
			150 °C	200 °C
Au–0.24Ge–0.05Sb	(Au)	As-produced	103[a]	103[a]
		1 day	97	94
		1 week	96	95
		3 weeks	96	86
	$AuSb_2$	As-produced	620[a]	620[a]
		1 day	619	623
		1 week	628	619
		3 weeks	625	567
	(Ge)	As-produced	320[a]	320[a]
		1 day	324	323
		1 week	325	321
		3 weeks	323	325

[a] Without heat treatment.

Table 2
Vickers hardness measurement of individual phases using 5 g load.

Candidate alloy	Phases	Aging time	Hardness (HV)	
			150 °C	200 °C
Au–0.18Ge–0.10In	ζ	As-produced	183[a]	183[a]
		1 day	199	197
		1 week	201	199
		3 weeks	204	202
	(Ge) phase distributed on Au rich phases	As-produced	230[a]	230[a]
		1 day	254	241
		1 week	249	240
		3 weeks	247	232
	α_1	3 weeks	–	162

[a] Without heat treatment – unstable.

Table 4
Vickers hardness measurement of individual phases using 5 g load.

Candidate alloy	Phases	Aging time	Hardness (HV)	
			150 °C	200 °C
Au–0.15Ge–0.12Sn	ζ	As-produced	150[a]	150[a]
		1 day	160	159
		1 week	165	162
		3 weeks	170	169
	Au_5Sn	As-produced	224[a]	224[a]
		1 day	226	227
		1 week	221	–
		3 weeks	225	–
	(Ge) phase distributed on (Au) rich phases	As-produced	265[a]	265[a]
		1 day	272	206
		1 week	258	192
		3 weeks	240	187

[a] Without heat treatment – unstable.

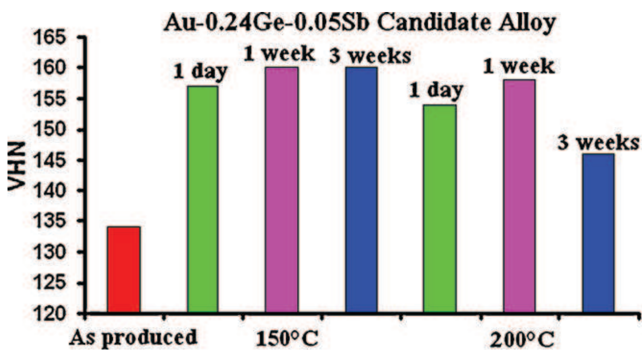

Fig. 10. Microhardness values of the Au–0.24Ge–0.05Sb candidate alloy using 100 g load before and after thermal aging.

Fig. 11. The microhardness of the Au–0.15Ge–0.12Sn candidate alloy aged at 200 °C decreased proportionally with the aging duration despite the solid solution strengthening of the ζ phase (Table 4) and also the refinement of the ζ phase. The content of Sn soluble in the ζ phase calculated thermodynamically at 150 and 200 °C in mole-fraction are 0.140 and 0.141, respectively. The high solubility of Sn in ζ phase was also confirmed by the SEM/EDX elemental mapping analysis. The age-softening effect observed at 200 °C can be attributed to the gradual disappearance of the brittle Au_5Sn phase from the microstructure during thermal aging. The AuSn phase too gradually vanished during aging at 200 °C. It was not possible to measure the Vickers hardness of the AuSn phase using the 5 g load without hitting other phases.

The microhardness of the Au–0.15Ge–0.12Sn candidate alloy aged at 150 °C was much higher than the ones aged at 200 °C as illustrated in Fig. 11. This effect could be attributed to the solid solution strengthening of the ζ phase, stabilization of the brittle Au_5Sn phase and also due to the presence of low-volume-fraction of Au rich phases (ζ and Au_5Sn phase) in the matrix. Though Au_5Sn is a hard phase, it is relatively softer when compared to (Ge) phase. The microhardness of the Au–0.15Ge–0.12Sn candidate alloy aged at 200 °C decreased proportionally with the aging duration. This age-softening effect could be attributed to the increase in the volume-fraction of relatively softer Au rich phases in the matrix during aging.

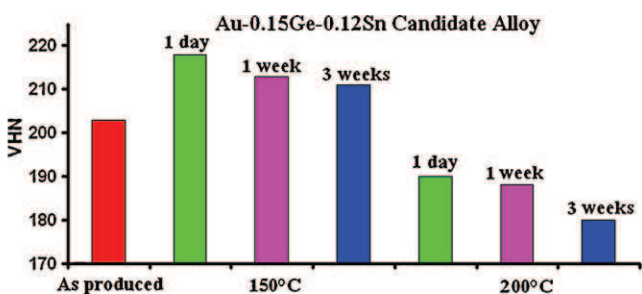

Fig. 11. Microhardness values of the Au–0.15Ge–0.12Sn candidate alloy using 100 g load before and after thermal aging.

The higher than expected strength in the case of Au–0.18Ge–0.10In and Au–0.15Ge–0.12Sn candidate alloys can be traced back to the changing microstructure. It appears that the lattice strains induced from an increased In and Sn concentration respectively are a more efficient strengthening mechanism than the refined (Ge) dispersed phase in the Au–0.24Ge–0.05Sb candidate alloy. However, the Au–0.15Ge–0.12Sn candidate alloy aged at 200 °C is a relatively soft alloy when compared to itself aged at 150 °C and also the Au–0.18Ge–0.10In candidate alloy.

Thus, among the three low melting point metals (In, Sb and Sn), it was determined in this work, that the addition of Sb to the Au–Ge eutectic would not only decrease its melting point but also would improve its ductility substantially despite the presence of very hard IMC ($AuSb_2$). Therefore, in this context, in addition to the solubility and reactivity of the alloying elements and the characteristics of their IMCs, the distribution of phases played a relatively more crucial role in determining the ductility of the bulk solder alloy. Though the effect of Sb on Au–Ge eutectic has been examined in this work with a holistic approach, it has to be mentioned that Sb is also in the list of toxic elements [5]. However, Sb is not as toxic as lead and even small proportions of Sb to the Au–Ge eutectic would make a significant difference in terms of ductility.

4. Concluding remarks

High-temperature solders are widely used in various types of applications. Since each application has its own specific requirement, a single high-temperature solder cannot cover all of the applications. Au–0.24Ge–0.05Sb is a promising candidate alloy for applications such as die-attach solders, circuit modules for step soldering, etc. where ductility of the solder alloy is an indispensable requirement to facilitate the relaxation of thermal stresses. The Au–0.15Ge–0.12Sn candidate alloy aged at 200 °C is a relatively soft alloy when compared to itself aged at 150 °C and also the Au–0.18Ge–0.10In candidate alloy. Au–0.18Ge–0.10In is a promising candidate alloy for applications such as optoelectronic packaging where high strength, low elastic modulus and stability of microstructure at high-temperatures are very crucial. The major drawbacks of developing Au–Ge based candidate alloys as an alternative to high-lead content solders are: the cost associated with the price of gold and also the fact that Ge cannot be easily electrodeposited which is important since electro-deposition is one of the

common ways of depositing solder alloys in a commercial scale. By using gold, the initial costs would be higher, but there would potentially be a value to the recycled product and no disposal cost associated with the solders, resulting in lower lifetime costs for the product.

Acknowledgment

The authors acknowledge the Danish Ministry of Science, Technology and Development for financial support through the innovation consortium “Matpack” (Project no. 07-003145).

References

[1] N. Kang, H.S. Na, S.J. Kim, C.Y. Kang, J. Alloys Compd. 467 (2009) 246–250.
[2] Y. Yamada, Y. Takaku, Y. Yagi, Y. Nishibe, I. Ohnuma, Y. Sutou, R. Kainuma, K. Ishida, J. Microelectron. Reliab. 46 (2006) 1932–1937.
[3] K. Suganuma, S.-J. Kim, K.-S. Kim, JOM 61 (2009) 64–71.
[4] V. Chidambaram, J. Hald, J. Hattel, J. Microelectron. Reliab. 49 (2009) 323–330.
[5] V. Chidambaram, J. Hald, J. Hattel, J. Microelectron. Electron. Pack. 6 (2009) 75–82.
[6] M. Rettenmayr, P. Lambracht, B. Kempf, M. Graff, J. Adv. Eng. Mater. 7 (2005) 965–969.
[7] US Environmental Protective Agency (EPA), <http://www.epa.gov/>.
[8] US Department of Labor, Occupational Safety and Health Administration (OSHA), <http://www.osga.gov/>.
[9] P.S. Schein, T. Smythe, D. Hoth, F. Smith, J.S. Mac Donald, P.V. Woolley, Cancer Treat. Rep. 64 (1980) 1051–1056.
[10] S.-K. Seo, S.K. Kang, D.-Y. Shih, H.M. Lee, J. Microelectron. Reliab. 49 (2009) 288–295.
[11] H. Schoeller, S. Bansal, A. Knobloch, D. Shaddock, J. Cho, J. Electron. Mater. 38 (2009) 802–809.
[12] Scientific Group Thermodata Europe (SGTE), SSOl2 Solutions Database Version 2.1, 1999/2002/2003.
[13] A.T. Dinsdale, A. Watson, A. Kroupa, A. Zemanova, J. Vrestal, J. Vizdal, COST 531 Database Version 3.0, 2008.
[14] R. Bergmann, P. Tang Torben, H.N. Hansen, P. Møller, In-situ Investigation of Lead-free Solder Alloy Formation using a Hot-plate Microscope IEEE Conf. Proc., 2007, pp. 252–256.
[15] V. Chidambaram, J. Hald, R. Ambat, J. Hattel, JOM 61 (2009) 59–65.
[16] C. Wei, Y. Liu, Z. Gao, R. Xu, K. Yang, J. Alloys Compd. 468 (2009) 154–157.
[17] R.A. Islam, B.Y. Wu, M.O. Alam, Y.C. Chan, W. Jillek, J. Alloys Compd. 392 (2005) 149–158.

Appendix IV

Design of lead-free candidate alloys for high-temperature soldering based on the Au-Sn system

Vivek Chidambaram, Jesper Hattel and John Hald

Materials and Design, 31: 4638-4645, 2010

Materials and Design 31 (2010) 4638–4645

Contents lists available at ScienceDirect

Materials and Design

journal homepage: www.elsevier.com/locate/matdes

Design of lead-free candidate alloys for high-temperature soldering based on the Au–Sn system

Vivek Chidambaram *, Jesper Hattel, John Hald

Department of Mechanical Engineering, Technical University of Denmark, Building 425, Produktionstorvet, Lyngby DK-2800, Denmark

ARTICLE INFO

Article history:
Received 30 March 2010
Accepted 16 May 2010
Available online 21 May 2010

Keywords:
Lead-free solder alloys
High-temperature soldering
Microstructure
Microhardness

ABSTRACT

Au–Sn based candidate alloys have been proposed as a substitute for high-lead content solders that are currently being used for high-temperature soldering. The changes in microstructure and microhardness associated with the alloying of Ag and Cu to the Au rich side as well to the Sn rich side of the Au–Sn binary system were explored in this work. Furthermore, the effects of thermal aging on the microstructure and microhardness of these promising Au–Sn based ternary alloys were investigated. For this purpose, the candidate alloys were aged at a lower temperature, 150 °C for up to 1 week and compared with aging at 200 °C for respective durations. It was determined in this work that the candidate alloys on the Sn rich side were relatively more stable, i.e. only the aging temperature had a substantial impact on the microstructure and not the aging duration. The candidate alloys aged at 200 °C were substantially softer on the Au rich side than the candidate alloys on the Sn rich side. However, the difference in hardness narrowed down considerably between the candidate alloys on the Au rich side and the Sn rich side when subjected to aging at 150 °C.

© 2010 Elsevier Ltd. All rights reserved.

1. Introduction

High-temperature soldering is a key technology for electronic components and assemblies and requires a high level of process control. This technology can provide value-added characteristics to the products including excellent heat conductivity, high reliability and also facilitate the drive for miniaturization [1]. High-lead containing solders have been commonly used as high-temperature solders. The main applications for high-temperature solders within the electronics industry are for advanced packaging technologies. Advanced packaging technology is required because electronic devices are operating faster and becoming smaller, lighter and more functional. As a result many advanced packaging technologies employing high-temperature solders such as ball grid array (BGA), flip-chip technology, chip-scale package (CSP) and multi-chip module (MCM) have been developed [2]. The development of high-temperature lead-free solders has become an important issue now because of the health and environmental concerns associated with lead usage. Unfortunately, limited choices are available as high-temperature lead-free solders [3].

The solder design for high-temperature applications needs to consider the proper regime of melting temperature because the soldered parts have to sustain with no melting until it passes the last step of the assembling process. Therefore, the melting temperature range (270–350 °C) has been defined by the industries in order to ensure efficient process control [4]. Modifying the Sn based solders towards higher temperatures by alloying with inexpensive metals, in order to achieve the required melting range remained unsuccessful till present. Thus, for soft solder alloys in the high-temperature regime, a suitable alternative to the high-lead containing alloys covering the whole spectrum of properties is still to be developed [5].

Au–20 wt.% Sn, which corresponds to the Au rich eutectic composition with a melting point of 280 °C, directly fits to the requirement. Au–20 wt.% Sn is an example of a hard solder, which is commonly used for opto-electronic packaging. It is brittle since it involves the ζ' (Au5Sn) hard phase. Phase-equilibria calculations show that the addition of small amounts of either Ag or Cu to the Au–Sn eutectic would suppress the precipitation of ζ' (Au5Sn) and instead precipitate relatively ductile phases. Thus, small additions of Ag/Cu to the Au–Sn eutectic would transform this hard solder to soft solder alloys [6]. Phase-equilibria calculations also show that the required solidification criterion could also be achieved on the Sn rich side of the Au–Sn–Ag/Au–Sn–Cu system. The region with high Sn content and still adhering to the required solidification criterion is of commercial interest since it involves less gold [7]. Thus, the effect of Ag/Cu on Au–Sn eutectic as well as on the Sn rich side with respect to microstructure and its corresponding mechanical properties has been investigated in this work.

The operating temperature that the high-temperature solders are being exposed to varies between 150 °C and 200 °C depending

* Corresponding author. Tel.: +45 4525 4880; fax: +45 4593 4570.
E-mail address: vchi@mek.dtu.dk (V. Chidambaram).

0261-3069/$ - see front matter © 2010 Elsevier Ltd. All rights reserved.
doi:10.1016/j.matdes.2010.05.035

on the applications [3]. At high-temperatures, the microstructure of these promising solder candidates could significantly change and consequently their mechanical properties could be affected [8,9]. Therefore, in this work, the high-temperature stability of microstructures and mechanical properties of Au–Sn based candidate alloys in the lower end as well as in the higher end of the operating temperature range are extensively reported. This work only characterizes the properties of bulk solders and does not consider factors such as reactions with joining materials, which may affect the mechanical performance of actual solder joints. Instead the work focuses on specific microstructural features that can explain solder performance at elevated temperatures.

2. Experimental methods

Phase-equilibria calculations in this work have been carried out using a thermodynamic description of the phases in COST 531 Version 3.0 [10] and SSOL2 [11] thermodynamic databases via the Thermo-Calc (Version R) software. The promising Au–Sn based candidate alloys with a diameter between 3.0 mm and 4.0 mm were produced accurately using a hot-plate microscope as illustrated in Fig. 1 [12]. This equipment consists of three main parts:

(1) Vacuum system.
(2) Specimen chamber with heating system.
(3) Microscope and imaging system.

The high purity metal powders were carefully weighed and mixed inside a specially designed pressing tool to form small tablets. The tablet was subsequently placed inside a cylindrical aluminium oxide crucible on a molybdenum plate that is mounted between the electrical contacts of the heating system inside the specimen chamber of the hot-plate microscope. The heating system can reach a temperature up to approximately 1400 °C and is equipped with water cooling. A high-vacuum ($<1 \times 10^{-3}$ mbar) was created in the specimen chamber and it was controlled by pressure measurements. The melting process was carried out under hydrogen flow to prevent further oxidation of the material and to start the reduction of oxides on the surface of the developing sphere. The solder spheres were held at the liquid state for a short time (5 min) to ensure homogeneity. The solder sphere was remelted a couple of times for homogenization [3,7]. A high cooling rate (300 K/s) was employed during the production of these solder spheres. The temperature inside the chamber was measured using a thermocouple positioned below the Mo-plate. The calibration of the thermocouple was done by relating the produced voltage (measured with a digital voltmeter) of the thermocouple to the known melting temperatures of pure metal spheres of Sn, Pb, Al, Ag and Au. This resulted in a linear relation between the measured voltage and the temperature inside the chamber.

To investigate the effects of aging temperature, the candidate alloys were aged at a lower temperature, i.e. 150 °C and compared with the ones aged at 200 °C. The samples were loaded into an ambient atmosphere resistant furnace and were heated to these respective temperatures and annealed at the same temperatures for 1 day and 1 week in order to investigate their structural stability. The as-produced and thermally aged samples were embedded in an epoxy resin, ground and polished in accordance with standard metallographic preparation methods for observations of the microstructure and also for the testing of microhardness. Both mechanical polishing and chemical etching were used to expose/examine different phases of the candidate alloys.

The metallographic microstructure and morphology of the various candidate alloys were examined using a Neophot optical microscope and a JEOL 5900 scanning electron microscope (SEM). The microstructural composition of the candidate alloys was analyzed with an energy dispersive spectrometer (Oxford, Link ISIS) and it was carried out on unetched samples. Since the mechanical properties of a material are frequently quantified by its hardness, the present study used a Vickers microhardness tester (FM-7000 Future Tech) with an indentation load of 5 g and 100 g and a dwell time of 5 s to measure the hardness of the various Au–Sn based candidate alloys. The 5 g load was used to determine the hardness of individual phases. However, in certain cases it was not possible to measure the hardness of individual phase without hitting other phases. The 100 g load was also applied so that the width of indentation was large enough to span multiple phases and many eutectic domains. Hence the test values reflect the overall microhardness of the candidate alloys. To ensure accurate results, 15 different indents were performed on each sample. The average of the individual measurements was evaluated as the results due to the slight variance of the 15 measurements especially in the case of the 100 g load.

3. Results and discussion

3.1. Design of candidate alloys

Au–20 wt.% Sn, is a fine mixture of hard ζ' (Au5Sn) phase and a relatively soft δ (AuSn) phase. Phase-equilibria calculations show that the small additions of Ag/Cu to the Au–Sn eutectic would suppress the precipitation of the brittle ζ' (Au5Sn) phase and in turn proportionally precipitate relatively ductile phases. However, it has been predicted that the liquidus temperature of the ternary

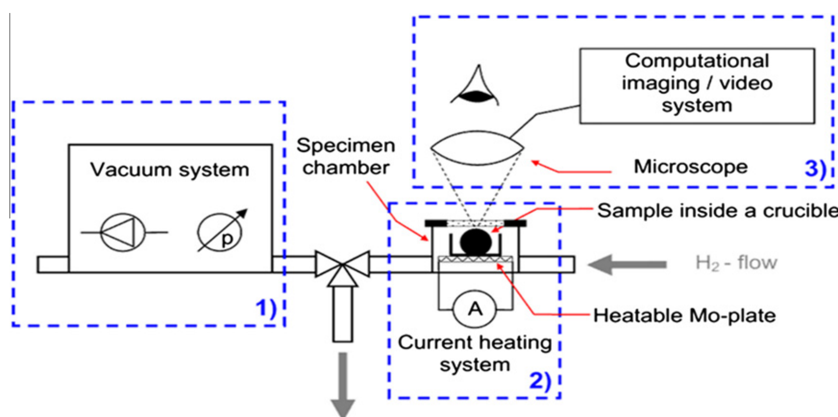

Fig. 1. Experimental setup of the hot-plate microscope [(1) vacuum system, (2) specimen chamber with heating system, (3) microscope and imaging system] [12].

alloy too would increase proportionally with the additions of Ag/Cu to the Au–Sn eutectic [6]. The equilibrium calculation has estimated that the liquid phase close to Au–Sn eutectic at 350 °C would extend up to 0.03Ag/0.04Cu respectively. Thus, the Au–Sn compositions close to eutectic with the maximum content of Ag and Cu in mole-fraction and still adhering to the solidification criterion are *Au–0.35Sn–0.03Ag* and *Au–0.33Sn–0.04Cu*, respectively.

Phase-equilibria calculations also show that the required solidification criterion could be achieved with a high tin content in these alloys varying roughly in the range of 0.60–0.70 (mole-fraction). These ternary combinations were optimized for a narrow solidification range since this is generally preferred for facilitating rapid production, efficient process control, preventing the movement of components during solidification and for minimizing segregation during solidification. In addition, too much liquid at reflow will destroy the package by large-volume expansion. Thus, the optimized ternary combinations in mole-fraction are *Sn–0.30Au–0.08Ag* and *Sn–0.29Au–0.08Cu*, respectively [7].

3.2. Structural variation during aging

3.2.1. Au–0.35Sn–0.03Ag candidate alloy

The metallographic microstructure of the as-produced Au–0.35Sn–0.03Ag samples as depicted in Fig. 2, before being subjected to thermal aging was comprised of δ (AuSn) phase dispersed on Au rich phases and also ζ' (Au5Sn) phase. The Au rich phases could be either (Au, Ag) or ζ. It was not possible to distinguish between these two phases by EDX due to the limitations of the technique. This can be attributed to the closer solubility limit of these two phases. The Au5Sn phase could be distinguished from the other Au rich phases using EDX since Ag is absolutely insoluble in this phase. SEM analysis showed that the volume-fraction of Au5Sn phase in the matrix of the as-produced samples was too low. This effect could be attributed to the fast cooling rate employed during the production of these alloys in the hot-plate microscope. Thus, it can be concluded that the fast cooling rate employed during the production of these alloys has suppressed the precipitation of the Au5Sn phase to a great extent.

It was observed that the volume-fraction of Au5Sn phase in the matrix of the Au–0.35Sn–0.03Ag alloys subjected to aging at 150 °C for different durations was much higher than that of the as-produced ones. In the samples that were subjected to thermal aging at 200 °C for 1 day, the volume-fraction of Au5Sn phase in the matrix was even lower than the as-produced samples. The Au5Sn phase did not exist in the matrix of the samples subjected to aging at 200 °C for 1 week.

3.2.2. Au–0.33Sn–0.04Cu candidate alloy

The microstructure of the as-produced Au–0.33Sn–0.04Cu candidate alloy as illustrated in Fig. 3 comprised of δ (AuSn) phase dispersed in the matrix. The matrix comprised of δ (AuSn) and ε (AuSn2) lamellae dispersed on Au rich phases [(Au, Cu)) or ζ] and ζ' (Au5Sn). The Au5Sn phase could be distinguished from the other gold rich phases since Cu is absolutely insoluble in this phase. The volume-fraction of Au5Sn phase was too low in the as-produced samples due to the lack of time for precipitation. The major difference that was observed in the as-produced Au–0.33Sn–0.04Cu candidate alloy when compared to that of the as-produced Au–0.35Sn–0.03Ag candidate alloy was related to the presence of a few AuSn2 lamellae in the matrix The presence of AuSn2 phase can be attributed to non-equilibrium solidification since this phase is not expected to precipitate for this specific composition.

The volume-fraction of Au5Sn phase increased proportionally with the aging durations when subjected to aging at 150 °C while decreased gradually during aging at 200 °C. SEM analysis also showed that the volume-fraction of AuSn2 lamellae in the matrix decreased gradually during aging at 150 °C and this phase did not exist in the microstructure of the samples that were subjected to aging for 1 week. Both the Au5Sn and the AuSn2 phases did not exist in the microstructure of the samples aged at 200 °C for 1 week.

3.2.3. Sn–0.29Au–0.08Ag candidate alloy

Before thermal aging, the microstructure of the as-produced Sn–0.30Au–0.08Ag candidate alloy comprised of the dark δ (AuSn) phase and the white Au rich phase dispersed in the matrix, as depicted in Fig. 4. The matrix consisted of ε (AuSn2) phase and an Ag rich ternary phase. It was not possible to identify the white Au rich phase with EDX. After thermal aging at different temperatures for different durations, the major difference observed in the aged

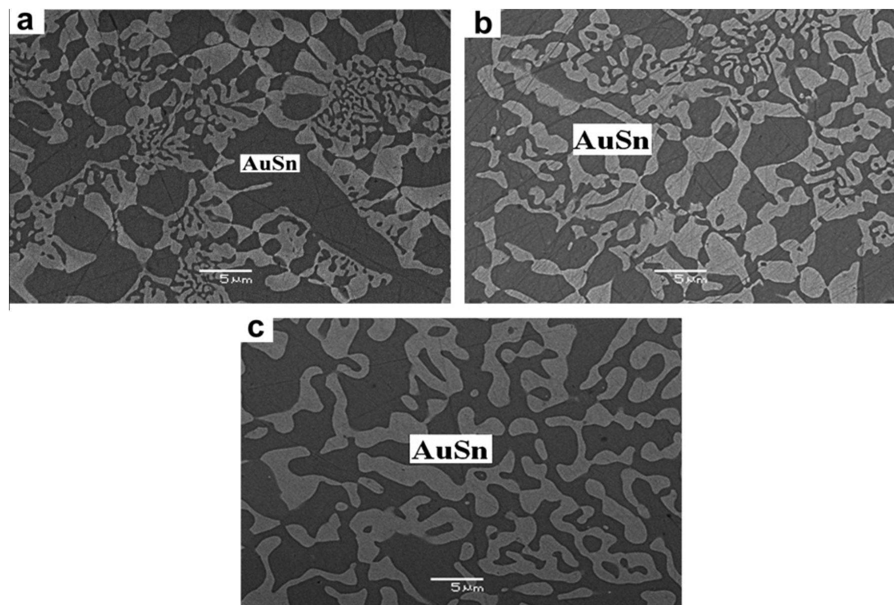

Fig. 2. SEM-BSE micrographs of the Au–0.35Sn–0.03Ag candidate alloy before and after thermal aging: (a) as-produced, (b) 150 °C – 1 week, (c) 200 °C – 1 week.

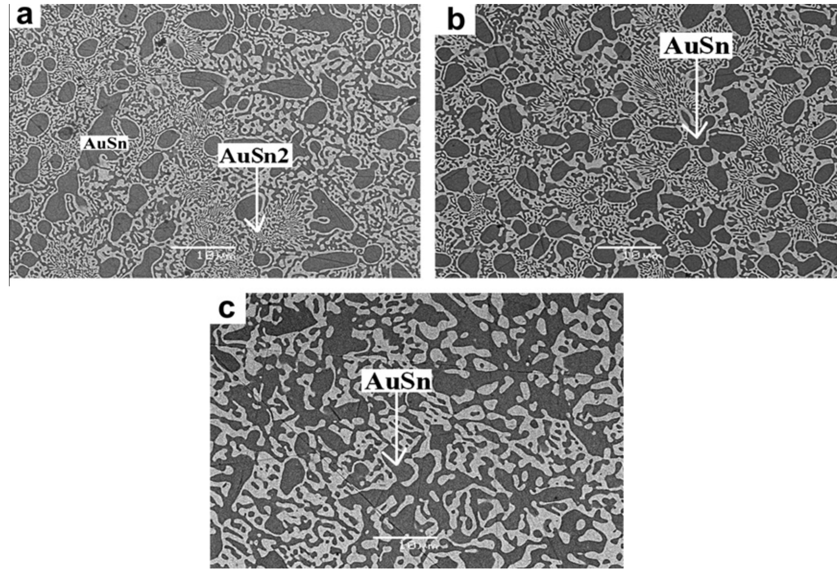

Fig. 3. SEM-BSE micrographs of the Au–0.33Sn–0.04Cu candidate alloy before and after thermal aging: (a) as-produced, (b) 150 °C – 1 week, (c) 200 °C – 1 week.

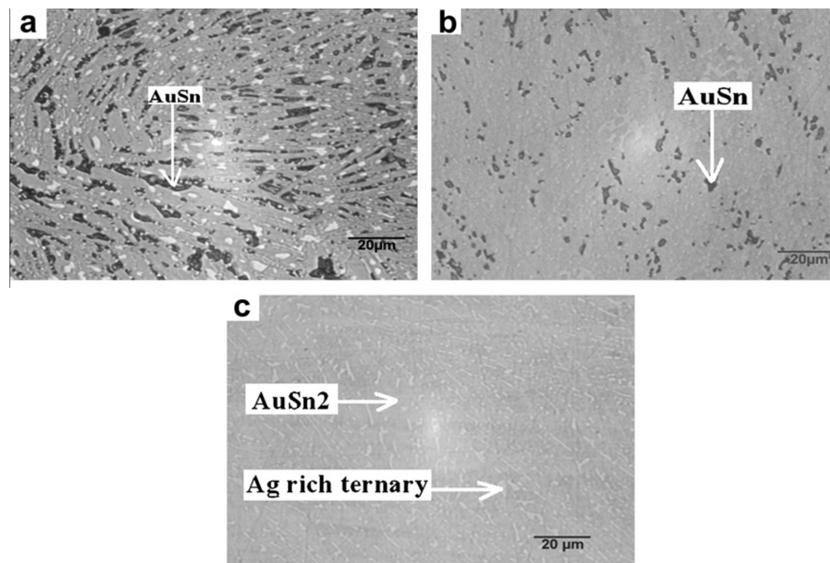

Fig. 4. Optical microstructures of Sn–0.30Au–0.08Ag candidate alloy before and after thermal aging for 1 week: (a) as-produced, (b) 150 °C, and (c) 200 °C.

samples was in relation to the dark AuSn phase dispersed on the matrix (Figs. 4 and 5). The volume-fraction of the Au rich phase was much lower in the aged samples when compared to that of the as-produced ones. It was determined that only the aging temperature had a dramatic impact on the precipitation of the dark AuSn phase and not the aging duration.

It was observed that the volume-fraction of the dark AuSn phase dispersed in the matrix of the samples aged at 150 °C for different durations was much lower when compared to that of the as-produced ones. The AuSn phase did not exist in the samples that were aged at 200 °C for different durations. EDX analysis of the as-produced samples and the samples that were aged at different

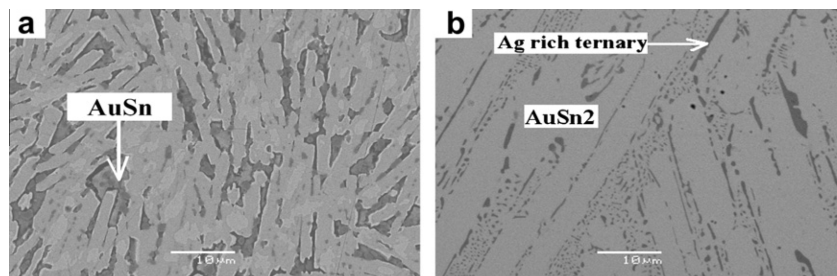

Fig. 5. SEM-BSE micrographs of Sn–0.30Au–0.08Ag candidate alloy after thermal aging for 1 week: (a) 150 °C and (b) 200 °C.

aging temperatures for different durations showed that the Ag content in the Ag rich ternary phase varied between 60 and 68 at.% while the Sn content varied between 24 and 30 at.% and the Au content varied between 4 and 14 at.%.

3.2.4. Sn–0.29Au–0.08Cu candidate alloy

Before thermal aging, the microstructure of the Sn–0.29Au–0.08Cu candidate alloy comprised of the dark δ (AuSn) phase and the gray Sn rich ternary phase dispersed on the ε ($AuSn_2$) matrix as depicted in Fig. 6. The volume-fraction of the dark δ (AuSn) phase dispersed in the matrix of the as-produced Sn–0.29Au–0.08Cu candidate alloy was higher when compared to that of the as-produced Sn–0.30Au–0.08Ag candidate alloy. After thermal aging at different temperatures for different durations, the major difference observed in the aged samples was in relation to the dark δ (AuSn) phase dispersed on the matrix as illustrated in Fig. 7. Similar to the Sn–0.30Au–0.08Ag candidate alloy only the aging temperature had a substantial impact on the precipitation of the dark δ (AuSn) phase and not the aging durations.

It was observed that the volume-fraction of the AuSn phase dispersed in the matrix of the samples aged at 150 °C for different durations was relatively lower than the as-produced ones. The volume-fraction of the AuSn phase in the samples aged at 200 °C for different durations was even lower than the ones aged at 150 °C. Slight coarsening of the dark AuSn phase was observed in the samples aged at 200 °C for different durations as depicted in Fig. 7. Thus, unlike for the Sn–0.30Au–0.08Ag candidate alloy, the AuSn phase existed in the samples aged at 200 °C for different durations. EDX analysis of the as-produced samples and the samples that were aged at different aging temperatures for different durations showed that the Sn content in the Sn rich ternary phase varied between 51 and 53 at.% while the Au content varied between 24 and 33 at.% and the Cu content varied between 15 and 25 at.%. The solubility of Cu in the ternary phase of the as-produced samples was much lower when compared to that of the samples that were subjected to thermal aging for different durations irrespective of the aging temperatures.

Thus, interestingly none of the brittle Cu–Sn intermetallics precipitated in any of the as-produced and the aged Sn–0.29Au–0.08Cu candidate alloy for this specific composition and temperatures. All the Cu in both the as-produced and the aged samples existed only in the Sn rich ternary phase. It has to be mentioned that Cu–Sn intermetallics are more brittle than any of the Au–Sn intermetallics.

Thus, both the aging temperature and the aging duration had a notable impact on the microstructure of the candidate alloys close to the Au–Sn eutectic. The candidate alloys on the Sn rich region were considerably more stable, i.e. only the aging temperature had a substantial impact and not the aging durations.

3.3. Microhardness of candidate alloys before and after aging

Microstructural features, such as grain size, particle distribution and phase distribution determine the microhardness of solder alloys [13]. The microhardness measurement technique is a very sensitive technique to detect structural changes of various candidate alloys at different temperatures. Microhardness testing is one of the easiest ways to determine the mechanical properties

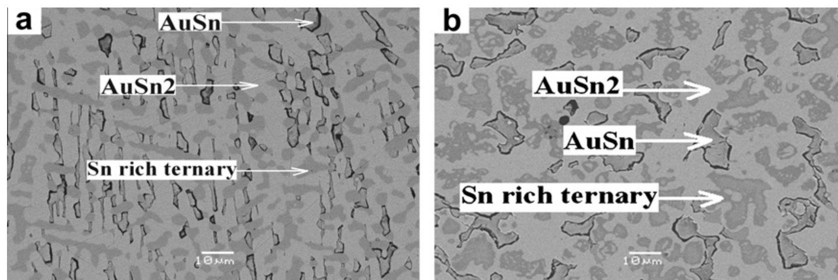

Fig. 6. SEM-BSE micrographs of Sn–0.29Au–0.08Cu candidate alloy after thermal aging for 1 week: (a) 150 °C and (b) 200 °C.

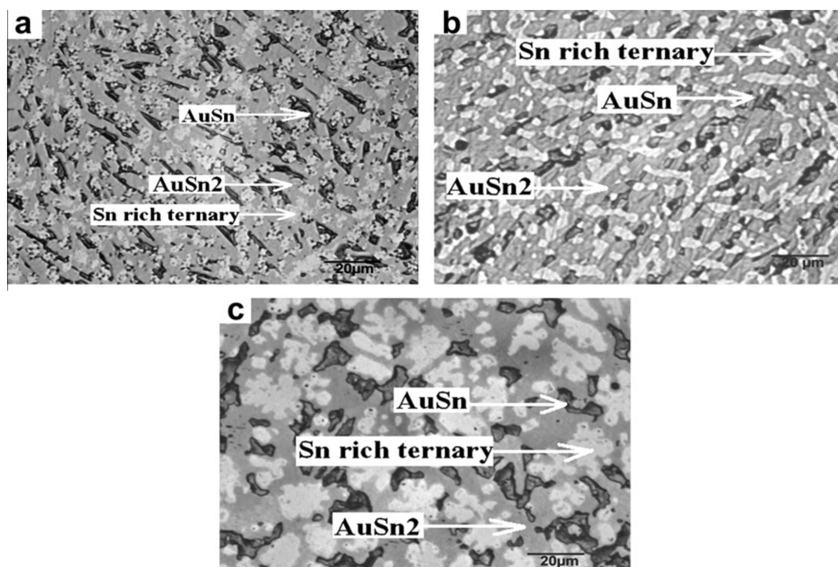

Fig. 7. Optical microstructures of Sn–0.29Au–0.08Cu candidate alloy before and after thermal aging for 1 week: (a) as-produced, (b) 150 °C, and (c) 200 °C.

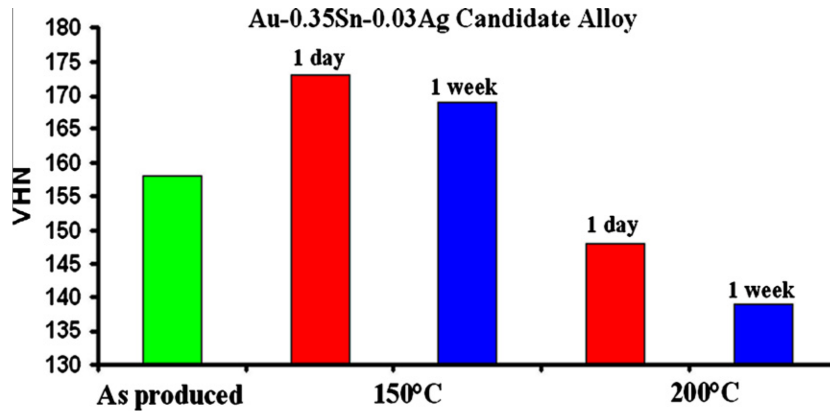

Fig. 8. Microhardness values of the Au–0.35Sn–0.03Ag candidate alloy using the 100 g load before and after thermal aging.

of the different phases of the structure. The rule of thumb is the higher the hardness, the higher the mechanical strength but with a compromise on ductility [14].

3.3.1. Au–0.35Sn–0.03Ag candidate alloy

The overall microhardness of the Au–0.35Sn–0.03Ag candidate alloy aged at 200 °C was lower than the as-produced ones while the overall microhardness of the Au–0.35Sn–0.03Ag candidate alloy aged at 150 °C was higher than the as-produced samples as depicted in Fig. 8. The microhardness of the Au–0.35Sn–0.03Ag candidate alloy aged at 200 °C decreased proportionally with the aging duration despite the solid-solution strengthening of the Au rich phases [(Au, Ag)/ζ] as listed in Table 1. This age-softening can be attributed to the gradual disappearance of the hard Au5Sn phase.

Table 1
Vickers hardness measurement of individual phases in the Au–0.35Sn–0.03Ag candidate alloy using the 5 g load.

Candidate alloy	Phases	Aging time	Hardness (HV)	
			150 °C	200 °C
Au–0.35Sn–0.03Ag	δ (AuSn)	As-produced	140[a]	140[a]
		1 Day	139	143
		1 Week	142	138
	(Au, Ag)/ζ	As-produced	144[a]	144[a]
		1 Day	148	154
		1 Week	155	160
	ζ' (Au5Sn)	As-produced	215[a]	215[a]
		1 Day	213	217
		1 Week	216	–

[a] Without heat treatment – unstable.

The relatively higher hardness of the Au–0.35Sn–0.03Ag candidate alloys aged at 150 °C can be attributed to the increase in the volume-fraction of the hard Au5Sn phase. The slight decrease in the hardness of the Au–0.35Sn–0.03Ag candidate alloy aged at 150 °C for 1 week when compared to the ones aged at 150 °C for 1 day can be attributed to the sensitivity of this technique not resulting in reproducibility within very narrow tolerances.

3.3.2. Au–0.33Sn–0.04Cu candidate alloy

Similar to the Au–0.35Sn–0.03Ag candidate alloy, the overall microhardness of the Au–0.33Sn–0.04Cu candidate alloy aged at 200 °C was lower than the as-produced ones while the overall microhardness of the Au–0.33Sn–0.04Cu candidate alloy aged at 150 °C was higher than the as-produced samples as depicted in Fig. 9. The overall hardness of the as-produced Au–0.33Sn–0.04Cu candidate alloy was higher than the as-produced Au–0.35Sn–0.03Ag candidate alloy. This can primarily be attributed to the presence of the hard AuSn2 lamellae in the matrix. Solid-solution strengthening of the Au rich phases [(Au, Cu)/ζ] too was observed irrespective of the aging temperatures as shown in Table 2. The solid-solution strengthening of the Au rich phases induced by the Cu atoms was determined to be relatively higher than the ones induced by the Ag atoms. It was not possible to measure the hardness of the AuSn2 phase without hitting the surrounding Au rich phases due to its lamellae structure as shown in Fig. 3. The slight increase in the hardness of the AuSn2 phase (Table 2) irrespective of the aging temperatures can be attributed to the solid-solution strengthening of the surrounding Au rich phases.

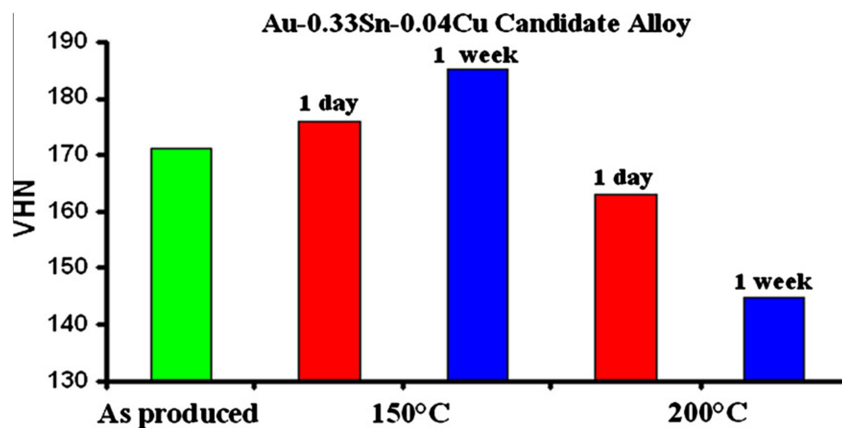

Fig. 9. Microhardness values of the Au–0.33Sn–0.04Cu candidate alloy using the 100 g load before and after thermal aging.

Table 2
Vickers hardness measurement of individual phases in the Au–0.33Sn–0.04Cu candidate alloy using the 5 g load.

Candidate alloy	Phases	Aging time	Hardness (HV)	
			150 °C	200 °C
Au–0.33Sn–0.04Cu	δ (AuSn)	As-produced	141[a]	141[a]
		1 Day	143	138
		1 Week	143	142
	(Au, Ag)/ζ	As-produced	157[a]	157[a]
		1 Day	158	161
		1 Week	163	168
	ε (AuSn2) distributed on Au rich phases	As-produced	180[a]	180[a]
		1 Day	183	185
		1 Week	–	–
	ζ′ (Au5Sn)	As-produced	214[a]	214[a]
		1 Day	216	211
		1 Week	216	–

[a] Without heat treatment – unstable.

The overall hardness of the Au–0.33Sn–0.04Cu candidate alloy aged at 150 °C was higher than the as-produced samples despite the gradual disappearance of the hard AuSn2 lamellae from the matrix. This age-hardening effect can be attributed to the increase in volume-fraction of the hard Au5Sn phase. The age-softening effect observed at 200 °C can be attributed to the disappearance of both the hard phases, i.e. Au5Sn and AuSn2 from the matrix.

3.3.3. Sn–0.30Au–0.08Ag candidate alloy

The trend in the overall hardness of the candidate alloys in the Sn rich region was different from the candidate alloys close to the Au–Sn eutectic. The overall hardness of the samples aged at 150 °C for different durations was higher than the as-produced ones. The overall hardness of the samples aged at 200 °C was even higher than the ones subjected to aging at 150 °C. Unlike the compositions close to the Au–Sn eutectic, only the aging temperature had a notable impact on the microhardness of the Sn–0.30Au–0.08Ag candidate alloy as depicted in Fig. 10 and not the aging duration. The slight difference in the overall hardness with respect to aging durations irrespective of the aging temperatures can be attributed to the sensitivity of the technique.

The overall hardness values of the Sn–0.30Au–0.08Ag candidate alloy were primarily controlled by the precipitation of the soft AuSn phase. This phase was measured to be relatively softer than the ones measured on the candidate alloys close to the Au–Sn eutectic composition as listed in Table 3. This could probably be attributed to the difference in the morphology of the AuSn phase.

Table 3
Vickers hardness measurement of individual phases in the Sn–0.30Au–0.08Ag candidate alloy using the 5 g load.

Candidate alloy	Phases	Aging time	Hardness (HV)	
			150 °C	200 °C
Sn–0.30Au–0.08Ag	ε (AuSn2)	As-produced	205[a]	205[a]
		1 Day	207	204
		1 Week	207	206
	δ (AuSn)	As-produced	104[a]	104[a]
		1 Day	106	105
		1 Week	104	106
	Ag rich ternary phase Ag: [60–68 at.%] Sn: [24–30 at.%] Au: [4–14 at.%]	As-produced	216[a]	216[a]
		1 Day	219	220
		1 Week	220	219
	Au rich phase	As-produced	161[a]	161[a]

[a] Without heat treatment.

The as-produced Sn–0.30Au–0.08Ag candidate alloy was much softer than the aged samples due to the high volume-fraction of this soft AuSn phase (Fig. 4). The Sn–0.30Au–0.08Ag candidate alloy subjected to aging at 150 °C was harder than the as-produced ones due to the presence of low volume-fraction of the soft AuSn phase. The Sn–0.30Au–0.08Ag candidate alloy subjected to aging at 200 °C was the hardest due to the complete disappearance of this soft AuSn phase. It was not possible to measure the hardness of the Au rich phase in the aged samples without hitting the matrix, i.e. Ag rich ternary phase dispersed on the AuSn2 phase.

3.3.4. Sn–0.29Au–0.08Cu candidate alloy

The trend in the overall hardness of the Sn–0.29Au–0.08Cu candidate alloy was similar to that of the Sn–0.30Au–0.8Ag candidate alloy as depicted in Fig. 11. The overall hardness of the aged Sn–0.29Au–0.08Cu candidate alloy was higher than the as-produced ones despite the solid-solution strengthening of the ternary phase induced by the Cu atoms as listed in Table 4. This age-hardening effect can be attributed to the slight reduction in the volume-fraction of the soft AuSn phase. The as-produced Sn–0.29Au–0.08Cu candidate alloy was even softer when compared to the as-produced Sn–0.30Au–0.08Ag candidate alloy. This could be attributed to the relatively higher volume-fraction of the soft AuSn phase.

Similar to the Sn–0.30Au–0.08Ag candidate alloy, the aging temperature had a notable impact on the microhardness of the Sn–0.29Au–0.08Cu candidate alloy and not the aging duration. The aged Sn–0.29Au–0.08Cu samples were substantially softer than the Sn–0.30Au–0.08Ag candidate alloy subjected to aging at the respective aging temperatures. This effect can be attributed

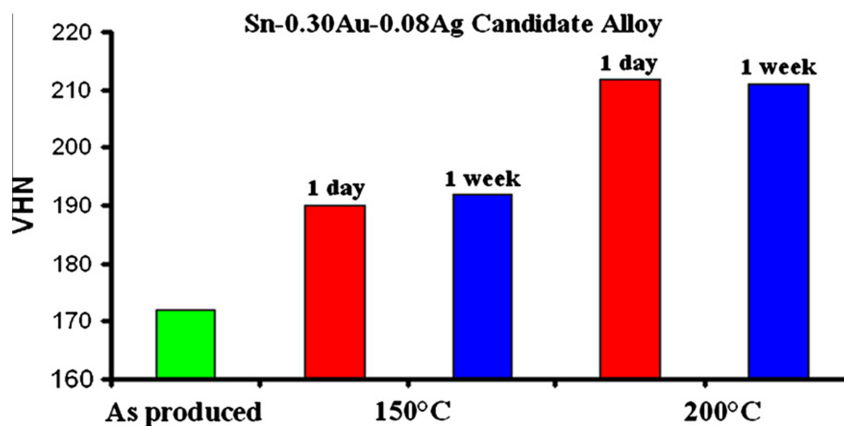

Fig. 10. Microhardness values of the Sn–0.30Au–0.08Ag candidate alloy using the 100 g load before and after thermal aging.

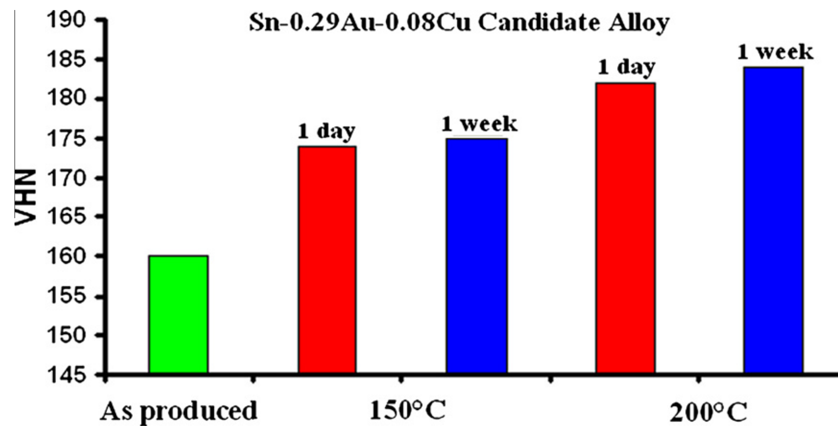

Fig. 11. Microhardness values of the Sn–0.29Au–0.08Cu candidate alloy using the 100 g load before and after thermal aging.

Table 4
Vickers hardness measurement of individual phases in the Sn–0.29Au–0.08Cu candidate alloy using the 5 g load.

Candidate alloy	Phases	Aging time	Hardness (HV)	
			150 °C	200 °C
Sn–0.29Au–0.08Cu	ε (AuSn2)	As-produced	204[a]	204[a]
		1 Day	204	203
		1 Week	204	204
	δ (AuSn)	As-produced	103[a]	103[a]
		1 Day	105	104
		1 Week	106	104
	Sn rich ternary phase	As-produced	241[a]	241[a]
	Sn: [51–53 at.%]	1 Day	270	277
	Au: [24–33 at.%]	1 Week	282	285
	Cu: [15–25 at.%]			

[a] Without heat treatment.

to the fact that the reduction in the volume-fraction of the soft AuSn phase during aging was substantially lower when compared to that of the Sn–0.30Au–0.08Ag candidate alloy. More importantly, the soft AuSn phase existed in the samples subjected to aging at 200 °C. No change in the hardness of the AuSn phase in the samples aged at 200 °C for different durations was noticed despite the slight coarsening of the AuSn phase.

Thus, among the four candidate alloys investigated in this work, the ones close to the Au–Sn eutectic were softer than the ones on the Sn rich side. For applications involving an operating temperature of 200 °C, candidate alloys close to the Au–Sn eutectic were relatively more ductile than the candidate alloys on the Sn rich side. However, for applications involving an operating temperature of 150 °C, the difference in hardness between the alloys on the Au rich side and the Sn rich side was small but still the Au rich candidate alloys had a slight edge over the latter with respect to ductility. This can be attributed to the stabilization of the brittle Au5Sn phase on the Au rich side and to the presence of a high volume-fraction of the soft AuSn phase on the Sn rich side.

4. Concluding remarks

The currently used high-lead content solders (Pb–Sn) are being applied for various applications irrespective of the operating temperatures (150–200 °C) and this is primarily because their microstructure does not consist of any intermetallic compound. Thus, the operating temperatures do not have a major impact on their microstructure. In the case of lead-free, a single high-temperature solder cannot coverall the applications ranging from 150 °C to 200 °C. Au–0.35Sn–0.03Ag and Au–0.33Sn–0.04Cu are promising candidate alloys for applications in the higher end of the temperature range, i.e. close to 200 °C. For applications, involving the lower end of the temperature range, i.e. close to 150 °C, both the candidate alloys close to the Au–Sn eutectic as well as the ones on the Sn rich side can be considered. In this work, the AuSn IMC was determined to be one of the softest Au–Sn IMCs.

Acknowledgement

The authors acknowledge the Danish Ministry of Science, Technology and Development for financial support through the innovation consortium “Matpack” (Project No. 07-003145).

References

[1] Suganuma Katsuaki, Kim Seong-Jun, Kim Keun-Soo. High-temperature lead-free solders: properties and possibilities. JOM 2009;61:64–71.
[2] Kim JH, Jeong SW, Lee HM. Thermodynamics aided alloy design and evaluation of Pb-free solders for high-temperature applications. Mater Trans, JIM 2002;43:1873–8.
[3] Chidambaram Vivek, Hald John, Hattel Jesper. Development of Au–Ge based candidate alloys as an alternative to high-lead content solders. J Alloys Compd 2009;490:170–9.
[4] Chidambaram Vivek, Hald John, Hattel Jesper. A feasibility study of lead free solders for level 1 packaging applications. J Microelectron Electron Pack 2009;6:75–82.
[5] Rettenmayr M, Lambracht P, Kempf B, Graff M. High melting Pb-free solder for die-attach applications. J Adv Eng Mater 2005;7:965–9.
[6] Chidambaram Vivek, Hald John, Hattel Jesper. Development of gold based solder candidates for flip chip assembly. J Microelectron Reliab 2009;49: 323–30.
[7] Chidambaram Vivek, Hald John, Ambat Rajan, Hattel Jesper. A corrosion investigation of solder candidates for high-temperature applications. JOM 2009;61:59–65.
[8] Seo Sun-Kyoung, Kang Sung K, Shih Da-Yuan, Lee Hyuck Mo. The evolution of microstructure and microhardness of Sn–Ag and Sn–Cu solders during high temperature aging. J Microelectron Reliab 2009;49:288–95.
[9] Schoeller Harry, Bansal Shubhra, Knobloch Aaron, Shaddock David, Cho Junghyun. Microstructure evolution and the constitutive relations of high-temperature solders. J Electron Mater 2009;38:802–9.
[10] Dinsdale AT, Watson A, Kroupa A, Zemanova A, Vrestal J, Vizdal J. COST 531 database. Version 3.0; 2008.
[11] Scientific Group Thermodata Europe (SGTE). SSOl2 solutions database. Version 2.1; 1999/2002/2003.
[12] Bergmann Rene, Tang Peter Torben, Hansen Hans Nørgaard, Møller Per. In-situ investigation of lead-free solder alloy formation using a hot-plate microscope. IEEE Conf Proc 2007:252–6.
[13] He M, Acoff VL. Effect of reflow and thermal aging on the microstructure and microhardness of Sn–3.7Ag–xBi solder alloys. J Electron Mater 2006;35: 2098–106.
[14] Islam RA, Wu BY, Alam MO, Chan YC, Jillek W. Investigations on microhardness of Sn–Zn based lead-free solder alloys as replacement of Sn–Pb solder. J Alloys Compd 2005;392:149–58.

Appendix V

A corrosion investigation of solder candidates for high-temperature applications

Vivek Chidambaram, John Hald, Rajan Ambat and Jesper Hattel

Minerals, Metals and Materials Society (JOM), 61: 59-65, 2009.

A Corrosion Investigation of Solder Candidates for High-temperature Applications

Vivek Chidambaram, John Hald, Rajan Ambat, and Jesper Hattel

The step-soldering approach is being employed in the multi-chip module technology. High-lead-containing alloys are among the solders currently being used in this approach. Au-Sn and Au-Ge based candidate alloys have been proposed as alternative solders for this application. In this work, a corrosion investigation was carried out on potential ternary lead-free candidate alloys based on these binary alloys for high-temperature applications. These promising ternary candidate alloys were determined by the CALPHAD approach based on the solidification criterion and the nature of the phases predicted in the bulk solder. This work reveals that the Au-Sn-based candidate alloys close to the eutectic composition (20 wt.% Sn) are more corrosion resistant than the Au-Ge-based ones.

INTRODUCTION

Multi-chip module (MCM) technology is a specialized electronic packaging technology recently gaining momentum due to the miniaturization drive in the microelectronics industry. The MCM technology is currently being used for servers; storage array systems; network infrastructure equipment for switching, signaling, and transmission; network management for telecommunication; automotive under-bonnet applications; and in aerospace industries. The step soldering approach is currently being used in the MCM technology.[1] High lead-containing alloys, where the lead levels can be above 85% by weight, are among the solders currently being used in this technology. Public awareness of environmental issues including the use and disposal of potentially toxic materials has never been greater, with lead being the subject of particular scrutiny. Thus, in industry there is now an increasing pressure to eliminate lead-containing materials despite the fact that materials for high-lead-containing alloys are currently not affected by any legislation.[2]

The primary requirement for replacing the high lead content solders used in the MCM technology is the solidification criterion. The solder alloy should possess a solidus temperature higher than 270°C in order to withstand peak temperatures of the second level soldering. It should also possess a liquidus temperature below 350°C in order to avoid thermal degradation of polymers commonly used in the substrate as dielectric materials.[3]

Miniaturization drive, multiplicity of materials, and globalization have resulted in corrosion being a significant issue for lead-free solder alloys. Corrosion in electronic components is insidious and cannot be readily detected and therefore, the cost of corrosion in the electronic sector can not be estimated. It has been suggested that a significant part of all electronic system failures is actually caused by corrosion but is generally not accounted for. Moreover, advanced packaging technologies like the MCM involve the reduction of the distance between components on a printed circuit board (PCB). The close spacing increases the electric field between points and reduces the size of the condensing water droplet needed for connecting the components together for corrosion.

The reduction in size and distance between components and the increase in the interconnect density makes the solder alloy susceptible to corrosion problems.[4] Thus, corrosion in the electronics industry has become a significant factor in recent years because of the extremely complex systems that have been developed and the increasing demand on their reliability.[5] Therefore, it is essential to take into account the effects of corrosion during the design of lead-free solder alloys for high-temperature applications.

See the sidebar for experimental procedures.

How would you…

…describe the overall significance of this paper?

Potential lead-free solder candidates for high-temperature applications that were determined by using computational thermodynamics were assessed from the corrosion perspective. This work reveals that, among the two primary candidate alloys for high-temperature solders, Au-Sn-based candidate alloys close to the eutectic composition are more corrosion resistant than the Au-Ge-based ones.

…describe this work to a materials science and engineering professional with no experience in your technical specialty?

The solder candidates that could adhere to the solidification criterion required for replacing the high-lead-containing solders were investigated from the corrosion perspective. An overview of corrosion-related problems that have to be thoroughly investigated before substituting the currently used one has been reported.

…describe this work to a layperson?

A drive for miniaturization, multiplicity of materials, and globalization has resulted in corrosion being a significant issue in the complex electronic packaging systems that are being developed. The possible corrosion scenario for the promising lead-free solder candidates in such packaging for high-temperature applications has been investigated in this work.

POTENTIAL LEAD-FREE SOLDER CANDIDATES

All the binary systems with the eutectic melting point close to the required solidification criterion for this application involve gold. The binary eutectic compositions in mole-fraction are Au-0.28Ge, Au-0.35Sb, Au-0.20Si, and Au-0.30Sn and the corresponding melting points in degrees Celsius are 360, 357, 364, and 280, respectively. Among these four eutectic compositions, Au-Sb is ruled out as antimony is also now being rated as a potential toxic element. Au-Si, too, is not appropriate for this application due to its wetting constraints.[11]

The Au-Ge system is interesting for this application since the tendency of germanium toward forming intermetallic compounds (IMCs) with the commonly used wetting layers of the under-bump metallization (UBM) is very low. However, its eutectic melting temperature slightly deviates from the required liquidus temperature. An investigation was carried out to determine if alloying the Au-Ge eutectic composition reduces its liquidus temperature thereby making it adhere to the required solidification criterion. The phase equilibria calculation shows that small additions of indium or antimony to the Au-Ge eutectic composition lower its liquidus temperature. These ternary combinations were then optimized for a narrow solidification range. Thus, the optimized ternary combinations in mole-fraction are Au-0.18Ge-0.10In and Au-0.24Ge-0.05Sb. Au-Ge-Sb has also been considered as a potential solder candidate since the antimony content in the alloy is relatively small when compared to the Au-Sb eutectic and antimony is not as toxic as lead.

Although the binary eutectic Au-Sn composition adheres to the required solidification criterion, it is generally less favored for this application since it involves brittle ζ′ (Au5Sn) phase as a major phase. It was determined that small additions of Ag/Cu to the Au-Sn eutectic could suppress the brittle ζ′ (Au5Sn) phase. The equilibrium calculation has estimated that the liquid phase close to Au-Sn eutectic at 350°C would extend up to 0.03 Ag or 0.04 Cu, respectively, in these ternary alloys.[12] The required solidification criterion could also be achieved with high tin content in these alloys varying roughly in the range of 0.60 to 0.70 (mole-fraction). These ternary combinations were also optimized for a narrow solidification range and the optimized ternary combinations in mole-fraction were Sn-0.30Au-0.08Ag and Sn-0.29Au-0.08Cu, respectively.[11] The partial isothermal sections of Au-Sn-Ag and Au-Sn-Cu at the minimum acceptable solidus temperature (i.e., 270°C) and the maximum permissible liquidus temperature (i.e., 350°C) for this application are illustrated in Figures 1 and 2, respectively. The region with high tin content and still adhering to the required solidification criterion is of commercial interest since it involves less gold.

EXPERIMENTAL PROCEDURES

The promising solder candidates were determined based on the solidification criterion and the nature of the phases predicted in the bulk solder by the CALPHAD approach. The phase equilibria calculation in this work was carried out using COST 531 v 3.0[6] and SSUB3[7] thermodynamic databases by Thermo-Calc (Version R software). The thermodynamic stability of chlorides for the promising solder candidates at different room temperatures was determined by coupling both these thermodynamic databases.

These promising solder candidates were precisely produced using the hot stage microscope.[8] The essential part of the equipment is the specimen chamber in which a high vacuum ($<1 \times 10^{-3}$ mbar) is created and is controlled by pressure measurements. Inside this chamber a molybdenum plate is mounted between the electrical contacts of the current heating system. The heating system can reach a temperature up to approximately 1,400°C and is equipped with water cooling. During heating an optional flow of reducing hydrogen gas is applied. The chamber is sealed by a removable glass lid for optical in-situ observations.

The high-purity metal powders are carefully weighed and are mixed inside a specially designed pressing tool to form small tablets. The tablet is then melted inside a cylindrical aluminum oxide (Al_2O_3) crucible to form a solder sphere. The process is carried out under hydrogen flow to prevent further oxidation of the material and to start the reduction of oxides on the surface of the developing sphere. Usually non-metal impurities pop up during the sphere-forming process. Therefore, it is necessary to clean the metal sphere. Normally it is done by washing it with ethanol followed by drying.

The electrochemical testing of these promising solder alloys produced using the hot stage microscope was carried out using a micro-electrochemical technique.[9,10] The micro-electrochemical setup consists of an electrochemical head containing the 250 ppm NaCl solution, counter, and reference electrode, which is attached to the carousel of an optical microscope. A 250 ppm NaCl solution was chosen since it is a standard for corrosion testing for electronic products. The cell is connected to a pipette, which makes contact with a local region of the working electrode (in this case, the solder alloy). The lateral resolution of the technique is determined by the dimensions of the pipette tip. Potentiodynamic polarization curves were measured to an Ag/AgCl reference electrode starting from the open circuit potential at a scan rate of 1.5 mV/s. All the solder alloys were ground on a 4,000 SiC paper prior to the experiment. All the surfaces were cleaned with alcohol followed by distilled water and then air dried. All measurements were carried out in naturally aerated 250 ppm NaCl. Separate experiments were used to measure the anodic and the cathodic reactivity. The results were affirmed after measuring the anodic and the cathodic reactivity in several duplicates. Corrosion morphology and the microstructure of the Au-Ge-based solder alloys after polarization tests were analyzed using scanning electron microscopy (SEM) (JEOL 5900). The chemical composition analysis was carried out using the EDX (Oxford, Link ISIS) system attached with the SEM.

THERMODYNAMIC STABILITY OF CHLORIDES

Presently electronic devices are used under service conditions that were never thought of a few years back.[13] Depending upon the design of the electronic component and the manner in which it is mounted in a substrate or printed wiring board, the solder connection can be exposed to the atmosphere. The solder is thus not only exposed to air but also moisture and other corrosives present in the atmosphere such as chlorine compounds.[14] Another source for chlorides is residual chemicals. These are generally introduced during manufacturing and include fluxes, cleaning compounds, plating solutions, and metal-processing fluids.

Also included here are chemicals from finger prints and saliva.[15] The likelihood of a metal forming a chloride and the stability of the chloride formed is represented by the standard Gibbs free energy of formation (ΔG_f^0) of that chloride. The thermodynamic parameter (natural logarithm of activity, LNAC) is a useful one for investigating metal-gas interaction systems involving formation of various forms of metal-involving oxides, chlorides, etc.:

$$LNAC = \mu/RT \quad (1)$$

where μ is the chemical potential. The compounds with the large negative LNAC of Cl_2 (g) value are highly stable. The ΔG_f^0 values and the LNAC of Cl_2 (g) of the most stable chlorides of the elements commonly being considered for the major constituents in solder alloys were calculated at different room temperatures using the SSUB3 thermodynamic database and are summarized in Table I. This table shows that all elements currently being considered for replacement solder alloy are prone to attack from chlorine that could be present in the atmosphere. The corrosion of the currently used Pb-Sn solder alloy was not a major concern although it easily reacts with chlorides because they form a lead oxide layer, which is fairly stable.

The thermodynamic parameter LNAC of Cl_2 (g) of the most stable chlorides for the promising solder candidates at different room temperatures were determined by coupling both the thermodynamic databases and are listed in Table II. Thermodynamic calculations for chlorides show that alloying gold with the elements commonly being considered for solder candidates would have an impact on the thermodynamic stability of chlorides for the respective alloy. However, this is unlikely in the case of germanium.

POTENTIODYNAMIC POLARIZATION CURVES

The anodic polarization curves of the Au-Sn and Au-Ge based solder alloy candidates in comparison with pure metals are depicted in Figures 3 and 4, respectively. There was a good agreement in the trend followed by the calculated thermodynamic parameter LNAC of Cl_2 (g) for the most stable chlorides and the experimentally determined E_{corr} values (potential) for the promising solder alloys in chloride environment. The tin was the least noble and it was anodically the most reactive in 250 ppm NaCl with highest anodic current density. It was evident that with the increase in the gold content in the Au-Sn-based solder alloys there was a gradual improvement in the noble E_{corr} value as well as the gradual reduction in the anodic current density. Germanium in comparison with tin showed ~300 mV noble E_{corr} and less anodic current density. Although, the E_{corr} values were different, both pure germani-

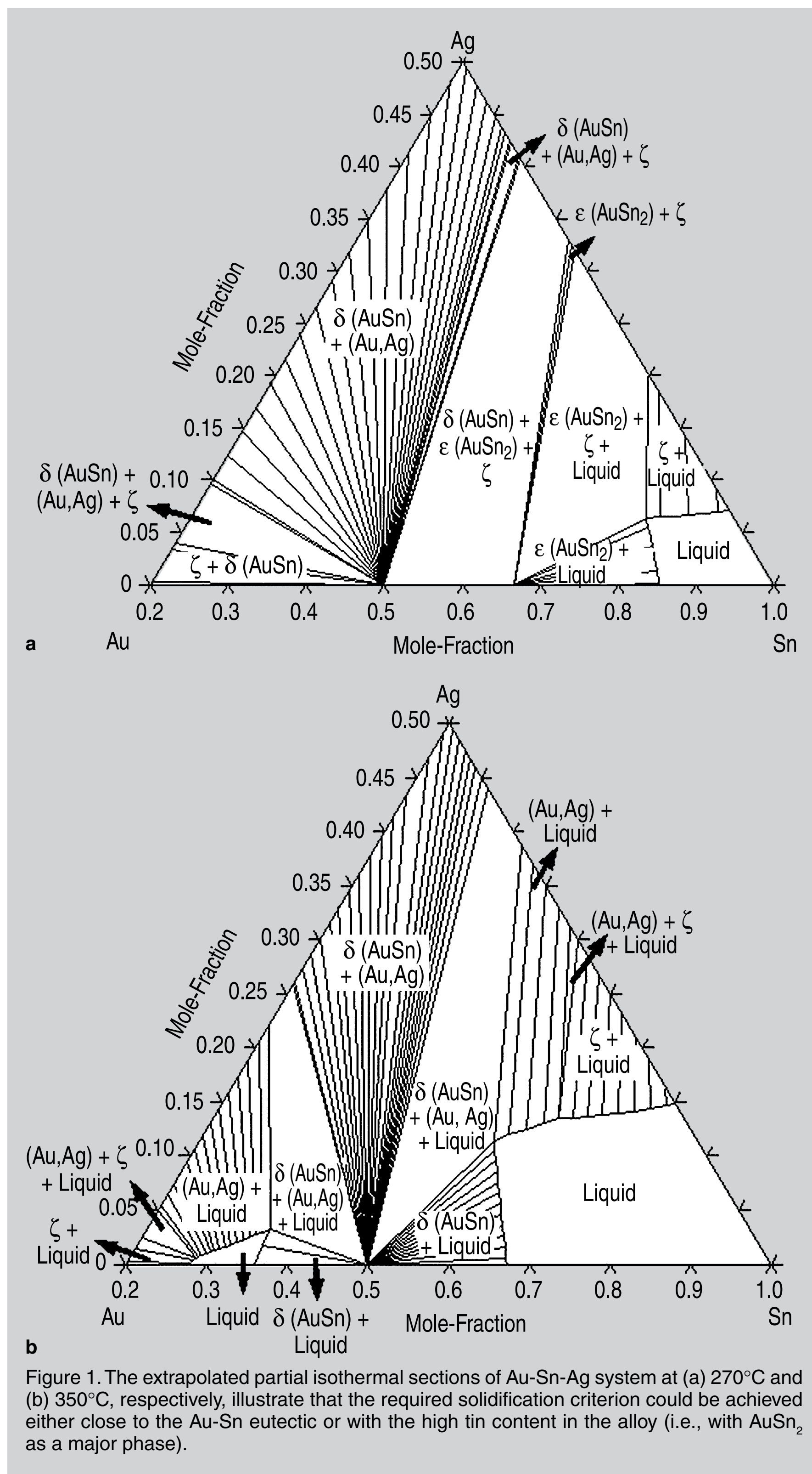

Figure 1. The extrapolated partial isothermal sections of Au-Sn-Ag system at (a) 270°C and (b) 350°C, respectively, illustrate that the required solidification criterion could be achieved either close to the Au-Sn eutectic or with the high tin content in the alloy (i.e., with $AuSn_2$ as a major phase).

um and Au-Ge-based solder alloys showed similar current densities over a range of potentials. Thus, it was determined that even by alloying germanium with substantial proportions of gold in order to adhere to the required solidification criterion no reduction in the anodic current density could be achieved and the passivation effect exhibited by pure germanium has been lost.

The cathodic polarization curves for the Au-Sn and the Au-Ge-based solder alloy candidates in comparison with pure metals are depicted in Figures 5 and 6, respectively. The cathodic activity exhibited by the Au-Ge- and Au-Sn-based solder candidates showed a trend similar to their respective anodic activity. Again, tin was cathodically the most reactive in 250 ppm NaCl with the highest cathodic current density and no reduction in the cathodic current density could be achieved even by alloying germanium with substantial proportions of gold. Thus, by alloying tin with gold, both the anodic and the cathodic reactivities of the alloy could be reduced while no significant reduction in both the anodic and the cathodic reactivities could be achieved by alloying germanium with gold.

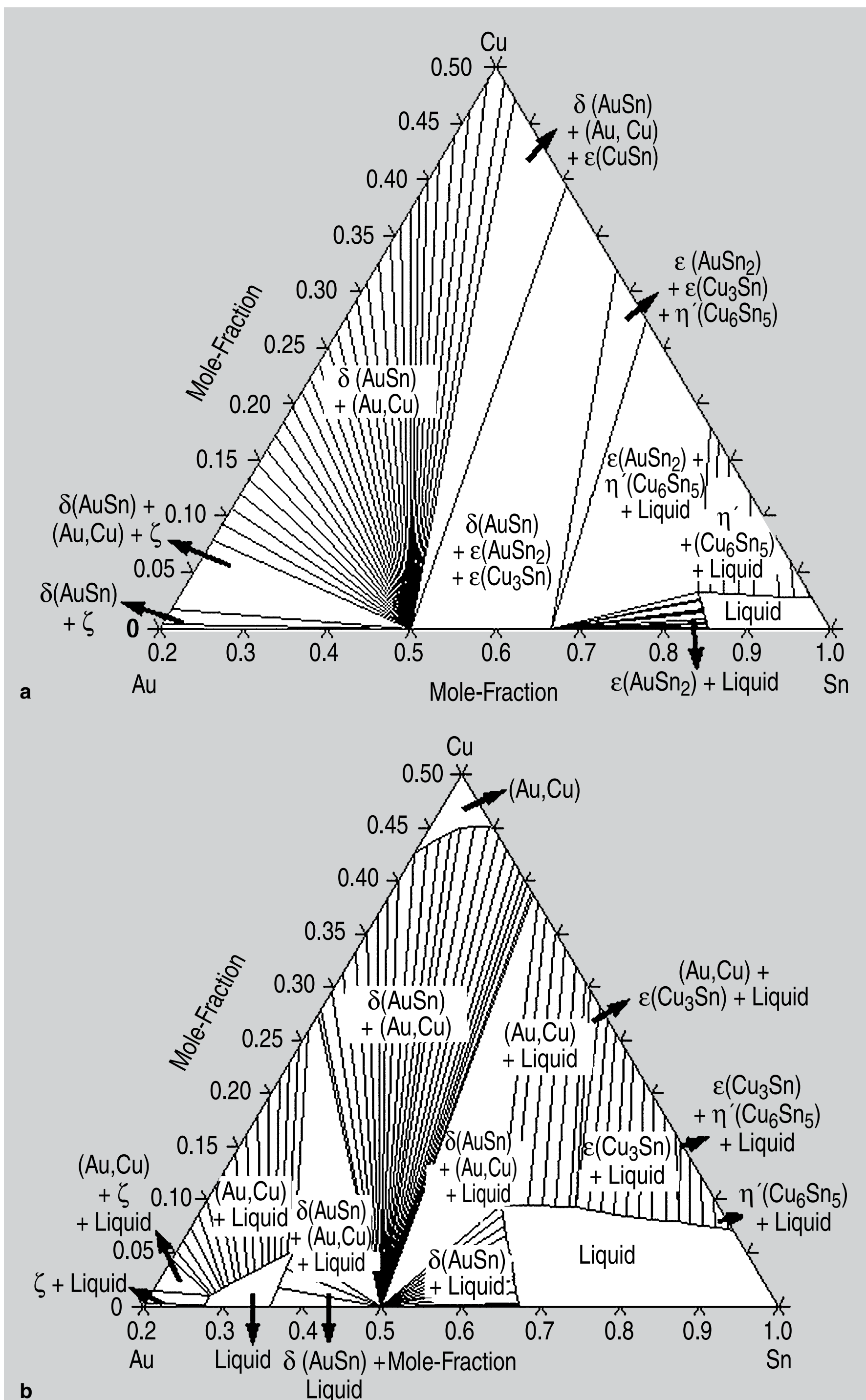

Figure 2. The extrapolated partial isothermal sections of Au-Sn-Cu system at (a) 270°C and (b) 350°C, respectively, illustrate that the required solidification criterion could be achieved either close to the Au-Sn eutectic or with the high Sn content in the alloy (i.e., with $AuSn_2$ as a major phase).

The MCM technology is being employed in applications involving high potential bias. All the solder candidates along with their pure metals were compared at a constant E_{corr} value of 1.5 V and are illustrated in Figure 7. Germanium exhibits both less anodic and cathodic current densities when compared to tin. However, substantial reduction in both the current densities could be achieved when tin is alloyed with gold while no significant reduction in any of the current densities could be achieved even by alloying relatively higher proportions of gold to germanium. Thus, Au-Sn-based solder alloy candidates close to the eutectic composition are more corrosion resistant compared to the Au-Ge-based ones and are much suited to MCM packaging involving high current density. However, the corrosion resistance property of the Au-Ge-based solder alloy candidates is almost similar to that of the Au-Sn-based solder alloy candidates involving high tin content.

ELECTROCHEMICAL AND GALVANIC COUPLING

Corrosion of solder alloys, in the presence of a suitable electrolyte can occur either due to the potential difference between the major phases in the alloy or galvanic coupling between one or more phases of the alloy and other parts of the microelectronics device since solder alloys are electrically connected with other metallic components in the electronic devices.[14] Moreover, all these materials including gold are soluble in chloride-containing environments at varied pH and potential conditions.[10]

Temperature fluctuations are common during storage and shipment.

Table I. Thermodynamic Stability of Chlorides

Metals	Chlorides	$\Delta G^0_{f,T}$ (KJ/ mole)		LNAC of Cl_2 (g) (dimensionless)	
		25°C	45°C	25°C	45°C
Ag	AgCl	–109.8	–108.7	–88.6	–82.2
Au	$AuCl_3$	–53.5	–49.1	–14.4	–12.4
Bi	$BiCl_3$	–315.2	–310.9	–84.8	–78.3
Cu	$CuCl_2$	–173.7	–170.8	–65.2	–59.1
Ge	$GeCl_4$	–462.7	–458.1	–93.3	–86.8
In	$InCl_3$	–455.4	–450.4	–112.9	–104.4
Pb	$PbCl_2$	–314.1	–311.1	–126.7	–117.6
Sb	$SbCl_3$	–324.4	–320.6	–87.3	–80.8
Sn	$SnCl_2$	–291.2	–288.4	–118.7	–109
Zn	$ZnCl_2$	–370.3	–367.3	–149.4	–138.8

These temperature swings can result in a large amount of condensation inside a package. During the warmer period, water vapor penetrates the packaging materials. This gives way to the cooler period. When the temperature reaches the dew point inside, the package condensation occurs. These water droplets (moisture) along with chlorides create conditions conducive to both electrochemical and galvanic corrosion.[16] The risk of corrosion in harsh/humid conditions for these potential ternary solder alloy candidates is higher as compared to the currently used Pb-Sn solder alloy for this application. This is because the galvanic potential difference between lead and tin is rather small while the galvanic potential difference between the constituents in these promising ternary alloys is higher.[15]

Copper and nickel are commonly being used as the solder wettable layers of the UBM. The solder alloys could interact with the wetting layers of the UBM in a hostile environment generating galvanic couples. The anodic and the cathodic polarization curves of these solder wettable layers are illustrated in Figures 8 and 9. Copper in comparison with nickel has ~300 mV noble E_{corr}. Nickel exhibited higher anodic current density when compared to copper over a range of potentials. However, copper was cathodically more reactive in 250 ppm NaCl solution than nickel.

A comparison between the electro-

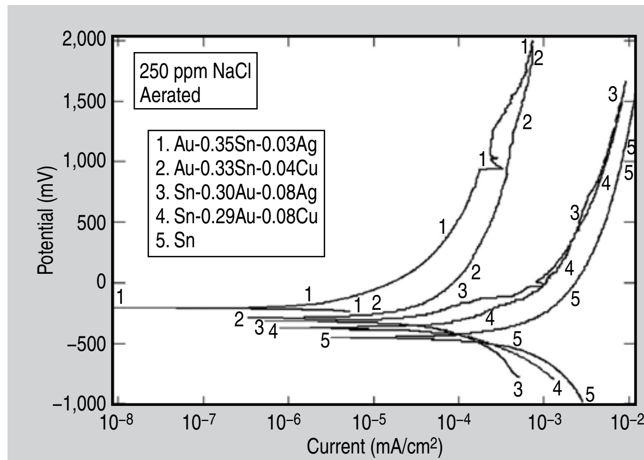

Figure 3. Anodic polarization curves for Au-Sn based solder candidates. A steady reduction in the anodic current density could be achieved with the increase in the gold content in the solder alloy.

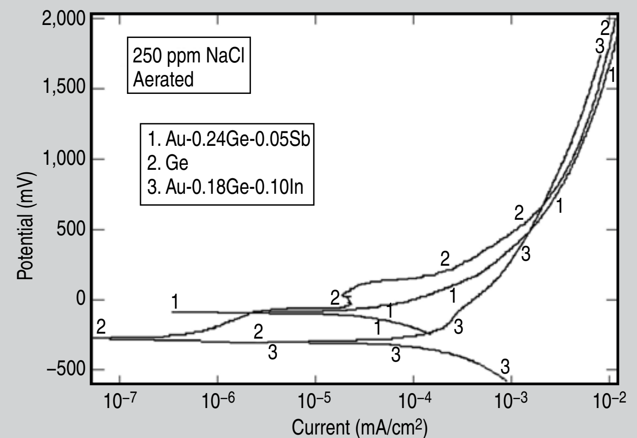

Figure 4. Anodic polarization curves for Au-Ge based solder candidates. No reduction in the anodic current density could be achieved even by alloying with substantial proportions of gold.

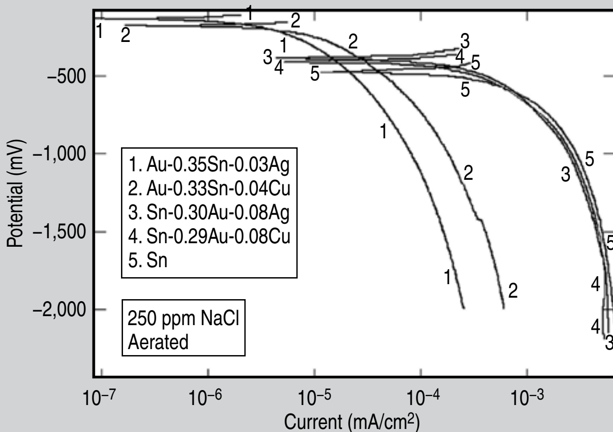

Figure 5. Cathodic polarization curves for Au-Sn based solder candidates. A steady reduction in the cathodic current density could be achieved with the increase in the gold content in the solder alloy.

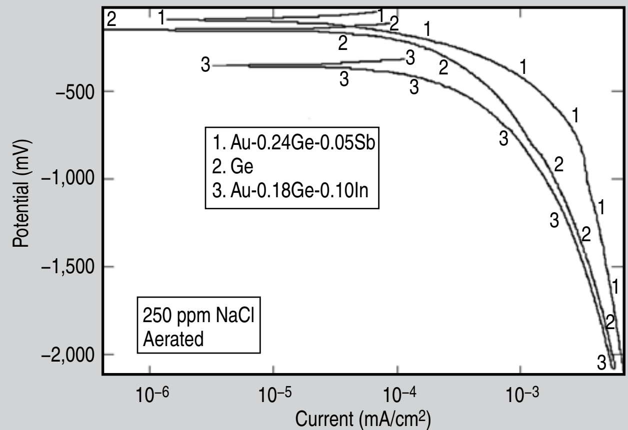

Figure 6. Cathodic polarization curves of Au-Ge based solder candidates. No reduction in the cathodic current density could be achieved even by alloying with substantial proportions of gold.

chemistry of potential solder alloys and the solder wettable layers of the UBM shows that a cross galvanic coupling could be feasible between them. Electrochemically as the E_{corr} value suggests, copper is nobler than all these potential solder alloys. Therefore, in hostile environments the Cu (UBM) could act as an additional cathode area to drive corrosion on these promising solder alloys. Moreover, the electrochemical results show that the copper is a good cathode. This could further exacerbate the corrosion mechanism. Similarly as the E_{corr} value suggests, all these potential solder alloys other than Sn-0.30Au-0.08Ag and Sn-0.29Au-0.08Cu are nobler than the Ni (UBM). Therefore, in hostile environments these solder alloy candidates could act as an additional cathode area to drive corrosion on the Ni (UBM). Generally, the potential bias between the solder-UBM would be a key factor in dictating how the corrosion proceeds. If the potential is high enough, it can cause even dissolution of nickel in the chloride solution in the latter scenario. Thus, there is a high risk of corrosion for both these potential solder alloy candidates and also the solder wettable layers of the UBM.

Table II. Thermodynamic Stability of Chlorides for Potential Solder Candidates

Potential Candidates (Mole-Fraction)	Predicted Phases		Stable Chlorides	LNAC of Cl_2 (g)	
	Matrix	Dispersed		25°C	45°C
Au-0.18Ge-0.10In	ζ	(Ge) (Au)	$InCl_3$	–109.7	–101.4
Au-0.24Ge-0.05Sb	(Au)	(Ge) $AuSb_2$	$GeCl_4$	–93.3	–86.8
Au-0.35Sn-0.03Ag	δ (AuSn)	(Au, Ag) ζ′ (Au_5Sn)	$SnCl_2$	–105.4	–97.8
Au-0.33Sn-0.04Cu	δ (AuSn)	(Au, Cu) ζ′ (Au_5Sn)	$SnCl_2$	–105.8	–98.2
Sn-0.30Au-0.08Ag	ε ($AuSn_2$)	ζ	$SnCl_2$	–115.5	–107.1
Sn-0.29Au-0.08Cu	ε ($AuSn_2$)	ε (Cu_3Sn) $η^1$ (Cu_6Sn_5)	$SnCl_2$	–116.0	–107.6

MICROSTRUCTURE CHARACTERIZATION

The electrochemical results of Au-Sn based solder candidates were anticipated. SEM analysis was carried out on Au-Ge based solder candidates after polarization tests to determine the corrosion surface morphology and also the corrosion products. A uniform distribution of phases in the solder sphere was achieved by homogenizing heat treatment during the forming of solder spheres in the hot stage microscope. The solders were thoroughly washed with water prior to SEM analysis to remove any residual NaCl on the surface. Small pits were found distributed throughout the surface of Au-0.18Ge-0.10In and Au-0.24Ge-0.05Sb solder alloys after polarization tests as shown in Figures 10a and 10b, respectively. In addition, the corrosion products that were predominantly germanium

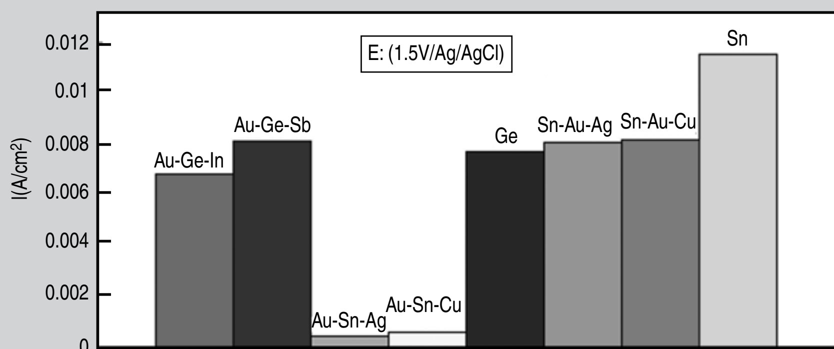

Figure 7. A comparison of Au-Sn and Au-Ge based solder candidates with respect to their current density. Au-Sn based alloys close to the eutectic composition are more corrosion resistant than the Au-Ge based alloys.

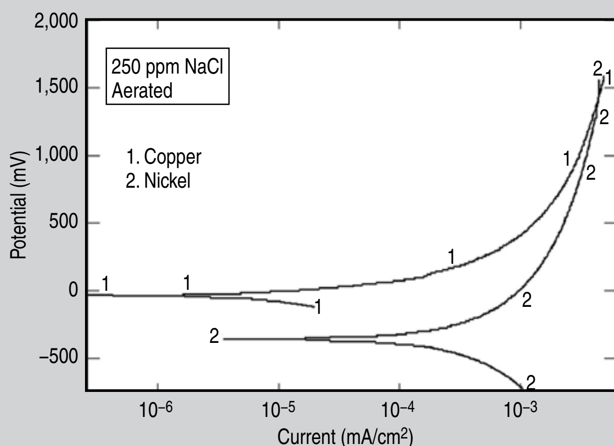

Figure 8. Anodic polarization curves for solder wettable layers. Ni exhibits more anodic current density than Cu over a range of potentials.

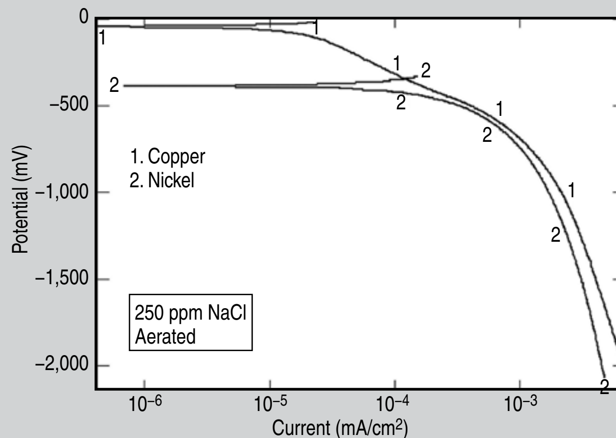

Figure 9. Cathodic polarization curves for solder wettable layers. Cu is an excellent cathode.

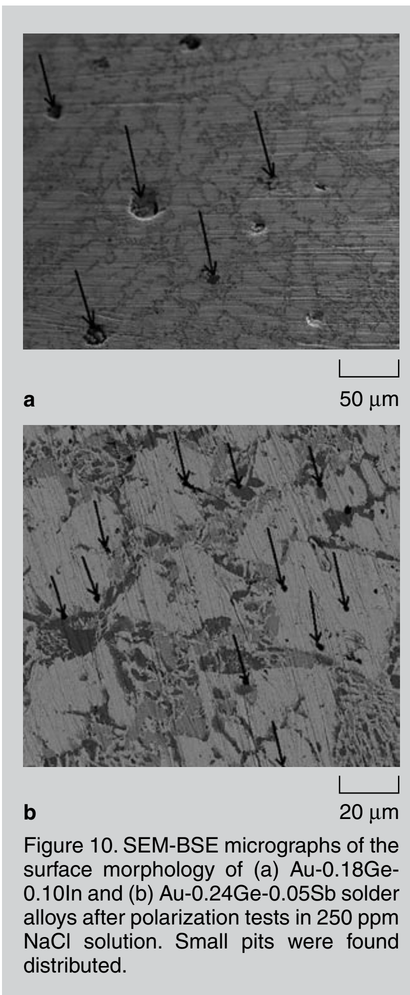

Figure 10. SEM-BSE micrographs of the surface morphology of (a) Au-0.18Ge-0.10In and (b) Au-0.24Ge-0.05Sb solder alloys after polarization tests in 250 ppm NaCl solution. Small pits were found distributed.

oxides and germanium chlorides were also found on the surfaces of both the Au-Ge-based solder alloys along with these pits as shown in Figure 11.

The anodic and the cathodic polarization behavior of the solder candidates are in close agreement with the predicted phase-fractions (Table II). The EDX spot analysis was used to identify the phases. The gray areas in Figure 10a were determined as (Ge) phase. The white areas in the Figure 10a could be either (Au) or ζ phase. These two phases could not be distinguished due to the limitations of the technique. The white, pale gray, and dark gray areas in Figure 10b were identified as (Au), $AuSb_2$, and (Ge) phases, respectively.

In the case of Au-Ge-based solder candidates, both gold and germanium exist in the microstructure as (Au) and (Ge) phases, respectively. The difference in the electromotive force between these phases is large and, hence, corrosion is likely to take place because the electrochemical coupling in the presence of chloride solution is high. Electrochemically, gold is nobler than germanium. Therefore, if there is an electrochemical coupling between the (Au) and (Ge) phases, (Au) phase could act as a cathode area to drive corrosion on the (Ge) phase. Moreover, Ambat et. al.[10] have determined gold to be an active cathode. Enhanced corrosion could occur because of the low anode [dispersed (Ge) phase]/cathode [matrix (Au) phase] ratio. Thus, the formation of these pitted areas could be attributed to the severe localized corrosion of (Ge) phase in the Au-Ge-based promising solder alloys.

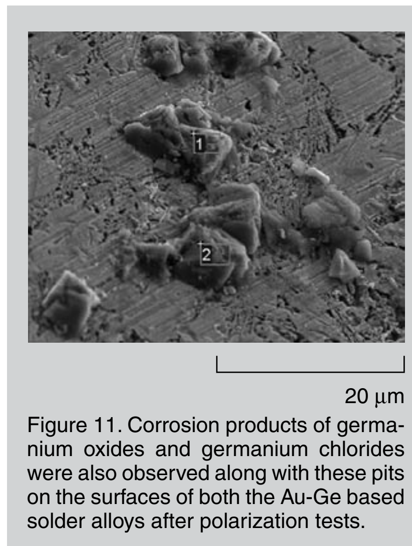

Figure 11. Corrosion products of germanium oxides and germanium chlorides were also observed along with these pits on the surfaces of both the Au-Ge based solder alloys after polarization tests.

CONCLUSION

Based on the present work's findings it can be stated that, among the two primary candidate alloys for high temperature solders, Au-Sn-based candidate alloys close to the eutectic composition are more corrosion resistant than the Au-Ge-based ones. The corrosion resistance property of germanium could not be improved even by alloying with very high proportions of gold due to the selective localized corrosion of (Ge) phase in the Au-Ge based solder alloy candidates. Overall, the results of this investigation present the possible corrosion scenario between these promising solder alloys and the UBM due to combination of materials with different electrochemical properties. Moreover, applications where MCM packagings are employed involve high potential bias and high current density and, hence, there could be additional issues in the MCM packaging due to combination of potential, environment, and material. Therefore, a thorough investigation has to be carried out on these issues related to corrosion before replacing the high lead-containing solder alloys with any of these potential solder candidates for high-temperature applications.

ACKNOWLEDGEMENT

The authors acknowledge the Danish Ministry of Science, Technology and Development for financial support through the innovation consortium "MatPack" (project no. 07-003145).

References

1. O. Ogunseitan, *JOM,* 59 (7) (2007), pp. 12–17.
2. COST ACTION MP0602, Memorandum of Understanding for the Implementation of a European Concerted Research Action, "Advanced Solder Materials for High-Temperature Application," Brussels (5 December 2006).
3. V. Chidambaram, J. Hald, and J. Hattel, "Development of High Melting Point, Environmentally Friendly Solders, Using the CALPHAD Approach" (Presentation at 2008 TOFA Conf., Krakow, Poland, 22–27 June 2008).
4. Morten S. Jellesen et al., "Corrosion in Electronics" (Paper presented at 2008 Eurocorr Conference, Edinburgh, Scotland, 7–11 September 2008).
5. R. Baboian, "Electronics," *Corrosion Tests and Standards: Applications and Interpretation*, ed. R. Baboian (West Conshohocken, PA: ASTM, 1996), *www.corrosionsource. com/events/intercorr/baboian.htm*.
6. A.T. Dindale et al., "COST 531 Database V 3.0" (Wien, Germany: Universität Wien, June 2008), *www.univie.ac.at/cost531/*.
7. Scientific Group Thermodata Europe, "SSUB3-Substance Database V 3.2," (2001/ 2002/ 2004), *www.sgte.org/*.
8. Rene Bergmann et al., "In-situ Investigation of Lead-Free Solder Alloy Formation Using a Hot-Plate Microscope" (Presentation at 2007 Electronics Packaging Technology Conf., Singapore, 9–12 December 2007).
9. Rajan Ambat, "Localized Corrosion Information Using High Resolution Measurement Devices" (Presentation at 2005 Eurocorr Conference, Lisbon, Portugal, 8–9 September 2005).
10. Rajan Ambat and Per Møller, *J. Corros. Sci.,* 49 (7) (2007), pp. 2866–2879.
11. Vivek Chidambaram, John Hald, and Jesper Hattel, *J. Microelectron. Electron. Pack.,* submitted.
12. Vivek Chidambaram, John Hald, and Jesper Hattel, *J. Microelectron. Reliab.,* 49 (3) (2009), pp. 323–330.
13. P.J. Martin, W.B. Johnson, and B.A. Miksic, "Corrosion Inhibition of Electronic Metals Using Vapor Phase Inhibitors" (Presentation at 1984 National Association of Corrosion Engineers Meeting, New Orleans, LA, 2–6 April 1984).
14. Mulugeta Abtew and Guna Selvaduray, *J. Mater. Sci. Eng.,* 27 (5-6) (2000), pp. 95–141.
15. C. Andersson and J. Liu, *J. Fatigue,* 30 (5) (2008), pp. 917–930.
16. Barry L. Rudman, "A Comparison of Several Corrosion Inhibiting Papers in Various Environments" (Presentation at 1998 National Association of Corrosion Engineers Meeting, San Diego, CA, March 1998).

Vivek Chidambaram, John Hald, Jesper Hattel, and Rajan Ambat are with the Department of Mechanical Engineering at the Technical University of Denmark. Mr. Chidambaram can be reached at vchi@mek.dtu.dk.

Appendix VI

Status of lead-free solders for high-temperature soldering

Vivek Chidambaram, Jesper Hattel and John Hald

Electronic Materials (Submitted).

Status of Lead-Free Solders for High-Temperature Soldering

Vivek Chidambaram*, Jesper Hattel and John Hald
Department of Mechanical Engineering, Technical University of Denmark, Building 425, Produktionstorvet, Lyngby, DK-2800, Denmark.
Tel.:+45-4525-4880; fax: +45-4593-4570
*Corresponding author: vchi@mek.dtu.dk

ABSTRACT

For lead-free solders in the high-temperature regime, unfortunately, a limited number of alloying systems are available. These are Bi based alloys, Au involving alloys and Zn-Al based alloys. Based on these systems, possible candidate alloys were designed to have a melting range between 270°C and 350°C. Each has its own superior characteristics as well as some drawbacks however none of them can fulfill all the requirements to replace the current high-lead content solders. Even the alternative technologies that are currently being developed cannot address several critical issues of high-temperature soldering. Therefore, further research and development of high-temperature lead-free soldering is obviously needed.

Keywords

High-temperature soldering, soft solder, thermal aging, intermetallics, die-attaching, thermal conductivity

INTRODUCTION

High-temperature soldering is a key technology for electronic packaging and requires a high level of process control.[1] This technology can eliminate wiring, connectors and cooling systems needed in a conventional electronic system. Furthermore, it provides value-added characteristics to the products including excellent heat conductivity as well as high reliability.[2] For these reasons, the high-temperature solders have wide applications in the electronics and automobile industries. High-lead containing solders have been commonly used as high-temperature solders.[3] These high-lead content alloys still hinder the recycling of electronic products even though the circuit boards are assembled with lead-free Sn based solders. Unfortunately, limited choices are available as high-temperature lead-free solders. Therefore, a robust design concept based on materials science is needed in order to fully benefit from this new technology.[4] This paper presents the possible candidate alloys that could replace the existing high-lead content solders currently being used for high-temperature soldering and also reviews the cost-effective substitute joining technologies for high-temperature soldering.

In designing new Pb-free high-temperature solder alloys, the melting behavior is important. The soldered parts have to sustain with no melting until it passes the last step of the assembling process. The solidus temperature of the high-temperature solder should be at least 50°C higher than the melting point of the solder used in the second level packaging and the liquidus temperature should be below the glass transition temperature of the polymers used in the substrate as dielectric materials. Therefore, the melting temperature range (270°C to 350°C) has been defined by the industries in order to ensure efficient process control.[5] Attempts to adjust the melting range (increase the solidus and liquidus temperatures) of Sn based solders by appropriate alloying with inexpensive metals have remained unsuccessful till present. Thus, for soft solder

alloys in the high-temperature regime, a suitable alternative to the high-lead containing alloys covering the whole spectrum of properties is still to be developed.[6]

The operating environment that the high-temperature solders are being subjected to varies between 150°C to 200°C depending on the applications. Therefore, the effects of thermal aging on the microstructure and its corresponding microhardness on the currently used high-lead content solders and the possible alternative candidate alloys at this operating temperature range have been reported. This work only characterizes the properties of bulk solders and does not consider factors such as reactions with joining materials which may affect the mechanical performance of actual solder joints. Instead the work focuses on specific microstructural features that can explain solder performance at elevated temperatures.[1,3]

EXPERIMENTAL METHODS

Sample preparation

The high-lead content solder alloys and the possible candidate alloys were precisely produced using a hot-plate microscope.[7] The high purity metal powders were carefully weighed and were mixed inside a specially designed pressing tool to form small tablets. The tablet was placed inside a cylindrical aluminium oxide crucible on a molybdenum plate that is mounted between the electrical contacts of the heating system inside the specimen chamber of the hot-plate microscope. A high-vacuum (<1x 10^{-3} mbar) was created in the specimen chamber and it was controlled by pressure measurements. The melting process was carried out under hydrogen flow to prevent further oxidation of the material and to start the reduction of oxides on the surface of the developing sphere. The solder spheres were held at the liquid state for a short time to ensure homogeneity. The solder sphere is remelted a couple of times for homogenization. A high cooling rate (300K/s) was employed during the production of these solder spheres.[1,3,8] For a comprehensive explanation with several illustrations about the production process of the samples employing hot-plate microscope is referred to Bergmann et. al.[7]

Thermal aging

The aging experiments were conducted at two different temperatures i.e. at 150°C and 200°C in order to investigate the stability of the respective microstructures both at the lower and the upper end of the operating temperature range for high-temperature solders. The samples were loaded into an ambient atmosphere resistant furnace and were heated to these respective temperatures and annealed at the same temperatures for 1 day & 1 week respectively.[1,3]

Cross sectioning

The as-produced and the thermally aged samples were embedded in an epoxy resin, ground for cross sectioning. They were ground with 500, 1000 and 4000 grade abrasive sand papers and then polished with 3 µm and 1 µm diamond suspensions. In the case of high-lead content solders, 0.04 µm alumina and 0.025 µm colloidal silica suspensions were used for final polishing since it is an extremely soft alloy. Appropriate chemical etching was also used to distinguish different phases of the possible candidate alloys.

Microscopy/Microhardness

The microstructure of the high-lead content solders and the possible candidate alloys were examined using a Neophot optical microscope and a JEOL 5900 scanning electron microscopy

(SEM). For the analysis of the microstructure, the back-scattered (BS) electron mode of SEM was used. Compositional analyses of the phases were conducted with energy dispersive spectrometer and it was carried out on unetched samples. Vickers hardness measurement was performed to clarify the relationship of microstructure and microhardness. An indentation load of 5g & 100g and a dwell time of 5s were used to measure the hardness of the high-lead content solders and also the possible candidate alloys. 5g load was used to determine the hardness of individual phases i.e. on the crystal in order to interpret the macro/overall hardness of the alloy. However, in certain cases it was not possible to measure the hardness of individual phases. 100g load was also applied so that the width of indentation was large enough to span multiple phases and many eutectic domains. Hence, the test values reflect the overall microhardness of the candidate alloys.[1,3] The Vickers hardness number was reported as an average value by measuring 10 indentations or more.

RESULTS AND DISCUSSIONS

High-lead content solders

Pb-Sn and Pb-Ag with a Pb content of more than 85 wt% are the currently used solders for high-temperature soldering. Common versions of high-temperature solders are Pb-5Sn and Pb-10Sn, having a melting range of 308-312°C and 275-302°C respectively.[9] The microstructure composed of Sn particles or (Sn) phase dispersed on the matrix (Pb) phase as depicted in Fig. 1. The microstructures of the high-lead content solders are very stable and both the aging durations and the aging temperatures do not have major impact on the microstructures. This facilitates in employing high-lead content solders in a wide range of applications since the microstructure does not consist of any intermetallic compounds (IMCs). Moreover, the corrosion of high-lead content solders was never identified as a reliability concern since they form a lead oxide layer, which is fairly stable. Furthermore, the galvanic potential difference between (Pb) and (Sn) is rather small, causing an insignificant corrosion effect even in harsh/humid conditions.[10]

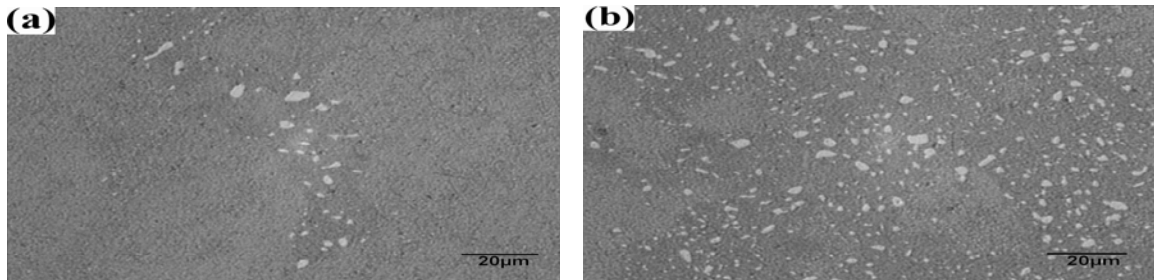

Fig. 1. Optical microstucture of Pb-5Sn and Pb-10Sn after thermal aging at 150°C for 1 week respectively.

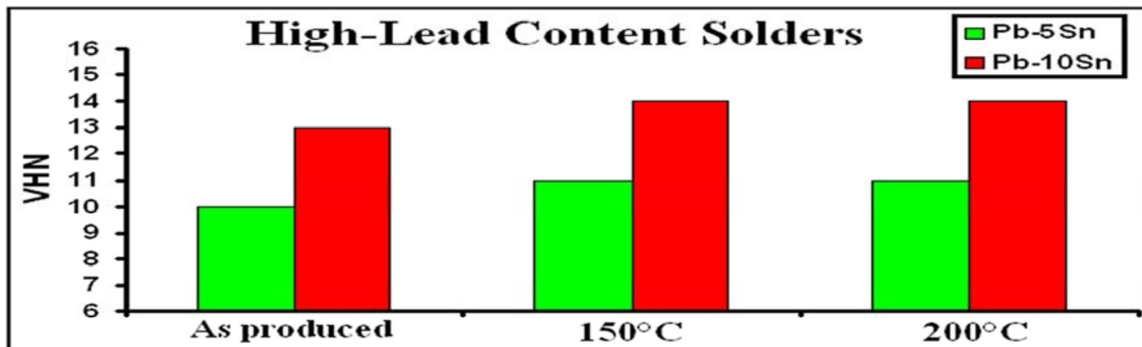

Fig. 2. Microhardness values of the high-lead content solder alloys using 100g load before and after thermal aging for 1 week.

High-lead content solders are an extremely soft alloy. It possesses excellent fatigue resistance since the softness of the alloy enables it to maintain a reliable joint structure by relaxation of thermal stresses.[11]On the other hand, because of this softness it is prone to thermo-mechanical failure due to creep. The overall hardness of the as-produced and the aged samples using 100g load are illustrated in Figure. 2. It was not possible to determine the hardness of individual phases even using the 1g load since the alloys are too soft. It was found that the hardness of the alloys during aging were almost similar irrespective of the aging temperatures. Pb-10Sn solder alloy was slightly harder than the Pb-5Sn alloy. This could be attributed to the dispersion hardening of the matrix (Pb) phase by Sn particles or (Sn) phase.

Possible candidates

Cheaper alternatives

The binary phase diagrams of Sn and further metallic elements indicate that generally the melting point of pure Sn (232°C) will be lowered by adding elements that are popular candidates for use in solder alloys.[12] Thus, Zn-Al based alloys & Bi based alloys are the only possible cost-effective alloys for high-temperature lead-free solder alternatives.[6,12] However, both these alloys possess weak bonding strength.

Zn-Al based candidate alloys

Zn-6Al (wt. %) with a eutectic melting point of 381°C is a very interesting candidate for this application. The corresponding phase diagram reveals that this alloy does not form any intermetallic compounds.[4] Zn-Al alloys have long been used as high-temperature solders for structural applications.[13,14] From the commercial perspective, this is a very prospective alloy since Zn is even cheaper than lead.[15] Small additions of either Mg or Ge to the Zn-Al eutectic would reduce the melting point of this alloy and make this ternary alloy adhere to the required solidification criterion for high-temperature soldering.[12]

However, having Al in the alloy for soldering electronic components would severely hamper the drive for miniaturization in the electronics industry due to the high natural radius of curvature possessed by Al.[1,3] Above all, the major drawback for developing Zn-based alloys as Pb-free solders for high-temperature soldering is the corrosion-oriented reliability issues. Zn is a highly corrosive metal and it can be advocated for solder alloys only as a minor constituent and definitely not as a major constituent since electronic devices are being subjected to service conditions that were never thought of a few years back.[8] It has been reported that Zn-Al eutectic is a relatively hard alloy when compared to the existing high-lead content solders.[12,16] Furthermore, it possesses poor wetting behaviour because of the high oxygen affinity of both Zn and Al. Taking into account its corrosive nature, high natural radius of curvature and wetting constraints, this alloy was not considered for further investigation in this work.

Bi based alloys

Bi is the least toxic of the heavy metals and with a melting point of 270°C is a natural choice for a high-temperature lead-free solder alternative. It should however be noted that at present Bi is mainly a bi-product of Pb production.[6] The development of Bi based alloys for Pb-free high temperature soldering is severely hindered by the poor thermal and electrical conductivity possessed by the Bi rich phases which is critical for the solder alloy. The thermal conductivity of Bi (k = 8 W/mK) is much lower when compared to the existing high-lead content solders like Pb-5Sn (k = 35 W/mK).[17]

It has been well documented that the addition of Ag to Bi would slightly improve the thermal and electrical conductivity of the alloy.[6,17,18] The Bi-Ag system has a eutectic melting point of 262°C corresponding to 2.6 wt% Ag. However, further increasing or decreasing the Ag content from the eutectic point entails an increase of only the liquidus temperature and not the solidus temperature. The microstructure of the Bi-Ag eutectic alloy consists of Ag rich dendrites dispersed on the matrix (Bi) phase.[6] Coupled growth of the eutectic phases has not been reported since the eutectic point lies on the region with a very high Bi content. Alloying small proportions of Ag cannot drastically improve the thermal and electrical conductivity of the alloy. Bi-2.6Ag alloy also possesses a higher wetting angle of 39° when compared to the existing high-lead content solders like Pb-5Sn (16°) on a Cu substrate.[11]

Bi-2.6Ag is the only possible alloy in addition of being close to the required solidification criterion, it is also close in hardness to the existing high-lead content solders.[6,11] Despite this advantage it cannot be used as an alternative since high-temperature solders are currently being employed in applications that generate high amounts of heat and it demands a high heat conductivity of the solder.

Expensive alternatives

There are several binary eutectic compositions involving gold that could either adhere or be very close to the required solidification criterion for high-temperature soldering. Au-0.30Sn (mole-fraction) is the only binary eutectic composition with a melting point of 280°C that directly fits into the requirement. Au-0.28Ge (mole-fraction) eutectic composition with a melting point of 360°C is still very close to the requirement.[19] Au-Sn as well as Au-Ge are existing hard solders currently being used for fluxless applications like opto-electronic packaging.[20,21] However, it cannot be used as a soft solder for high-temperature applications without inducing some softness in it by micro-alloying. In addition to fulfilling the solidification criterion, both Au-Sn (k=57 W/mK) and Au-Ge (k=44 W/mK) eutectic alloys possess better thermal conductivities than the existing high-lead content solders like Pb5Sn (k=35 W/mK).[17]

Although Au-0.20Si (mole-fraction) and Au-0.35Sb (mole-fraction) eutectic compositions with a melting point of 363°C and 357°C too are close to the requirement, they are still not prospective candidate alloys. The former is not an appropriate candidate alloy due to the wetting constraints and the latter is not promising due to the high proportions of Sb involved in it since Sb is also in the list of toxic elements.[22,23]

Au-Sn based candidate alloys

Au-Sn eutectic alloy is currently being used as a hard solder due to the presence of the brittle ζ' (Au5Sn) phase. The microstructure of the as-produced Au-Sn eutectic alloy was comprised of the brittle ζ' (Au5Sn) and ζ phases dispersed on the matrix of the Au-Sn eutectic structure (ζ' + δ) as illustrated in Fig. 3. The presence of ζ phase can be attributed to the fast cooling rate employed during the production of these alloys in the hot-plate microscope. The microstructure of the thermally aged Au-Sn eutectic alloy at 150°C for 1 week was comprised of large Au5Sn IMCs dispersed on the Au-Sn eutectic structure. The ζ phase did not exist in the Au-Sn eutectic alloy subjected to aging at 150°C. The microstructure of the thermally aged Au-Sn eutectic alloy at 200°C was comprised of ζ and δ phases only. Therefore, it can be concluded that at 200°C, the brittle ζ' phase of the Au-Sn eutectic alloy has transformed into ζ phase.

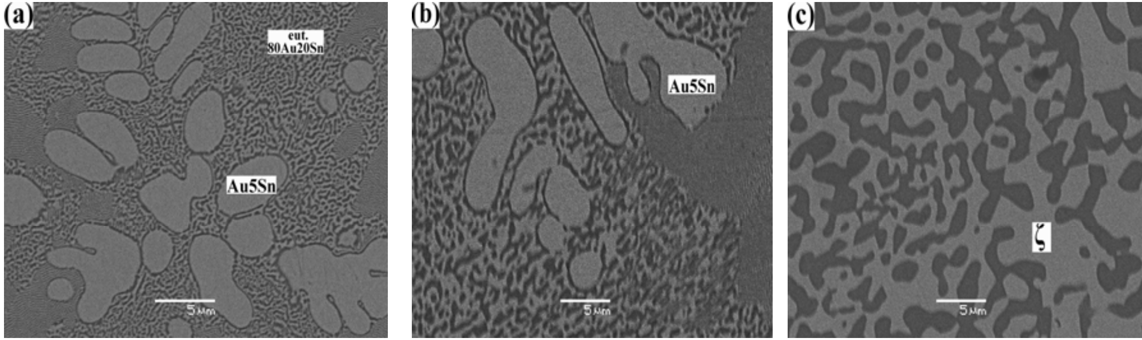

Fig. 3. SEM-BSE micrographs of the eutectic Au-Sn alloy before and after thermal aging (a) as-produced (b) 150°C-1week (c) 200°C-1 week.

Phase equilibria calculations show that the small additions of Ag/Cu to the Au-Sn eutectic would suppress the precipitation of the brittle Au5Sn phase and in turn proportionally precipitate relatively ductile phases. However, it has been predicted that the liquidus temperature of the ternary alloy too would increase proportionally with the additions of Ag/Cu to the Au-Sn eutectic. The equilibrium calculation has estimated that the liquid phase close to Au-Sn eutectic at 350°C would extend up to 0.03Ag/0.04Cu respectively. Thus, the Au-Sn compositions close to eutectic with the maximum content of Ag and Cu in mole-fraction and still adhering to the solidification criterion are Au-0.35Sn-0.03Ag and Au-0.33Sn-0.04Cu, respectively.[19]

Phase equilibria calculations also show that the required solidification criterion could also be achieved on the Sn rich side of the Au-Sn-Ag/Au-Sn-Cu system, with Sn content varying roughly in the range of 0.60 to 0.70 (mole-fraction). This region with high Sn content is of commercial interest since it involves less gold. These ternary combinations were optimized for a narrow solidification range and the optimized ternary compositions in mole-fraction are Sn-0.30Au-0.08Ag and Sn-0.29Au-0.08Cu.[1,5,8]

Au rich side of the Au-Sn System

Micro-alloying of Ag/Cu to the Au-Sn eutectic would to some extent suppress the brittle ζ' (Au5Sn) phase as illustrated in Fig. 4. This was very evident at 150°C. Ag was determined to be a better alloying element since in addition to the suppression of the most brittle ζ'phase, ε (AuSn2) phase did not exist in the matrix. Unlike the Au-0.35Sn-0.03Ag candidate alloy, a few refined ε (AuSn2) lamellae existed in the matrix of the as-produced Au-0.33Sn-0.04Cu candidate alloy. However, these refined AuSn2 lamellae disappeared when subjected to aging. The presence of AuSn2 lamellae in the as-produced Au-0.33Sn-0.04Cu can be attributed to the fast cooling rate employed during the production of these alloys in the hot-plate microscope. It has to be mentioned that among the Au-Sn intermetallics, ε (AuSn2) is the second most brittle IMC next only to ζ' (Au5Sn).[1]

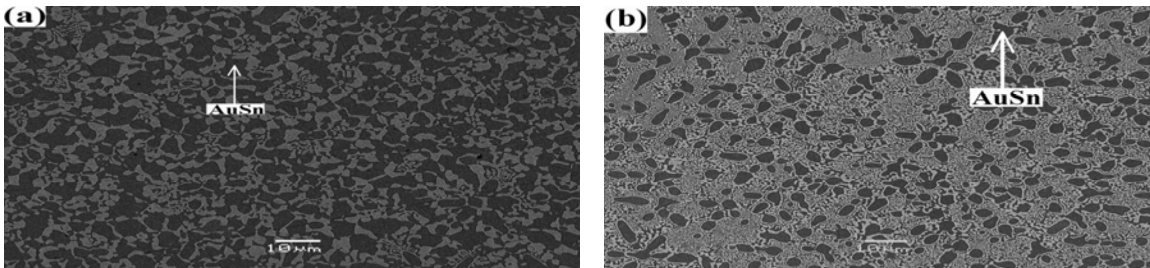

Fig. 4. SEM-BSE micrograph of the candidate alloys subjected to aging at 150°C for 1 week (a) Au-.35Sn-0.03Ag (b) Au-0.33Sn-0.04Cu.

Au-Sn eutectic is a hard alloy at 150°C and a relatively soft alloy at 200°C due to the presence of high volume-fraction of ζ' at 150°C and due to the gradual disappearance of ζ' phase at 200°C. Micro-alloying of Ag/Cu has induced some softness to the hard solder as illustrated in Fig. 5. The magnitude of softness induced to the hard solder was relatively higher at 150°C than at 200°C. However, the degree of softness induced to the hard solder by micro-alloying is still not promising enough to be regarded as a soft solder. Despite being hard, Au-Sn eutectic alloys have been reported to exhibit superior thermal fatigue resistance by Suganuma et. al.[4]

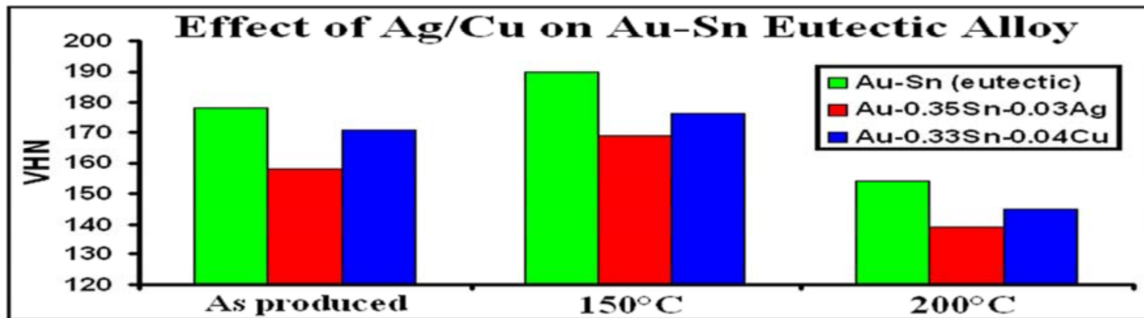

Fig. 5. Microhardness values using 100g load before and after thermal aging for 1 week.

Sn rich side of the Au-Sn System

The major difference that was observed in the Sn rich alloys during aging at different aging temperatures for various durations was with respect to the dark δ (AuSn) phase as illustrated in Fig. 6. The volume-fraction of this soft phase decreased with the increase in the aging temperatures. The reduction of this soft phase during aging was substantially lower in the case of the Sn-0.29Au-0.08Cu (mole-fraction) candidate alloy when compared to the Sn-0.30Au-0.08Ag (mole-fraction) candidate alloy at the respective aging temperatures.

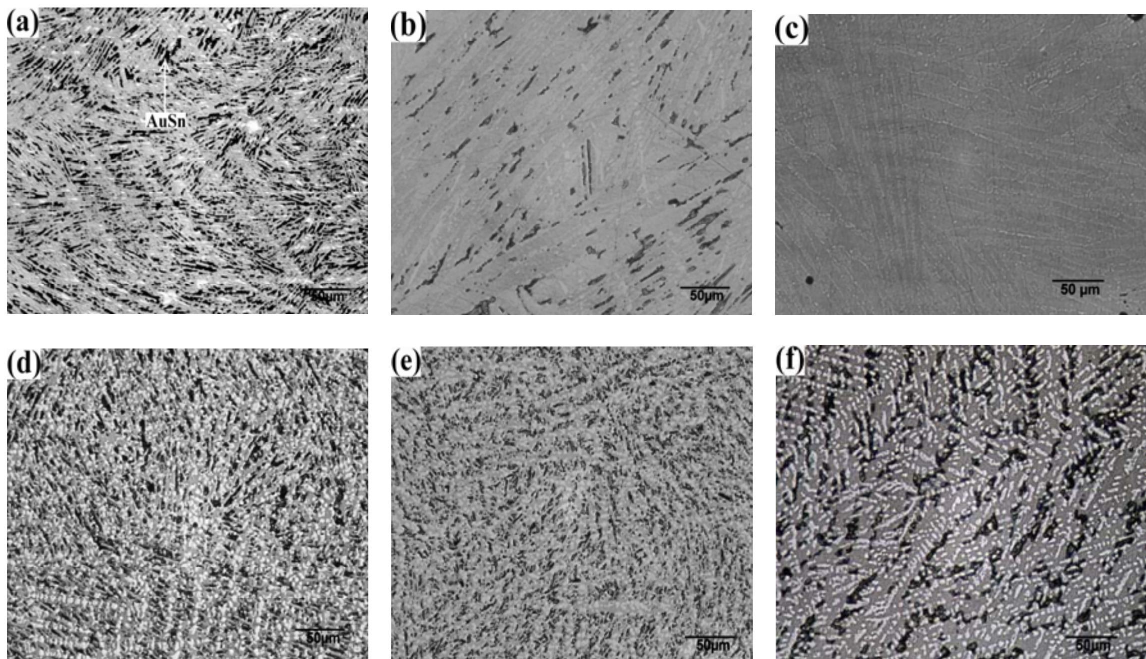

Fig. 6. Optical microstructures of Sn-0.30Au-0.08Ag (a) as-produced (b) 150°C-1 week (c) 200°C-1week, and Sn-0.29Au-0.08Cu (d) as-produced (e) 150°C-1week (f) 200°C-1week.

The hardness profile in the Sn rich region was primarily governed by the volume-fraction of the soft δ phase. The Sn-0.29Au-0.08Cu was a relatively soft alloy when compared to Sn-0.30Au-0.08Ag candidate alloy due to the higher volume-fraction of this soft phase as illustrated in Fig. 7. None of the brittle Cu-Sn IMCs was observed both in the as-produced as well as in the aged Sn-0.29Au-0.08Cu samples. It has to be mentioned that Cu-Sn intermetallics are relatively more brittle than any of the Au-Sn intermetallics. The Sn-0.29Au-0.08Cu candidate alloy aged at 150°C is a relatively soft alloy when compared to itself aged at 200°C due to the higher volume-fraction of AuSn phase. The difference in hardness between the Au rich side and the Sn rich side narrowed down when subjected to aging at 150°C. This is due to the precipitation & stabilization of the hard ζ' phase on the Au rich side and the presence of higher volume-fraction of the soft AuSn phase on the Sn rich side. Thus, for applications involving the operating temperature close to 150°C even the Sn rich side i.e. in particular the Sn-0.29Au-0.08Cu candidate alloy too can be considered.[1]

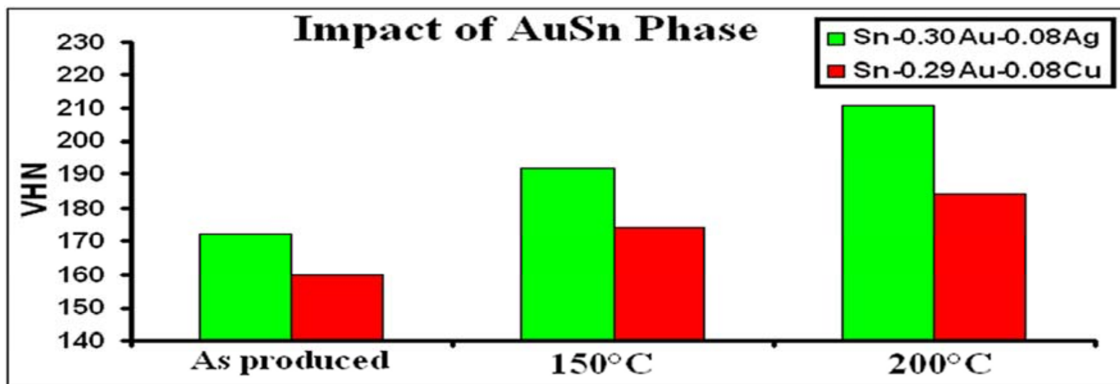

Fig. 7. Microhardness values of Sn rich candidate alloys using 100g load before and after thermal aging for 1 week.

Au-Ge based candidate alloys

Au-Ge is a promising system for high-temperature soldering since it does not have any intermetallic phases.[19] The microstructure of the Au-Ge eutectic was comprised of the dark (Ge) phase dispersed on the bright (Au) phase as illustrated in Fig. 8. The melting temperature of the Au-Ge (28 at. %Ge) eutectic composition is 360°C. It slightly deviates from the permissible liquidus temperature for high-temperature soldering. Addition of small proportions of In or Sb or Sn to the Au-Ge eutectic decreases the melting point of this alloy thereby adhering to the required solidification criterion. The most interesting fact is that Ge does not have affinity towards any of these low melting point metals. [3,22]

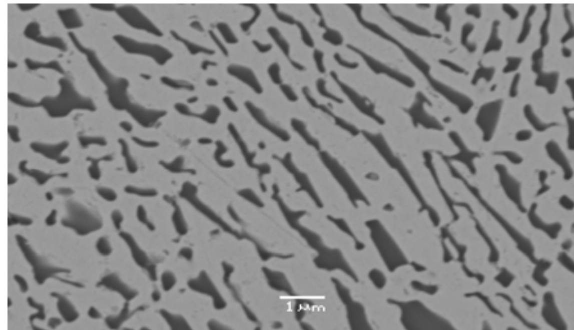

Fig. 8. SEM-BSE micrograph of the as-produced Au-0.28Ge eutectic alloy

Generally, the eutectic microstructure has a very high surface area per unit volume and it is very hard for a dislocation line to move within the eutectic structure which causes this structure to be hard. It was determined that among the low melting point metals, the addition of Sb to the Au-Ge eutectic would not only decrease its melting point but also would improve its ductility substantially despite the presence of a very hard IMC (AuSb2). This softening effect can be attributed to the expansion of the bright (Au) phase as illustrated in Fig. 9.

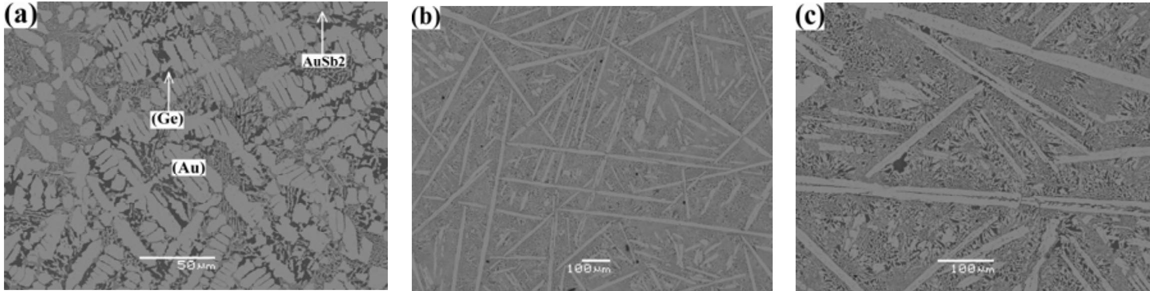

Fig. 9. SEM-BSE micrographs of the Au-0.24Ge-0.05Sb candidate alloy before and after thermal aging (a) as-produced[3] (b) 150°C-1week[3] (c) 200°C- 1 week.

Thus, a small fraction of Sb to the Au-Ge eutectic would transform this hard solder to a soft solder alloy (Fig. 10). The increase in hardness during aging despite the softening induced by the expansion of the (Au) phase can be attributed to the refinement of the dark (Ge) phase. It was determined that the addition of In to the Au-Ge eutectic would further enhance the hardness of the alloy due to the effective lattice strains induced by the In atoms.[3,22] In the case of Sn, much softening could not be achieved because of the formation of massive intermetallic compounds. Therefore, alloying Au-Ge eutectic with Sn or In would facilitate in adhering to the required solidification criterion for high-temperature soldering but will not induce the required softness to the otherwise hard solder.

The Au-Ge-Sb candidate alloy is vulnerable to corrosion since the difference in the electromotive force between the (Au) and the (Ge) phases is large.[8]A small proportion of Sb to Au-Ge eutectic could make a significant difference in terms of ductility and certainly Sb is not as toxic as lead.[23,24] In addition to the cost associated with the price of gold, the other major drawback for developing Au-Ge based candidate alloys for high temperature lead-free soldering is the fact the Ge cannot be easily electro-deposited which is important since electro-deposition is one of the common ways of depositing solder alloys in a commercial scale.[3]

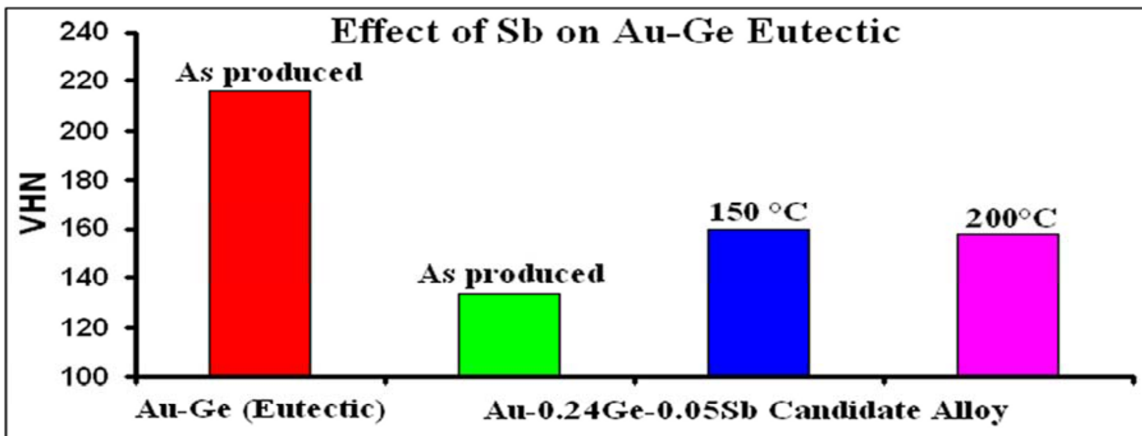

Fig. 10. Microhardness values using 100g load.

Alternative technologies

There is still no obvious cost-effective replacement for high-lead content solders. Even the expensive candidate alloys involving Au too could not cover the spectrum of properties required for being accepted as a standard soft solder for high-temperature applications. The other option is to find substitute joining technologies for high-temperature soldering. The two emerging cost-effective technologies that are identified as potential technologies for future electronics and manufacturing are: conductive adhesive technology and the transient-liquid phase bonding. These are briefly evaluated with respect to replacing high-lead content soldering, in the following.

Conductive adhesive technology

Electrically conductive adhesives (ECAs) provide a promising alternative for the high-temperature soldering. The major advantage of ECAs over the proposed Pb-free candidate alloys is that the former can be used on a wide range of surfaces including ceramics, glass and other non-solderable surfaces. ECAs are generally composed of two groups of materials: polymer binders that provide mechanical adhesion and conductive fillers that offer electrical conduction. Polymer binders are either thermosets or thermoplastics. For conductive fillers, metallic materials such as gold, silver, copper, and nickel, and nonmetallic materials such as carbon have found applications in ECAs.[25]

The use of epoxies as polymeric matrix in ECAs formulations has been the state of the art for a long time due to their beneficial properties like low shrinkage, good adhesion and resistance to thermal and mechanical shocks.[26,27] The most popular filler material in ECAs is Ag which is cheaper than Au and has superior conductivity and chemical stability. Also, it is easy to precipitate into a wide range of controllable sizes and shapes, and silver oxides too show high conductivity. Flakes or fibers are the most preferred morphology for the filler material due to their high aspect ratio which may provide easy contact within the composite and thereby the desired electrical conductivity can be achieved.[28]

However, this technology has to address a series of critical reliability issues before being adapted by the electronics industry as an alternative technology to high-temperature soldering. Notable among them are impact strength, electrical and thermal conductivity, adhesion capability of ECAs, compatibility with non-noble metal finished components and environmental reliability.[29,30] It also has to be noted that the thermal conductivity of ECAs (k=3 W/m K) are even worse than the Bi based candidate alloys.[17]

With the advent of nanotechnology, some of the critical reliability issues with respect to ECAs could be addressed. Nano-sized metal particles are being used in ECAs to improve electrical conduction and mechanical strength. The desirable properties of the ECAs could further be improved with a suitable choice of solvents, colorants, flame retardants, flexibilizers, cure accelerators, coupling agents etc.[27,31,32]

Transient liquid-phase bonding

The transient liquid phase (TLP) bonding combines the characteristics of liquid-phase joining (soldering and brazing) and diffusion bonding. The process relies on the reaction between a thin low melting interlayer and metal on the components. During the heating cycle, the low melting layer diffuses into the high melting point component and by that intermetallic phases are formed due to diffusion. After that the remelting temperature of the system is raised and the joint will not remelt thereafter unless it is heated to a higher temperature at which one of the intermetallic

phases melts. TLP bonding could easily be achieved around 280°C by using metals with low melting point metals like Bi/ In/ Sn as interlayers.[33-35]

By judicious selection of the component materials or metallizations applied to them, interlayer and process parameters, it is possible to design a joining method that combines the beneficial characteristics of soldering, namely rapid joint filling, tolerance to surface preparation and the formation of fillets, together with the advantages of completeness of joint filling and high remelt temperature of diffusion bonded joints. However, it is usually necessary to apply compressive stress to the assembly in the beginning to minimize the joint gap and a further heat treatment to the assembly after diffusion soldering so that the diffusion of the solder interlayer into the parent materials continues until, ultimately, the joint is homogenous.[36,37]

Nevertheless, several critical issues are hindering the wide acceptance of TLP bonding as an alternative to high-temperature soldering. These include production delays i.e. the duration of this process could be much longer when compared with seconds for soldering. Most of the possible intermetallic phases that could precipitate between the low melting point metals and the commonly used pad materials & the under-bump metallizations are more brittle than any of the proposed candidate alloys. The possibility of having Kirkendall voids right at the joint is also a matter of great concern.

CONCLUDING REMARKS

The currently used high-lead content solders are used mainly in the form of wires or ribbons for die-attaching. The high hardness of the possible candidate alloys other than Bi-Ag alloys causes some obstacles in introducing these alloys to actual products since it is hard to supply these alloys in the form of wires or ribbons. Thus, applying these alloys entails an expensive development effort for die-attach machines that handle solder in different forms. The possible candidate alloys are relatively more creep resistant than the high-lead content solders due to their higher strength. However, their thermo-mechanical fatigue resistance has to be investigated in a comprehensive way in order to ensure reliability of the electronic packaging. Considering gold as a potential substitute for lead would substantially increase the cost of high-temperature solders. Although the initial costs would be higher but there would potentially be a value to the recycled product and no disposal costs associated with the solders, resulting in lower life time costs for the product.

ACKNOWLEDGEMENT

The authors acknowledge the Danish Ministry of Science, Technology and Development for financial support through the innovation consortium “MatPack” (project no. 07-003145).

REFERENCES

1. V. Chidambaram, J. Hald and J. Hattel, J. Mater. Design., DOI 10.1016/j.matdes.2010.05.035.
2. N. Kang, H.S. Na, S.J. Kim and C.Y. Kang, J. Alloys Compd. 467, 246 (2009).
3. V.Chidambaram, J. Hald and J. Hattel, J. Alloys Compd. 490, 170 (2010).
4. K. Suganuma, S-J. Kim and K-S. Kim, JOM 61, 64 (2009).
5. V. Chidambaram, J. Hald and J. Hattel, J. Microelectron. Electron. Pack. 6, 75 (2009).
6. M. Rettenmayr, P. Lambracht, B. Kempf and M. Graff, J. Adv. Eng. Mater. 7, 965 (2005).
7. R. Bergmann, P.T. Tang, H.N. Hansen and P. Møller, IEEE Conf. Proc., 252 (2007).
8. V.Chidambaram, J. Hald, R. Ambat and J. Hattel, JOM 61, 59 (2009).
9. T. Yoshikazy, O. Ikuo, K. Ryosuke, Y. Yasushi, Y. Yuji, N. Yuji, J. Electron. Mater. 35, 1926 (2006).
10. C. Andersson and J. Liu, Int. J. Fatigue 30, 917 (2008).

11. Y. Shi, W. Fang, Z. Xia, Y. Lei, F. Guo and X. Li, J. Mater Sci: Mater Electron., DOI 10.1007/s10854-009-0010-5.
12. M. Rettenmayr, P. Lambracht, B. Kempf and C. Tschudin, J. Electron. Mater. 31, 278 (2002).
13. E. Gervais, R.J. Barnhust and C.A. Loong, J. Metals 37, 43 (1985).
14. F. Cay and C. Kurnaz, J. Mater. Design. 26, 479 (2005).
15. London Metals Exchange, < http://www.lme.co.uk/>.
16. T. Shimizu, H. Ishikawa, I. Ohnuma and K. Ishida, J. Electron. Mater. 28, 1172 (1999).
17. J.N. Lalena, N.F. Dean and M.W. Weiser, J. Electron. Mater. 31, 1244 (2002).
18. Y. Yamada, Y. Takaku, Y. Yagi, Y. Nishibe, I. Ohnuma, Y. Sutou, R. Kainuma and K. Ishida, J. Microelectron. Reliab. 46, 1932 (2006).
19. V.Chidambaram, J. Hald and J. Hattel, J. Microelectron. Reliab. 49, 323 (2009).
20. S.J. Kim, K-S. Kim, K. Suganuma and G. Izuta, J. Electron. Mater. 38, 873 (2009).
21. S.J. Kim, K-S. Kim, S-S. Kim, K. Suganuma and G. Izuta, J. Electron. Mater. 38, 2668 (2009).
22. V. Chidambaram, J. Hald and J. Hattel, IMAPS Conf. Proc., 000338 (2009).
23. US Environmental Protective Agency (EPA), <http://www.epa.gov/>.
24. US Department of Labor, Occupational Safety and Health Administration (OSHA), < http://www.osha.gov/>.
25. Z. Wu, J. Li, D. Timmer, K. Lozano and S. Bose, Int. J. Adhes. Adhes. 29, 488 (2009).
26. D. Wojceichowski, J. Vanfleteren, E. Reese and H-W. Hagedorn, J. Microelectron. Reliab. 40, 1215 (2000).
27. F. Tan, X. Qiao, J. Chen and H. Wang, Int. J. Adhes. Adhes. 26, 406 (2006).
28. I. Mir and D. Kumar, Int. J. Adhes. Adhes. 28, 362 (2008).
29. J.E. Morris, J. Microelectron. Reliab. 47, 328 (2007).
30. M. Yamashita and K. Suganuma, J. Microelectron. Reliab. 46, 850 (2006).
31. H-H. Lee, K-S. Chou and Z-W. Shih, Int. J. Adhes. Adhes. 25, 437 (2005).
32. Y. Li and C.P. Wong, Mater. Sci. Eng. R 51, 1 (2006).
33. N.S. Bosco and F.W. Zok, Acta Mater. 52, 2965 (2004).
34. E. Lugscheider, K. Bobzin and A. Erdle, J. Surf. Coat. Technol. 174, 704 (2003).
35. A. Kodentsov, Technical Program Abstract, TMS Symposium, Seattle, WA, United States, 14-18 February 2010, p. 272.
36. G. Humpston, D.M. Jacobsen and S.P.S. Sangha, Endeavour 18, 55 (1994).
37. W.F. Gale and D.A. Butts, J. Sci. Technol. Weld. Joining 9, 283 (2004).